INVESTIGATION OF METHODS OF DELAYING
OR CONTROLLING VENTILATION
ON SURFACE PIERCING STRUTS

by

Richard Stone Rothblum

THESIS SUBMITTED TO
THE UNIVERSITY OF LEEDS
FOR THE DEGREE OF
DOCTOR OF PHILOSOPHY

DEPARTMENT OF MECHANICAL ENGINEERING
THE UNIVERSITY OF LEEDS

January 1977

NOTE: Flow velocity U, is from left to right

in all photographs and drawings unless

otherwise indicated.

ABSTRACT

The problem of undesired ventilation of partially submerged foils and appendages on hydrofoils is traced from the earliest hydrofoils which appeared toward the end of the last century. Ventilation is assessed in the context of other problems in the development of hydrofoils, and is found to be still a serious problem. The elements of the mechanism of ventilation inception are identified as a region of low energy and low pressure flow, a surface seal, and the existence of a means of rupturing the surface seal. Two modes of rupture are identified, corresponding to nose and tail ventilation. The mechanism is used to explain the use of taper, dihedral, camber, and fences to prevent ventilation. The extension of these techniques is discussed, as well as the possible application of some novel techniques and some techniques presently in use in the aerodynamic field. These include separation control by boundary layer suction and blowing, air bleed, solid and liquid fences, flaps, and controlled ventilated cavities. Observed differences between model and prototype behaviour is the basis of a discussion of modelling ventilation phenomena. Most existing data for similar geometries can be reduced to functions of the dimensionless cavitation and Froude numbers. An empirical correlation between surface drawdown and a dimensionless velocity is shown to have wide applicability independently of geometry. Two experiments were performed to gauge the effect of parameters suspected to influence model tests, primarily roughness, wettability and speed. It was found that the effects of roughness and size and speed may be analogous in certain respects. High speed cine photography revealed a mixed subsurface mode of ventilation not previously observed. It also enabled a description of the interaction of separation, cavitation and ventilation. The present methods for prediction of separation are presented and used as the basis for semi-empirical predictions of the amount of blowing and suction required to eliminate separation from struts of finite length in the presence of the free water surface. Suction and blowing in the amounts predicted were used to retard the inception of ventilation. The greatest success was achieved with a roughened model, which it is believed simulated full scale conditions more accurately. The results of the experiments with separation nearly completely eliminated call into question the hypothesis that separation is a necessary precursor of ventilation. The results of an experiment with a liquid fence barrier were mixed, but were also more successful with a roughened model.

i

TABLE OF CONTENTS

LIST OF FIGURES

NOMENCLATURE

A	submerged planform area
A_j	jet slot area
C_L	$L/\left(\frac{1}{2}\rho\,U_\infty^2\right)$, lift coefficient
C_P	$\dfrac{P}{\frac{1}{2}\rho\,U_o^2}$ or $\dfrac{P}{\frac{1}{2}\rho\,u_{eo}^2}$, pressure coefficient based on minimum pressure or initial velocity along flat plate
C_S	sideforce coefficient (see C_L, lift coefficient)
C_μ	$V_j^2\,A_j/\frac{1}{2}\,U_\infty^2\,A$, jet momentum coefficient
c	chord length
d	surface drawdown at trailing edge of strut
F_c	$\dfrac{U_\infty}{\sqrt{gc}}$, a Froude number based on chord length
F_h	$\dfrac{V}{\sqrt{gh}}$, Froude number based on depth L
F_δ	$\dfrac{U_\infty}{\sqrt{g\delta}}$, a Froude number based on seal thickness
$F(\eta)$ $G(\eta)$	functions in one-parameter family of curves in boundary layer theory
g	acceleration due to gravity
g_1	downward acceleration due to pressure
h	submergence
k	roughness height above boundary
$k(\bar{z})$	ratio of two dimensional ideal pressure to presumed three dimensional pressure
L	reference length in boundary layer theory
n	weak function of R_x, $n \sim 7$ usually
P_A	atmospheric pressure

P_V	vapour pressure of water
P, p	pressure (ideal)
p	local pressure
p_o	pressure initially
Q	volume flow rate
R	$U_\infty c/\nu$, Reynolds number
R_k	$u_k k/\nu$, Reynolds number (roughness)
R_x	$U_\infty x/\nu$, Reynolds number
R_x, u_{eo}	$x u_{eo}/\nu$, Reynolds number
R_s	Reynolds number R_x at $x = x_s$, point of separation
R_θ	$u_e \theta/\nu$, Reynolds number
$(R_{\rho t})_n$	Reynolds number
t	time or section thickness or maximum section thickness
U_o	maximum ideal velocity along boundary or initial velocity along flat plate
U_∞	velocity of water far upstream
u	local velocity parallel to boundary
u'	flat plate comparison velocity
u_e	local velocity outside boundary layer (ideal)
u_k	velocity at roughness height
V	speed of foil or strut
V_j	jet exit velocity
v	local velocity perpendicular to boundary
v_o	uniform suction velocity to prevent separation
x	distance from nose or start of turbulent boundary layer
$\bar{x}$	arc length along boundary non-dimensionalised in terms of chord length

x_{eq}	$\int_0^{x_o} \dfrac{u_e}{u_{eo}}\,dx$, the Stratford equivalent flat plate distance which corresponds to the length of flow over a flat plate which would give the same momentum thickness as laminar flow in a favourable pressure gradient
y	perpendicular distance from boundary
y'	perpendicular distance from boundary, flat plate comparison profile
$\bar{z}$	vertical distance above or below water surface, nondimensionalised by chord length
$\bar{z}_s$	nondimensional height above midspan of point of separation
$\bar{z}_{ss}$	nondimensional height of effective free surface above midspan at point of separation
α	incidence angle or angle of attack
β	sideslip angle or empirical constant in separation theory
β_R	sideslip angle, maximum linear range
β_S	sideslip angle, separation range
β_V	sideslip angle, normal ventilation inception
δ	boundary layer thickness
$\underline{\delta}$	thickness of surface seal
δ'	boundary layer thickness, flat plate comparison profile
δ^*	$\int_0^{\infty} 1 - \dfrac{u}{U_{\infty}}\,dy$, boundary layer displacement thickness
η	height above mean free surface or $\dfrac{y}{\delta}$ in boundary layer theory
η_o	height above mean free surface at time 0
θ	$\int_0^{\infty} \dfrac{u}{u_e}\left(1 - \dfrac{u}{u_e}\right)dy$, boundary layer momentum thickness
Λ	shape factor in boundary layer theory
λ	wavelength of a disturbance to water surface
μ	viscosity (of water)
ν	kinematic viscosity of water

ρ	mass density of water
σ	$\dfrac{P_A - P_V}{\rho U_\infty^2}$, the cavitation number or index
σ_i	cavitation number of inception of cavitation
ψ	$\displaystyle\int_o^y u\, dy$, stream function

Subscripts

e	denotes "outside boundary layer"
i	denotes "inner boundary layer"
n	indicates measurement normal to leading edge
o	denotes "at point of minimum pressure"
s	denotes "at point of separation" or "streamwise measurement"
t	denotes "at the wingtip"
tr	denotes "at point of transition," e.g., x_{tr} is distance from leading edge at transition to turbulent flow
ρ	referred to leading edge radius

ACKNOWLEDGEMENTS

FORWARD

It is the intent of the author that, in addition to being a contribution to the understanding of the phenomenon of ventilation on hydrofoil lifting surfaces and appendages, this thesis be of practical value to hydrofoil designers. The mechanism of ventilation is explored, historically, analytically, and experimentally. Guidance is given to the designer and model scale experimentalist as to the practical implications of results. Current techniques for treating the problems which arise in designing for prevention of ventilation are presented. The thesis is divided into ten chapters and a Summary of Conclusions.

Chapter One establishes an historical perspective and places the problem of hydrofoil ventilation in the context of other problems of hydrofoil development. It is shown that ventilation of surface piercing struts and foils is a problem that has been underestimated and unrecognized, is insufficiently understood, and which remains as an important limitation on the performance of hydrofoil craft.

One of the difficulties in the approach to the study of hydrofoil ventilation has been the lack of a consistent and general definition. *Chapter Two* formulates such a definition, which provides the basis for a discussion of the mechanism of ventilation. The discovery of each of the elements of the mechanism is traced, and the present understanding is summarised.

An historical exposition is also used in *Chapter Three* to describe techniques that have been developed for suppression and control of ventilation. The success of these techniques is then explained in terms of the mechanism of ventilation postulated in Chapter Two. The extension of the present techniques is discussed, and some entirely new possibilities are mooted, some of which form the basis for the experimental and analytic chapters.

Model scale testing has long been a powerful tool of the naval hydrodynamicist. Unfortunately, little is known about the phenomenon of ventilation at full scale. *Chapter Four* analyses, in terms of the mechanism of Chapter Two, the probable differences between model studies and ventilation as it occurs at sea. Methods are then proposed to minimise the influence of these differences in model tests. Scaling laws are presented, along with an empirical correlation which should prove useful.

In *Chapter Five*, the results of an experiment are described in which two factors which may have been responsible for model test anomalies were studied. The effect of roughness and surface wettability are explained in terms of the mechanism of ventilation.

The roughness experiment raised some interesting questions, particularly in view of a possible analogy between the effect of roughness and the effect of higher speeds and larger sizes corresponding to prototype conditions. *Chapter Six* reports and discusses the results of an experiment which extended the work of Chapter Five on roughness to a speed range in which vapour cavitation played a significant role. This experiment provided an explanation of several puzzling phenomena, as well as revealing a mode of ventilation not previously observed.

The analytic and empirical tools which are used for predicting two- and three-dimensional separation on aerofoils are reviewed in *Chapter Seven*. As well as suggesting a design procedure, this chapter provides a basis for prediction of the effects of boundary layer suction and blowing on surface piercing struts, which forms the subject matter of the following two chapters.

To test the proposition that a region of low energy fluid is a prerequisite for ventilation inception, an attempt was made to delay or eliminate ventilation on a surface piercing strut by eliminating a region of nose separation using boundary layer suction. *Chapter Eight* describes the results of this experiment and an empirically modified theory to predict the amount of suction required to eliminate separation to a given depth below the free water surface.

While the suction experiment was designed strictly to test the model of the mechanism of ventilation, a second boundary layer control experiment, reported in *Chapter Nine*, was undertaken with possible practical application in mind. Boundary layer blowing was applied to eliminate a region of tail separation from a surface piercing strut. A semi-empirical theory was developed, based on an analogy with elliptic cylinders, which proved surprisingly accurate in predicting the amount of blowing required.

Interposition of a mechanical barrier to the path of air was one of the first solutions to the problem of ventilation of surface piercing appendages on watercraft. *Chapter Ten* describes how this intuitively appealing idea was carried one step further by replacing the solid mechanical barrier with a barrier of horizontally ejected water.

Extensive use was made of flow visualisation techniques in the experimental work, and many photographs of oil smear patterns, stroboscopic photos and prints of high speed cine films are included. The illustrations and photographs should provide the physical insight which is the basis of practical knowledge, the principal objective of this work.

CHAPTER 1

THE ROLE OF VENTILATION
IN HYDROFOIL DEVELOPMENT

HYDROFOILS AND AEROPLANES

Aeroplane Analogy. A simple definition of a hydrofoil boat – one implied by the word
"Hydrofoil" – might be "a craft which flies in the water as an aeroplane flies in the air." In
fact, such a definition would be more usefully applied to a modern submarine. The hydrofoil
boat "flies" partly in air, and partly in water. The analogy with the aeroplane is tempting
but accurate only insofar as the weight of the ship is supported by dynamic fluid forces,
rather than by buoyancy, as a conventional hull.

To say that the analogy is tempting accords with historical fact as well as intuition. The
concept of hydrofoil boats was contemporary with the idea of heavier-than-air flight, and
many of the pioneers of aeroplanes, including the Wright brothers and T. Curtiss, A. Crocco,
C.A. de Lambert, H. Phillips, S. Dumont, contributed to the development of
hydrofoils.*[1.1, 1.2, 1.3, 1.4, 1.5, 1.6]

Theoretical Advantages of Hydrofoils. A superficial examination of the analogy between
flight in air and the "flight" of a hydrofoil boat might lead one to think that, for transporta-
tion over water, development of the aeroplane was a waste of time. On a hydrofoil, the non-
lifting surfaces, analogous to the fuselage of an aircraft, travel in a medium where the drag
forces are an infinitesimal fraction of the drag which would be borne by the same vehicle
travelling in a homogeneous medium and generating the same lift forces. For the same size
of lifting element, 800 times as much force is generated at the same speed in water as in air.
Because the ratio of viscosity to density in water is less than that in air, drag due to frictional
losses is a smaller proportion of total drag. If the advantages of greater lift for smaller lifting
surfaces at lower speeds and less drag were not enough, the speed of sound in water is seven
times that in air, making compressibility effects and the "sound barrier" practically irrelevant.

---

*Superscripts refer to the numbered references at the end of each chapter. The integral part of the superscript
refers to the Chapter Number. Unless otherwise stated, historic facts are based primarily on Hayward,[1.1]
Von Schertel,[1.2, 1.3, 1.4] or Crewe.[1.5] Patroclus[1.6] pursues the aeronautical analogy.

A eulogy to hydrofoil boats could continue by enumerating the theoretical advantages the hydrofoil has over conventional displacement ships – such as negligible wave and form drag. But enough has been recounted already to cause one to wonder why there are no 2000 mph hydrofoils, each carrying hundreds of passengers and tons of cargo thousands of miles, as aircraft now do, and why there are no hydrofoil supertankers of 500,000 tons displacement. In spite of apparent advantages over both aeroplanes and ships, hydrofoils have had extremely limited success in competition with either of them. Ironically, the development of sophisticated aircraft and space technology is responsible for the present hope for future utilisation of the aeroplane's neglected step-sister.

TECHNOLOGICAL DEFICIENCIES

At the end of the nineteenth century, the aeroplane was an invention whose time had come, while its contemporary, of equal if not brighter promise, has until recently withered on the vine. Part of the reason – the lesser part – is that the technology to support the hydrofoil through its infancy did not exist.

Materials Science. The greater lift loads developed on hydrofoils in proportion to their size meant that working pressures and stresses were higher. Even today there is no wholly satisfactory material from which to construct the foils. The requirements of high strength, resistance to corrosion and cavitation erosion, resistance to fatigue, and repairability under field conditions, have not all been met simultaneously.[1.7] The requirements become even more stringent as sizes increase beyond even the most modest craft. For example, the US Navy Hydrofoil Gunboat FLAGSTAFF, displacing 68 metric tons when hullborne, had foils of solid forged 6061 aluminium coated with laminar urethane. For the next generation of military hydrofoils, the PHM NATO Missile Patrol Boat, the material selected for the foil system will be chosen from an even more exotic collection – the high yield low carbon steels such as HY-80, HY-100 and HY-130 (developed for submarine construction) and the precipitation-hardening corrosion-resistant steels such as 15-5PH and 17-4PH. These are the materials which have already been used in the present developmental prototypes of military hydrofoil craft, the largest of which is still only 320 tons.[1.8]

It is felt that present materials science will suffice for a craft of 1000 tons to be constructed. Baron Hanns von Schertel,[1.3] one of the most important figures in the development of the commercial and military hydrofoil, estimates that a 2000 ton craft is the absolute upper limit in size, and 70 knots the maximum speed that can be expected from hydrofoils in the foreseeable future.

Propulsive Systems. Besides materials science, the second major technological constraint on hydrofoil development was the propulsion system. One of the major advantages of a hydrofoil mentioned was that non-lift producing elements were not submerged in the high drag water medium. The propulsion system mostly falls into the category of a non-lift producing element. It is an unfortunate fact of life that the balance of forces on hydrofoil craft requires that the propulsive impetus be applied below the water surface for maximum efficiency and stability. This poses the problem of transmitting huge amounts of power from the engine above the surface to the propelling element below the surface. For example, the 320 ton USS PLAINVIEW, AGEH-1, transmits 28,000 horsepower through two right angle "Z" drives to the propellers six meters below the keel. Both the power plant (General Electric LM-1500 gas turbines) and the transmission are offshoots of aircraft technology.[1.8] While the aircraft was able to successfully adapt the ship's screw, the hydrofoil's requirements were so different that propellers of adequate efficiency have only just been developed. The system that will be used for the PHM will be water jet propulsion, a unique synthesis of ship and aircraft technology, which although reliable, is still inefficient by aircraft or conventional ship standards.

Control Techniques. The development of the present potential of hydrofoils had to wait upon the advent of control theory and technology. The lack of stability and controllability of the early hydrofoil craft was their main defect. Horatio Phillips, the holder of an 1881 hydrofoil patent, wrote after an experiment on the Thames with a 20 foot craft towed alongside a fast steam launch, "Everything went well, until one day we were passed by a tug running light, and the way that model behaved when it encountered the waves thrown up by the tug will never be forgotten by me, and I at once came to the conclusion that the system possessed no commercial value, and the subject dropped."[1.1] Von Schertel, in his early attempts to create a seaworthy hydrofoil craft, experimented with rudimentary feedback control systems, but eventually gave up.[1.2] Christopher Hook, in the 1950's solved the problems of the mechanical feedback loop,[1.9] but the high degree of complexity made the system impractical. The success of feedback systems in achieving the controllability and seaworthiness of the NATO PHM can

again be credited to developments in aircraft technology, computors and radar. However, the real inadequacy, for which automatic control systems have partially compensated, is the fact that aerofoils are not analogous to hydrofoils, nor do hydrofoil boats fly on the water as aeroplanes fly in the air, as first suggested. It is the failure of this analogy that is the principal reason for the retarded development of hydrofoils, rather than the lack of adequate technological resources.

HYDROFOIL DIFFERENCES

Aeroplanes operate in a single medium which at low speeds is virtually incompressible, whereas hydrofoils operate in the interface between two fluids. This is what gives them their theoretical advantages over vessels which operated purely in either medium. It is also a very serious constraint. The advantages hold unequivocally only in a very specific regime — that for which the interface is smooth and initially unperturbed and for which the flow about the hydrofoil is dynamically similar to airfoil flow. The first condition holds to a sufficient extent on inland waterways most of the time. The second holds, provided the speed is lower than that at which the pressure minima in the flow about the hydrofoil cause the water to boil locally at ambient temperature — the now familiar phenomenon of vapour cavitation. This means that, far from being incompressible, the relationship between pressure and volume is discontinuous, non-linear and non-single valued at all but the lowest speeds. Practically, this means speeds below 35 - 40 knots.

If the early hydrofoil boats could have fulfilled their initial promise only on inland waterways and at speeds below 40 knots, they still would have quickly found a useful niche in transportation technology, as they do at present, in countries with under-developed road and rail systems. However, even in relatively smooth water, and at subcavitating speed, the aerofoil analogy may still fail to be maintained. This occurs when air is introduced into the flow which should be entirely of a single fluid in the airfoil analogy.

VENTILATION

Effect of Lower Pressure below Water Surface. An aerofoil derives its property of producing a force normal to the incident flow (lift) mainly by virtue of a lowering of pressure, below ambient, on its upper surface. The hydrofoil boat operates at the air-water interface. By its nature, part of the craft operates submerged in the water, and part in the air. To accomplish this, certain elements must connect the two parts. These connecting elements are generally similar to aerofoils in that, when making forward progress through the air and water, a lower than ambient pressure is developed on one or more surfaces piercing the interface. Because the flow pressures produced by water are roughly 800 times greater than those produced by air flowing at the same speed, the air at the intersection of the interface and the surface piercing element remains essentially at ambient pressure, while the pressure in the water just below the interface may be much lower. This pressure difference tends to cause air to flow to the region of low pressure water. Under certain conditions, which frequently occur in practice even at very low speeds, massive amounts of air can be entrained in the water flow, creating a cavity which springs from the leading edge of the surface piercing element and extends downstream to a depth and extent determined by geometric factors and the ratio of the force due to the weight of the displaced water and the inertial forces due to the flow (Froude number). Generally, the velocity of the air in the cavity is still low enough so that it can be considered to be at the ambient pressure. Because the air cavity replaces flowing water which was at less than ambient pressure, the balance of forces on the affected surface piercing element is changed, often astonishingly strongly. This is because the entire flow pattern is altered as a result of the introduction of the air, rather than being a simple matter of raising the pressure in one particular area.

This flow condition has been called many things, including air leakage, aeration, reefing and, most misleading but semantically correct, cavitation. The term which has been used in most references in the past 15 years or so has been "ventilation". The cavity which results is called a "ventilated cavity" or a "vent".

Bistable Characteristic of Ventilated Flow. The flow pattern of an ideal fluid which obeys Laplaces equation, with fixed boundaries, is unique. The flow around a streamlined body piercing a water surface has a curious, and, for early hydrofoil designers, unfortunate property of having at least two stable states – ventilated and unventilated. Furthermore, the transition between the two states can occur after only an infinitesimal change in measurable macroscopic flow parameters, such as incidence angle or velocity.

It was undoubtedly the ventilation phenomenon which stymied even the most limited development of hydrofoil craft. Technological constraints ruled out large sizes, and cavitation limited speed. Had these limitations been accepted, the difficulty of preventing the erratic entrainment of air into the flow about the hydrofoil was sufficiently great that it was not until 1936 that Von Schertel[1.2] solved the problem of hydrodynamic instability due to ventilation. He considers this his most significant achievement.

Horatio Phillips. That ventilation was a problem which plagued early hydrofoil experimenters can be inferred from accounts of their work and what we now know about the phenomenon. Ventilation probably accounts for Horatio Phillips' conclusion that there was no commercial value to hydrofoil craft after observing the behaviour of a model in waves. Because the speeds attainable at the time were sub-cavitating, and, as we now know, ventilation inception may be triggered by an encounter with a disturbance, he must have observed the characteristic behaviour of a craft subjected to ventilation on one or more of its surface piercing elements. That he observed ventilation also accords with what we know about the possible changes in forces on struts and foils after ventilation. Depending upon the flow incidence angle at which inception occurs complete reversal of direction of the forces is possible.[1.10] Catastrophic lateral instability can result, and hydrofoils have been observed to slew wildly to one side or another or even to spin completely around. Phillips' discouragement can be easily understood in this context.

Comte de Lambert. After the model tests of Phillips, the next significant event in hydrofoil history was the demonstration of a steam-driven hydrofoil on the Seine in 1891 by the Comte de Lambert. De Lambert adopted an approach which is considered today to have the best chance of overcoming the cavitation and ventilation speed barriers. The lifting elements on De Lambert's craft were simple wedge shapes. (Figure 1.1) From modern tests of similar shapes, the upper and back surfaces of the wedges must have been fully ventilated as they approached the water surface. At the highest speeds, they probably functioned as individual planing hulls, rather than as hydrofoils. In this mode, they undoubtedly suffered from the wave pounding characteristic of planing boats. This is confirmed by a later version of the De Lambert craft where the foils were mounted on springs to cushion the shocks.

Because De Lambert's hydrofoils did not provide lift in the way that a conventional aerofoil does, Von Schertel[1.2] does not consider that it was the earliest hydrofoil boat and it is true that the craft must have had all the drawbacks of planing craft, such as poor response to waves and insufficient lateral stability, but it would have to be a very strained definition of hydrofoil boats which would exclude De Lambert's. One of the most advanced modern hydrofoils, HMCS BRAS D'OR, (FHE-400)[1.11] has a modified wedge shape for its forward foil. (Figure 1.2) It functions as a "super-ventilated" foil, sometimes planing and sometimes submerged in much the way De Lambert's "foils" must have behaved. A fully ventilated cavity is always attached to the low pressure faces of the wedge in normal operation.

Wedge-like shapes piercing or near the water's surface tend always to be ventilated, thus, they avoid the instability arising from the abrupt change between the ventilated and fully wetted states. These shapes suffer from poor efficiency compared to conventional aerofoil shapes, which is why they are not used to carry significant loads in modern hydrofoils. The forward foil of the BRAS D'OR carries only 10 percent of the foilborne weight of the boat. The efficiency of superventilating foils is increased if they are able to function very close to the surface in the planing mode. This is probably responsible for De Lambert's modest success. Had he tried to counter the adverse effect of waves on his planing wedges by submerging them well below the surface, he would then have been faced with the problems of low efficiency and washing out of the ventilated cavity that prevents present day designers from adopting this solution.

Rather than excluding De Lambert's efforts from the mainstream of hydrofoil developments, it may be that his craft was the precursor of hydrofoils yet to come.

Forlannini Ladder Foil. The man whose name competes with that of De Lambert for the status of builder of the first successful hydrofoil is Enrico Forlannini.[1.1] Unquestionably, Forlannini was the first to use a fully submerged, cambered aerofoil shape to provide the lift for his craft. He also contributed the concept of the ladder foil as a means of achieving vertical stability. By correctly (almost) surmising that lift and drag varied as the square of the velocity and directly with span, he designed a ladder arrangement of foils of decreasing span such that, with increasing speed, the longer spans would be lifted out of the water, resulting in constant drag force with increasing speed. (Figure 1.3) In fact, in model tests he achieved weight to drag ratios of 20 to 1, which is good even by modern standards. He designed a craft by this formula to reach a speed of 56 knots. On Lago Maggiore in 1906 it actually achieved 38 knots. The failure to achieve design speed tells us something about the nature of the problems he encountered – probably excessive resistance to cavitation in
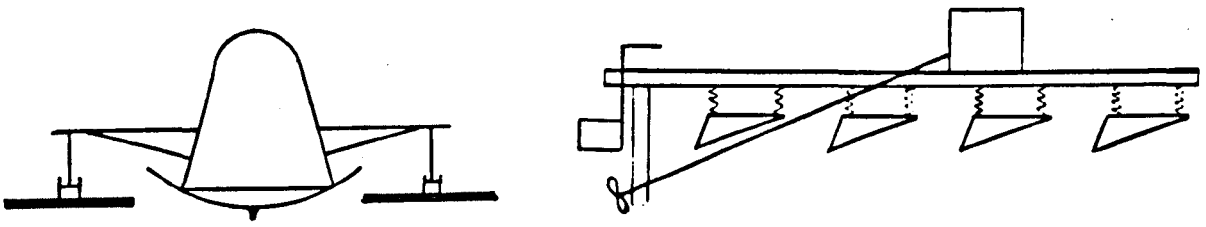
Figure 1.1 – De Lambert Hydrofoil, from Hayward[1.1], Probably Based
on Patent Sketch (1891-1904).

FLOW
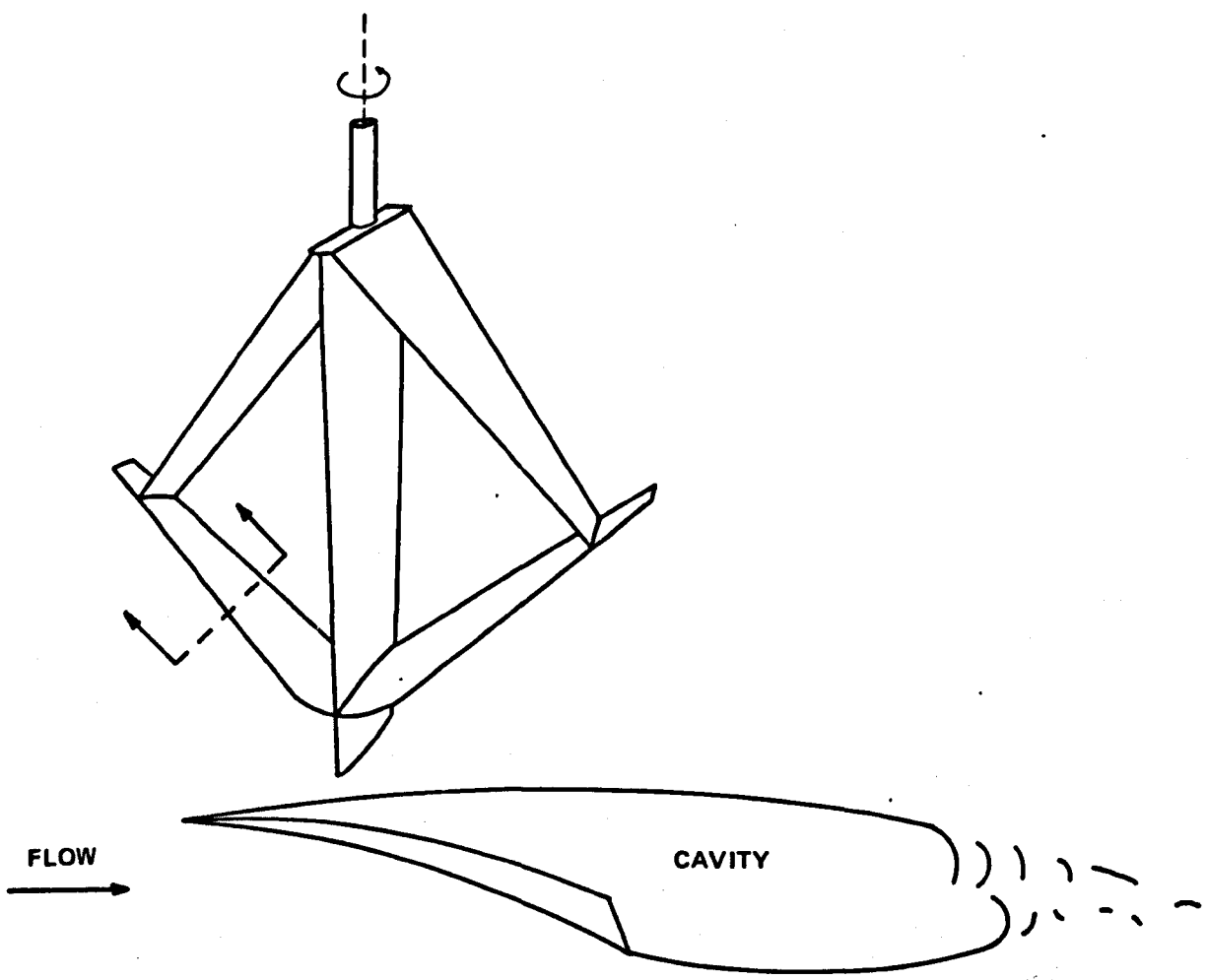
CAVITY

Figure 1.2 – Sketch Representing the Configuration of the Bow Foil of
HCMS Bras d'Or (FHE 400), Based on Millman[1.11].
A Supercavitating Foil Section is Also Shown.

straight ahead running. From the appearance of the system there was no lateral stiffness in turns, and the unprotected vertical surface piercing struts were surely prone to ventilation. It is also fairly obvious now that the ladder system is unsuitable for use in waves. Broaching of foils in waves is troublesome on today's monowing craft. With the ladder system, broaching and re-submergence is the principal means of height control. Forlannini attempted to alleviate the problem of excessive foil broaching in a later design (never built) in which the take-off foils were retractable once the craft became foilborne.

Bell-Baldwin Ladder Foil. Although Forlannini's ideas were more sophisticated than De Lambert's, and more firmly grounded on aeronautical principles, it can be said that he left a false scent which has been followed from time to time by hydrofoil designers right up to the present. Even though his craft did not attain its design speed, 38 knots was a spectacular achievement. This induced Alexander Graham Bell to buy the American rights to Forlannini's patents. Using Forlannini's basic system, as shown in Figure 1.4, Bell, in collaboration with Casey Baldwin, achieved a truly remarkable success in 1919 when his "hydrodrome" HD-4 attained a speed of 61½ knots on the Bras d'Or lakes in Canada, a world waterborne speed record which was not broken for 30 years.[1.5] Again, this apparent breakthrough in hydrofoil design encouraged many imitators, especially in Canada, where the ladder system has only just been discarded with the advent of the FHE 400.[1.11]

Forlannini's ladder system is illustrative of the problem of hydrofoil development in general – a tantalising success which failed to develop into a workable system even after years of effort. It is also typical that, because the development of hydrofoils has been so slow, the blind alleys of earlier investigators tend to be forgotten and the same fruitless paths are chosen by later experimenters. An example was the successful hydrofoil sailboat built in the 50's by Gordon Baker, sponsored by the US Navy. This craft, the MONITOR, attained speeds of 35 knots as measured by pace boats, and reported speeds of nearly 40 knots. The MONITOR used ladder foils with large dihedral and complicated mechanical linkages to control foil incidence. As a consequence of the MONITOR success 20 years ago, present day sailing hydrofoil designs include many ladder systems. The MONITOR itself is being re-fitted for an attempt on the John Player/RYA Sailing Speed Record.[1.12]

The initial success of the ladder system was due to the fact that, under good conditions, the lift producing elements were isolated from the effects of the air-water interface, including ventilation, except for the uppermost foil, which as it rose to the surface, experienced a decreasing lift and eventual ventilation. The system was inherently stable with respect to height. With the additon of dihedral, lateral stability was also gained at the expense, perhaps,
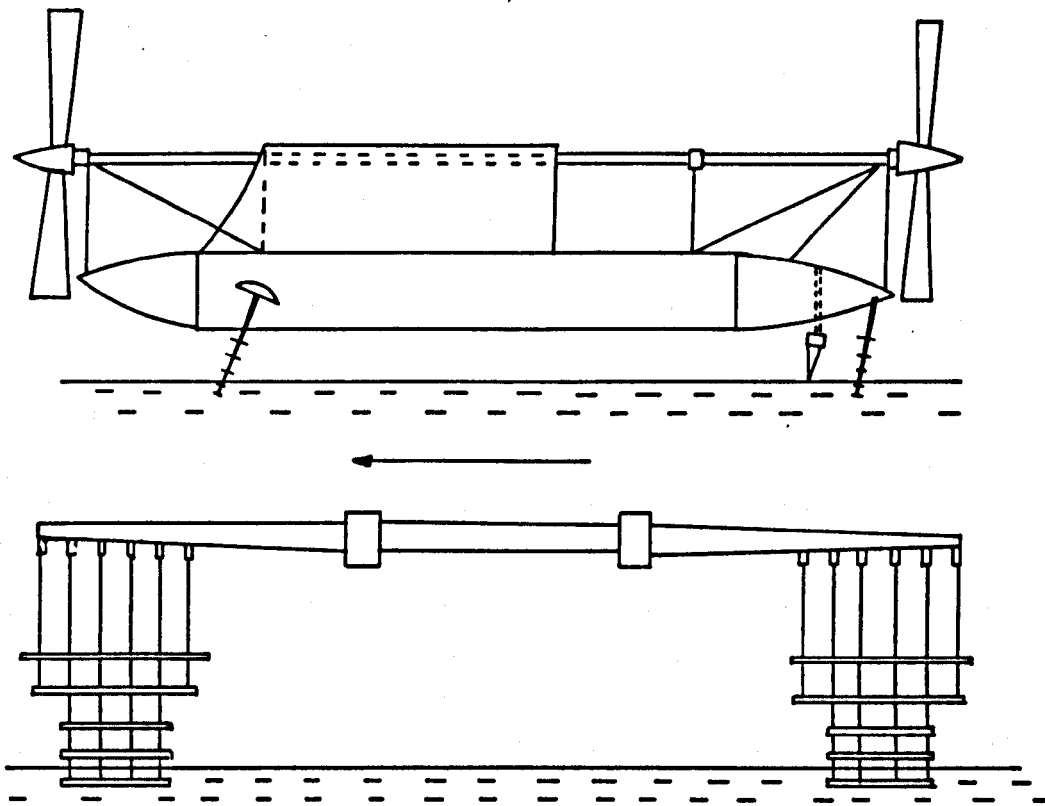
Figure 1.3 – Forlanni Ladder Foil, from Hayward[1.1], Probably Based on Patent Sketch (1905).
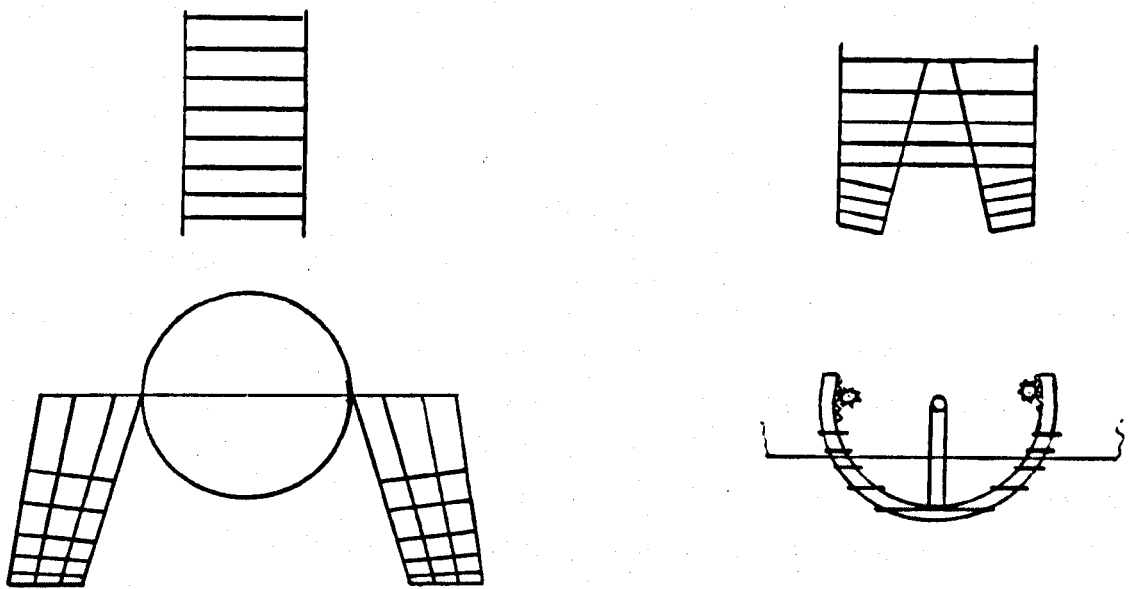
Figure 1.4 – Bell-Baldwin "Hydrodome" Showing Use of Ladder Foils, from Hayward[1.1], Probably Based on Patent Sketch (1920).

of aggravating ventilation problems. Dihedral meant that the lift-producing elements pierced the surface, possibly more than one at a time, depending on span and dihedral angle.

Surface Piercing and Fully Submerged Systems. There are two other approaches to isolate the lift producing elements from the "free" water surface. The first, suggested in a patent by William Meacham in 1896,[1.1] is to have incidence controlled, fully submerged foils with the hull supported on vertical surface piercing struts. The height of the craft is sensed, and foil incidence adjusted to maintain level "flight". (Figure 1.5) The second, developed by Hanns von Schertel, utilizes V-shaped foils which pierce the water surface in such a way that the craft is inherently stable. (Figure 1.6) The fully submerged system depends upon an active feedback control system to maintain stability. With one exception, these are the two systems which have won acceptance on every contemporary commercial and military hydrofoil boat. The exception is the fully submerged foil without incidence control used on many Russian hydrofoils for inland operation. The stability of height of these craft is accomplished by the normal decrease in lift as a submerged foil rises towards the surface. This system works only over a limited speed range, and cannot cope with waves.

Development of Fully Submerged Foil Systems. Of the two major systems presently in use, the fully submerged incidence controlled hydrofoil has had the longest, and until 1958 with the advent of aircraft electronic controls and sensors, the least successful history. Mechanical systems for sensing and control were too clumsy for practical application, even though several demonstration craft were built. In particular, in the 1950's, Christopher Hook and Gordon Baker developed the basic ideas necessary for feedback control of hydrofoil boats at the time when the electronics to make the systems practical also emerged.[1.9]

In 1958, the Gibbs and Cox hydrofoil craft SEA LEGS, with incidence controlled fully submerged foils and electronic sensors made a demonstration run down the Atlantic coast of the US, accompanied by Von Schertel who wrote that it "showed to what extent the disturbing effect of waves can be reduced by lift variations, controlled by sensors. A smoother run than ever achieved before with a watercraft (was) demonstrated."[1.2]

In 1960, based on the success of SEA LEGS, the US Navy ordered their 110 ton prototype hydrofoil patrol boat HIGHPOINT (PCH-1) from Boeing Aircraft Corporation. Shortly thereafter, orders were placed for two patrol gunboats of about 60 tons and an experimental craft of 320 tons, the PLAINVIEW, at present the largest hydrofoil craft.[1.13] All of these boats shared the fully submerged automatically controlled foil system, with some individual variation, as will the NATO hydrofoil missile patrol craft.

12

COUPLED HEIGHT
SENSOR
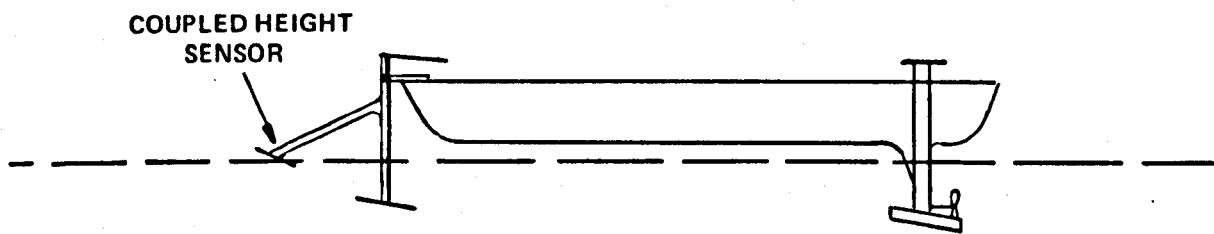
Figure 1.5 – Meacham Incidence Control System, from Hayward[1.1], Probably
Based on Patent Sketch (1896).
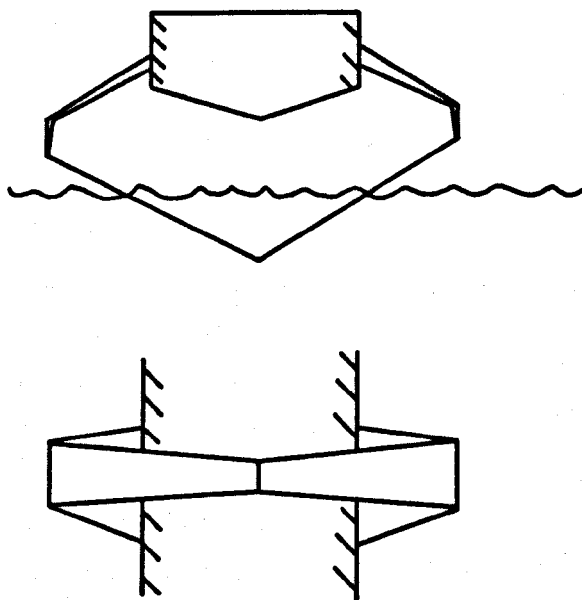
Figure 1.6 – Schertel-Sachsenberg Foil System, Based on Von Schertel[1.2, 1.3]
Photographs and Sketches.

13

Ventilation Problems on Fully Submerged Systems. In spite of this evidence of eager acceptance for fully submerged foil systems, all the problems of the air-water interface had not been eliminated. It was true that vertical, surface piercing struts used to support the hull and having section shapes based on aerofoil designs will not suffer from ventilation or cavitation at the present speeds of operation of these craft, which is generally in excess of 50 knots, provided the incident flow seen by the struts is head-on – zero sideslip angle. Unfortunately, in a seaway, or in a turn, a fully submerged system depends upon developing a sideforce on the vertical struts to provide lateral stability and restoring forces to counter the centrifugal forces of the turn. This means that the struts must operate at sideslip angles to generate side-forces (sideways lift). If "lift" is generated, low pressure regions are created with the attendant possibility of ventilation or cavitation.

Ventilation Experience on Modern Fully Submerged Foil Systems. A 1968 report[1.14] on the steering characteristics of PCH-1 in calm water noted the following anomalies:

- port yaw rate greater than starboard
- high turn rate with small increment in rudder
- 4° starboard rudder required to maintain straight course
- 8-12° starboard rudder or 6-8° port required to maintain straight course

During rough water trials, the rudder was insufficient to control the yaw rate. These deficiencies, since corrected, were attributed to ventilation of the vertical surface piercing struts. They were manifestations of the discontinuous force change and hysteresis associated with transitions to the ventilated state.

In the case of PCH-1, the anomalies were corrected by the application of ventilation fences and by removing discontinuities in the section shape of the strut. Ventilation problems frequently occur on craft with vertical surface piercing struts, and these are either solved on an ad hoc basis, or remain to pose a limitation on craft performance.

Development of Surface Piercing Foil Systems. Von Schertel was attracted to the concept of the fully submerged feedback controlled foil system in 1929.[1.2] After seven boats and five years, he came to the conclusion, which history has supported, that fully submerged mechanically controlled systems were impractical. He then turned his attention to the surface piercing system which he had used on a boat he built as a boy in 1919. Although there are historical antecedants to the surface piercing system prior to Von Schertels' work, including a boat built and sailed by A. Crocco,[1.1] Von Schertel was probably unaware of them. The relevant

patents are nearly all held by Von Schertel, and he was certainly responsible for bringing the idea to fruition.

Ventilation on Surface Piercing Systems. While the developers of fully submerged systems considered the problem of ventilation to be a secondary one due to the isolation of lifting elements from the surface, the prevention of ventilation was the main problem on surface piercing foils, particularly in waves. After years of trial and error, by using a combination of fences, proper section shape (changing along the span), and dihedral angle, Von Schertel was able in 1936 to sail foilborne from Mayence to Cologne and back in bad weather without "falling off the foils" due to ventilation.[1,2] As a result of this demonstration, the first hydrofoil to be built as a commercial passenger carrier was ordered. Due to the war, the boat never saw commercial service.

Ventilation Experience on Modern Surface Piercing Systems. Although Von Schertel was able to "solve" the problem of ventilation on surface piercing foils for specific cases, difficulties still arise in modern hydrofoils using this system. HMCS BRAS D'OR (FHE-400) went through several modifications of its forward surface piercing foil before ending up with a superventilating configuration. All other attempts at suppressing ventilation had failed.[1,11] The loss in efficiency was made tolerable by the fact that the forward foil carried only 10 percent of the total foilborne load.

RELATIONSHIP OF VENTILATION TO FUTURE PROGRESS

It can be seen that the factors retarding the development of hydrofoils compared to the development of aircraft are interdependent. Technological limitations prevented certain solutions being applied to the fluid mechanical problems of operation in the air-water interface. Thus, the fully submerged foil system could not be used by the early inventors to avoid ventilation of lifting elements, because only the advent of avionics technology made such a system practical. The development of the technology could not be "driven" by the simultaneous development of the hydrofoil as it was by the development aircraft, because the rewards were not great enough for the effort applied. For aircraft, each small improvement in technology brought a corresponding improvement in performance and profitability or ability to accomplish a military mission. Thus each improvement contained the seeds of further

advancement of the technology. For hydrofoils, a great leap in technology was required before even a modicum of reward was earned. Primarily, the leap was performed on the back of the aeroplane. The situation is the same at the present. Improvements in hydrofoil performance will depend on the advancement of a technology on which hydrofoils will have little influence. Therefore, the problems which are unique to hydrofoils assume an added importance, since they are the ones for which there is the least hope of solution without specific application of effort. These problems are concentrated in the areas of propulsion and operation in the air-water-vapour-interface, of which ventilation is an important component of both.

No systematic method exists for designing surface piercing hydrofoil elements to avoid or control ventilation. Ventilation is largely dealt with on a cut and try basis after a craft has been built and it is discovered that the problem exists. Practical experience has taught hydrofoil builders some obvious errors to avoid, so ventilation prevention is not entirely ad hoc. However, the fundamental mechanism of ventilation as it occurs on commercial and military sized craft under realistic conditions is completely unverified.

Chapter 1 References

1.1   Hayward, Leslie, *"The History of Hydrofoils,"* Hovering Craft & Hydrofoils, Vols. 4 & 5, 1965.

1.2   Von Schertel, Hanns, *"Hydrofoil History,"* Hovering Craft & Hydrofoils, Vol. 13, No. 7, April 1974.

1.3   Von Schertel, Hanns, *"The Design and Application of Hydrofoils and Their Future Prospects,"* Trans. I. Mar. E., Vol. 86, 1974.

1.4   Von Schertel, Hanns, *"Hydrofoil Boats as a New Means of Transportation,"* SNAME, Presented Oct 30, 1958.

1.5   Crewe, M.A., *"The Hydrofoil Boat; Its History and Future Prospects,"* Trans. Inst. Naval Architects, March 26, 1958. (Also Qrtrly Trans. Vol. 100, No. 4, Oct 1958)

1.6   Yangos, Patroclus J., *"The Interest of Aeronautical Engineers in Hydrofoil Development,"* AGARD Rep 473, July 1963.

1.7   Ellsworth, William M., *"Hydrofoil Development – Issues and Answers,"* AIAA/SNAME Advanced Marine Vehicle Conf., AIAA Paper No. 74-306, Presented February 1974.

1.8   Ellsworth, William M., and O'Neill, William C., *"The U.S. Navy Hydrofoil Development Program – A Status Report,"* Naval Ship R & D Center Technical Note SDD-OH50-62, Nov 1970.

1.9   Johnston, Ralph J., and O'Neill, William C., *"The Development of Automatic Control Systems for Hydrofoil Craft,"* International Hovering Craft, Hydrofoil and Advanced Transit Systems Conference, Brighton, England, Kalerghi Publications, London, May 1974.

1.10 Rothblum, Richard S., Mayer, Dennis A., and Wilburn, Gene M., *"Ventilation, Cavitation, and Other Characteristics of High Speed, Surface Piercing Struts,"* Naval Ship R & D Center Report 3023, July 1969.

1.11 Milman, John W., *"The Canadian Hydrofoil Programme,"* Trans. RINA, presented Mar 24, 1965.

1.12 Grogono, James, *"Hydrofoil Sailing – The State of the Art,"* International Hovering Craft, Hydrofoil and Advanced Transit Systems Conference, Brighton, England, Kalerghi Publications, London, May 1974.

1.13 Goss, LaVaughn B. (Ed.), *"The Centerline"* U.S. Naval Ship R & D Center, Vol. 2, No. 7, April 12, 1968.

1.14 Boeing Company Report, *"Hydrofoil Patrol Craft High Point (PCH-1) Analysis of Strut Hydrodynamic Characteristics in Calm Water,"* HYSTU PLAN BE049AP044, Contract NOO 600-69-c-0618, 1968.

CHAPTER 2

MECHANISM OF VENTILATION

DEFINITIONS

Difficulty in Terminology. One of the difficulties in the investigation of the problem of ventilation arises from a lack of agreed terminology to describe the phenomenon. Ventilation is a phase of general free surface behaviour and as such is difficult to distinguish logically from vapour cavitation and the "usual" deformation of the water surface as it passes obstacles. It is also possible to confuse ventilation with the mixing of air with water as occurs in the wake of a ship.

Suggested Definitions of Earlier Investigations. S.F. Hoerner[2.1] defines ventilation as

> *"the formation of a more or less steady cavity, which is connected to the atmosphere, past or behind a surface piercing body."*

K. Wadlin[2.2] defines ventilation by the use of photographic examples.

Wetzel[2.3] states that it is the formation at a certain speed of

> *"an air pocket ... that will expose part or all of the rear portion of the (surface piercing) body to the atmosphere."*

J. Breslin and R. Skalak[2.4] define ventilation as

> *"the occurrence of atmosphere connected cavities, usually on one side and abaft a moving, surface piercing body."*

Features of a General Definition. It would be too complicated, and not very helpful to try to formulate a perfectly general definition of ventilation. However there are unique features of ventilation which nearly every definition recognises. First, the term applies to cavities connected directly to the atmosphere. If the air is introduced through pipes or other internal structures, we speak of artificial or forced ventilation, even if the air supplied is at atmospheric pressure. The connection to atmosphere distinguishes a ventilated cavity from a vapour cavity which may include air as a component of the gases within it.

Ventilation does not specifically apply only to surface piercing bodies. Fully submerged hydrofoils can ventilate if they approach the surface too closely or if the tip vortices breach the surface. Even though the mechanism of ventilation of fully submerged bodies is probably similar to that of surface piercing bodies, it will not be considered here.

The other feature of ventilation common to every definition is that it is an "occurrence". Ventilation is a distinctive change in the flow pattern which occurs more or less abruptly, after only infinitesimal changes in other flow parameters such as speed or incidence angle, or

after encountering a particular type of disturbance. The fact that the onset of ventilation is an occurrence implies at least two distinctive possible flow states given the same external conditions of speed, geometry and other independent flow parameters. This distinguishes a ventilated cavity from the "ordinary" surface deformation in flow around surface piercing or above shallowly submerged bodies.

While it is not included in the definitions quoted, ventilation is always characterised by a marked hysteresis effect. Once the transition is made to the ventilated state, a return to the ordinary previous state requires more than a small reversal of the independent flow parameters to the values they had in the non-ventilated state.

Descriptive Definition Using a Specific Example. To go further in a general definition would become cumbersome. Therefore, consider a streamlined fine untapered symmetric strut of constant section (or uncambered hydrofoil) moving through a body of water piercing the surface vertically, submerged to a depth of several chord lengths, and terminated with a simple truncation. The strut rises above the surface to such a height that the upper termination does not influence the flow of water around the strut. (Figure 2.1)

Deformation at Small Sideslip Angle. At a particular speed, if the sideslip (incidence) angle is increased slowly from zero, a sideways force will be generated on the strut as is normally the case with an aerofoil at an angle of attack. Ignoring minor flow features such as spray sheets, the surface of the water flowing past the strut will deform to be generally higher on the high pressure side of the strut and lower on the suction side. To be more specific, consider that the speed of the strut is sufficiently high that the pressure gradient due to the inertia of the flowing water is much greater than the static pressure gradient due to gravity in the still liquid (high Froude number). Thus the initial deformation of the surface will be nearly independent of speed. This is the case in all present hydrofoil applications. The strut is also assumed to be of a sufficient size that the effects of surface tension and wetted contact angle are unimportant.

Ventilation Inception. As sideslip angle is increased, the surface drawdown on the suction side progresses smoothly. For some value of sideslip angle, a ventilated cavity will suddenly form on the suction side of the strut. When it becomes fully established, one wall will probably spring from a line nearly on the leading edge of the strut and extend for many chord lengths behind the strut. The walls of the cavity will be well defined. The wall terminating on the high pressure face will spring from the trailing edge, eventually intersecting

21
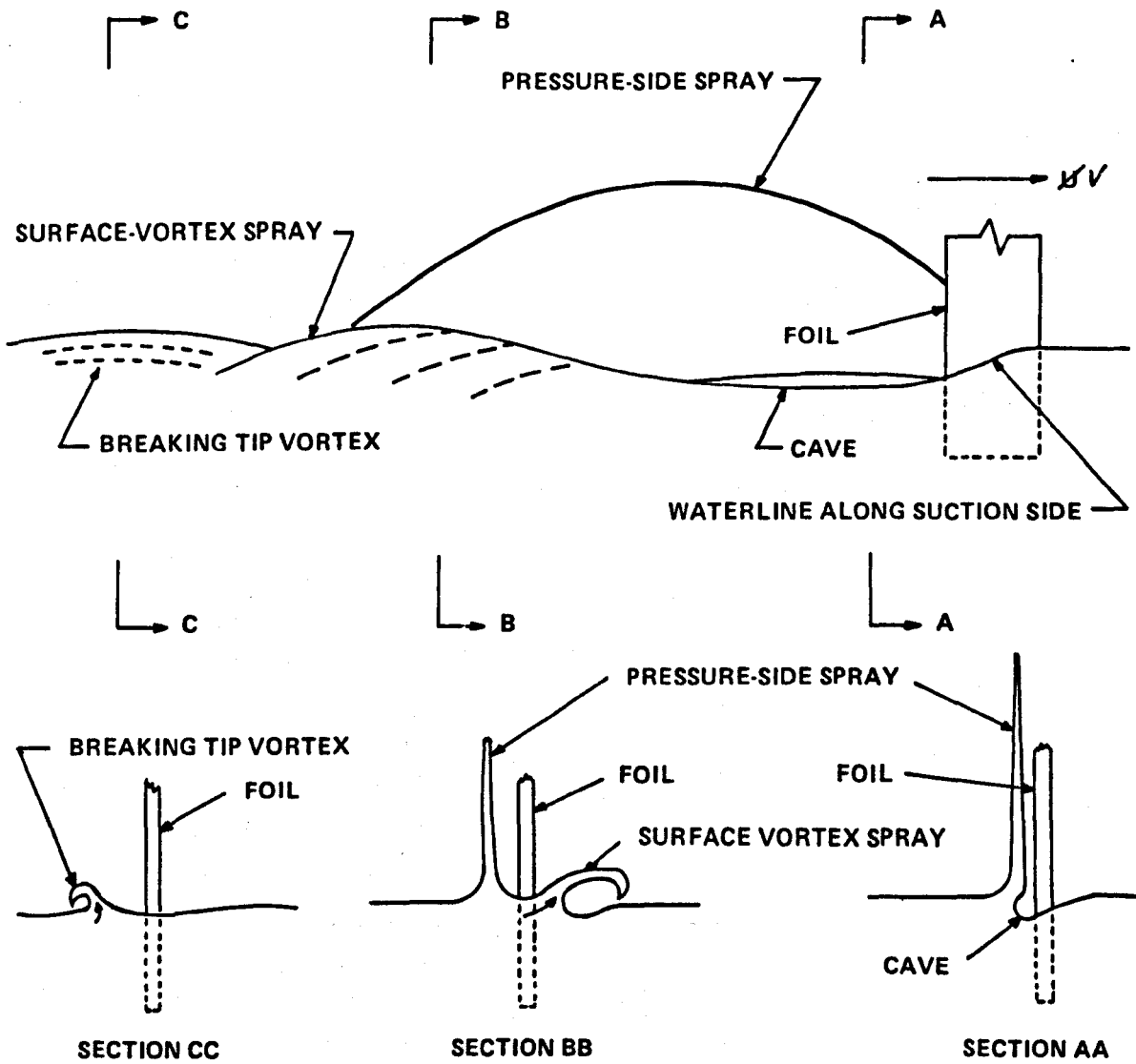
Figure 2.1(a) — Typical Flow Prior to Ventilation at High Froude Number, from Breslin and Skalak[2.4].

22

PRESSURE-SIDE SPRAY

A

CENTER ROACH

FOIL

$\cancel{1/2} V$

SUCTION-SIDE SPRAY

BOTTOM OF CAVITY

A

PRESSURE-SIDE SPRAY

CENTER ROACH

FOIL

SUCTION-SIDE SPRAY

SECTION AA
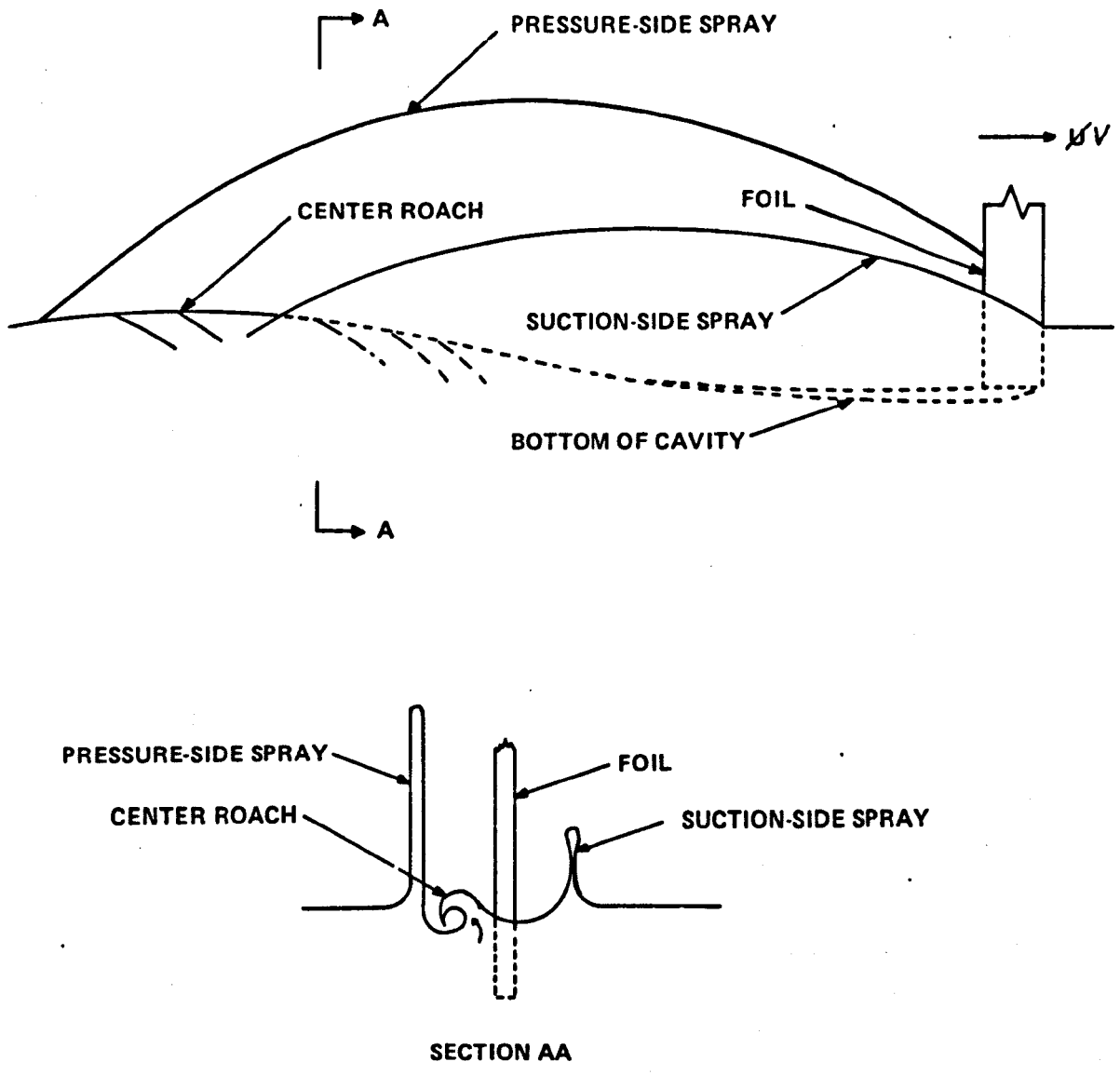
Figure 2.1(b) — Flow Pattern after Ventilation at High Froude Number,
from Breslin and Skalak[2.4].

23

the opposite cavity wall downstream. The cavity walls will be nearly vertical except at the bottom of the cavity. The top of the cavity is open to the atmosphere. (Figure 2.1)

Partial Ventilation. If the cavity extends to the bottom of the strut, it is said to be fully ventilated, or ventilated. The cavity may not extend to the bottom of the strut. (Figure 2.2) If the speed of the strut is not great enough so that the dynamic pressure of the flow at the bottom of the strut is not sufficient to support the static load of the weight of the water at that depth, the cavity will not reach the bottom. Furthermore, if the sideslip angle continues to be increased, the cavity will not get much deeper. This situation is likely to occur if the Froude number based on depth, F_h, is less than about two,[2.1,2.4]

where
$$F_h = \frac{V}{\sqrt{gh}}$$

V = the speed of the strut

g = the acceleration due to gravity

h = the submergence

Under certain circumstances, even at Froude numbers much greater than that required for full ventilation the ventilated cavity will not extent to the bottom of the strut. In these cases, a new surface having similar properties to the unventilated surface re-forms at the bottom of the cavity. With further increase in sideslip angle, the depth of the cavity will increase abruptly in the same manner as the original ventilation. This process will continue, until at some sideslip angle, the bottom of the strut and the bottom of the cavity will coincide.

If a ventilated cavity does not extend to the bottom of the strut, that will be referred to as a "partial vent." In the case where the Froude number is insufficient to allow full ventilation to the bottom of the strut, it is perhaps unjustified to call ventilation to the maximum depth "partial" ventilation. However, this case is avoided in all the discussion and experimental work presented here, and it is not representative of most hydrofoil craft, although it conceivably could be.

Washout. Once a full or partial ventilated cavity has been established, and the sideslip angle is reduced, the process of restoration of the normal flow occurs in a similarly abrupt fashion to the way in which the cavity was established. However, partial cavities are much more likely to occur in this stage. The hysteresis effect is manifested as sideslip angle is decreased.
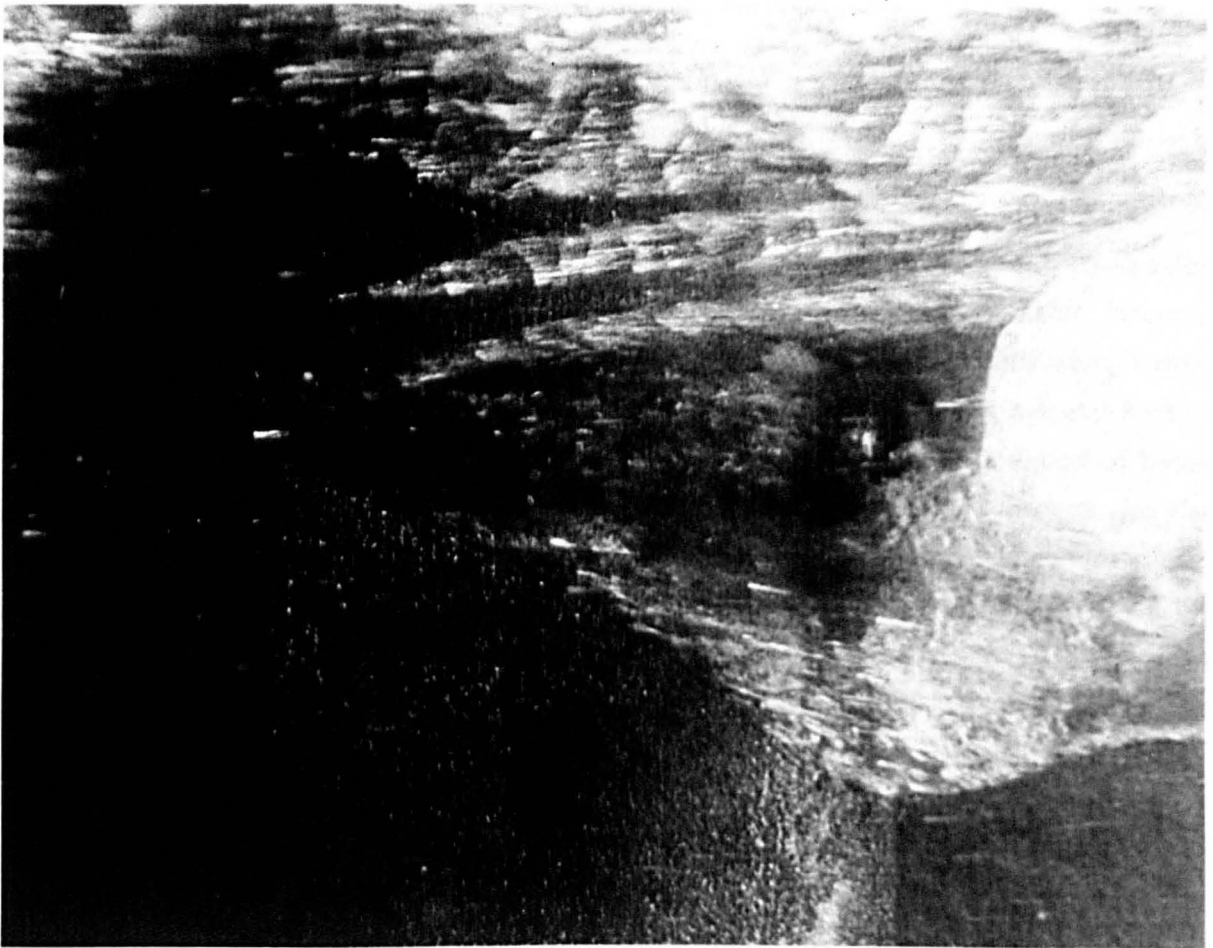
Figure 2.2 – Example of Partial Ventilation.

25

Partial Washout. Restoration of ordinary flow may not be complete, in certain circumstances, until the sideslip angle has reversed its sign. The re-establishment of normal flow is called "washout." The establishment of a partially ventilated cavity which was preceded by a more full (deeper) one is called "partial washout."

HISTORICAL DEVELOPMENT OF THE
BASIC MECHANISM OF VENTILATION

Earliest Description of Elements of Mechanism. Interest in the mechanism of ventilation certainly dates back to the efforts of Von Schertel[1.2] in the 1930's. The earliest paper discovered on the subject during the present investigation was that of Sottorf,[2.5] 1940, referred to in the 1953 paper by Hoerner.[2.1] Although the original paper was not available, Hoerner reproduced much of the data. In his hypothesis about the mechanism of ventilation, Hoerner relied only on experimental work already accomplished by his references, principally Sottorf's. Hoerner stated that the necessary conditions for ventilation were "an accumulation of boundary layer material and a negative pressure within the separated region...and a speed...so that the critical Froude number F_h is attained or exceeded." Since the Sottorf paper was concerned with the effects of dihedral angle on ventilation, a refinement not yet reached by present day investigators, it is probably a safe assumption that these elements of the mechanism of ventilation were known at this rather early stage in hydrofoil development, probably coinciding with German interest in them as military vehicles.

Unseparated Region Near Surface Identified. Flow studies carried out by J. Breslin and R. Skalak[2.4] at the Stevens Institute and by K. Wadlin[2.2] at the National Advisory Committee on Aeronautics (NACA), Langley, utilising an oil smear flow visualisation technique developed by D. Loving of NACA, were able to clarify the nature of the separated flow region that preceded ventilation. They found that near the water surface was a region of unseparated flow, the momentum of which was apparently sufficient to prevent the ingress of air into the low pressure separated region.

Search for Airpaths. They postulated that low energy paths must exist from the atmosphere to the separated region for ventilation to occur. Breslin and Skalak[2.4] identified what they called "Rankine Vortices" in the wake of surface piercing struts, which they observed to

create air paths to initiate the ventilated cavity. They also observed ventilation via the tip vortex when the vortex found its way to the surface in the case of slightly submerged struts. Wadlin[2.2] also favoured the idea of wake vorticity as providing the air path. T. Kicenuik[2.6] in a discussion of Wadkin's proposed mechanism, presented photographs which he had taken in his studies of ventilation at the California Institute of Technology. These purported to show vorticity in the wake of two bodies – one a circular cylinder which had just ventilated, and the other a strut apparently not yet ventilated.

"Taylor Instabilities". Also evident in the photograph of the surface piercing strut were surface instabilities of the type, described by G.I. Taylor,[2.7] which are characteristic of liquid surfaces undergoing downward acceleration. These Taylor instabilities and what appeared to be aerated vortex cores were reported by Rothblum et al [2.8] in 1969. (Figure 2.3) The instabilities were apparent in a thin, unseparated sheet of water dividing the free surface from a vapour cavity just below the waterline. The existence of a vapour cavity just below a free surface on a surface piercing body had been previously reported by C.W. Coffee and R.E. McKann[2.9] of NACA. The vapour cavity was found by Rothblum et al,[2.7] at the David W. Taylor Naval Ship Research and Development Center, to fulfill the same role as the separated region of low pressure in the ventilation mechanism. The downward acceleration in the unseparated liquid layer at the interface were estimated to be of the order of twenty times the acceleration due to gravity. A comparison of photographs of the instabilities with photographs and calculations by Emmons and Chang[2.10] of Taylor instabilities in downwardly accelerating liquid surfaces showed remarkable similarities. R. Waid[2.11] calculated the growth rate of the instabilities in the flow above the vapour on one of the Rothblum surface piercing struts after performing similar experiments on the same models at lower speeds and reduced pressures at Lockheed's towing facility (LUMF). He found that the expotential growth rate of the instabilities as they were accelerated downward in the pressure gradient of the suction side of the strut coincided with that predicted by Taylor.

Interaction of Taylor Instabilities and Vorticity. Waid observed the characteristic vortex cores in the wake of the strut and speculated that the interaction of the Taylor mechanism and the vorticity in the flow may combine to generate a low energy path. Swales[2.12] et al also observed the Taylor instabilities. From their careful observations it was discovered that the Taylor instabilities did degenerate in the wake of a surface piercing strut to form the cores of vortices from which air was fed into separated regions in contact with the strut. They observed that the air was fed into the separated regions in pulses, each one corresponding to

an individual vortex core. The flow of air into the separated region was choked off as the vortex filament elongated and was swept downstream. This corroborated Waid's[2.11] finding of a stepwise change in side force as ventilation occurred. However, Rothblum et al [2.8] observed only once an intermediate single step in the change from normal ventilated flow. Although the Lockheed tests utilised the same struts as the Taylor Center tests, the Center speeds were much greater, and the transition to ventilated flow was quicker. This was probably due to the greater pressure and density difference between the air and the vapour cavity in the Center tests. The LUMF tests were conducted at reduced ambient pressures.

Small Incidence Angle Ventilation. Swales[2.12] et al identified a further mechanism of breach of the "surface seal" besides the growth of instabilities. It had been recognised for some time (e.g. J. Wetzel)[2.3] that there were two "types" of ventilation, one associated with small incidence angles and the other with large angles. The large angle ventilation had been associated with full stall and the small angles were thought to be associated with laminar separation and turbulent reattachment at the leading edge. In fact, a careful reading of the early work reveals three types of ventilation, corresponding to small, medium and large angles.

Two Modes of Ventilation - Nose and Tail. The work by Swales et al has clarified this picture considerably. They showed that there were two distinct modes of ventilation that occur on surface piercing struts, ignoring the very large angles where the strut behaves as a blunt body – indistinguished in the past from large angle ventilation.

Using the oil smear technique (developed by Loving, Wadlin, and Breslin) in the University of Leeds Variable Pressure Free Surface Recirculating Water Channel, Swales et al [2.13] were able to study comprehensively ventilation associated with four different types of separation, in addition to vapour cavitation. They selected four struts, chosen to exemplify long (growing) leading edge "bubble" separation, short (shrinking) leading edge bubble separation, leading edge vortex, and turbulent tail separation.

Tail Ventilation / Taylor Instabilities. For the strut which was chosen to exhibit tail separation, they verified that the mechanism of ventilation was due to breach of the surface seal by aerated vortices in the wake, associated with the growth of Taylor instabilities in the accelerating surface seal. Air ingress was from the rear of the strut. They found that only at the lowest speeds was ventilation associated with full stall. At higher speeds, "tail" ventilation occurred after only 50 percent of the foil area showed separation.

Nose Ventilation / Ambient Disturbances. One of the most significant discoveries was that the mode of inception or breach of the surface seal took place at the nose of a strut exhibiting nose separation. They did not find much to distinguish between a leading edge vortex and long (growing) bubble separation, but they were unable to observe ventilation associated with short shrinking bubble separation. By qualitatively interpreting the intensity of the scouring effect on the oil of the reversed flow in the nose separation bubble, they formed the opinion that the likelihood of inception increased with the strength of the vorticity in the separation bubble. They estimated that nose ventilation was most likely to occur with a separated region at the nose of either about 10 percent or just before complete stall. Besides ordinary separation, they also found a small nose cavity would suffice for ventilation inception. This was contrary to the findings of Rothblum et al [2.8] at the Center towing tank, who found that even at the very high speed of 55 knots (28 m/s) ventilation did not occur on struts exhibiting nose cavitation until the cavity covered nearly 100 percent of the submerged area excluding the surface seal and the submerged termination (tip).

Swales also observed that inception of ventilation at the nose was due to breach of the surface seal by an ambient disturbance, rather than amplification of an infinitesimal disturbance by the Taylor mechanism as was responsible for inception at the tail of a surface piercing strut. The conclusion that might be drawn from this is that sufficient disturbances are not present in towing tanks to initiate nose ventilation, even in the presence of a separated or cavitating region at the nose. An alternative explanation, which cannot be disregarded, is that the Center tests were conducted at speeds 3 to 4 times as great as the Leeds tests. It is possible, and there is some evidence, that the surface seal is proportionately stronger at higher speeds and larger sizes. Since the "strength" of the surface seal is due to its momentum, increased size and speed should result in greater resistance to disturbances.

Swales et al found that nose ventilation could be provoked by droplets of water falling from the top of the water channel, and Breslin and Skalak reported that a pencil point in the water ahead of their towed strut would provoke ventilation. However, Rothblum et al found that considerable effort was required with a 2 x 4 inch (nominal cross section) piece of lumber to artificially provoke ventilation in their experiments, and that with increasing speed it was nearly impossible. A recent series of experiments at the Center was performed, in which a steel rod was fixed vertically to the side of one of the struts tested earlier and protruding about 2 inches (50 mm) below the water surface – well into the vapour cavity, near the strut leading edge.[2.14] This was found to reduce the sideslip angle required for ventilation only by about 2 percent, over the speed range tested, from 14½ to 13½ percent at 35 kts (18 m/s) and from 10½ to 8½ percent at 45 kts (23 m/s). In fact, the rod itself ventilated at

Figure 2.3a – Taylor Instabilities Photographed in Leeds Free Surface
Water Channel at 10 ft/s (3 m/s), 100 mm chord model.
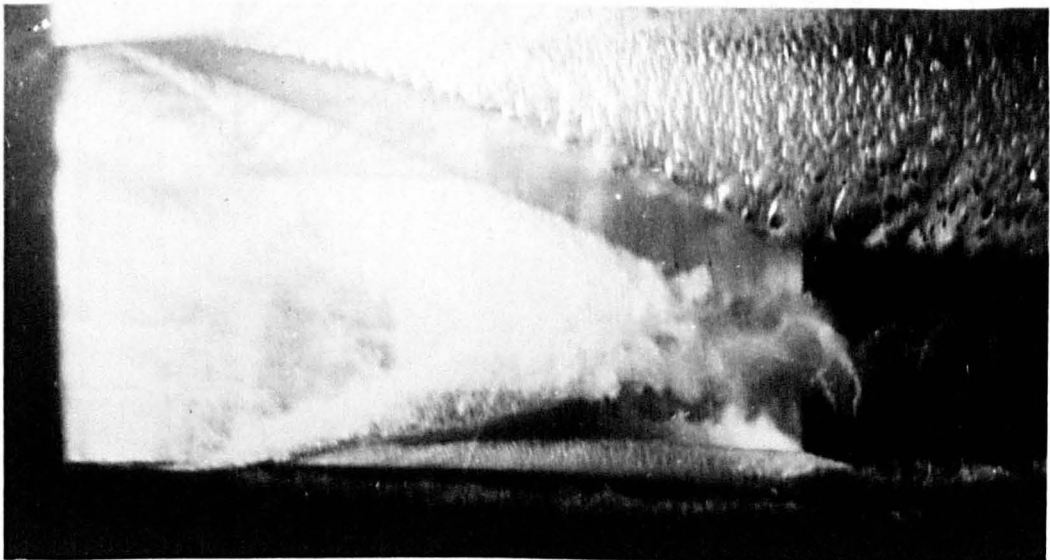
Figure 2.3b – Taylor Instabilities Photographed at the David W. Taylor Center
Towing Tank at 55 kts (28 m/s), 600 mm chord model.

RANDOM DISTURBANCES
(Nose Triggering Mechanism)

SURFACE SEAL OF
UNSEPARATED FLOW

MEAN WATER
LINE

COLLAPSED TAYLOR
INSTABILITIES

FLOW

SEPARATED FLOW OF LOW
NET MOMENTUM AND
PRESSURE (May be a Vapour
Cavity or Due to Wetted Nose
or Tail Separation)

TIP VORTEX
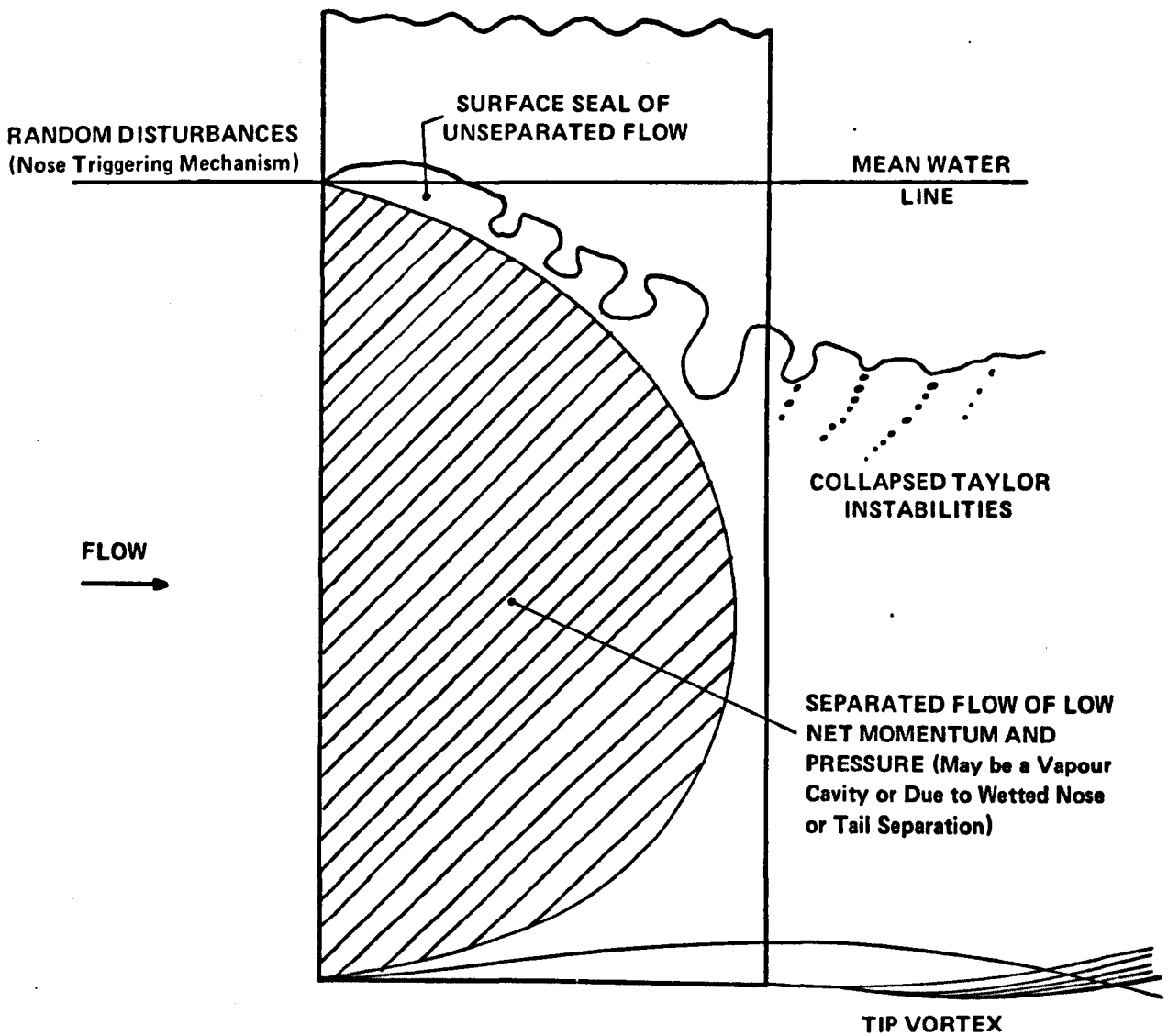
Figure 2.4 – Principal Features of Flow Immediately Before Ventilation Inception.

an early stage and formed a new free surface which was relatively unperturbed, and below which the vapour cavity formed on the strut.

Summary of Elements of Mechanism. The three elements of ventilation inception have been established as (shown schematically in Figure 2.4); (1) the existence of a region of low momentum and (2) low pressure, satisfied by ordinary wetted separation at less than ambient pressure, or vapour cavitation, and (3) the surface seal, a layer of unseparated flow isolating the atmosphere from the low pressure, low momentum region, including a mechanism for the breaching of the surface seal by the atmosphere.

Two important modes of disruption of the surface seal have been established – instability due to the downward acceleration of the surface seal associated with a relatively large region of tail separation or cavitation (tail ventilation), or breach of the surface seal at the nose of a surface piercing strut associated with leading edge cavitation or separation (nose ventilation). This nose separation or cavitation region may be of the order of 10 percent of chord, and the breaching is due to the encounter with an ambient disturbance.

Chapter 2 References

2.1   Hoerner, S.F., *"Some Characteristics of Spray and Ventilation,"* Gibbs and Cox Report 1351/S1/1,S1/10(1-1504), ONR Contract No. NONR -507(00), Sept 1953.

2.2   Wadlin, Kenneth L., *"Mechanics of Ventilation Inception,"* Second Symposium on Naval Hydrodynamics, Office of Naval Research, 1958.

2.3   Wetzel, Joseph M., *"Ventilation of Bodies Piercing a Free Surface,"* Second Symposium on Naval Hydrodynamics, Office of Naval Research, 1958.

2.4   Breslin, John P., and Skalak, Richard, *"Exploratory Study of Ventilated Flows about Yawed Surface-Piercing Struts,"* NASA MEMO 2-23-59W, April 1959.

2.5   Sottorf, *"Experimental Investigation of Hydrofoils,"* Inst. Seeflugwesen, Hamburg, ZWB Document FB 1319, 1940. (Note: This reference is as it appeared in Reference 2.1)

2.6   Kicenuik, Taras, *"A Preliminary Experimental Study of Vertical Hydrofoils of Low Aspect Ratio Piercing a Water Surface,"* Cal. Inst. Tech. Rept. E55.2, 1955.

2.7   Taylor, G.I., *"The Instability of Liquid Surfaces When Accelerated in a Direction Perpendicular to Their Planes.I.,"* Proc. Roy. Soc. Vol. A201, pp. 192-6, 1950.   .

2.8   Rothblum, Richard S., Mayer, Dennis A., and Wilburn, Gene M., *"Ventilation, Cavitation and Other Characteristics of High Speed Surface Piercing Struts,"* Naval Ship R&D Center Rept. No. 3023, 1969.

2.9   Coffee, Claude W., and McKann, Robert E., *"Hydrodynamic Drag of 12- and 21-Percent Thick Surface-Piercing Struts,"* NACA TN 3092, 1953.

2.10   Emmons, H.W., Chang, C.T., and Watson, B.D., *"Taylor Instability of Finite Surface Waves,"* Jour. Fluid Mech., Vol 7, Part 2, Feb 1960.

2.11   Waid, Robert L., *"Experimental Investigation of the Ventilation of Vertical Surface-Piercing Struts in the Presence of Cavitation,"* Lockheed Missiles & Space Company Rept. LMSC/DO19597, May 1968.

2.12   Swales, P.D., Wright, A.J., McGregor, R.C., and Rothblum, R.S., *"The Mechanism of Ventilation Inception on Surface Piercing Foils,"* Jour. Mech. Eng. Sci., Vol. 16, No. 1, 1974.

2.13   Swales, P.D., Wright, A.J., McGregor, R.C., and Cole, B.N., *"Separation and Ventilation Interaction Studies,"* Hovering Craft and Hydrofoil, Vol. 13, No. 3, pp. 8-12, 1973.   -

2.14   Rothblum, R.S., Dailey, N.L., and Pattison, J.H., *"Effect of a Protuberance and Aspect Ratio on the Inception of Ventilation on a Surface-Piercing Strut in Cavitating Flow,"* Naval Ship R&D Center Ship Performance Dept. Eval. Rept. 479 H 02, June 1972.

CHAPTER 5

GENERAL APPROACH TO
SURFACE SHIP CONTROL

CHAPTER 3

GENERAL APPROACH TO
SUPPRESSION/CONTROL

EARLY APPROACH TO SUPPRESSION/CONTROL

Von Schertel was the first to recognize and solve the problem of ventilation on surface piercing hydrofoils.[3.1] Exactly how this was accomplished is not part of published literature. However, from his statements, and from photographs of hydrofoil boats designed by his company, the basic techniques can be ascertained. Figure 3.1 is a schematic sketch of a generalised Schertel-Sachsenberg foil.

Taper. The most striking feature of the foils is that they are tapered in the opposite manner that one finds in aeroplane design. The V-shaped dihedral lifting foils are wider (greater chord) at the outside of the "V" than at the middle. This is not completely contrary to aeroplane design from a structural standpoint, since in the hydrofoil case the "wing" is supported at the tips of the "V" rather than at the center in aeroplane fashion.

Dihedral. In the Schertel system, the foils provide inherent stability of the craft. The dihedral angle is an important factor in roll stiffness and in efficiency. It will also be seen to be a factor in ventilation of V-foils.

"Baffles." Besides taper and dihedral, another feature of the Schertel foils is readily apparent – a series of thin plates, two to three times wider than the foil section thickness, arranged normal to the foil surface and parallel to the oncoming flow direction.

Camber. Not too surprisingly, the foils are cambered, as is usual in aircraft practice, but which has added significance in terms of ventilation prevention.

EXPLANATION OF VON SCHERTEL
SUPPRESSION/CONTROL TECHNIQUES

In view of the gross features of the mechanics of ventilation inception, these characteristics of the Schertel foils are readily understood, if not quantifiable. It is also instructive to note that nearly everything which is done to affect the ventilation characteristics of a craft must necessarily affect its performance in other areas – such as efficiency, stability, speed – but not necessarily adversely.

Features of Pre-Ventilation Flow. The three principal features of the flow around a surface piercing strut just prior to ventilation according to the ventilation mechanism presented in
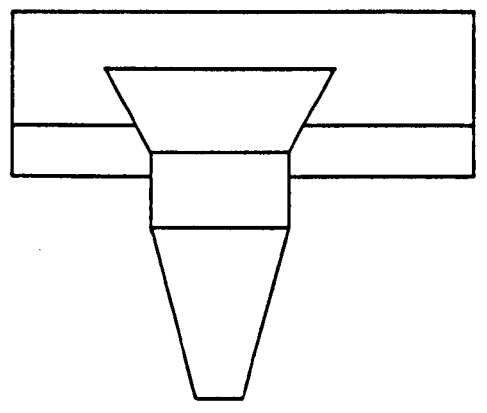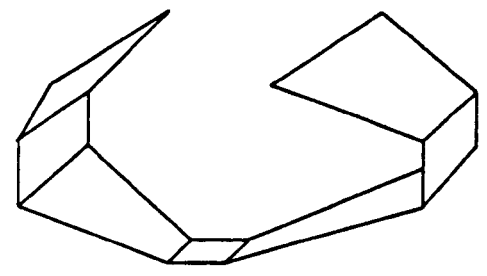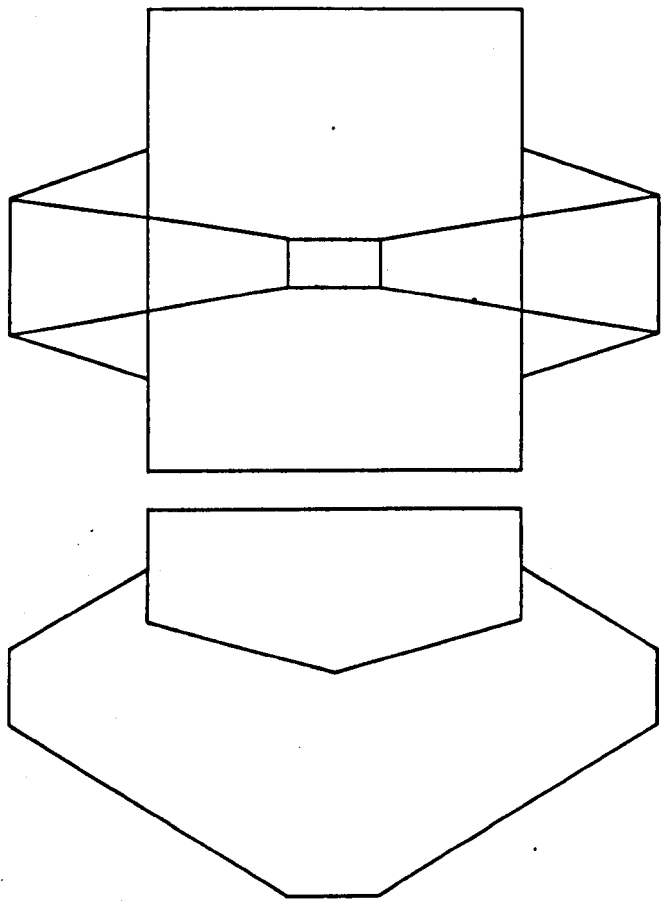
Figure 3.1 — Schertel-Sachsenberg Foil System, Based Primarily on Photographs and Drawings from Von Schertel[3.1].

Chapter 2 are:

1. Region of low momentum
2. Low pressure in the low momentum region
3. Surface seal

Principles of Suppression/Control. From these three features of the flow prior to ventilation can be deduced the means of prevention of ventilation. In general, the object is to reduce the separated region, decrease the (spanwise negative) pressure gradient near the surface, and stabilise or strengthen the surface seal. Of course, it is very easy to prescribe this solution if one fails to mention the details of execution. The complications which arise can be seen by considering Von Schertel's solution.

Explanation of Use of Taper and Camber in Schertel System. The tapered foils of Von Schertel can be seen as means to reduce the lift coefficient as the water surface is approached by changing section shape. By increasing foil chord, thus increasing the lifting area, the actual lift per unit span is kept high enough for good roll stability in spite of the decreasing lift coefficient. The reduced lift coefficient near the surface produces less of a spanwise pressure gradient, reducing the downward acceleration of the free surface and making it less susceptible to acceleration induced (Taylor) instabilities. The reduced lift coefficient requirements allow a foil cross section to be chosen with a higher minimum pressure coefficient, which makes cavitation near the water surface less likely. Because the minimum pressure coefficient does not have to be high, neither does the chordwise pressure gradient, which makes wetted separation less likely. The use of camber also allows a flatter pressure distribution and higher lift coefficients without approaching the stall regime with attendant separation. Under optimum foilborne conditions, only the smallest chord sections with the least dihedral will be submerged, due to the taper and dihedral change at the bottom of the "V". This section is the most efficient because of its high aspect ratio, low dihedral and presumably higher lift coefficient. Under less than optimum conditions, when the craft must ride lower in the water, or on takeoff, the maximum stability is achieved with the least tendency to ventilate.

Considerations in Use of Dihedral in Schertel System. As dihedral is decreased (90 degrees of dihedral is taken to be a vertical foil) the low pressure regions of a foil approach the surface more closely. Thus, if there are separated regions, ventilation is more likely to occur. From the model of ventilation of Chapter 2, it is not entirely obvious why, but the Sottorf data quoted by Hoerner[3.2] show that the maximum lift coefficient obtainable before ventilation

decreases with decreasing dihedral. This is probably the reason that hydrofoil designers have found that more dihedral is necessary for stability than is usual in aircraft design. Because part of the lifting surface of a hydrofoil emerges from the water during roll, the analogy with aircraft falters, as usual.

Role of "Baffles" or Fences on Schertel Foils. The thin plates used by Von Schertel on the low pressure face of the foils were referred to as "air baffles." Mostly they have been called ventilation or, misleadingly, cavitation fences. Although their function is fairly obvious, in terms of the model of ventilation, fences can be thought of as acting to supplement the surface seal. The fence guides the flow and tends to act as a physical barrier between air and regions of separation or cavitation. The action of fences is somewhat equivocal, however, as will be shown later.

EXTENSION OF SCHERTEL TECHNIQUES AND EXPLORATION OF POSSIBLE NEW METHODS

The methods employed by Von Schertel to avoid ventilation exemplify the present state of the art. Virtually no progress has been made beyond ad hoc treatment of the problems as they arise. Although some conclusions have been drawn on the basis of previous model scale studies in the laboratory, no practical applications have been made of them. This is possibly because there has been no verification of what factors in the laboratories correspond to full scale conditions. Also, the failure in the past to distinguish between the different modes of ventilation has led to apparently contradictory results. Enough progress has now been made, including the work presented here, that essentially all the observed phenomena can be explained, if not quantified.

By considering the model of ventilation presented in Chapter 2, possible new ways of avoiding, suppressing and controlling ventilation, and the extension of present ones, may be determined.

Elimination of Separation. The most elegant, and useful technique for promoting resistance to ventilation is to ensure that surface piercing elements, struts or foils, are free of separation (including cavitation) under design conditions. This solution may sound somewhat facile to the person who has actually dealt with the problem. The aeronautical engineer usually considers that he has no separation problem if his force coefficients are linear with angle of attack. However, ventilation has been shown to occur under laboratory conditions with less than 10 percent of the chord separated, and no evidence of separation ascertainable from the

39

force coefficients. Therefore, the absence of separation must be more strictly interpreted for hydrofoils. In spite of these reservations, designing to avoid, limit, or control separation (and cavitation) must be considered a primary method of avoiding ventilation.

Separation Control by Section Design. As far as is known, no wing sections have been designed especially for use by hydrofoils – yet all hydrofoils, with limited exceptions, use aerofoil sections for both struts and lifting elements. Generally, aerofoils are designed to give high lift. But because the loads on hydrofoils are so much higher than those on aerofoils, high lift coefficients create problems, not the least of which is a tendency towards vapour cavitation.

Special Case of Struts. Aerofoil struts are designed to give flat pressure distributions at zero attack angle. In fact, it is much easier to assure low attack angles on struts in aircraft applications. On a hydrofoil with a fully submerged foil system, the struts must provide the side forces required for lateral stability. For example, in a heavy beam wind, the craft assumes a sideslip angle and the hydrodynamic side forces developed on the vertical struts counter the aerodynamic forces.

"Coordinated" Turns. In a turn, if a hydrofoil could imitate an aeroplane and bank in such a way that the turn was "fully coordinated", then the sideslip angle experienced by vertical surfaces would be minimal. A fully coordinated turn implies that the angle of bank is sufficient for the centrifugal forces to be completely balanced by the reaction of the gravity forces and the wing lift, with no contribution from rudder or vertical stabiliser.

Limited Hydrofoil Bank Angle. On a hydrofoil, the bank angle is limited by the tendency of the submerged foils to breach. If the turn rate were limited to that which could be accommodated in the fully coordinated mode, its manoeuvrability might be unnecessarily restricted.

Reaction to Wave Motion. Aside from manoeuvring, there is no way lateral stability in a seaway can be provided by fully submerged horizontal lifting elements. The orbital motion of waves is a significant component of total velocity. The sea in general does not run in the direction of the craft course. This implies sideslip angles being developed on the vertical surface piercing struts with the attendant possibilities of separation and ventilation. Aerofoil struts were apparently not designed to cope with these factors, probably because they are not as significant to aeroplanes.

Aerofoil Section Design Techniques. Because aerofoils and struts are not generally designed for use as hydrofoils an obvious solution is to adapt the current techniques which have been developed by aeronautical scientists and apply these allowing for the special considerations demanded by the ocean environment. With this objective, the techniques presently being used for aerofoil design are reviewed in Chapter 7 with a view towards their applicability to hydrofoil design. These techniques include empirical methods as well as a description of a mathematical method of generating a practical two dimensional profile from a specified input pressure distribution. Just as aerofoil sections are not quite suitable for hydrofoil applications, so wholesale transfer of aerofoil design techniques to hydrofoil design cannot be made. The major considerations are the presence of the air-water interface (the free surface) and cavitation.

Empirical Corrections Required. A complete theory of three dimensional flow including viscous effects (separation) still eludes the aeronautical engineers. Therefore in the final stages, empirical methods must be applied. The important aspect of this process to the hydrofoil designer is that the empirical corrections reflect the special problems of waterborne operation.

Separation Control Using Passive Devices. Besides section design, there are a number of what could be called "gadgets" employed in aircraft and in fluid machinery for preventing separation. Generally, these take the form of turning vanes, turbulence stimulators and vorticity generators. The limited experimental evidence available, and what is known of the physics of ventilation inception, suggests that any beneficial effects of turbulence or vorticity stimulators would be counterbalanced by the adverse effect on the surface seal and cavitation properties. These solutions cannot be dismissed out of hand without a careful appraisal of individual cases. A tantalising prospect exists for combining the function of ventilation fences with some form of flow control. As presently applied, fences are probably detrimental to overall hydrofoil performance, except ventilation.

Control of Separation by Active Devices. Consideration of separation control by active devices may be divided into two categories: boundary layer control by suction or blowing, and control by leading or trailing edge flaps, which may or may not be slotted.

Boundary Layer Suction and Blowing. The prospects of using suction or blowing for boundary layer energisation to delay the onset of separation as a practical means of ventilation control on hydrofoil boats seems remote at the present time. This opinion is based not on a low estimation of the efficacy of these techniques, but on the observation that they have failed

thus far to gain acceptance in the aircraft field for production craft, civil or military, in spite of the principle being known since the 1930's. Obviously, the penalty associated with the weight and complexity of the necessary apparatus, plus the extra power requirements, make application of the principle unfeasible. There are indications that boundary layer control techniques will be applied to special cases in the fairly near future, such as helicopter blades, and short and vertical take-off craft.

Prospects for Blowing Applied to Hydrofoil Craft. It is possible that the hydrofoil craft will prove to be one of these special cases because of its requirement of high lift coefficients at low speeds for take off, and low lift coefficient at cruising for cavitation and ventilation suppression. Because of the proven feasibility and attractiveness of the water jet propulsion system and its selection for use in the NATO PHM, the prospects for the inclusion of a water blowing boundary layer control system may be enhanced. The supply of high momentum water could simply be bled from the propulsion system in a simpler manner than could be accomplished in the case of an aeroplane, because of the shorter distances involved for pipes and manifolds. The elimination of mechanical devices for lift control and rudder control could more than offset the additional apparatus needed for water blowing lift control and rudder. The possibilities seem attractive enough to warrant a careful investigation of the problems.

Prospects for Suction Applied to Hydrofoil Craft. The case for ventilation control by elimiating separation by suction seems considerably more tenuous. By its nature, a suction device would be more prone to cavitation problems. It is more susceptible to fouling. The maximum pressure difference attainable is the difference between the ambient pressure and the vapour pressure of water, therefore the control range is inherently limited.

Besides the practical considerations of ventilation suppression, the use of either suction or blowing to eliminate a region of separation is a useful device to study the properties of pre-ventilated flow. The results and a full discussion of an experiment performed utilising suction to eliminate a nose separation region are given in Chapter 8. As a practical means of ventilation suppression, the experiment confirmed that it is a very delicate procedure, likely to be upset by any of several factors commonly encountered in the ocean.

Elimination of Tail Separation by Blowing. An experiment to investigate the effects of the elimination of tail separation by blowing was performed and the results discussed in Chapter 9. For purposes of assessing the practical prospects of blowing for ventilation suppression, it may

be said that the known facts are promising, but the problem has many more aspects which must be investigated before an application to a full scale craft can be considered.

Leading and Trailing Edge Flaps and Slotted Flaps. The second category of "active" control of separation besides suction and blowing devices are flaps. The slotted flap in particular is analogous to boundary layer energisation techniques because it is a device to effectively reduce the influence of the boundary layer while still achieving high lift coefficients by re-directing the flow in much the same way as the blown foil. In fact, a slotted foil can be considered as several individual foils and flaps. The slotted flap is different only in that it needs no external supply of momentum or energy. In this sense flaps could be considered a passive flow control device, except that their geometry is generally variable in actual application, requiring in practice an external source of power. To consider flap actuation power may seem a trivial point, but, in fact, the hydraulic power consumed by the present craft using fully submerged systems with active feedback control is a significant proportion of total installed power.

Early attempts to use flaps for lift control on fully submerged systems have been abandoned in favour of total foil incidence control. The complexity and power requirements of flaps were found to be beyond the state of the art. There is no doubt that flapped systems will eventually find a use in hydrofoils as they have in aircraft, as hydrofoils advance from their primitive forms. A significant increase in cruising speed practically mandates the use of variable geometry foils, since for fixed geometry the takeoff speed effectively limits the top speed, much as for aircraft.

The advent of supercavitating or superventilating foil systems will undoubtedly depend on the use of variable geometry, with subcavitating configurations used for takeoff, changing to supercavitating for cruise or sprint.

Limiting Low Pressures. After the separated region, the next flow feature of a surface piercing element just prior to ventilation is a lower than atmospheric pressure in the separated region. The phenomenon of step-wise ventilation, observed by Swales et al,[3.3] and Waid[3.4] in tail ventilation, suggests a possible method of delaying ventilation inception. The explanation given for the steps in Chapter 2 on the mechanism, was that a Taylor instability collapsed into a vortex core which allowed atmospheric air into the separated low pressure region. The air continued to be sucked into the low pressure region until the elongation of the vortex core choked off the passage of air. The low pressure region was then fed by the next successive instability, which continued until a sufficient cavity had formed for massive entrainment of air to occur, when a full ventilated cavity would spring forth. Typically, before the series of

consecutive injections of air into the separated region resulting in transition to full ventilation would occur, so called "false strikes" would be observed. The false strikes consisted of a single instability in a train of instabilities allowing air into the separated region, but which was not followed by successive strikes. A review of the cine photographs of this effect showed that after a false strike, air would enter the separated region, and the free water surface could be seen to spring upwards. Succeeding instabilities would then be out of reach of the separated region. This can be understood in terms of the mechanism of tail ventilation and amplification of instabilities. The air injected by the false strike, or initial instability, into the separated, low pressure region would immediately expand, raising the pressure of the separated region and causing the water surface to fail to be accelerated downward as much, making it appear to spring upwards to an observer stationary at the strut. According to Taylor,[3.5] the amplification of instabilities in an accelerating surface increases with increasing acceleration. Two effects were therefore incurred by the ingestion of air: the water surface sprang away from the separated region, and the Taylor instabilities were not amplified as much. Therefore an initial strike of air into the separated region had the effect of isolating the instabilities from the region thereby preventing or delaying further strikes.

"Bleeding" air into the suction side of a submerged hydrofoil is now an established technique of decreasing the lift coefficient. The phenomenon of false strikes suggests that it might also be used in ventilation suppression. Because air bleed generally involves a decrease of lift coefficient, the usefulness of this technique for ventilation suppression would be limited, since in most cases, it is the lift coefficient which is the important ventilation boundary. However, there are cases where this is not so.

Air Bleed Experiment. Impromptu experiments with air injection to suppress ventilation using the water blowing or suction apparatus indicated that the air would have to be extremely finely controlled if it were not to have the opposite effect intended. Generally, air bubbles of all but the finest seemed to have an adverse effect on the sideslip angle which could be maintained without ventilation. Therefore, while it cannot be rejected out of hand as a means of ventilation suppression, air bleed is not a particularly promising approach. Perhaps where it could be combined with lift control, as in a surface piercing rudder, an investigation might reveal a fruitful application.

Stabilising and Strengthening the Surface Seal. The surface seal is the last flow element characterising the pre-ventilated state to be considered from a standpoint of ventilation suppression.

Fences. As mentioned in the discussion of Von Schertel's approach, the category of strengthening and stabilising the surface seal includes the use of fences. The oldest, most obvious and, one is tempted to think, most ham-fisted approach to ventilation control is the interposition of a solid barrier between the submerged lifting element and the atmosphere. The "cavitation plate" above the propellers of outboard motors is probably an early example of the technique.

In spite of their antiquity and widespread application, no systematic laboratory investigation has been made of the optimum application of fences up to the present study, described in Chapter 10. One of the most surprising conclusions drawn from this study is that fences usually affect tail ventilation adversely. This, coupled with the finding that relatively tiny fences on the first 25 percent of chord sufficed to prevent nose ventilation, and the fact that hydrofoil designers have found by trial and error that nose fences will usually do as well as full chord fences, implies that tail ventilation is usually not a problem on full scale hydrofoils. Tail ventilation is the most commonly observed mode of ventilation in the laboratory, however. Part of this enigma was resolved in a series of experiments described in Chapters 5 and 6 designed to answer just this question – how model scale tests and the mechanism of ventilation postulated relate to full scale speeds and sizes. It was found that with increasing speed, the point of inception tended to move forward. Also, ventilation occurred at lower sideslip angles, implying that at the highest speeds, the sideslip angle would be so low that tail separation might be unlikely.

In terms of suppression of ventilation, further investigation into fences would undoubtedly be the most fertile and rewarding area for the least effort. Even after the possibilities of optimising fences for their present use have been exhausted the prospects remain of using fences for dual purposes such as separation control, spray control, drag reduction and lift enhancement.

"Liquid" Fences. The study of solid fences suggested that a dynamic liquid fence might be a feasible method of ventilation suppression that could have advantages under certain circumstances. Particularly, the result that large full chord solid fences usually had an adverse effect on ventilation characteristics and on drag suggested that a liquid fence that would naturally conform to flow lines might preserve the effectiveness without the detrimental aspects. The experiments using boundary layer suction and blowing near the free surface could also be considered liquid fence techniques, but here the name will be reserved for the use of a liquid sheet ejected roughly horizontally near the free surface around the low pressure side of a strut

with a sideslip angle. The results of an experiment performed with this configuration, presented in Chapter 10, were somewhat promising. Any eventual practical application would depend upon how badly the designer wished to avoid solid fences – for example, on a strut designed to retract inside a hull.

Controlled, Stable, Ventilated Cavities. A survey of ventilation suppression techniques would not be complete if it did not touch on the concept of avoiding the instabilities inherent in the transition from ventilating to ordinary flow by ensuring at an early stage that the flow regime was firmly in the ventilated state. The problems of this technique are much the same as the problems of maintaining a strictly non-ventilated flow, except that the critical speeds are at the low end of the operating range instead of the highest. In addition to the problems of maintaining a stable ventilated cavity, the force coefficients achievable in the ventilated state are much smaller than those obtained in fully wetted flow, and the lift to drag ratios are much less favourable. In certain regimes, the rate of air entrainment from the cavity to the water can be so high as to create a further type of instability, as when the dynamic pressure of the air flow becomes great enough to influence the cavity dimensions.

SUMMARY OF APPROACHES TO SUPPRESSION

It is possible to explain the efficacy of the current approach to suppression of ventilation, exemplified by Von Schertel's system, by examining the geometric properties of the foils in terms of their influence on the known features of the flow prior to ventilation, as follows:

    (1)   Elimination of separation by the use of camber

    (2)   Reduction of the pressure gradient (raising the pressure in the low pressure region) by the use of taper and varying section shape

    (3)   Reinforcement of the surface seal by the use of fences

Other techniques which might in the future be used for ventilation suppression can be evaluated for effectiveness and practicality in terms of the same three flow features; separation, low pressure and the surface seal.

Separated Region. For eliminating separation, passive means may be used, such as section shape and camber, possibly relying on recently developed aeronautical techniques. Other passive methods borrowed from aeronautics may include the use of devices, such as turbulence stimulators. The use of these may be limited by the problem of cavitation. Flaps and other variable geometries are "semi-active" devices that have been found useful in aircraft design,

and are potentially useful for hydrofoils, but have been found in the past to entail excessive complications and power consumption. Avoidance of separation by active means such as boundary layer suction and blowing are probably far in the future as practical ventilation suppression devices, if aircraft history may be used as a guide, but experiments presented here using these techniques revealed a considerable amount of information about the properties of the flow preceding ventilation. Boundary layer blowing was shown to warrant further investigation as a practical preventive device, particularly if it could be used in conjunction with some other applications of boundary layer control, such as lift control, propulsion, or possibly cavitation suppression.

Low Pressure. In addition to the use of section design, taper, and camber for reduction of the (absolute value of) low pressures in the separated region, air bleed was briefly considered. Preliminary experiments show that this would be a delicate procedure. But, should it prove feasible it would be attractive if combined with a lift control function in, for example, a surface piercing air-controlled rudder.

Surface Seal. The area of investigation with the greatest promise of reward for ventilation suppression is the surface seal, particularly mechanical (solid) fences. Besides the refinement of these devices to their minimum size or drag, they could be designed to enhance lift, reduce drag, control spray or otherwise direct flow. As part of this study, and in conjunction with a study of solid fences, a liquid fence was investigated, which might possibly be useful under special circumstances where a solid fence would interfere with the functioning of some other aspect of the boat, such as retractability of foils or struts.

RESERVATIONS ABOUT THE APPLICABILITY
OF LABORATORY TECHNIQUES TO FULL SCALE CRAFT

The model of ventilation developed was completely based on laboratory experiments. It is true that the known successful techniques of ventilation suppression can be explained in terms of this model, but there is no direct evidence of the extent to which the individual features of the model retain their relative importance at full scale speeds and sizes. Certain observations have been made of ventilation on full scale craft which have no correspondence with observed small scale behaviour. To overcome some of these reservations, and to provide more insight into the mechanism, a series of experiments was performed concerning the effects of increased speed, roughness, and wettability on laboratory scale models. These are described in succesive chapters.

Chapter 3 References

3.1 Von Schertel, Hanns, *"Hydrofoil History,"* Hovering Craft & Hydrofoils, Vol. 13, No. 7, April 1974.

3.2 Hoerner, S.F., *"Some Characteristics of Spray and Ventilation,"* Gibbs and Cox Report 1351/S1/1, S1/10(1-1504), ONR Contract No. NONR-507(00), Sept 1974.

3.3 Swales, P.D., Wright, A.J., McGregor, R.C., and Rothblum, R.S., *"The Mechanism of Ventilation Inception on Surface Piercing Foils,"* Jour. Mech. Eng. Sci., Vol. 16, No. 1, 1974.

3.4 Waid, Robert L., *"Experimental Investigation of the Ventilation of Surface Piercing Struts in the Presence of Cavitation,"* Lockheed Missiles & Space Co. Rept. LMSC/DO19597, May 1968.

3.5 Taylor, G.I., *"The Instability of Liquid Surfaces when Accelerated in a Direction Perpendicular to their Planes.I.,"* Proc. Roy. Soc. Vol. A201, pp. 192-6, 1950.

CHAPTER 4

SCALING

At the Second Office of Naval Research Symposium on Naval Hydrodynamics in 1958, many people who had been instrumental in hydrofoil ventilation studies contributed to the discussion of the papers given by Wadlin[4.1] and Wetzel.[4.2] One of the few there who had actual experience with hydrofoils outside of the laboratory was Mike Eames of the Canadian Naval Research Establishment. In discussing the paper by Wadlin, "Mechanics of Ventilation Inception", in which the concept of the unseparated layer of flow near the water free surface which isolates the separated region on a yawed surface piercing strut from the atmosphere is presented, Eames made the following statement:[4.3]

> ...Experience in the full-scale operation of hydrofoil craft suggests that
> significant retardation of ventilation by the influence of the constant-
> pressure water surface can only be obtained under laboratory conditions.
> In open water even the smallest ripples appear to be sufficient to initiate
> ventilation at the water surface. This of course is an advantage to full-
> scale operation since ventilation proceeds smoothly as speed is increased.
> The explosive type of phenomenon which results when large negative
> pressures are supported in calm water and subsequently tripped by a
> small disturbance could represent a very dangerous situation for a
> hydrofoil craft...

In the same discussion, Breslin[4.4] suggested that the path of the air to the separated low-pressure region consisted of vortex cores in the wake of the strut, as he had earlier in his Stevens Institute of Technology report.[4.5] Probably with this in mind, Eames continued in his statement:

> ...In an "ad hoc" search for the smallest effective fence we have found
> that on a particular section designed for uniform pressure distribution it
> is only necessary to extend the fence over the leading 50 percent of the
> chord...I would have expected most of the low energy paths to exist
> behind this, and therefore the success of the half-fences surprises me...

Besides illustrating the fact that the significance of the consequences of ventilation are generally underestimated by hydrofoil designers, Eames implicitly raised three questions of the utmost importance to the correct interpretation of laboratory studies for application to full scale.

These questions cannot be unequivocally answered at present, and the purpose of the investigation described in this Part is largely directed towards clarifying the answers. Specifically, the questions raised by full scale experience with ventilation are:

1. Does the surface seal degenerate at full scale speeds and sizes, so that the only effect of the preventilation flow model developed in Chapter 2 is from the separated region and low pressure? And if this is so, are discussions of Taylor instabilities and ambient disturbances irrelevant?

2. What are the characteristics of the open water environment and their effect on the proposed mechanism of ventilation?

3. Since the vast majority of the observations of the mode of ventilation in the laboratory have been of the tail mode, in which air ingress takes place largely in the wake region, and the nose ventilation mode is principally associated with laminar separation at the nose, what is the explanation for the success of partial, nose-only ventilation fences? And what are the implications for the model of ventilation?

The well documented[4,6] experience of the PCH-1 with its uncontrollable yaw rates in rough water, and the many other identifiable problems now associated with ventilation have disposed of the unjustified optimism which led to the belief that the dire consequences intimated by model tests would not be realised under full scale conditions. The implication is that the surface seal still plays an active role in the prototype phenomenon, since the gradual onset of ventilation suggested by Eames would not explain the behaviours observed. But before attempting a detailed answer to the questions raised of the influence of prototype conditions on the mechanics of ventilation, the evidence of the observed differences between ventilation as it occurs on prototypes as compared to model studies should be examined. The word "evidence" is used loosely, because prototype observations are scanty and ill-documented as well as difficult to make.

OBSERVED DIFFERENCES BETWEEN MODEL AND PROTOTYPE

Smaller Sideslip Angles Implied in Prototype. The most distinctive feature of prototype ventilation as observed on craft with fully submerged systems is that it probably occurs at sideslip angles much smaller than those observed on models in the laboratory. The qualification "probably" is required, because there is no satisfactory way to measure local sideslip seen by a strut on a full scale vessel at sea. Generally, the behaviour attributed to the effects of ventilation on struts is inferred from tests in relatively calm water, in which the reaction

51

of the craft to the onset of flow anomalies manifested by observable changes in the flow pattern, particularly the spray sheets, is recorded. By tracking the course of the boat, measuring accelerations in strategic places, and making simultaneous cine films of the flow around the struts, the flow anomalies are correlated with craft behaviour. The sideslip angles are calculated based on mathematical models of the craft behaviour. Of course, the mathematical model makes use of assumptions about the forces generated on the struts as a function of sideslip angle. These forces functions are in turn dependent upon the flow state – whether ventilated, cavitated or separated. Therefore the quantity to be determined must be used as an input. If the course is also recorded, as was done in certain of the PCH-1 trials, then the data and theory can at least be made self-consistent. Base lines may also be established by running in circles in fairly constant conditions, providing another self consistent point of reference. Discussions with designers familar with the results of tests like these indicate that the sideslip angles expected are of the order of 2 to 3 degrees. This will vary depending on the conditions. In calm water, considering only fully coordinated turns, the sideslip angles are probably half or less than the amounts indicated. Even allowing for a generous margin of error in the estimation of full scale sideslip angles, (some people would concede up to 6 degrees of sideslip) the ventilation angles observed under laboratory conditions are largely outside the range of those apparently occurring naturally. Rothblum et al[4.7] observed ventilation at angles of about 6 degrees on surface piercing struts tested at full scale speeds of 55 knots in the Taylor Center towing tank in calm water. The only other data obtained besides the present study, which demonstrated angles this low were these of Wetzel[4.2] and Kramer,[4.8] obtained in rough water and waves, respectively, at much lower speeds. Chapter 5 describes an experiment with roughnesses applied to a model in which ventilation angles were reduced to 4 and 5 degrees.

Foils vs. Struts. The case of surface piercing foils (as opposed to struts) is being excluded from this discussion, as it has been from the great majority of experimental work. Moreover, full scale data concerning surface piercing foils does not seem to be available at all. The fundamental difference between foils and struts, besides dihedral angle, is that foils are allowed to assume asymmetric shapes. The conclusions reached for struts may be extended, by and large, to foils which are not too close to the horizontal (large dihedral). The angle of attack deviation from design conditions is roughly comparable to sideslip angle. In many ways, the designer has more flexibility with foils than with struts. Struts are by definition symmetric and uncambered, and are liable to sideslip angles of either sign. The foil designer can generally count on positive attack angles and he is free to use camber and asymmetrical section shapes to achieve his desired pressure distribution.

Visual Appearance. To establish the flow anomalies observed on full scale craft as being the manifestation of ventilation on the struts is not trivial. The existence of a fully ventilated cavity on a surface piercing strut on a full scale boat has never been reported. The films of ventilation on a hydrofoil strut in open water available to the author have shown partial cavities in a very unstable state, generally not as is observed under laboratory conditions. The laboratory test which reproduced behaviour most similar to that reported in full scale tests was the model test at cavitating speeds with roughness applied to a surface piercing strut in rather turbulent flow, presented in Chapter 5.

Cine films of ventilation taken on full scale craft must necessarily be shot through the water surface if the camera is carried aboard the craft. Even the calmest open water surface is less than ideal for looking through. Therefore details of underwater occurrences are difficult to observe. Ventilation is usually easiest identified under these circumstances by the characteristic change in the spray pattern. This has led to the identification of a phenomenon called water line ventilation, in which the spray pattern at the water surface is observed to change to that associated with ventilation, and the typical behaviour of the craft is observed simultaneously, but there is no evidence of an underwater cavity. The nearest analogy to this phenomenon observed in laboratory experiments was in the present work on solid and liquid fences. For fences of either sort, ventilation down to the barrier occurred at rather low angles, of about 4 degrees. While the cavity thus formed was extremely shallow, the spray pattern was still markedly different from ordinary flow.

Difference in Forces Experienced by Model and Prototype. Eames' speculation[4.1] that the large changes in forces implied by the retardation of ventilation inception due to the effect of the surface seal would not be experienced under full scale conditions was not entirely wrong. It is true that we would not expect, based on the full scale evidence available, that the large sideslip angles achieved in the laboratory prior to ventilation could be sustained under prototype conditions. However, in the laboratory, at the largest angles attained before ventilation, separation or cavitation are so extensive that the force coefficients had long started to flatten or tail off at much lesser angles (Figure 4.1). That is, the force coefficients had reached a maximum at a particular angle due to the influence of the separated or cavitated region associated with the flow prior to ventilation. The fact that the occurrence of ventilation was delayed until a rather greater angle did not mean that the forces on the strut fell from a higher point than would have been the case had ventilation occurred at the lower angle. The reverse effect is in fact achieved. Breslin noted that the post-ventilation force coefficients behave as though a sudden change in camber had occurred upon ventilation.

The new force coefficients, plotted as function of sideslip angle were roughly parallel and below the fully wetted values (Figure 4.2). Of course, the ventilated coefficients do not show the dropoff with angle due to separation or cavitation reflected in the fully wetted, or nominally fully wetted, coefficients. Therefore, the delaying of ventilation to higher angles beyond the point where the pre-ventilation coefficients started to fall off actually had the effect of bringing the two force curves closer together, thereby decreasing the total change which would have been observed had ventilation occurred at a lower angle (Figure 4.3).

Because of the camber analogy to post-ventilated forces, Breslin foresaw, although he did not actually measure, changes in sign of forces if ventilation took place at a sufficiently low angle. In fact, from the same argument, it is easy to see that the lower the angle at which ventilation takes place, the greater will be the force reversal in terms of the magnitude of the pre-ventilation forces. Rothblum et al[4.7] measured force reversals of 200 percent.

The constant camber change interpretation of post-ventilated forces obviously breaks down at some point, as the sideslip angle approaches zero. One would not expect ventilation occurring at zero sideslip angle to produce a force of very great magnitude, whether in the ventilated or non-ventilated states. Ventilated cavities have been observed in the laboratory to persist through a change in sign of sideslip angle,[4.7] so the occurrence of ventilation at zero sideslip angle cannot be ruled out. The persistence of ventilation through zero sideslip to negative angles was regularly observed in the present experiments with roughened struts. However, these were inevitably partial cavities by the time the sideslip angle had approached zero. Apparently, the physical process that "saves" hydrofoil craft from experiencing the drastic forces reversals that might be anticipated from model tests is the tendency of partial ventilation to occur at the low angles. Unfortunately, the situation is not quite as happy as it might have been had the prediction been correct of a gradual change to the ventilated state in the complete absence of the retarding effect of the surface seal.

An interesting aspect of the forces associated with partial ventilation is revealed in the work of Rothblum et al[4.9] on the effect of a protuberance on the ventilation and force characteristics of a surface piercing strut. As mentioned previously, this test consisted of attaching a vertical piece of cylindrical rod near the leading edge of the strut, and measuring the forces and ventilation angles as a function of the distance aft of the leading edge that the rod was placed. When the rod was at or within 10 percent of chord of the leading edge, the rod itself would ventilate to the submerged tip of the rod, which was designed to be less than 10 percent of the total strut submergence below the previously unperturbed surface existing at the same speed. In spite of the shallowness of the artificially created waterline
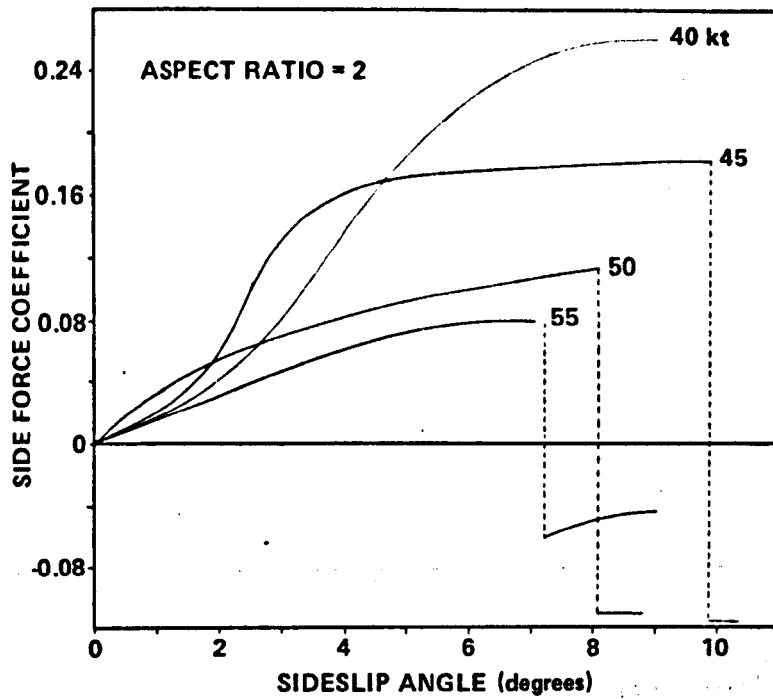
Figure 4.1 — Falloff of Sideforce Coefficient Prior to Ventilation, from Rothblum and Mayer[4.7].
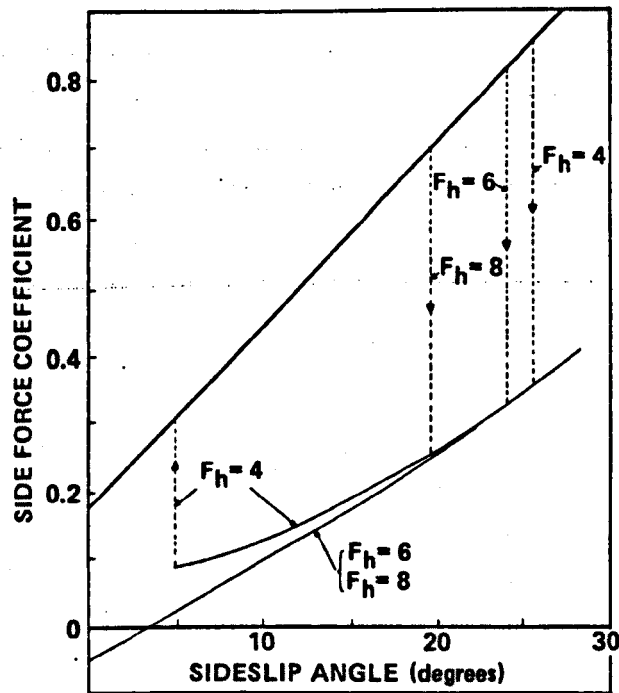
NACA 4412 STRUT: 3.0 inch (76 mm) CHORD

Figure 4.2 — Effective Camber Change Due to Ventilation, from Breslin and Skalak[4.5].

55

cavity (less than 10 percent of total submergence) the effect on the side forces was remark-able (Figure 4.4). At 5 degrees, to cite the worst case, the rod attached to the leading edge reduced the side force coefficient from 0.12 to 0.02, a change of more than 60 percent, corresponding to a cavity covering a nominal 10 percent of submerged area. Furthermore, analogous to full ventilation, the change in force coefficient seemed to correspond more to a change in camber than to a simple spoiling of lift, as is the case in aerofoil stall. The slope of the side force coefficient versus sideslip angle was virtually unchanged except for a displacement downward. Unfortunately, the range of sideslip angles was not extended to negative values, so it was not possible to determine whether the effective change in camber extended over the entire range of angles available before full ventilation inception. This experiment was performed using a strut of nearly full scale size (two foot chord (0.61 m)) and at speeds up to 50 knots (26 m/s), so the results were nearly directly comparable to prototype hydrofoil boats. This phenomenon provides ample corroboration of the association of steering anomalies on PCH-1 with the appearance of water line ventilation.

Difference in Ambient Conditions Between Model and Prototype. The character of the oncoming flow seen by a strut is probably the most important difference between conditions attainable in the laboratory and the ocean. The effect of waves and background turbulence is also the most difficult to assess on the basis of theoretical considerations without actual observations to provide a baseline. Full scale observations are difficult to make under the best of conditions, as described previously. In bad weather it is nearly impossible to accurately correlate flow conditions with craft behaviour. One thing certain is that rough water has an immensely adverse effect on the tendency of struts and foils to ventilate. It is puzzling in some respects as to why this is so. The available experimental evidence is somewhat contra-dictory, in much the same way, perhaps, that the calm water experiments were apparently contradictory until the concepts of nose and tail ventilation were sorted out. Work at the Taylor Center at high speeds showed that waves had little effect on ventilation inception boundaries (speed and angle). The investigation (unpublished) was conducted only in head seas, but included breaking waves as well as regular waves. Kramer,[4.8] at Lockheed, who tested the same models at lower speeds in waves and reduced pressures to obtain the same values of the cavitation scaling parameter, found vastly reduced sideslip angles compared to the calm water tests under similar conditions, and a tremendous amount of scatter of the boundary points. Kramer investigated both head and following seas, and suggested that ventilation was likely to occur in crests in head seas and in troughs in following seas. From this observation, he attempted to reduce the scatter of his data by correcting the inception cavitation parameter
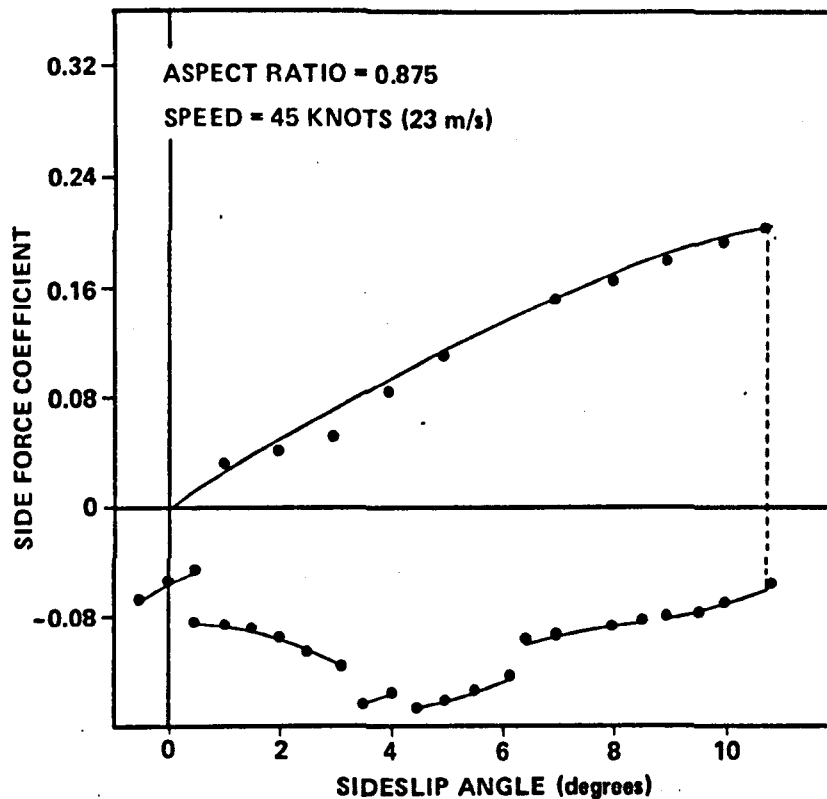
Figure 4.3 – Side Force Coefficient vs Sideslip Angle for Taylor Center Model 4, Ventilated and Non-Ventilated. From Rothblum, Mayer and Wilburn[4.7].
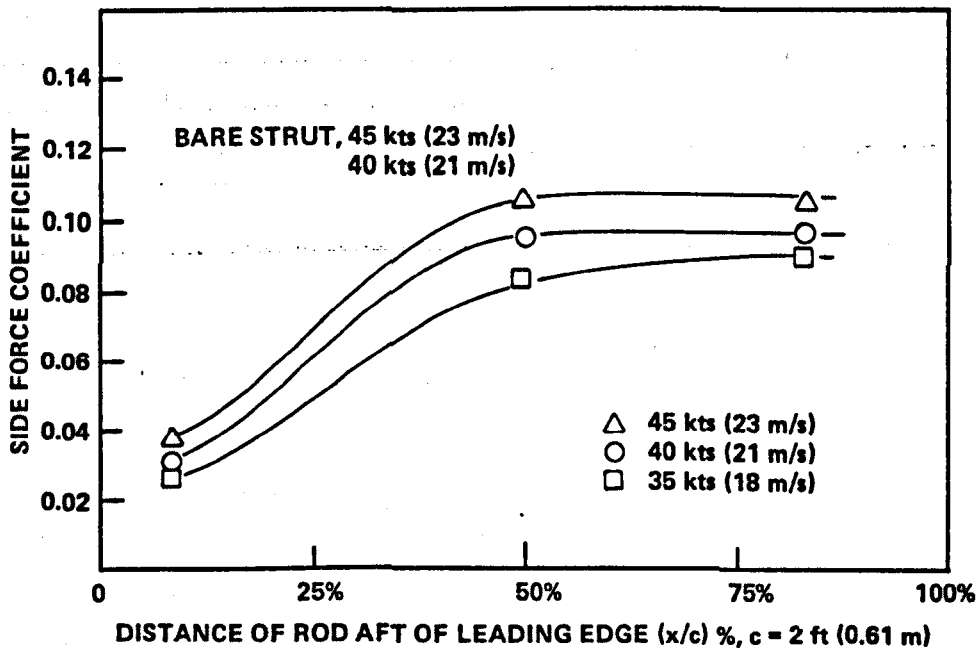
Figure 4.4 – Effect of Chordwise Position of Protuberance on Sideforce Coefficient at a Constant Angle of 5 degrees. From Rothblum, Dailey and Pattison[4.10].

57

for the orbital velocity of the waves. He was able to collapse his data somewhat, but the results were insignificant compared to the total scatter.

McGregor et al,[4.10] in tests conducted in the Mathematics Department of the University of Leeds in atmospheric conditions at comparitively low speeds, reported that inception took place predominately at wave crests in both head and following seas. By adding the effect of the acceleration of the water surface around the struts to the acceleration under calm conditions, he was able to obtain an empirical correlation between calm water and wave inception boundaries for limited circumstances. Swales et al[4.11] were able to include some representative points of the McGregor et al experiment in a different empirical correlation of calm water ventilation boundaries with considerable success, which will be discussed later in this chapter in relation to scaling laws.

Difference in Surface Finish Between Model and Prototype. Model construction methods and the highly polished finish of most models used in hydrodynamic testing bear little relationship to the finished product of shipyards. Many examples of the deleterious effects of weld beads, seams and cavities have been discovered. The ability to specify the maximum allowable roughness and waviness which can be tolerated without adversely affecting performance is of prime economic importance. Yet, up to the present work, there has been no study of the effect of roughnesses on ventilation. We still have no quantitative criterion that could be used by a shipyard, but at least some understanding of the effect of roughness on ventilation has been gained, as well as a deeper understanding of the mechanism of ventilation, which was the prime motivation of the study.

Different Effect of Fences in Model and Prototype. The third anomalous effect noted by Eames in comparing model results with prototype experience was the success of leading edge fences on full scale craft, while the results of model studies would seem to indicate that the low energy paths for air ingress to the low pressure separated region would be nearer the after part of the strut, if not in the wake. Part of this apparent anomaly was explained by Swales et al, when they identified the phenomenon of nose ventilation.[4.12] In nose ventilation, the air path is at the leading edge of a strut, and enters a separated region or vapourous cavity in the same vicinity. Typically, nose ventilation occurred at smaller sideslip angles than tail ventilation, so if nose ventilation were the predominate mode of full scale ventilation, it would explain both the experience of ventilation at lower angles under full scale conditions as well as the success of nose fences. However, there were still some disturbing features of full scale ventilation that were difficult to reconcile with the picture of nose ventilation being the

predominant mode. Firstly, nose separation is generally associated with small sizes and low speeds (low Reynolds numbers) and is explainable in most cases, except where the nose radius is exceptionally small, by the phenomenon of laminar separation, transition to turbulent flow, and reattachment. Therefore, in most full scale situations, nose separation would not be expected to occur. The second possible objection is not nearly so strong. It is that nose cavitation is not likely to be present under all the conditions where ventilation has been observed, nor was nose cavitation observed in cine films of full scale ventilation on the PCH-1. Cavitation at the strut-foil intersection was present, however.

A further mystery is posed by the observation in the Leeds tests[4.13] of fences that full chord fences actually aggravate the tendency towards tail ventilation in the model case, while doing no more to prevent nose ventilation than a 25 percent of chord nose fence of minimal horizontal width. Generally, although nose fences are found to be as effective as full fences in the prototype hydrofoils, conservative designers use full chord fences anyway. Apparently this does not provoke the deterioration in effectiveness predicted from the model studies. The reason for this may be indicated by the results of the investigation into the effect of higher speeds on the elements of the model of ventilation presented here in Chapter 6. Specifically, at low speeds, inception was predominately at the tail, until the speeds became high enough for nose cavitation to appear, at which time the mode of inception could be either nose or tail, with the appearance of a hitherto unobserved coupled nose and tail mode.

With still increasing speed, the nose initiated mode disappeared, but the air paths associated with the tail mode moved forward. The most likely explanation for the success of nose fences and the absence of failure of full chord fences would seem to be that under prototype conditions, the air paths for both the nose and tail mode move forward. Although there is yet no experimental evidence for this, the implication also is that the previous air paths further aft somehow cease to exist at the higher speeds. A possible explanation is the elongation of the vertical paths in the wake observed by Swales et al,[4.11] which choked off the air being supplied to the separated tail regions in the phenomenon of false strikes discussed earlier. With increasing speed, the elongation would take place more quickly, allowing proportionately less air to pass before being choked off. Since the pressure difference between the atmosphere and the low pressure separated region is limited by vapour cavitation, the speeding up of the process of elongation could not be compensated by the higher pressure gradient ordinarily associated with faster flow.

Implication of Observed Differences Between Model and Prototype. Because of the paucity of full scale observations, it would be a fairly safe conclusion that not all the possible

differences between model tests and prototypes have been discovered. Furthermore, it is not likely that they will be in the foreseeable future – assuming that the experimental techniques and resources available for the study of this problem do not undergo any substantial improvement.

Besides the obvious differences made by waves in a seaway, there are many other characteristics of the open ocean which could conceivably affect ventilation on surface piercing struts and foils. Background turbulence has been mentioned, and this factor is already suspected of being responsible, along with differing surface disturbances, for the disparity in results obtained between towing tanks and among water channels.[4.14] Also to be considered are wind driven surface currents, which can be as high as eight to nine knots and strongly varying with depth in the first twenty feet or so closest to the ocean surface. In bad weather, large amounts of air can be entrained in the water near the surface. Typically, besides air entrained in the gaseous state, the water near the ocean surface is supersaturated with dissolved air. Capillary waves as well as gravity waves may influence ventilation.[4.10] Theoretically, since cavitation can supply the requisite low pressure separated region condition preceding ventilation, anything which influences cavitation inception could be considered to have an effect on ventilation. This would include such things as temperature, dissolved air content and gaseous air content (which have already been mentioned as possibly affecting ventilation directly), the existence of solid nuclei, atmospheric pressure, salinity and a host of other factors.[4.15] Because of the near impossibility of sorting these factors out in experiments performed at sea, the only rational approach is to conduct model tests which vary possibly important parameters in the direction of the full scale values.

Since in general the actual full scale values of most parameters cannot be attained in the laboratory, it is necessary to refine the picture of the mechanics of ventilation to the greatest extent possible to permit the maximum extrapolation of the laboratory results. The remainder of this chapter will be devoted to examining the basic elements of the mechanism of ventilation (developed in Chapter 2) with regard to the effect and influence of prototype conditions. The results of the roughness, high speed and wettability experiments presented in the following two chapters will also be utilised in this context.

EFFECT OF SIZE AND SPEED ON SURFACE SEAL

The unseparated region at the water surface which separates the atmosphere from the low pressure separated region, the surface seal, is difficult to study in the laboratory. In general, the only portion that can be studied is the part actually touching the strut, which can be

observed by its effect on an oil film spread over the strut. Because it can only be observed as a two dimensional phenomenon, there is a tendency to think of it in those terms. In fact, it seems reasonable that the most important phases of the phenomenon of breakdown may properly be considered as two dimensional. If a slice of the flow just next to the strut is considered to represent a plane, ignoring the contours of the strut, then certain conclusions may be drawn about the effect of greater speed and size on the surface seal (Figure 4.5).

Important Properties of the Surface Seal. The function of the surface seal is separation of the atmosphere from the low pressure separated region. It accomplishes this by virtue of its momentum, and its final failure to maintain the separation results from its disintegration due to acceleration instabilities or encountering a discontinuity already present in the flow.

Taylor Instabilities. From ideal flow considerations, G.I. Taylor[4.16] calculated that the amplification factor by which small disturbances in an interface between two fluids of different densities which being accelerated in the direction of the more dense one were multiplied was given by

$$\frac{\eta}{\eta_0} = \cosh \left[\left\{ -\frac{2\pi}{\lambda} (g_1 - g) \right\}^{1/2} t \right] \tag{1}$$

where η = the height above the mean surface of the denser fluid

η_0 = the surface at $t = 0$ (initial disturbance)

λ = the wavelength of the initial disturbance

g = the acceleration due to gravity

g_1 = the *downward* acceleration of the surface due to pressure forces

t = the elapsed time from the initial conditions

These instabilities may be observed in a glass of water if one pulls the glass downward more quickly than it would otherwise fall due to the attraction of gravity. The effect is the same, but more difficult to observe due to starting transients, if one simply turns the glass upside down and holds it still.

The flow around a surface piercing strut may be thought of as a surface which is being accelerated downward. Time $t = 0$ corresponds to the position of the surface at the leading edge, and at the trailing edge

$$t = \frac{c}{U_\infty}$$

where c = the length of the strut chord

U_∞ = the velocity far upstream

Taking the case of a vapour cavity below the surface seal, if it is assumed that the pressure below the surface seal is P_V, the pressure above is P_A and the curvature and the deviation of the surface from the horizontal is negligible – i.e. the component of gravity parallel to the surface can be ignored, then the downward acceleration due to pressure difference is (c.f. Figure 4.5)

$$g_1 = \frac{P_A - P_V}{\rho \underline{\delta}}$$

(2)

where ρ = the mass density of water

$\underline{\delta}$ = the thickness of the surface seal

P_V = the vapour pressure of water under the test conditions

P_A = atmospheric pressure

Substituting (2) and $t = c/U_\infty$ in (1), gives

$$\frac{\eta}{\eta_0} = \cosh\left\{-\frac{2\pi}{\lambda}\left(\frac{P_A - P_V}{\rho \underline{\delta}} - g\right)\frac{c^2}{U_\infty^2}\right\}^{1/2}$$

$$\frac{\eta}{\eta_0} = \cosh\left\{-\frac{2\pi}{\lambda \underline{\delta}}\left(\frac{P_A - P_V}{\rho U_\infty^2} - \frac{g\delta}{U_\infty^2}\right)\right\}^{1/2}$$

(3)

Three dimensionless groups in expression (3) can be identified

$$\sigma \equiv \frac{P_A - P_V}{\rho U_\infty^2}, \qquad \text{the cavitation or pressure index}$$

(4)

$$F_\delta \equiv \frac{U}{\sqrt{g\underline{\delta}}}, \qquad \text{a Froude number based on seal thickness}$$

(5)

$$\frac{c^2}{\lambda \underline{\delta}}, \qquad \text{a geometric ratio}$$

(6)

Rewriting (3) using (4), (5), and (6) gives

$$\frac{\eta}{\eta_0} = \cosh\left\{-2\pi \frac{c^2}{\lambda \underline{\delta}}\left(\sigma - \frac{1}{F_{\underline{\delta}}^2}\right)\right\}^{1/2}$$

(7)

62

If $c^2/\lambda\underline{\delta}$ is preserved with geometric similarity, and if η/η_0 is taken as a measure of the stability of the surface seal, then preservation of σ and $F_{\underline{\delta}}$ will model the important property of the surface seal. Since it is being assumed that $c^2/\lambda\underline{\delta}$ will be preserved with geometric similarity, the analysis will not suffer if it is assumed that $F_{\underline{\delta}}$ will be preserved if F_c, is preserved,

where
$$F_c = \frac{U_\infty}{\sqrt{gc}} \, .$$

The advantage is that $F_{\underline{\delta}}$ must be measured empirically whereas F_c is easily calculated.

The thickness of the surface seal, $\underline{\delta}$, depends on the extent of the separated or cavitating region. In the case of a vapour cavity, which we are now considering, above certain Reynolds numbers, say $R = 5 \times 10^5$

where
$$R = \frac{U_\infty c}{\nu} \, ,$$

and ν = the kinematic viscosity of water under the test conditions,

the extent of the vapour cavity will depend only on F_c and σ for similar geometries. Therefore, for similar geometries, in calm water, the ventilation boundary should be a function only of F_c and σ.

Figure 4.6 shows the results of a series of tests by Rothblum et al at the Taylor Center, Kramer and Waid at Lockheed, Wright and McGregor at Leeds, and the present study, with the ventilation inception boundaries plotted as a function of σ and F_c. Except for the Leeds data, the results are for a series of three geometrically similar models, ranging in size from $c = 1/2$ ft (1/6 m), $c = 1$ ft (1/3 m) and $c = 2$ ft (2/3 m). All the models had a thickness to chord ratio (t/c) of 0.12. The Center and Lockheed models were modified biogives with blunted leading edges. The Leeds model was a NACA 0012 of 1/3 ft (100 mm) chord. The aspect ratios based on submerged area/chord (AR) were 1.0 for the biogives and 2.1 for the NACA 0012, except for the 62 ft/s (19 m/s) test with the NACA 0012, where AR $\cong$ 3, but was effectively greater because the model was fastened to the bottom of the test water channel. Speeds ranged from 15 ft/s (4 1/2 m/s) to 93 ft/s (55 kts, 28 m/s), for the various test facilities and experiments represented.

For the Center and Lockheed modified biogive boundary points, an excellent fit is obtained by the function

$$\sigma = \sigma\,(F_c \to \infty) - \frac{0.4}{F_c^2}$$

63
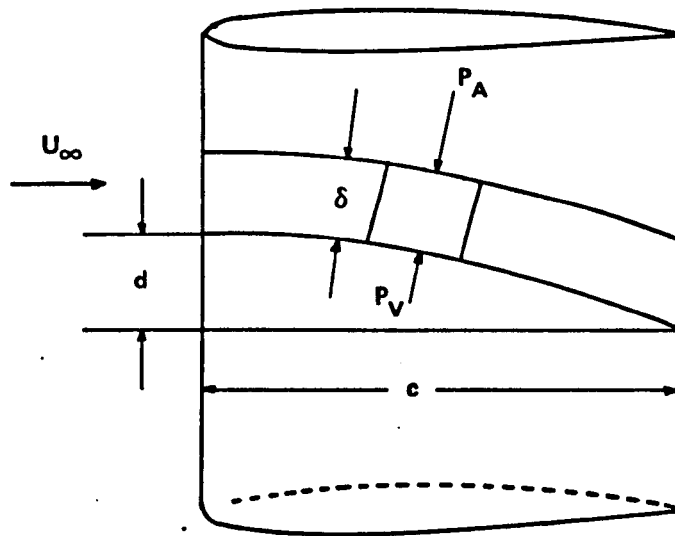
Figure 4.5 – Idealised Diagram of Surface Seal.

$$g_1 = \frac{P_A - P_V}{\rho \underline{\delta}}, \; t = \frac{c}{U_\infty}$$

KEY:

CHORD IN FEET	SIDESLIP ANGLE (degrees)			
	4	6	8	10
0.33			◖	●
0.5		⬠	▽	
1.0	◇	○	△	⬡
2.0		◇	◁	
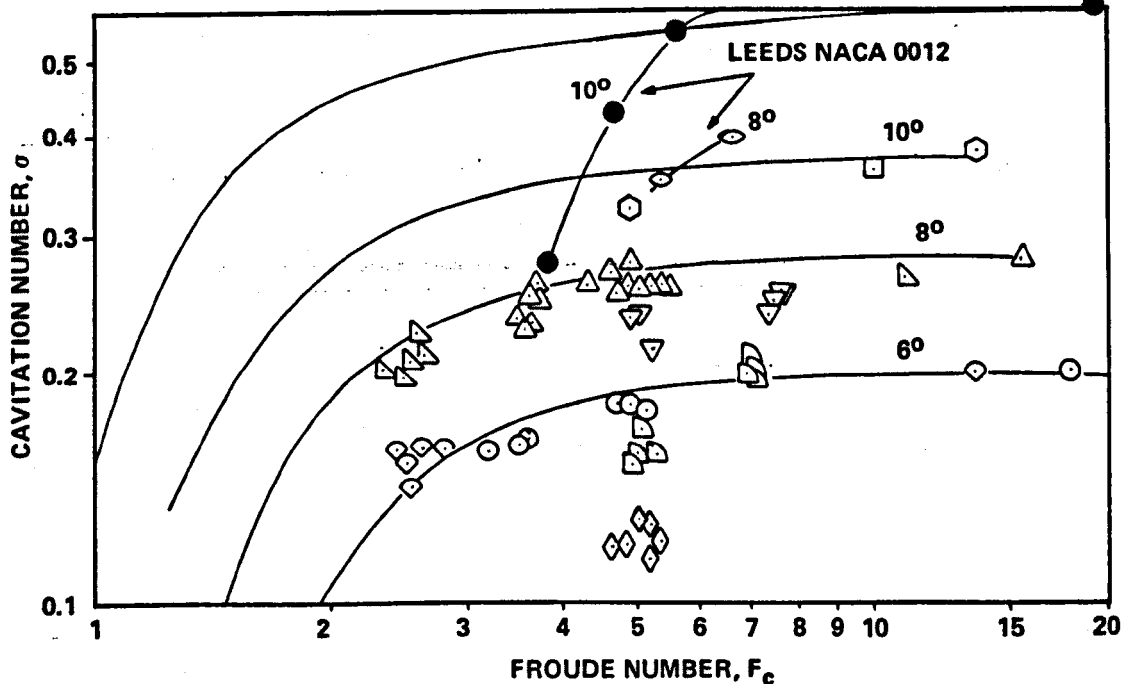
Figure 4.6 – Ventilation Boundary Correlation for Geometrically Similar Versions of NSRDC Strut Model 2 (similar to NACA 16-021). Also Shown are Boundary Points for NACA 0012. Data Taken from Present Tests and Rothblum et al,[4.7] Waid,[2.11] and Wright et al.[4.10]

– 64 –

where $\sigma(F_c \rightarrow \infty)$ is the value of σ on the boundary for large values of F_c. These are the solid lines in the figure. The factor 0.4 does not appear to be universal as other data from different geometries (not shown) contradict it. The Leeds data, while it shows the same trend as the Center – Lockheed results, should not be expected to exactly coincide since the geometry was not similar.

The figure shows the expected dropoff in dependence on F_c as predicted by the factor

$$\left(\sigma - \frac{1}{F_c^2}\right).$$

analogous to $(\sigma - 1/F_\delta^2)$ in expression (7).

Obviously, this analysis neglects several factors that may be important in the full scale case. For example, with higher Reynolds number, the thickness of the boundary layer in the surface seal will grow, with consequent loss of momentum. The proportionate thickness of the boundary layer with increasing chord length becomes smaller, while with increasing speed the actual thickness decreases, as can be seen from the expression governing growth of the turbulent boundary layer in the absence of a pressure gradient.[4.17]

$$\delta = \frac{(n+1)(n+2)(0.036)\,x}{n\,R_x^{1/5}}$$

where x = the distance from the start of the turbulent boundary layer

$R_x = U_\infty x / \nu$

n = a weak function of R_x, $n \sim 7$ for most purposes

δ = is the perpendicular distance from the boundary at which the fluid velocity is nearly equal to that which would obtain in the absence of friction

For example, if c is doubled, the value of δ at x = c will not quite double because of the increase in the factor $R_x^{1/5}$ in the denominator. Likewise if U_∞ is increased, then x stays the same while $R_x^{1/5}$ increases, resulting in an absolutely smaller value of δ.

For zero pressure gradient, the momentum thickness, θ, defined as

$$\theta \equiv \int_0^\infty \frac{u}{u_e}\left(1 - \frac{u}{u_e}\right) dy$$

where   u = local velocity

u_e = local velocity outside the boundary layer, e.g. as computed for frictionless flow

and   y = perpendicular distance from boundary

65

remains a constant proportion of δ. The momentum thickness is a measure of the momentum flux in the boundary layer. However, with increasing speed, although the momentum thickness decreases, as does δ, the total momentum lost increases. The net effect of this is difficult to project.

An additional effect of increasing size and speed is the increased tendency for air and water to become mixed, as can be observed over the side of a fast ship. The mechanism of this mixing is not fully understood, but may be associated with the increased vorticity as the turbulence becomes greater with increased size and speed. Its effect, if any, on the surface seal cannot be anticipated, although it may be presumed, as was done by Eames, that the net effect of all these factors is to weaken the surface seal.

Because the Taylor treatment of surface disturbance amplification was linear, it can be expected that the longer residence times and larger initial disturbances of full scale conditions would result in the growth rates passing into the non-linear regime, also with probably adverse effect.

In sum then, attempts to model ventilation based on scaling F_c and σ have met with reasonable success over a wide range of velocities and sizes in calm water, where the separated region is due to a vapour cavity. An analysis of the amplification of disturbances in the surface seal appears to justify this procedure. However, factors relating to turbulence and non-linearities may eventually limit this approach. Because the method is based on geometric similarity, no guide is given for performance of dissimilar shapes or incidence angles. Special interest in the viscous or other aspects of the flow could require the scaling of other parameters.

EFFECT OF SIZE AND SPEED ON THE
LOW PRESSURE SEPARATED REGION

Factors Affecting Surface Seal Stability for Fully Wetted Separation. The effect of size and speed on the surface seal was not discussed in the case where the low pressure separated region was fully wetted rather than due to vapour cavitation. That is because the thickness of the surface seal depends in the wetted case on the extent of the separation. In the vapour cavitating case, the same factors governed the extent of the cavitation as determined the stability of the surface seal.

In the fully wetted case, a buoyancy term cancels out the factor g in expression (2). g also becomes insignificant in the cavitating case for $F_c > 5$, i.e., when the acceleration $g_1 \gg g$. The modified version of (1) is then

$$\frac{\eta}{\eta_0} = \cosh\left\{-\frac{2\pi}{\lambda} g_1 t^2\right\}^{1/2} \tag{1'}$$

But $1/2\, g_1 t^2$ is just the total drawdown of the surface, d, at the tail of the strut. Therefore

$$\frac{\eta}{\eta_0} = \cosh\left\{-\frac{4\pi d}{\lambda}\right\}^{1/2} \tag{8}$$

The fact that this did not depend on geometry led to an attempt to correlate ventilation inception with surface drawdown. However, although the problem had been simplified, the factors governing stability of the surface seal are no longer adequate to govern the separated region as for the cavitating area.

2-D Equation Governing Onset of Turbulent Tail Separation. The equation developed in Chapter 7, due to B.S. Stratford,[4.17] for predicting two dimensional turbulent separation is

$$\overline{C}_p \left(\frac{x\, d\overline{C}_p}{dx}\right)^{1/2} = 0.39\,(10^{-6}\, R_s)^{1/10} \tag{9}$$

where $\overline{C}_p = \dfrac{P}{\frac{1}{2}\rho U_0^2}$,   a pressure coefficient based on the minimum pressure

R_s = Reynolds number at $x = x_s$, the point of separation

U_0 = the maximum velocity on the strut (calculated from potential flow)

P = pressure (calculated from potential flow)

From an examination of this equation it can be seen that with increasing Reynolds number, the point of separation will move aft and, in three dimensions, because of the decreased streamwise gradient near the free surface, will shrink from the surface leaving the surface seal proportionately thicker. However, the dependence on Reynolds number is only slight. To first order, the main factor is $\overline{C}_p$. If $\overline{C}_{p\,min}$ is chosen as a scaling parameter $d\overline{C}_p/dx$ will be closely related. An empirical factor relating the surface drawdown to the minimum pressure coefficient was found to be the cavitation number normalised by the incipient cavitation number σ_i at 2 degrees sideslip angle.[4.11] In fact, this turns out to be a ratio of velocities,

$$\frac{\sigma_i}{\sigma} = \frac{U_\infty^2}{U_{i\infty}^2}$$

Empirical Correlation of Tail Ventilation Boundary Points Based on d/c and $U_\infty/U_{i\infty}$.

Figure 4.7 shows values of d/c versus $U_\infty/U_{i\infty}$ on the ventilation boundary of a wide variety of surface piercing struts, including Center and Leeds models. Considering that this criterion is independent of all details of geometry, the correlation is excellent and should be extremely useful. Of course, the parameters d and $U_{i\infty}$ must be empirically measured. However, $U_{i\infty}$ may be calculated on the basis of two-dimensional ideal flow, and d may be estimated from flat plate results, (Figure 4.8), since at or near the ventilation boundary, extensive separation will obscure details of section profile. This criterion, and the preceding criterion for cavitating struts, applies only to the tail ventilation mode.

OTHER SCALE EFFECTS

The suggested scaling criteria presented have been shown to have moderate success in correlating laboratory measured ventilation inception boundaries. Some discussion was given of the possible effect full scale conditions might have on the factors governing the behaviour of model tests. Besides Reynolds number effects on the surface seal and the separated region due to increased turbulence and decreased boundary layer momentum, there are effects of roughness of the model and prototype surface to consider, and water surface tension and contact angle.

Wettability and Surface Tension. Wetzel[4.2] and Perry[4.18] found that surface tension and "wettability" had an effect on the ventilation boundaries of very small models – 1/4 inch diameter (6 mm) rods and 2 inch chord (50 mm) struts. It is unlikely that surface tension and wettability will have any effect on full scale ventilation, but it is important to determine how it may affect model results.

Roughness. The effect of roughness is twofold.

First, it is unlikely that the surface finish of a prototype will correspond to that of a model, as mentioned previously.

Second, the use of roughness at model scale to stimulate turbulence has long been a standard technique of ship and aircraft model studies. It is possible that the addition of roughness to struts will simulate the additional turbulence and momentum loss that may be present at full scale and thus provide some insight into the effect of large sizes on the surface seal. In the present study, the effects on the surface seal of roughness were comparable to the hypothesised effects of turbulence due to full scale size. A weakened action of the surface
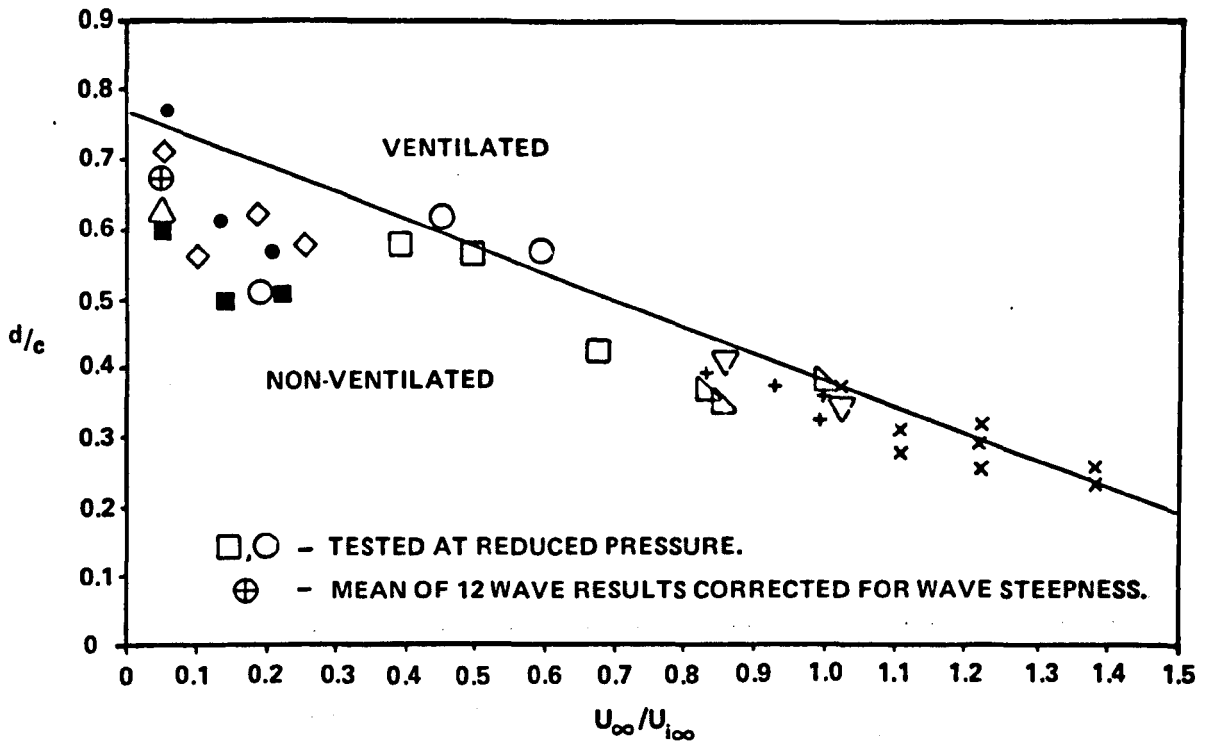
Figure 4.7 – A Criterion for Tail Ventilation
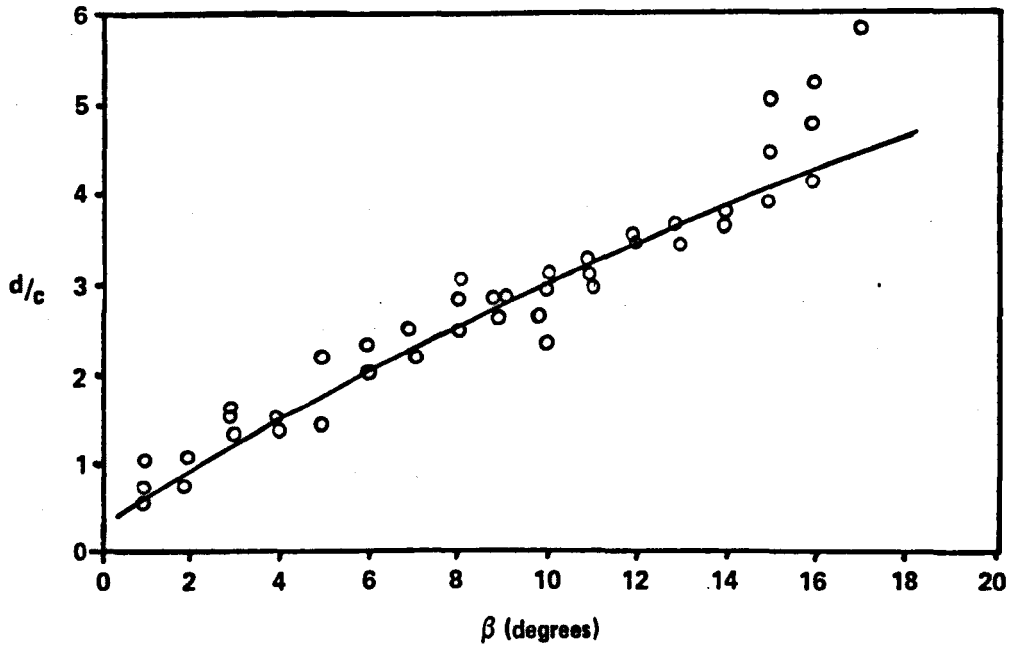
Figure 4.8 – Values of d/c Against Sideslip Angle β for a Flat Plate, Which Can Be Used to Determine Approximate Inception Angles for Tail Ventilation. From Swales, Wright, McGregor & Rothblum[4.11].

— 69 —

seal and a behaviour of the ventilated cavity similar to that of prototype observations was noted.

A series of experiments designed to test the effect of roughness, wettability and high speed on the ventilation characteristics of a NACA 0012 strut are described and discussed in the following two chapters.

CONCLUSIONS

● The effect of prototype speeds and sizes on the elements of the mechanism of ventilation can be inferred from model studies.

● For similar geometry, a large variation in size and speed can be reduced to a function of cavitation number and Froude number alone.

● For nearly arbitrary geometry, an empirical relationship between a dimensionless velocity and the ratio of surface drawdown to chord length collapses the inception points for a great variety of data, including some obtained in waves.

Chapter 4 References

4.1   Wadlin, Kenneth L., *"Mechanics of Ventilation Inception,"* Second Symposium on Naval Hydrodynamics, Office of Naval Research, 1958.

4.2   Wetzel, Joseph M., *"Ventilation of Bodies Piercing a Free Surface,"* Second Symposium on Naval Hydrodynamics, Office of Naval Research, 1958.

4.3   Eames, M.C., Discussion of Ref. 2.2, Second Symposium on Naval Hydrodynamics, Office of Naval Research, 1958.

4.4   Breslin, John P., Discussion of Ref. 2.2, Second Symposium on Naval Hydrodynamics, Office of Naval Research, 1958.

4.5   Breslin, John P., and Skalak, Richard, *"Exploratory Study of Ventilated Flows about Yawed Surface-Piercing Struts,"* NASA MEMO 2-23-59W, April 1959.

4.6   Boeing Company Report, *"Hydrofoil Patrol Craft High Point (PCH-1) Analysis of Strut Hydrodynamic Characteristics in Calm Water,"* HYSTU PLAN BE049AP044, Contract NOO 600-69-c-0618, 1968.

4.7   Rothblum, Richard S., Mayer, Dennis A., and Wilburn, Gene M., *"Ventilation, Cavitation and Other Characteristics of High Speed Surface Piercing Struts,"* Naval Ship R & D Center Rept. No. 3023, 1969.

4.8   Kramer, Ray L., *"An Experimental Study of the Effects of Waves on the Ventilation of Surface-Piercing Struts,"* Lockheed Missiles & Space Co. D029678, Nov 1970.

4.9   Rothblum, R.S., Dailey, N.L., and Pattison, J.H., *"Effect of a Protuberance and Aspect Ratio on the Inception of Ventilation on a Surface-Piercing Strut in Cavitating Flow,"* Naval Ship R & D Center Ship Performance Dept. Eval. Rept. 479 H 02, June 1972.

4.10 McGregor, Robert C., Wright, A.J., Swales, P.D., and Crapper, G.D., *"An Examination of the Influence of Waves on the Ventilation of Surface-Piercing Struts,"* J. Fluid Mech., Vol. 61, Part 1, pp. 85-96, 1973.

4.11 Swales, P.D., Wright, A.J., McGregor, R.C., and Rothblum, R.S., *"The Mechanism of Ventilation Inception on Surface Piercing Foils,"* Jour. Mech. Eng. Sci., Vol. 16, No. 1, 1974.

4.12 Swales, P.D., Wright, A.J., McGregor, R.C., and Cole, B.N., *"Separation and Ventilation Interaction Studies,"* Hovering Craft and Hydrofoil, Vol. 13, No. 3, pp. 8-12, 1973.

4.13 McGregor, Robert C., Swales, P.D., Rothblum, R.S., *"The Influence of Fences on Surface Piercing Struts and Foils,"* Tenth Symposium on Naval Hydrodynamics, Office of Naval Research, 1974.

4.14 Wright, A.J., McGregor, R.C., and Swales, P.D., *"Time Dependency of Ventilation,"* Hovering Craft and Hydrofoils, Vol. 12, No. 9, 1973.

4.15 Shen, Young T., *"General Scaling Problems on Fully Cavitating and Ventilated Flows,"* Part of Report on Cavitation, 17th American Towing Tank Conference, Cal. Inst. of Tech., 1974.

4.16 Taylor, G.I., *"The Instability of Liquid Surfaces When Accelerated in a Direction Perpendicular to Their Planes.I.,"* Proc. Roy. Soc. Vol. A201, pp. 192-6, 1950.

4.17 Stratford, B.S., *"The Prediction of Separation of the Turbulent Boundary Layer,"* J. Fluid Mech., Vol. 5, pp. 1-16, 1959.

CHAPTER 5

ROUGHNESS AND WETTABILITY
EXPERIMENT

GENERAL CONSIDERATION OF
ROUGHNESS AND SURFACE FORCES

Turbulent Flow Resistant to Separation. Roughness has an important effect on boundary layer phenomena. The use of controlled roughness is well established as a means of provoking transition from laminar to turbulent flow in the testing of ship and aircraft models. This is done to obtain greater similarity between the model flow and the prototype flow, if the prototype flow is likely to be turbulent. Because of the greater mixing of momentum from the free stream into the boundary layer, turbulent flow is less likely to become separated than laminar flow, where the only means of momentum transfer is usually considered to be through ordinary shearing stresses.

Roughness and Cavitation. A less recognised effect of roughness is to increase the tendency of a body towards cavitation. Because of surface tension forces, it can be shown that it is impossible for cavitation to occur without a "nucleus" of more than infinitesimal radius. Besides providing these nuclei, roughness elements may also be responsible for localised regions of separation, now also thought to be a precondition for the occurrence of vapour cavitation.

Other Possible Effects of Roughness. Even if cavitation is not influenced in a particular case by the existence of roughness, there is the possibility that the local regions of separation may link together to form a low energy path for air, or that vorticity induced by the roughness may provide a similar path.

In the preceding chapter, the likely effect that roughness might have on the difference between model and full scale performance was discussed. It was noted that the effect of the greater full scale turbulence and boundary layer thickness, as well as surface imperfections due to cruder manufacturing methods, might be simulated at model scale by the use of controlled roughness.

Roughness and Possible Explanation for Model Scale Differences. In addition to the foregoing incentives to test the effect of roughness in a controlled experiment, the Leeds University hydrofoil team reported the experience that two foils of ostensibly identical section when tested were found to have different ventilation boundaries.[5.1] The only apparent difference between the foils was their method of manufacture. It was speculated that because of the difference in surface finish obtained by casting, as one was, and profile milling, the method

of manufacture of the other, that the ventilation properties might have been affected. A test of the effect of known roughness was decided upon as necessary to eliminate or confirm this possibility, and to establish a smoothness criterion for future model tests.

Surface Tension Influence on Models. In the discussion of the differences between model and prototype scale, surface tension and surface contact angle were mentioned as possibly affecting model results, but not able to influence full scale flows. Perry,[5.2] Kicenuik[5.3] and Wetzel[5.4] each found that surface tension was an important parameter in the ventilation of small objects, such as cylinders of less than 1/4 inch (6 mm) diameter. Breslin speculated that surface tension effects might make ventilation scaling impossible. Wetzel also found that changing the surface contact angle by coating his small cylinders with "Teflon" spray eliminated the effects of surface tension, which indicates that the forces of attraction between the body and the water are important, rather than just surface tension.

Effect of Surface Tension on Instabilities in the Surface Seal. The effect of acceleration on the surface seal is similar to the effect which turning a tumbler of water upside down has on the surface of the water in the tumbler, as was explained in Chapter 3 on the mechanism of ventilation. Continuing with this example, after the water is nearly gone from the glass, a few droplets will still cling to the edges and perhaps the bottom of the tumbler. The forces of surface tension and contact have stabilised the surface and counteracted the force due to gravity. If the droplets are below a certain radius (the surface tension forces are inversely proportional to the local radius of curvature of the surface) their growth is arrested. Therefore, surface tension acts as a cutoff filter in the Taylor amplification mechanism for wave numbers above a certain spatial frequency. The size of water droplets provides a good indication of the scale of this effect.

Since surface forces do not depend upon flow, the magnitude of surface forces relative to inertial forces becomes small very quickly with increasing sizes and speeds. Surface forces are also inversely proportional to radii of curvature, and therefore usually decrease with increasing size for this reason as well. However, if model sizes and speeds are too small, the effects of surface tension and contact angle may result in spurious phenomena which do not relate to full scale situations.

Effect of Surface Tension on the Present Experiments. In order to ensure that the present work and similar studies at the Leeds University facility were comparable with other apparently similar studies, an experiment was designed, to be performed along with the

roughness studies, to change the surface contact angle between the water and the model, to test whether this was an important variable. Ideally, the surface tension in the water in the entire facility should also have been changed independently in order to make the experiment more comprehensive. This was not feasible within the experimental constraints. However, surface tension and contact forces are similar in nature and in magnitude. Therefore a null result in the case of variation of surface contact angle was taken to imply that surface tension also had no effect on ventilation at the sizes and speeds of interest.

OUTLINE OF THE EXPERIMENT

In order to study the effects of roughness and wettability on ventilation, a NACA 0012 section strut of 4 inch (102 mm) chord was mounted vertically piercing the water surface in the 14 x 14 inch (355 x 355 mm) test section of the University of Leeds free surface recirculating water channel at atmospheric pressure, with varying angles of sideslip (incidence) up to ventilation, and at speeds from 5 to 20 ft/s (1 1/2 to 6 m/s) in increments of 2 1/2 ft/s (3/4 m/s). The runs were made at constant speed while sideslip angle was slowly increased to the ventilation inception angle. The model was first tested with the surface finish as furnished by the manufacturer. It was then polished and re-tested, and then tested with four grades of spherical glass bead roughness applied with varnish. The effect of the varnish alone was tested. The model was tested with wax applied to change the surface contact angle, and with a coating of Dow Corning "Silanox", a "hydrophobic" material, also applied with varnish. A further test was made with a previously manufactured NACA 0012 model. The ventilation and washout angles were recorded. Details of the experimental facility are presented in the following section. Details of the experiment are given in the "Procedure" section.

EXPERIMENTAL APPARATUS

The Variable Pressure Free Surface Recirculating Water Channel. The principal facility used for the roughness and wettability experiment was the Variable Pressure Free Surface Recirculating Water Channel purpose built for testing surface piercing hydrofoils and struts, commissioned in 1968.[5.5] The working section was 14 x 14 inches square (355 mm) and 9 ft long (2 3/4 m). The design speed was 20 ft/s (6 m/s) although speeds up to 25 ft/s (7 1/2 m/s) could be maintained with loss in flow quality. The unusual feature of this facility was the combination of a free surface test section with the ability to operate at

reduced pressures. The layout of the channel, shown in Figure 5.1, was in a vertical plane to reduce cavitation and leakage problems in the main circulating pump. The contraction section ahead of the working section had a circular cross section which gradually changed to a square cross section. The small amount of available space dictated the use of the minimum contraction ratio, 8:1, required for uniform flow.

Quality of Channel Working Section Free Surface. Above 6 ft/s (1.8 m/s) the flow in the working section was supercritical – the velocity greater than the wave celerity. The quality of the free surface at supercritical speeds (which includes the majority of the test conditions investigated in this work) was not exceedingly smooth. Wright[5.6] conducted an investigation of the surface quality, the results of which are presented as Figures 5.2 and 5.3. Smoothness of the surface was aided by the additon of a knife edge exit from the contraction section. The hydraulic jump which would exist at supercritical speeds was drawn away by another knife edge flow splitter, at the end of the working section, which carried away the surface flow through "cyclones" to a settling tank, where it rejoined the main circulation in the air removal section.

Water Channel Air Removal. Removal of entrained air, a major consideration in a facility designed to test surface piercing models, was accomplished by allowing the flow to slow to 5 ft/s (1 1/2 m/s) maximum velocity, and passing it through closely spaced separation trays. During the present work, these trays had suffered somewhat from distortion and were replaced. The replacement trays were not aligned as well as the original ones, and the experiment suffered from excessive recirculation of air bubbles at the higher speeds. This did not appear to affect any of the results except possibly the experiments involving boundary layer suction, where this will be discussed.

Range of Ambient Pressures Available. Evacuation of the working section could be effected by an oversized rotary water seal pump, which could reduce the working pressure to less than 1/20 atmosphere, or alternatively, pressurise to more than 2 atmospheres (absolute). Although this capability was not used in the present investigation, comparison results obtained by other investigators in this facility at low pressures are presented. The vacuum pump was used in the boundary layer suction experiment to supply the suction.

Velocity Cross Section. G. Smith[5.7] performed a survey of the mean velocities distributed over a cross section of the working section using a pitot tube rake. The contour maps
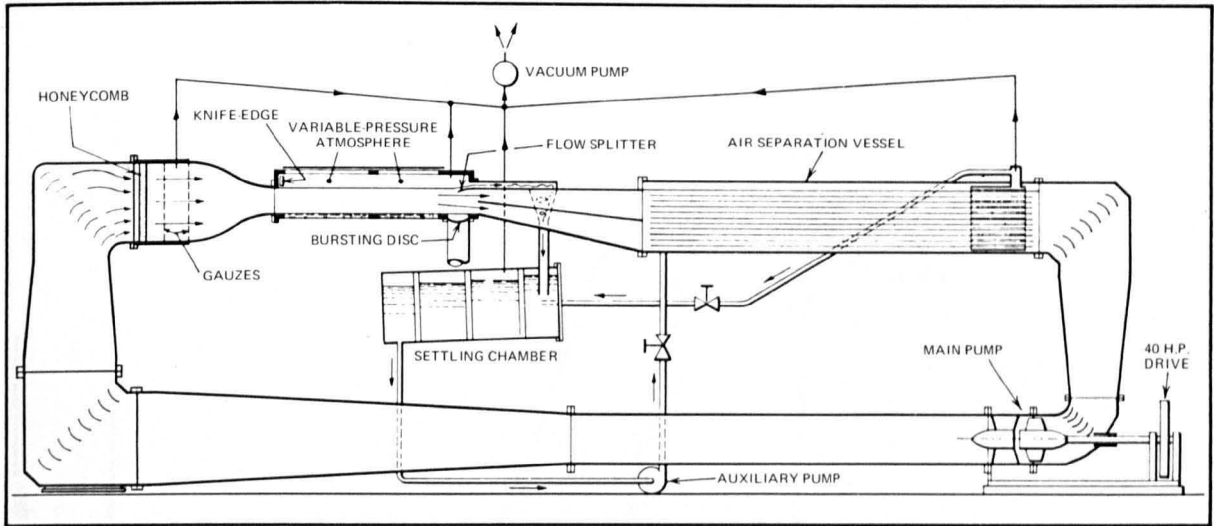
Figure 5.1a — Schematic Diagram of the Variable Pressure Recirculating Water Channel. From Hunter et al.[5.5]
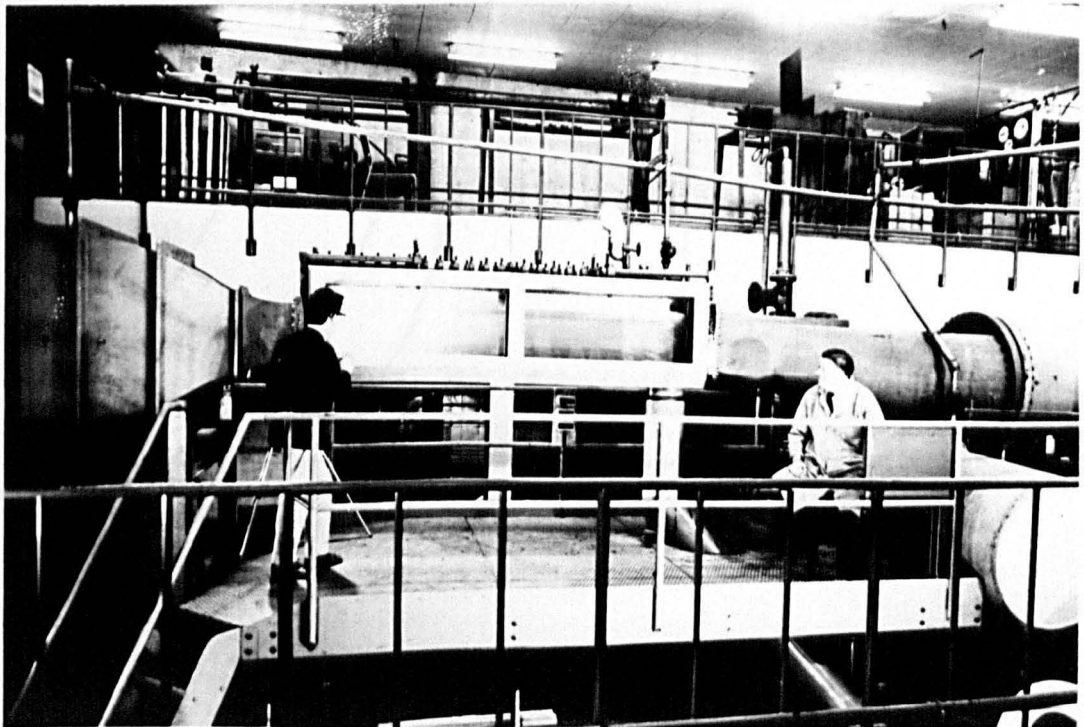
Figure 5.1b — Photograph of Test Section
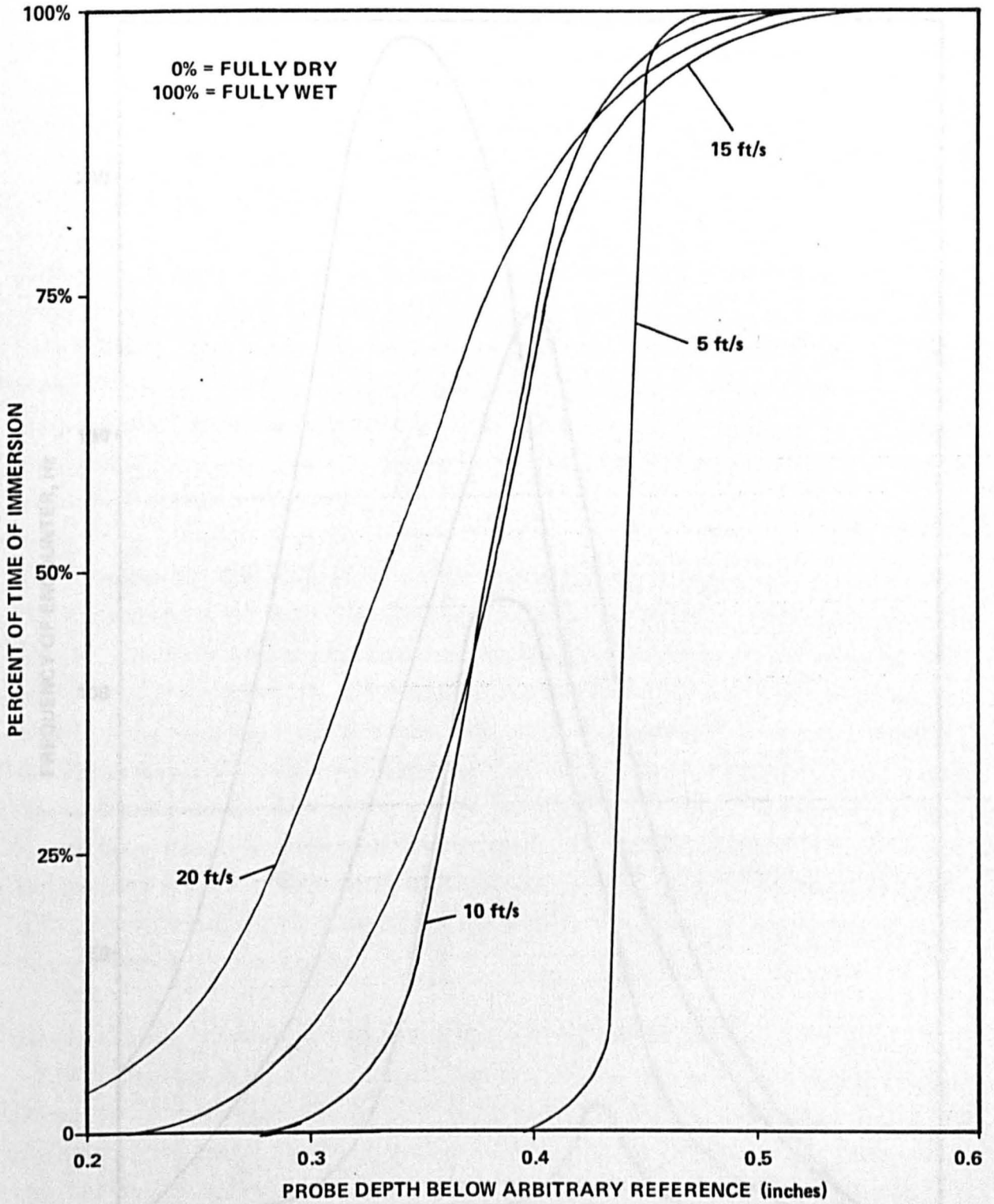
Figure 5.2 – Surface Quality of Channel: Percent of Time for Which a Probe Was Wetted vs Probe Depth. From Wright.[5.6]
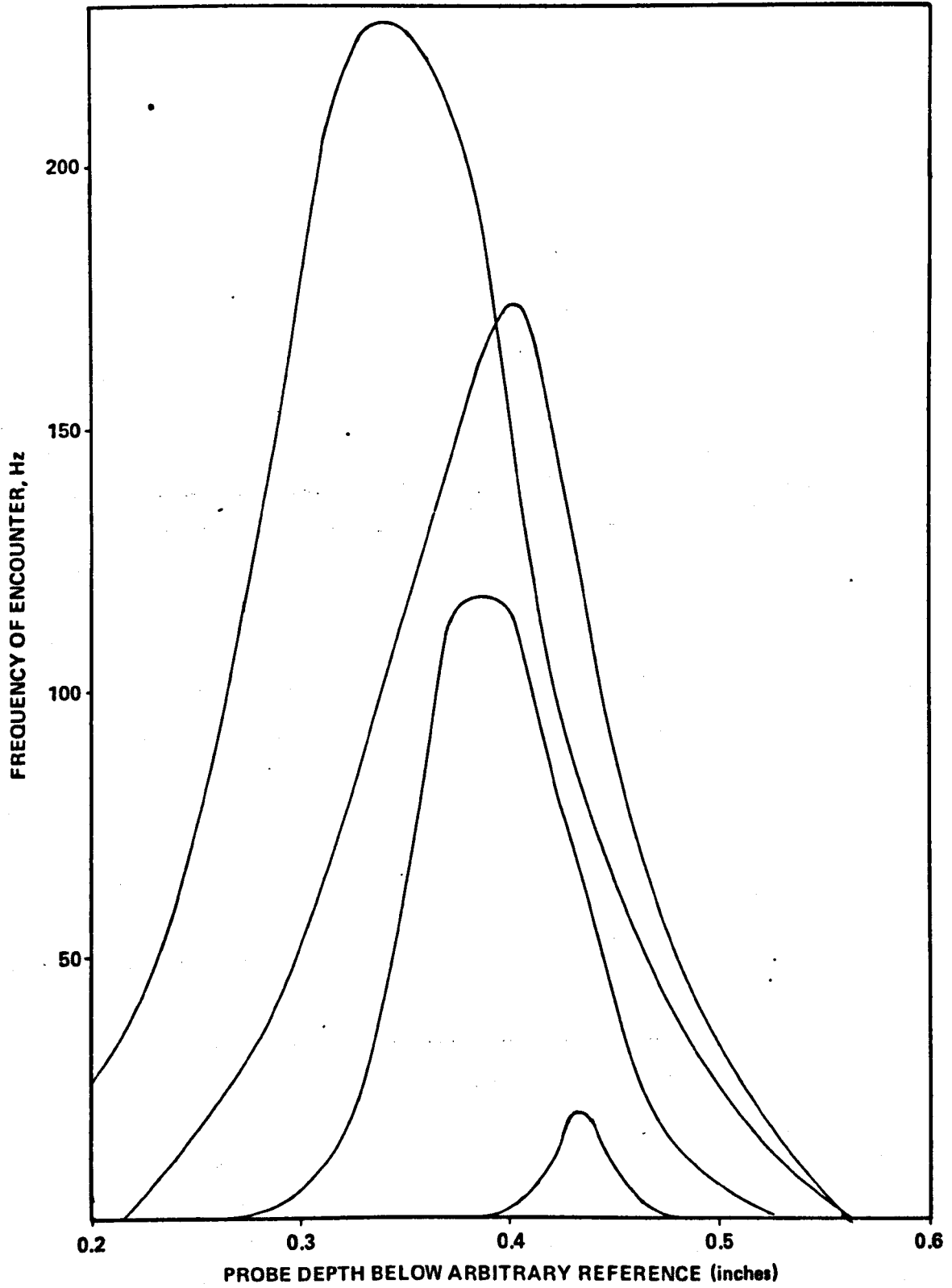
Figure 5.3 – Surface Quality of Channel: Frequency of Encounter with
Disturbances vs Probe Depth. From Wright.[5.6]

produced by him are shown in Figures 5.4 to 5.6. They are for one subcritical velocity and two supercritical velocities. For the subcritical case, there is a variation across the channel of +4 percent in the center to −3 percent at the channel walls. The deviations from the average velocity and the asymmetry of the patterns are somewhat reduced at supercritical speeds, as may be seen from the Figures.

Calibration of Mean Velocity. Smith also calibrated the motor driving the main circulation pump to correlate pump RPM with channel velocity over the central section, using a pitot tube and water manometer. This calibration was spot checked using an impellor type velocity meter with a magnetic pulse pickup coupled with a gated clock. With the model in place, the pump RPM was then relied upon as the indicator of nominal velocity. This was considered an acceptable measure of velocity because of the considerable blockage effects of the model, particularly at large sideslip angles.

Wall Interface and Blockage. McGregor[5.8] evaluated the interference effects due to the channel walls using the method of images and replacing the model by a vortex singularity of like lift. The theoretical pressures were only changed by a few percent. However, because of the free surface, which was not considered in the analysis, and the finite thickness of the models, particularly significant at high sideslip angles, the mathematical estimate must be considered only a very rough approximation. In a closed channel, or in an analysis where the free surface is not allowed to deform greatly, the effect of blockage is to increase the velocities around the obstruction. With a free surface, particularly at lower speeds, the blockage increases the height of the surface rather than increasing the velocity. Once ventilation has occurred, with great deformation of the free surface and massive entrainment of air, the situation becomes hopelessly complicated.

Blockage Effects Obtained by Comparison with Wetzel, NSRDC and Breslin. A good indication that blockage effects were not significant from a standpoint of ventilation inception is that the boundary points for the smooth foil agree with Wetzel,[5.4] who conducted his tests in a rotating arm tank. His NACA 0012 models had 2 and 3 inch chords, respectively, (51 and 76 mm), and wall effects were negligible. The agreement shown in Chapter 4 with David Taylor Center towing tank data based on Froude and cavitation number scaling is also reasonable, considering the different strut cross sections and the different water surface conditions. The data are in good agreement with Breslin's test of a NACA 4412 strut of 3 inch chord, conducted in the Stevens Rotating Arm Towing Tank.[5.9]
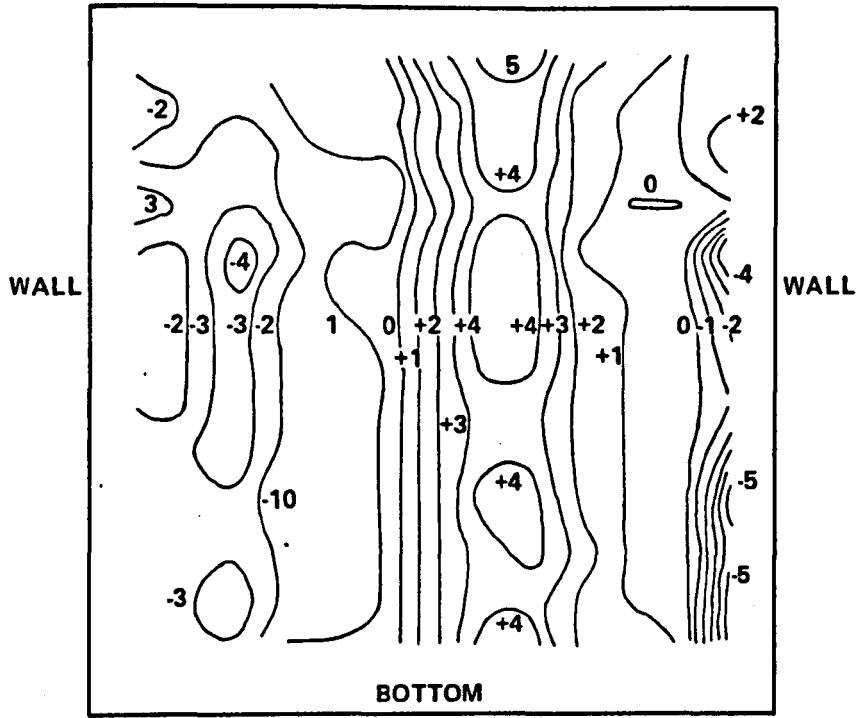
AVERAGE VELOCITY 3.84 ft/s

Figure 5.4 – Velocity Contour Map of Working Section of Channel Showing Percent Variation from Mean. From Smith.[5.7]
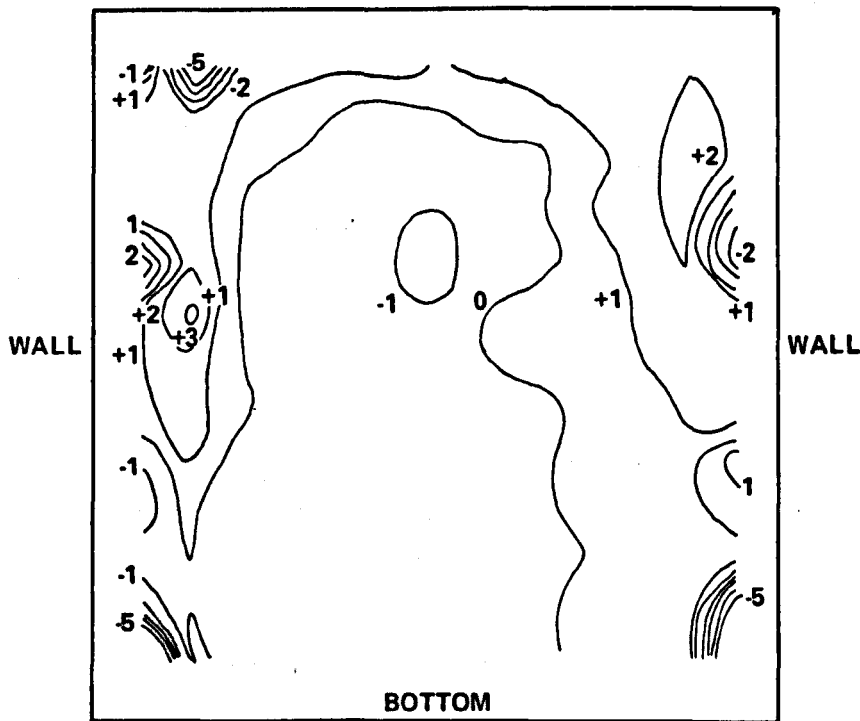
AVERAGE VELOCITY 7.45 ft/s

Figure 5.5 – Velocity Contour Map of Working Section of Channel Showing Percent Variation from Mean. From Smith.[5.7]

Blockage Effects Estimated by Comparison with Smaller Channel. The best estimation of the effects of blockage can be obtained by a comparison of the data obtained in the high speed single shot channel, where the high speed tests were conducted on the same model. The working section of the high speed facility was only 9 x 9 inches (229 mm). Also, in this facility the model was mounted flush with the channel bottom, instead of clearing it by 5 inches (125 mm), which further increased the blockage. In spite of this, at 10 ft/s, (3 m/s) the ventilation angle increased from 18.5 degrees to only 23 degrees, and at 20 ft/s (6 m/s) the ventilation angle went from 21.5 degrees to 24 degrees. Furthermore, the shape of the boundary curves were similar for similar velocities. Therefore, it was concluded that blockage in the larger channel was insignificant, but that the effects of blockage were distinctly measurable in the smaller high speed facility.

EXPERIMENTAL PROCEDURE

The Model. A NACA 0012 section strut was manufactured in an aluminium bronze material. The theoretical offsets are given in Table 5.1. The method of manufacture was to grind a milling cutter to the chordwise profile, and then mill the strut on both sides for the full spanwise length, leaving sufficient unprofiled material at the end for purposes of attachment. Figure 5.7 shows the nominal dimensions of the strut. The nominal chord length was 4 inches (102 mm), and it was tested at a nominal submergence of 2 chord lengths, with approximately one chord length of profiled span remaining above the mean free water surface. Another NACA 0012 model had been previously cut from the same milling cutter. This was designated Mk I, and the other, Mk II.

Measurement of Model Offsets and Nose Radius. A thin acrylic plastic cast was made of the strut profile at a representative depth. The casting was then carefully measured using an optical comparator, and the offsets recorded. For comparison, the same procedure was applied to the previously tested Mk I NACA 0012 model. Figure 5.8 shows the theoretical offsets compared with the measured ones for both NACA struts. Except at the extreme leading edge, the measured offsets for the new foil differed from the theoretical by no more than 1/4 percent of chord length. The old, comparison model (Mk 1) was somewhat less accurate. Tracings were made of 50X enlargements of the profiles, and best-fit circles were drawn to fit the nose curvature. Both models were found to have nose radii of 1.38 percent of chord, compared to the theoretical value for the 0012 profile of 1.58.

WALL   WALL

BOTTOM
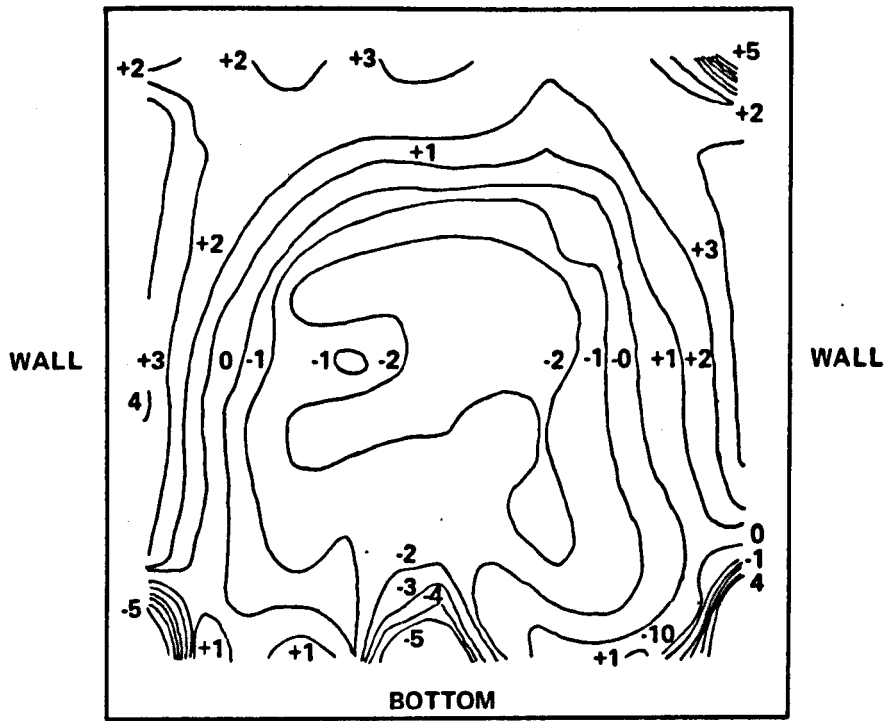
AVERAGE VELOCITY 12.36 ft/s

Figure 5.6 – Velocity Contour Map of Working Section of Channel Showing
Percent Variation from Mean. From Smith.[5.7]
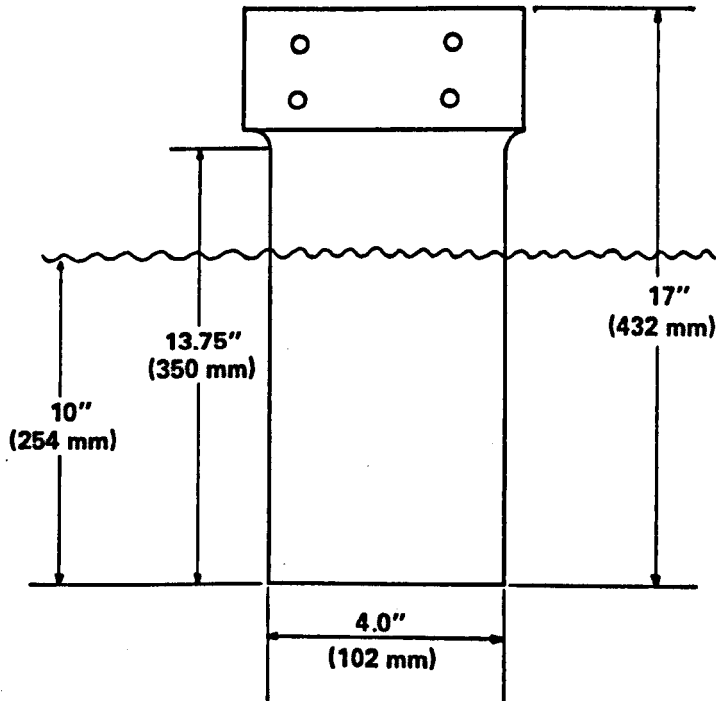
OFFSETS	
x	y
100·000	0
97·095	0·530
89·025	1·565
77·055	2·940
62·530	4·345
46·970	5·470
31·930	5·990
18·760	5·670
8·565	4·440
4·835	3·510
2·125	2·460
0·520	1·290
0	0

13.75"
(350 mm)

17"
(432 mm)

10"
(254 mm)

4.0"
(102 mm)

Figure 5.7 – NACA 0012 Struts, Mk I & Mk II, Nominal Planform Dimensions
and Table of Offsets in Percent Chord.
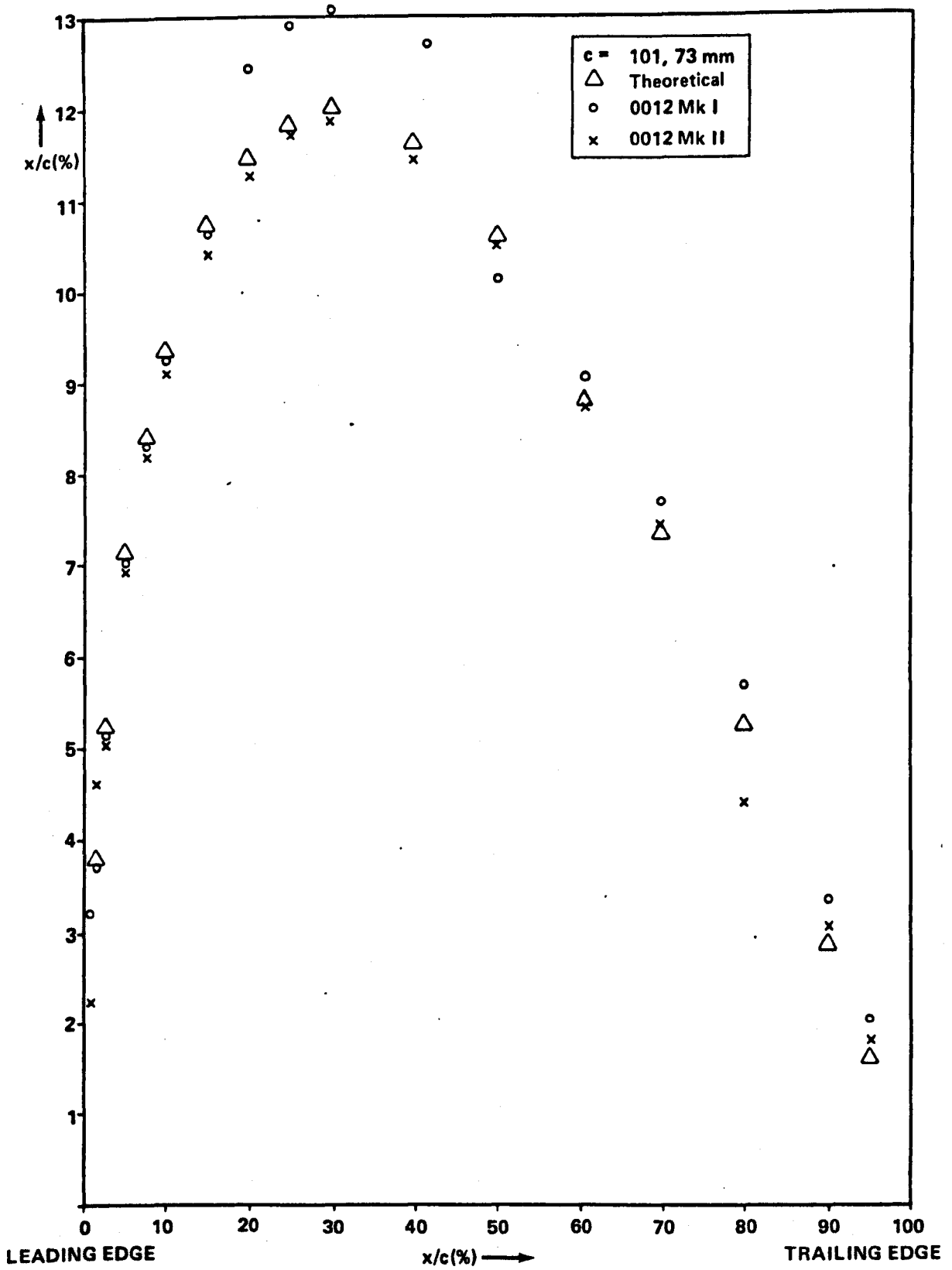
Figure 5.8 — Theoretical and Measured Profiles of NACA 0012 Models Mk I & Mk II.

Measurement of Model Microscopic Roughness. "Tallysurf" profilometer measurements were taken of the microscopic surface profile at four representative depths for both foils. The apparent resolution of this instrument was of the order of a few microinches. After the Mk II model had been tested initially, it was returned to the manufacturer for fine polishing. The surface profile measurements were then repeated. The comparison between the model as furnished orignially and after repolishing to a high shine can be seen in Figure 5.9. The detailed characterisations of the profile and the surface of the model were required by the experimental objective of testing the influence of small perturbations. The possibility of the results being due to imperfections of manufacture had to be eliminated.

Mounting, Alignment, and Incidence Control. The model was attached to a force balance and turning apparatus as shown in Figure 5.10. The incidence angle could be read directly from an inscribed brass protractor and index mark as a primary scale, but for convenience, a secondary plastic scale with much larger marks and a long extension was used. There was some uncertainty about the hydrodynamic zero of incidence, as well as the mechanical. Therefore all runs were made to both the port and starboard side, and the ventilation angle finally plotted was a mean of at least four runs to either side. In any case, runs were repeatedly made until the results could command confidence. Overall error in angular measurement was probably less than ± 1/2 degrees, including all factors.

The NACA 0012 shape was particularly chosen because of its regular behaviour and freedom from the influence of duration of run. However, incidence control was manual. Strut rotation was achieved by means of a thumbscrew driving a right angle gearbox. In general, port and starboard runs were alternated, sweeping rather quickly through the intermediate and zero angles and then quite slowly approaching the range where ventilation was possible. It was realised that this technique could lead to errors of the type which arise when the most time is spent at the incidence angles where ventilation is expected, which makes ventilation at the "expected" angles more likely. A conscientious attempt was made to avoid this situation.

Velocity Matrix. As mentioned in the Outline of the Experiment, all configurations of the NACA 0012 foil were tested at velocities of 5 ft/s (1 1/2 m/s) to the maximum acceptable velocity of 20 ft/s (6 m/s) in increments of 2 1/2 ft/s (3/4 m/s). Speeds lower than 5 ft/s (1 1/2 m/s) were not tested because that was nearly the minimum velocity for which ventilation to the full depth of the model occurred.
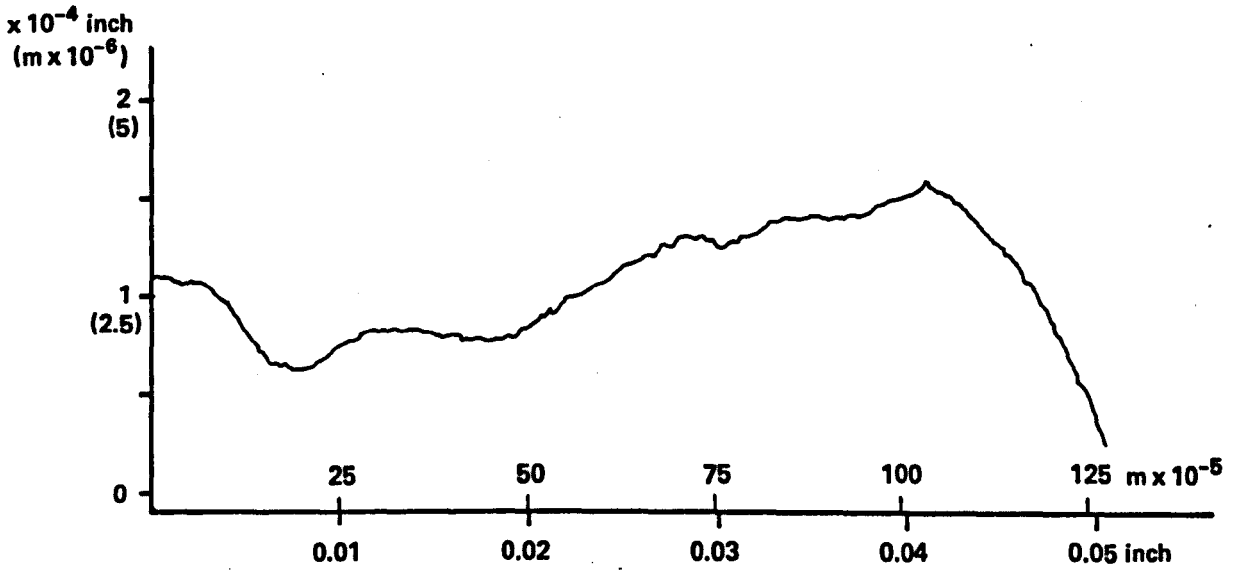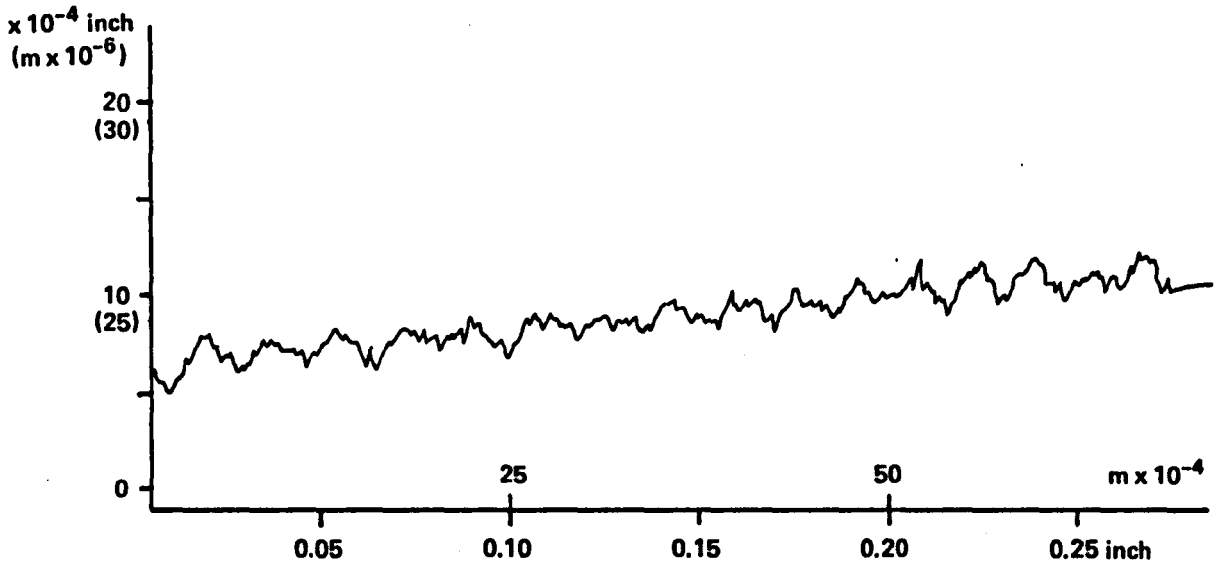
Figure 5.9 – Mk II NACA 0012 Foil Before and After Polishing (Note scale change on graphs). Reproductions of Tallysurf Roughness Traces.
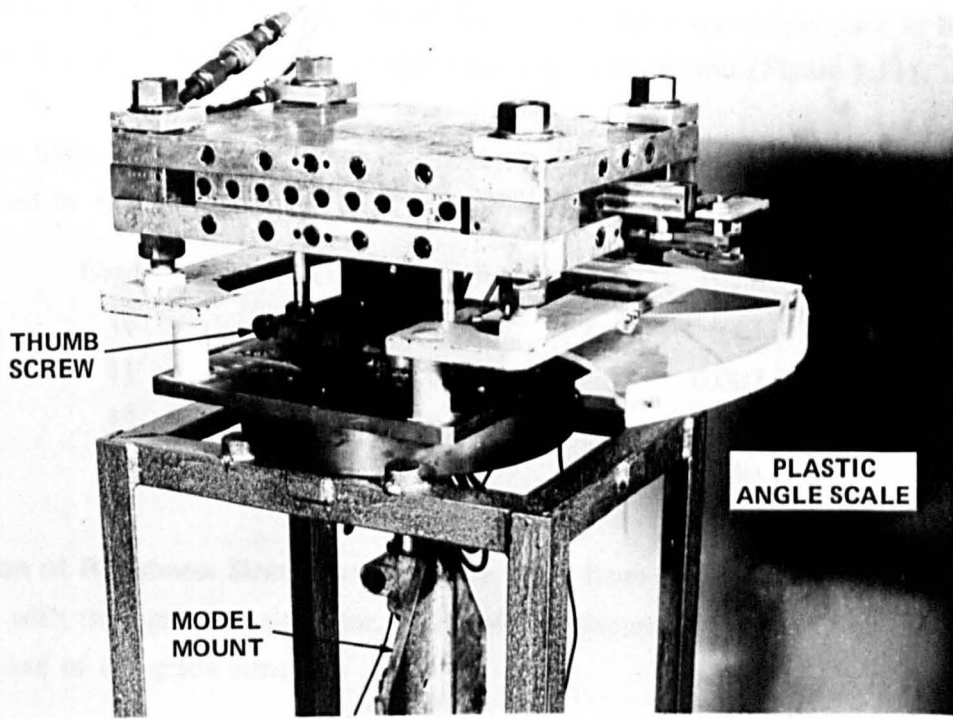
Figure 5.10 – Force Balance and Turning Apparatus.

Application of Roughnesses. After testing the foil as furnished by the manufacturer and retesting when it was returned after very fine polishing, polishing was found to have no effect. It was then tested with four grades of spherical glass roughness stuck to the foils with an undercoat of varnish.

Choice of Roughness Shape. After preliminary tests using emery paper glued to the models, glass spheres were chosen for the applied roughness because they were obtainable in relatively uniform grades, and, because of their near sphericity, their geometric and hydrodynamic properties were well defined. A profile of the commercial emery paper used in the preliminary work illustrates the difficulty of characterising its roughness (Figure 5.11).

Roughness Sizes. The nominal range of diameters corresponding to the four grades applied, as furnished by the manufacturer, were as follows:

Grade	Diameter (mm)	Diameter (in)
10	0.249 – 0.318	0.01 – 0.0125
11	0.176 – 0.249	0.007 – 0.01
15	0.065 – 0.090	0.0025 – 0.0035
20	0.053	0.002

Verification of Roughness Sizes. Samples were taken from each of the roughness grades and examined with the optical comparator. Most of the diameters measured were close to the lowest bound of the grade sizes.

Roughness Application Technique. After a series of preliminary experiments in which it was found that lumps of glass beads which tended to coagulate in the application process had a distinct effect upon the ventilation boundaries, and in particular upon post ventilation flow, a method of application was developed which resulted in a relatively uniform coating in which the beads were embedded in varnish, but not fully wetted or coated with the varnish themselves. This was achieved by allowing the varnish, after having been rather sparingly applied, to dry to a tacky consistency and then pouring the glass beads over the foil and brushing off the excess. It was never possible to completely eliminate minute singularities from the surface finish. For this reason, the angles of washout of ventilation are not considered meaningful in a quantitative sense.

Attempts to Influence the Wetted Contact Angle. A demonstration of the properties of a Dow Corning chemical called "Silanox" on the television programme, "Tomorrow's World", instigated the attempt to use it to influence the contact angle of water with a surface piercing strut. Silanox is described by the manufacturer as a "hydrophobic" material. Its general appearance is that of a fine powder, but microscopically it has the appearance of tiny goose down feathers. These "feathers" have the effect of making surfaces to which they are applied nearly completely unwettable, although not affecting their permeability to air, for example. Small water droplets placed on the surface of the NACA 0012 strut, which had been treated with Silanox in the same way that the roughnesses had been applied, retained nearly perfect sphericity or zero contact angle, compared to an angle of about 100 degrees for both the polished and original untreated surfaces, for both the Mk I and Mk II models. (180 degrees would be defined as fully wetted – the droplet would be completely flat.)

Measurement of Surface Contact Angle. The surface contact angles were measured by mounting the struts in a beam of collimated light on an optical comparator and aligning crosshairs with the edges of the enlarged image. This method was not wholly satisfactory, particularly when the drops were nearly spherical, as the droplets acted like lenses which considerably distorted the images on the ground glass screen.

Effect of Immersion on Properties of Silanox. Unfortunately, after the strut coated with varnish and Silanox was immersed in the Channel for testing, the coating quickly became "poisoned" so that after a few runs, its effect resembled that of blotting paper. This was probably due to the effect of residual oils, anti-corrosion and fungicidal chemicals present in the Channel water. Instead of a test of extreme unwettability, it became a test of great wettability.

Application of Wax. Further attempts were made to influence the contact angle by the application of automobile wax to the foil surface. Waxing changed the contact angle from 100 to about 70 degrees. This was considered significant because the change was from somewhat attractive surface forces to slightly repellant. Immersion did not change the characteristics of the waxed surface. In view of the null effect that all of these changes in contact angle had on the ventilation boundaries, (except for some spurious changes induced by the Silanox which will be discussed in the results), no additional attempts were made to study the effect of wettability.

Effect of Roughness on Ventilation: Speed Dependence. The effect of glass-sphere roughness and Silanox-varnish coating on ventilation inception are shown in Figures 5.12 and 5.13. It can be seen that the finest grade of roughness, grade 20, had virtually no effect except at 20 ft/s (6 m/s). At 5 ft/s (1 1/2 m/s), none of the roughnesses had any effect. As speed and roughness increased, the ventilation inception angle decreased. Thus, dependence of inception angle on speed was introduced by the roughness. This was a result not previously observed at subcavitating speeds. At cavitating speeds, the dependence of ventilation angle on speed was related to the increase of the cavitating region with speed. Previous tests by Wright and McGregor[5,6] of the Mk I NACA 0012 model using oil film flow visualisation techniques showed that the area of separation did not change greatly at least between 10 and 15 ft/s (3 and 4 1/2 m/s). The analysis of the last chapter also indicated that for ordinary turbulent separation, the extent will not be highly dependent upon speed, and will probably decrease with increasing speed. Later flow visualisation work with the boundary control models of the present work also demonstrated that the grade 11 roughness did not significantly affect the pattern of separation below the surface seal, although there were some difficulties in using the oil film technique with roughness. This evidence suggests that the important changes affecting the ventilation boundaries took place in the surface seal.

Requirement for Separated Region Decreased. Figure 5.14 shows the extent of the separated region on the NACA 0012 foil as measured by Wright and McGregor at 10 and 15 ft/s (3 and 4 1/2 m/s) as a function of incidence angle. It will be noted that at 10 degrees, there is no tail separation evident. This has been verified by inspecting the original flow visualisation photographs used in the Wright and McGregor tests. However, ventilation was repeatedly encountered at $\beta = 10$ degrees with the grade 10 roughness at 20 ft/s (6 m/s). This implies that the roughness induced earlier tail separation, or that the rate of growth of the boundary layer was such that a sufficient region of low momentum fluid was established for ventilation to occur, without the onset of separation, strictly defined as zero shear stress. If this is truly the case, the implications are very serious for large sizes of hydrofoils, where substantial boundary layer growth will occur in spite of all precautions of smoothness.

Maximum Effect of Roughness. Since the largest roughness continued to produce an increase in effect, it is not possible to say what is the maximum roughness size which would still increase the dependence on velocity. If the effect of the roughness on the surface seal is
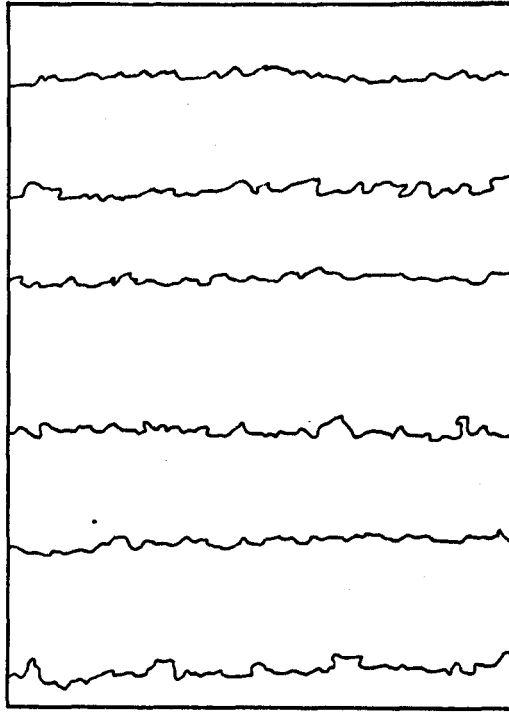
Figure 5.11 – Typical Surface Profiles of 180 Grit Emery Paper (magnification x 50).
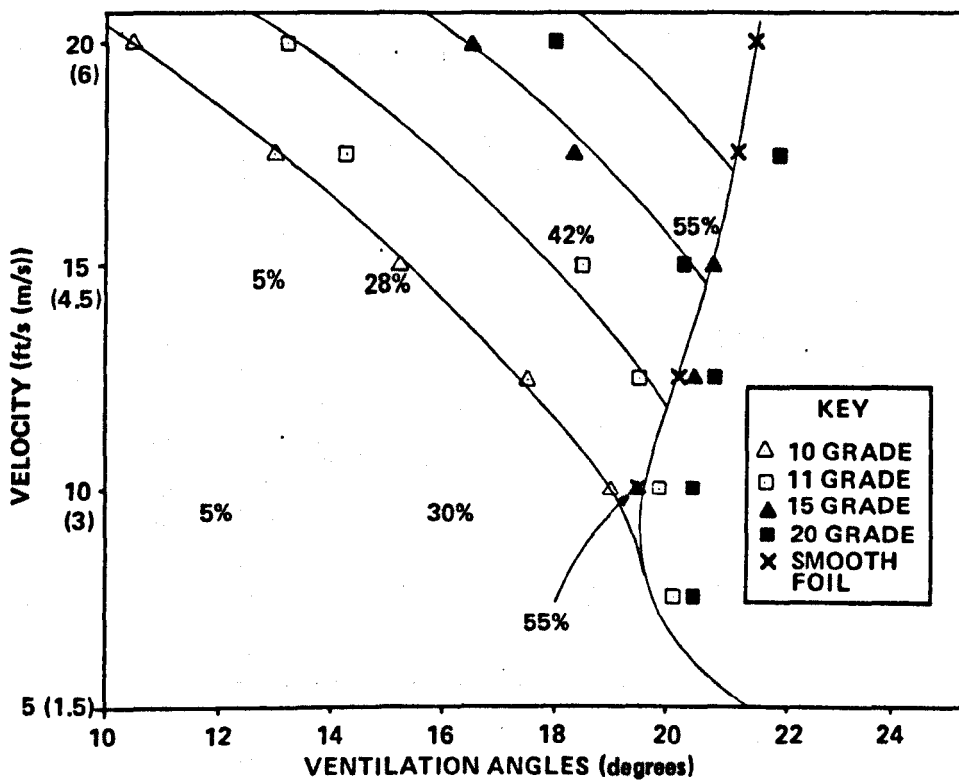
Figure 5.12 – Effect of Roughness on NACA 0012 Strut. Figures Show Amount of Separation Measured in Percent of Chord on Smooth Foil.
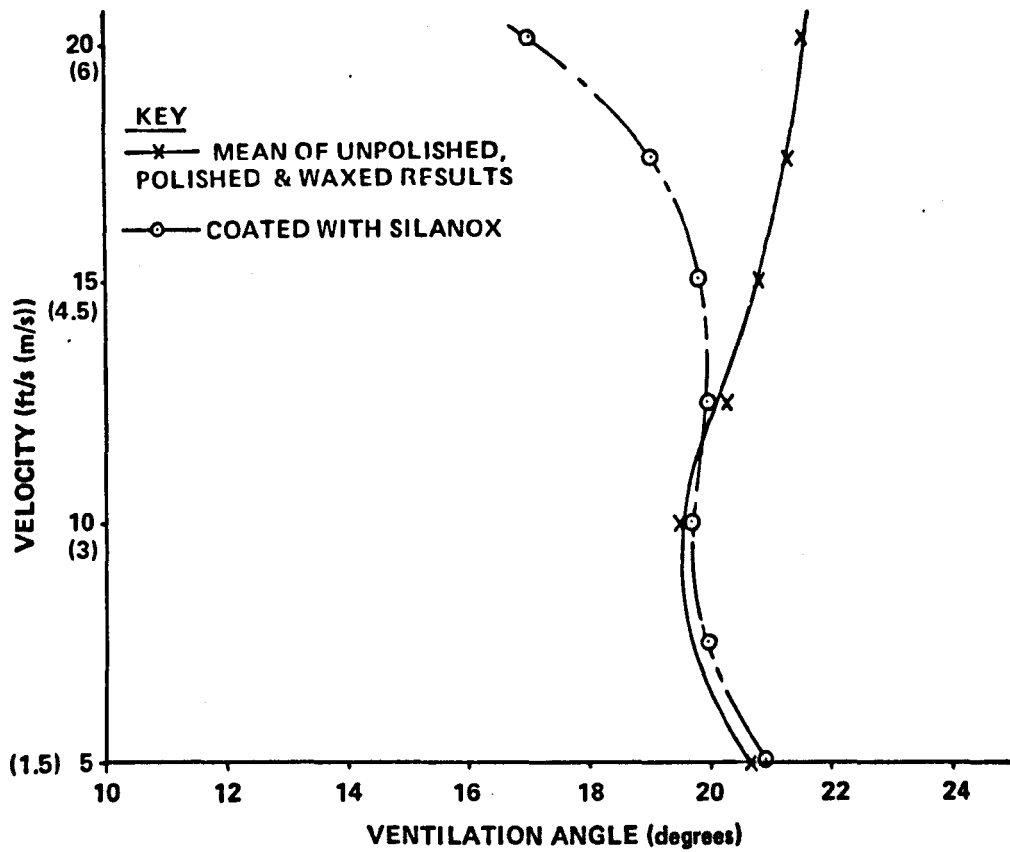
Figure 5.13 — Effect of Surface Contact Angle.
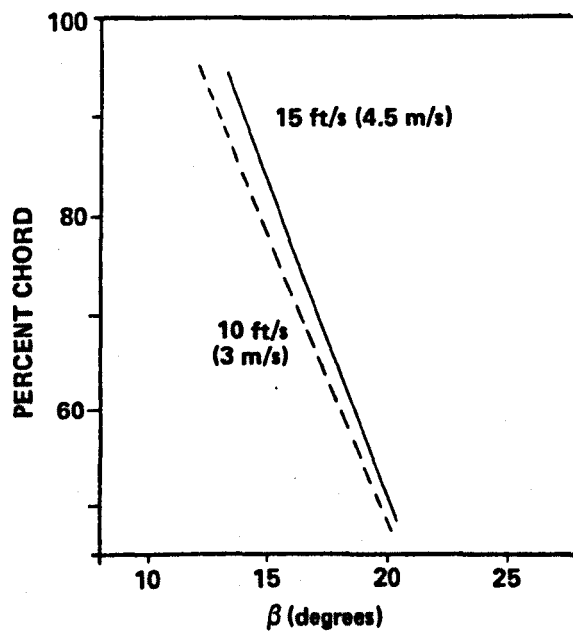
Figure 5.14 — Turbulent Tail Separation as a Percent of Chord for
NACA 0012 Foil. From Wright and McGregor.[5.6]

similar to the effect of the rough water in the tests of Wetzel,[5.4] his results, shown in Figure 5.15, indicate that there is still quite some scope for a decrease in the ventilation angles.

No Gradual Transition Observed. The suggestion of Eames[5.10] that weakening the surface seal . would result in a gradual transition to the ventilated state, was not observed at all. Transition seemed to occur in approximately the same time and in the same manner in both the rough and smooth conditions.

Effect of Silanox on Ventilation. The Silanox powder affixed with an undercoat of varnish had nearly exactly the same effect on inception angles as did the grade 15 roughness, which relates to the subjective impression of roughness given by the coating.

Effect of Polishing, Waxing, and Varnishing on Ventilation and Washout. The finer surface finish achieved by polishing, and the change in surface contact angle achieved by waxing, and the surface change caused by the application of varnish had no measurable effects whatsoever on the ventilation properties of the strut throughout the range of conditions tested.

Effect of Roughness and Silanox on Washout. The effect of roughness on washout angles was difficult to assess because individual roughness singularities, which were impossible to avoid in the application of the glass beads and the Silanox, tended to cling to partial and isolated vented cavities long past the point where the experience with the smooth foil would have indicated. Because the cavities clinging to the roughnesses were often isolated, if the angle was held still for long enough, they would eventually wash away. This meant that the washout angle was very dependent upon the rate of decrease of angle. Therefore determination of the washout angle was a somewhat subjective operation. Once a cavity had collapsed to the point where it was thought to be no longer stable, the angle was held constant for a few moments to see if washout would complete. No systematic procedure was adopted, so the results are not meaningful except in a gross sense. Figure 5.16 shows the washout angles as a function of speed for the various surface treatments. As expected, contradictory trends may be observed. For example, the second coarsest and the second finest roughness had no effect on washout, while the coarsest and finest delayed washout by 2 degrees or 3 degrees. Significantly, no roughness coating increased washout angle. Therefore it is interesting that the Silanox coating increased washout angle by from 2 degrees to 3 degrees, independently of speed. Observations suggest that the increased wettability, or blotting paper effect, allowed

94
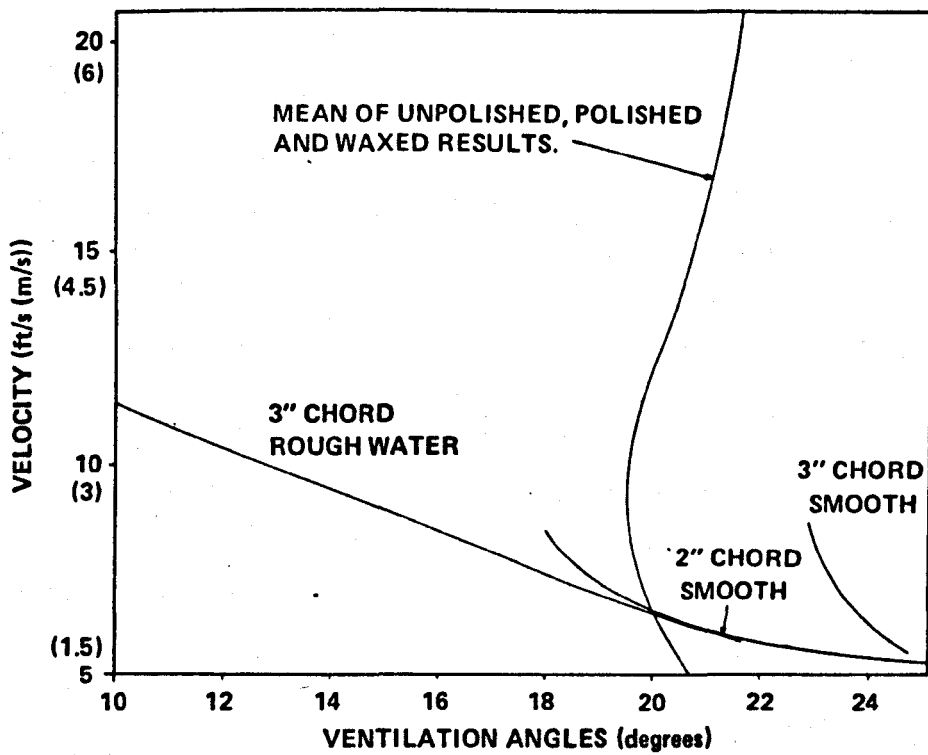
Figure 5.15 — Wetzel[5.4] Results with NACA 0012 Foil, in Smooth and Rough Water Compared to Results of Present Smooth Foil Tests.
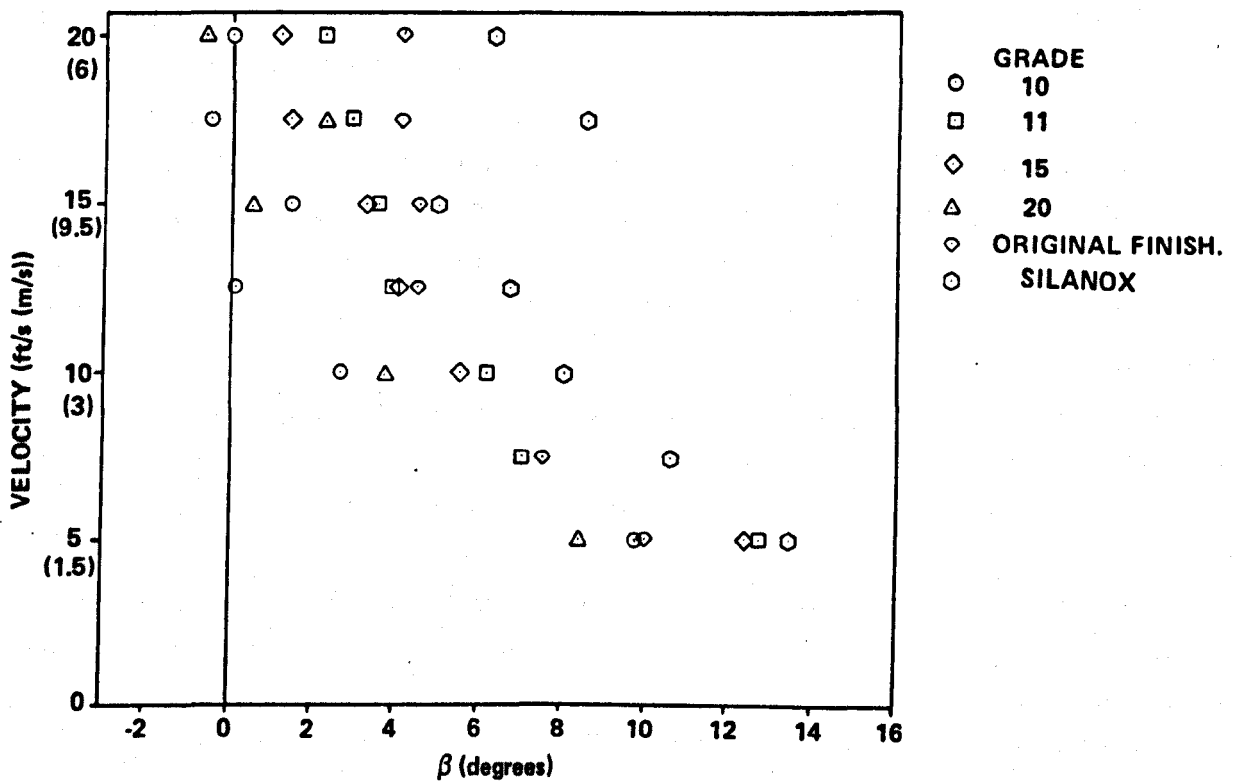
Figure 5.16 — Washout Angle vs Speed for NACA 0012 Mk II with Roughness, Silanox Coating and Plain.

95

the cavity closure sheet to attach itself to the strut more readily. These observations of cavity closure also indicate that the mechanism of closure at this scale may be spurious in respect to full scale boats. As the sideslip angle is decreased, a thin film of water bridges the cavity at the nose of the strut, and slowly works its way aft, choking off the air supply and isolating the cavity from the atmosphere after which it collapses. The thinness of the sheet and its glassy appearance clearly indicate that surface tension is an important factor in its formation. The attractive effect of the blotting paper surface provided by the Silanox is also apparently important. Obviously, neither of these effects would be significant at full scale speeds. Similar observations were made by Breslin.[5.9] Furthermore, because of the relatively low levels of turbulence at the model scale in the wake, the demand for air to replace entrained air is relatively slight. A similar sheet to the closure sheet observed in the model case would have to disrupt an air flow of far greater momentum at full scale conditions.

Differences Between Mk I and Mk II Models. A comparison was made of the results of previous tests of the Mk I NACA 0012 model in the Channel due to Wright and McGregor and the present tests of the Mk II. In order to clarify the discrepancy between the two, the tests on the Mk I were repeated, using only port angles of sideslip, as was the case in the previous tests. The results obtained in this way were in fair agreement with the previous tests, but still lay outside of what was thought to be the experimental error. Averaging port and starboard runs with the Mk I brought the results into complete agreement at the lowest and highest speeds with the Mk II data, but left a maximum difference of about 1 1/2 degrees at the intermediate range between 6 and 17 ft/s (2 1/2 and 5 m/s). This is only just outside the routine variation between runs, and the slight difference can probably be attributed to the microscopically greater thickness of the Mk I model as shown by the measured offsets of Figure 5.8. This experience emphasised the importance of making runs to port and starboard, no matter how much care is taken to center and align the model. The possibility of major discrepancies being caused by minor differences in surface finish or composition was eliminated, at least for models whose characteristic mode of ventilation is tail ventilation.

Implications of the Null Effect of Wettability. The result of the wettability variation on ventilation inception shows that the model size and velocities used in the experiment, and similar experiments at the University of Leeds, are outside the range of influence of molecular effects, probably including surface tension. The fact that there was a small effect due to contact angle on the cavity closure indicates that the use of smaller models would be inadvisable.

Implications of the Roughness Results. The important question which the roughness results raise is whether an increase in Reynolds number would have the same effect as the roughness. As discussed in Chapter 4, the greater thickness of the boundary layer and the increased turbulence as well as the effect of shipyard construction would all tend to have an effect similar to that of roughness. The pronounced effect that roughness had on both inception and washout is grounds for hesitation in applying the results of smooth model tests directly to full scale.

Laminar vs Turbulent Surface Seal. It is possible that the flow in the surface seal was laminar in the cases studied. In flow visualisation studies on thicker foils reported in Chapters 9 and 10, transition from laminar to turbulent flow was observed with increasing incidence angle in the speed range of the tests. The flow near the surface did not show any evidence of transition, but the oil smear pattern was difficult to interpret in the region. Based on the smooth flat plate criterion,[5.11] the flow in the zero pressure gradient surface seal should have been laminar at least to the 50 percent of chord point at the highest speed tested of 20 ft/s (6 m/s). Because of the background turbulence of the tunnel, the ordinary criterion of transition may not have applied. However, it may have been that the effect of roughness was primarily to trigger transition to turbulent flow where it would not otherwise have occurred. It is difficult to say whether the surface seal would be stronger if the flow in it were laminar or turbulent. The turbulent boundary layer has more net local momentum in the region close to the strut surface, which would have the effect of making it less permeable, but, the greater overall momentum loss due to turbulent mixing from the free stream and the higher incidence of velocity fluctuations would tend to weaken the seal.

Calculation of Boundary Layer and Roughness Reynolds Number. If the boundary layer in the surface seal is assumed to be laminar, at least for the first 0.1 ft of flow past the strut (30 mm), then the velocities in the surface seal can be calculated from the following formula which governs the growth of a laminar boundary layer in the absence of a pressure gradient (flat plate analogy). The momentum thickness, θ, as previously defined may be found from the expression, based on exact theory (from Schlichting,[5.11] attributed to Blasius).

$$\theta = 0.664 \sqrt{\frac{\nu x}{U_\infty}}$$

The velocity at a point a distance y from the strut surface is given by an empirical formulation from Schlichting

$$\frac{u}{U_\infty} = \frac{3}{2}\frac{y}{\delta} - \frac{1}{2}\left(\frac{y}{\delta}\right)^3$$

where δ is the distance from the boundary at which $u/U_\infty = 0.99$. The value of δ is approximately given by $\delta = 8.51\,\theta$, another empirical relationship, from Rosenhead,[5.12] attributed to Young and Winterbottom.

If a roughness Reynolds number $R_k \equiv u_k k/\nu$ is defined,

where $\quad$ k = the roughness height

$\quad\quad\quad$ u_k = the streamwise velocity in the boundary layer at the height of the roughness

and the other symbols are as previously defined, then according to experimental evidence presented by Dommet,[5.13] transition to turbulence will not occur if $R_k < 200$ and transition will definitely occur if $R_k > 600$. $\cdot R_k$ can be calculated from the above expressions. Table 5.1 below gives the values of R_k and the velocity u_k in the boundary layer at the roughness height, k, for the four grades of roughness used in the experiment and for the speeds at which the roughnesses just started to take effect, U_{eff}. Also shown are values of δ, δ^*,

where $\quad$ $\delta^* = \displaystyle\int_0^\infty 1 - \frac{u}{U_\infty}\,dy$, θ, k/θ, and k/δ^*.

TABLE 5.1

k inches x 10⁻³	k mm	U_{eff} ft/s	U_{eff} m/s	R_k	δ inches x 10⁻³	δ mm	δ* inches x 10⁻³	δ* mm	θ inches x 10⁻³	θ mm	k/δ	k/δ*	k/θ	u_k ft/s	u_k m/s	u_k/U_{eff}
2	.053	20	6	60	15½	.40	4¾	.12	1.8	.047	.13	.42	1.1	3.8	1.2	.19
3½	.090	17½	5¼	150	16½	.43	5	.13	2.0	.050	.20	.69	1.8	5.4	1.6	.31
10	.249	15	4½	870	18	.46	5½	.14	2.1	.054	.55	1.83	4.7	11.2	3.4	.74
12½	.318	12½	3¾	1000	20	.50	6	.15	2.3	.059	.63	2.10	5.4	10.2	3.1	.82

From the table, it appears that there is no correlation between the roughness Reynolds number required for transition to turbulence and the velocity at which the roughnesses became effective. Because of the approximations used, this analysis cannot be considered conclusive proof that the explanation for the effect of roughness is not the triggering of transition to turbulent flow in the surface seal. The principal error is probably the assumption that the laminar boundary layer grows in the same manner as it does on a smooth surface, until the transition point is reached. The magnitude of the roughnesses compared to the momentum thickness which would result from this assumption, shown in the table, indicates that the roughnesses would have been a significant factor in the initial development of the boundary layer.

Effect of Trip Wire Compared to Uniform Roughness. Breslin[5.9] tested the NACA 4412 strut with a 0.01 inch (0.25 mm) diameter trip wire, apparently about 5 percent of chord behind the leading edge. His results are shown in Figure 5.17 compared with the roughness results of the present study. The effect of the trip wire is about the same as the grade 11 roughness which had an upper boundary limit on diameter of approximately 0.01 inch (0.25 mm), the same as the trip wire diameter.

Effect of Trip Wire Not Piercing Surface Seal. That the principal effect of the trip wire in encouraging ventilation is on the surface seal is corroborated in an article by I.I. Isayev.[5.14] Although no ventilation data was reported, trip wires of 0.04 inch (1 mm) diameter applied at 7 percent aft of the leading edge of one foot (300 mm) chord struts tested at Reynolds numbers between 5 and 10^5 (5-10 ft/s, 1 1/2-3 m/s) resulted in premature ventilation of the struts, presumably at angles of less than the largest for which force coefficients were presented, which was 10 degrees. When the trip wire was installed a distance below the free water surface of 3 to 5 percent of chord below the surface seal, the premature ventilation was no longer observed. The aim of the Isayev work was to quantify force coefficients. Interestingly, he found that use of the trip wire increased lateral forces on struts by more than 200 percent, which he attributes to elimination of laminar separation. Thus the effect of trip wires, and by implication of all roughnesses, is to increase the spanwise pressure gradient by ensuring fully turbulent flow, to provide microscopic areas of separation, and to disrupt the surface seal. In flow which would otherwise be fully turbulent, the first effect would not arise. In the present tests of the NACA 0012 foil, previous investigations had already shown that the laminar separation area was not significant so far as force coefficients were concerned. Therefore, in the present tests, the effect of roughness on the spanwise pressure gradient would not be important, at least at the higher speeds. It is not possible on present evidence to separate the other two effects, microscopic separation and disruption of the surface seal.

Other Possible Explanations. Other possible effects besides the initiation or supplementation of turbulence could account for the effect of roughness. For example, the microscopic regions of separation associated with individual roughnesses might link together to form a low energy path. This would not explain the speed dependence or the dependence on roughness size. Likewise vorticity created by the microscopic spheres could do the same. At higher speeds than those tested, individual roughness elements could cavitate and individually ventilate to trigger a path to the low pressure separated or cavitating region. All of these alternate explanations are closely linked to the phenomenon of turbulence generation.
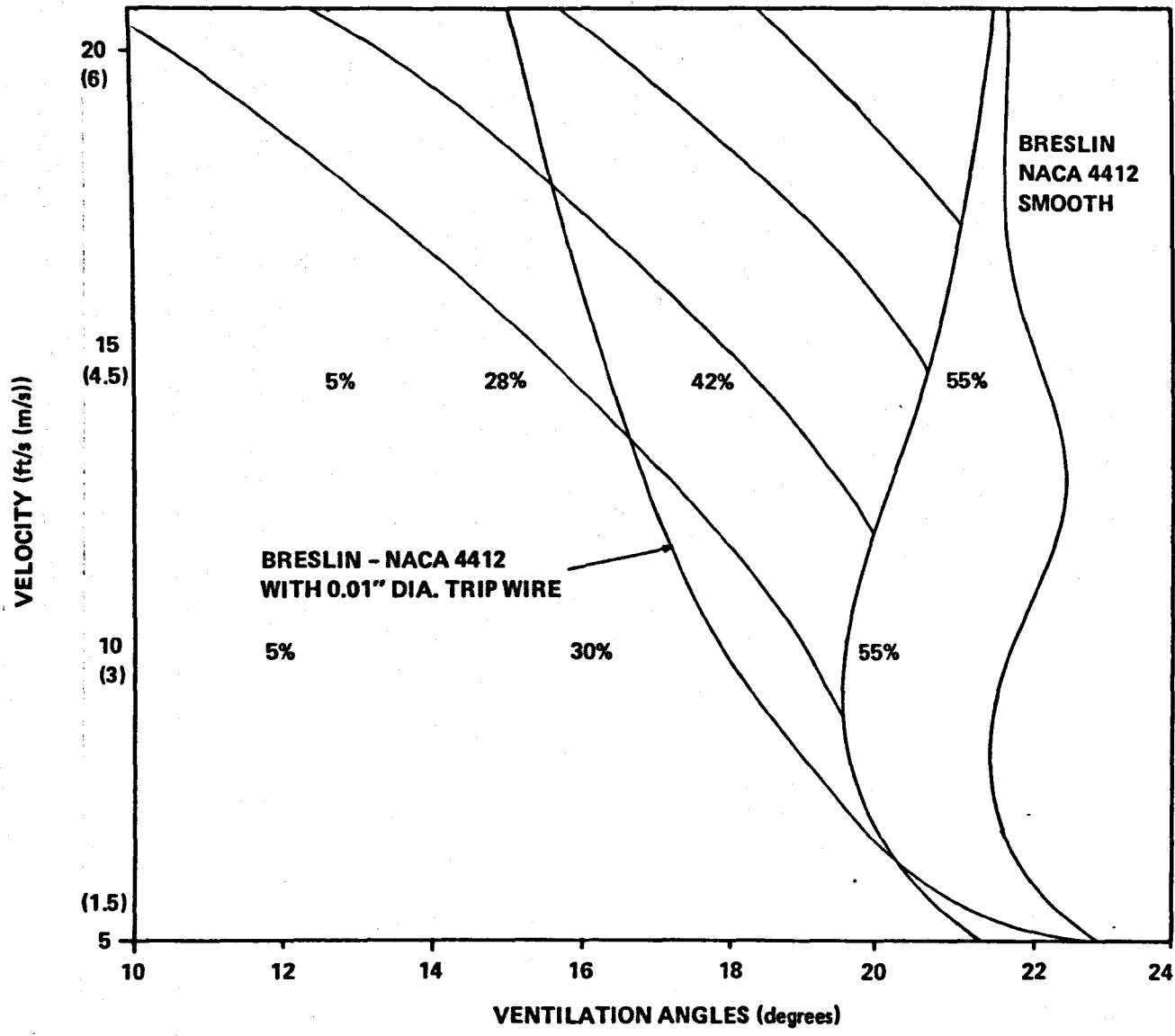
Figure 5.17 — Breslin[5.9] Trip Wire Data Compared to Results of Present Study.

A study in greater detail than the present one would be necessary to give the definitive explanation of the effect of roughness.

Enough evidence has been presented to create a good circumstantial case for the effect of roughness being similar to that of increased speed. To be useful, criteria will have to be developed to correlate to exact size of roughness required in model test to simulate full scale conditions. At some point, more carefully controlled tests than have yet been performed will have to be accomplished under full scale conditions. As a first step in this direction, and to shed further light on the effect of roughness, an additional test was performed with the model used in this study in the University of Leeds High Speed Single Shot Water Channel, at speeds up to 62 ft/s (19 m/s), which is described in the following chapter.

CONCLUSIONS OF THE ROUGHNESS AND WETTABILITY STUDY

The application of roughness above a minimum size to a surface piercing strut reduced the ventilation angle at a given speed, the effect becoming more pronounced with increasing speed and increasing roughness size. Probably, the principal action of roughness is to weaken the surface seal, first by causing transition to turbulence and then encouraging the growth of the boundary layer. The effect may be similar to that of increased speed or size.

Roughness probably does not have a great effect on the extent of the separated region, except possibly by the elimination of laminar nose bubbles, but the thickening of the boundary layer caused by roughness may effectively behave as a separated region.

Data of Wetzel and the trends observed with increasing roughness diameter suggest the maximum effect of applied roughness in reducing ventilation boundaries was not reached in the present work.

Weakening of the surface seal did not result in a gradual transition to the ventilated state.

Treatment of the strut surface with Silanox had approximately the effect that a comparable roughness had.

Contact angle had no effect on ventilation or washout except an anomalous effect on washout observed in the case of Silanox treatment.

Roughness generally had a delaying effect on washout, with a tendency of cavities to cling to isolated roughnesses to negative incidence angles.

Effects due to surface finish variations between models finished to ordinary hydraulic smoothness standards are insignificant.

The null effect of contact angle implies that surface tension is not important at the sizes and speeds used in this study.

5.1   Swales, P.D., Wright, A.J., McGregor, R.C., Cole, B.N., *"DREA Hydrofoil Project Interim Report, 1st April - 31st July 1971,"* Univ. Leeds Dept. Mech. Eng. Res. Rept. TP/DREA/2, July 1971.

5.2   Perry, Byrne, *"Experiments on Struts Piercing the Water Surface,"* Cal. Inst. Tech. Rept. No. E-55.1, 1954.

5.3   Kiceniuk, Taras, *"A Preliminary Experimental Study of Vertical Hydrofoils of Low Aspect Ratio Piercing a Water Surface,"* Cal. Inst. Tech. Rept. E55.2, 1955.

5.4   Wetzel, Joseph M., *"Ventilation of Bodies Piercing a Free Surface,"* Second Symposium on Naval Hydrodynamics, Office of Naval Research, 1958.

5.5   Hunter, B., Swales, P.D., Cole, B.N., *"Variable Pressure Water Channel,"* The Engineer, Vol. 225, pp. 515-519, March 1968.

5.6   Wright, Alastair J., and McGregor, Robert C., *"DREA Hydrofoil Project Interim Report, 1st Dec 1971 - 31st March 1972,"* Univ. Leeds Dept. of Mech. Eng. Res. Rept. TP/DREA/4, March 1972.

5.7   Smith, Gary L., *"An Investigation of Ventilated Cavities Associated With Bodies Piercing a Free Water Surface,"* Ph. D. Thesis, Univ. of Leeds, Dept. of Mech. Eng., 1970.

5.8   McGregor, Robert C., *"DREA Hydrofoil Project Interim Report, Appendix F,"* Univ. of Leeds Dept. Mech. Eng. Res. Rept. TP/DREA/3, Nov 1971.

5.9   Breslin, John P., and Skalak, Richard, *"Exploratory Study of Ventilated Flows about Yawed Surface-Piercing Struts,"* NASA MEMO 2-23-59W, April 1959.

5.10   Eames, M.C., Discussion of Ref. 2.2, Second Symposium on Naval Hydrodynamics, Office of Naval Research, 1958.

5.11   Schlichting, Hermann, *"Boundary Layer Theory,"* McGraw-Hill, 1960.

5.12   Rosenhead, L., *"Laminar Boundary Layers,"* Oxford, Clarendon Press, 1963.

5.13   Dommet, R.L., Journal Royal Aeronautical Society, Vol. 63, pp. 722, 1970.

5.14   Isayev, I.I., *"Scaling Effect on the Magnitude of the Lateral Force Acting on an Isolated Hydrofoil Strut,"* Sbornik Statey po Gidromekhanike i Dinamike Sudna, (Russian) pp. 158-162, 1967.

CHAPTER 6

ROUGHNESS AND HIGH SPEED
EXPERIMENT

CORRELATION OF ROUGHNESS WITH SPEED

Background. The experiment of the previous chapter showed that the principal effect of roughness was to weaken the surface seal, probably by promoting turbulence and boundary layer growth. The experimental results also raised the possiblity that boundary layer growth below the surface seal may relax the constraint that a region of separation exist prior to ventilation in the strict sense of zero shear or reverse flow. The earlier discussion in Chapter 4 as well as Chapter 5 suggested that the effect of high speed and large size might well be similar to that of roughness, by encouraging turbulence and boundary layer growth. To test this hypothesis, the same NACA 0012 Mk II model used in the Roughness and Wettability Experiment in the Recirculating Channel was mounted in the High Speed Single Shot Water Channel. In the High Speed Channel, this model, which had been thoroughly characterised at low speed and with roughness, could be subjected to a much higher flow velocity to explore the analogy of high speed to roughness. In addition, it was hoped that the difference between the types of ventilation reported at high speeds and at low speeds could be explained. As discussed in Chapter 2, tests at high speeds at the David W. Taylor Center did not reveal evidence of the nose mode of ventilation reported by investigation at Leeds in testing at lower speeds.

Outline of the Experiment. Tests were performed in the High Speed Channel, which had a 9 inch wide (229 mm) working section. The 4 inch (102 mm) chord NACA 0012 Mk II strut was suspended vertically piercing the free water surface to a depth of 10 inches (254 mm). The tip of the strut was held in a bearing flush with the floor of the test section. The model was tested at constant speed during a run, over a speed range from 15 ft/s (4 1/2 m/s) to 62 ft/s (19 m/s), the maximum possible in the channel. For each run, the incidence angle was increased at a controlled rate to the ventilation boundary, then reversed to the point of ventilation on the opposite side, if run time permitted. Port and starboard angles were not averaged, but presented separately in the results. Tests were made with the smooth strut and again with grade 10 glass spheres imbedded in varnish on the strut surface. Cine films synchronised with stroboscopic lighting were taken, at frame rates of 2000 to 10,000 frames/s, of ventilation inception on both the rough and smooth struts over a range of speeds.

High Speed Single Shot Water Channel. The High Speed Channel[6.1] was a free surface water channel capable of operating at speeds up to 62 ft/s (19 m/s). (Figure 6.1) These speeds were achieved by discharging 10,000 gallons (51 cubic metres) from a head tank 80 ft (25 m) above the laboratory floor through an 18 inch diameter (457 mm) pipe and appropriate valves and connections pipes to the working section and thence to a sump. The working section size was 9 in. square by 4 1/2 ft long (229 mm x 1.37 m). The circuit layout can be seen in Figure 6.1. The headtank was recharged in about 5 minutes between runs with a single centrifugal pump, due to the unavailability of the second pump designed for use with the system. Another 5 minutes was usually allowed for settling and de-aeration. A manually operated butterfly valve before the stilling section isolated the equipment when not in use. When the channel was in use, the valve was fully opened. The disc was shaped to provide minimal interference with the flow. The rate of flow was set by a second valve of the same type but pneumatically controlled, which was situated 17 diameters upstream of the working section. Thin turning vanes at each of the corners after the flow control valve, and an aluminium honeycomb upstream of the contraction acted as flow straighteners. The stilling section was short because of the limited space available, and the contraction ratio of only 4.5 : 1 gave rise to some doubts about the uniformity of the flow. Hunter et al [6.1] performed a velocity survey using a pitot-static tube, and acceptably uniform distributions were found – a typical result is shown in Figure 6.2. The free surface was level and remained at a constant height but was rendered opaque by the mass of capillary waves associated with supercritical flow. To ensure smooth starting, there was a flap valve downstream of the working section, which automatically operated in concert with the velocity control valve to maintain the free surface at a more or less constant height during starting. Downstream of the flap valve, the water discharged freely into a large chute and thence into the sump. A splitter plate reduced the froth from the wake, and a baffle reduced surface disturbance and air entrainment in the sump. In spite of the plate and baffle arrangement, or perhaps because of it, the tip vortex from the NACA 0012 strut frequently became aerated in the sump, provoking premature ventilation. This problem was overcome by mounting the model so that the tip was nearly flush with the channel bottom, thus eliminating the tip vortex.

Blockage Effects. The effect of blockage in the High Speed Channel was discussed indirectly in the last chapter, in which it was noted that for a comparable speed, the results of the Recirculating Channel agreed well with towing tank data for which no blockage or wall effects
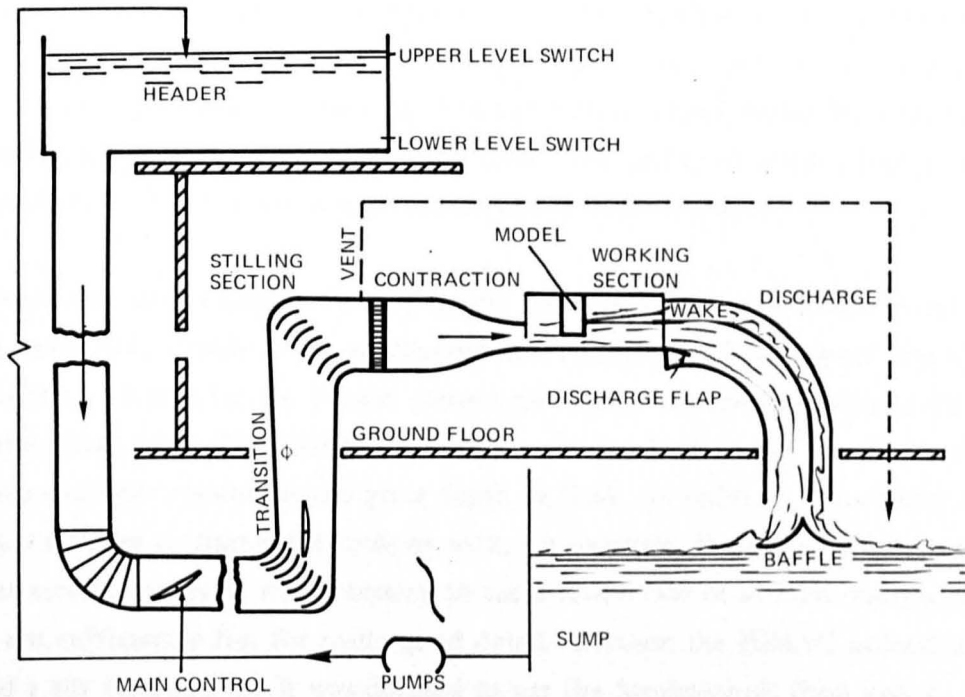
Figure 6.1a – Circuit Diagram of High Speed Channel.
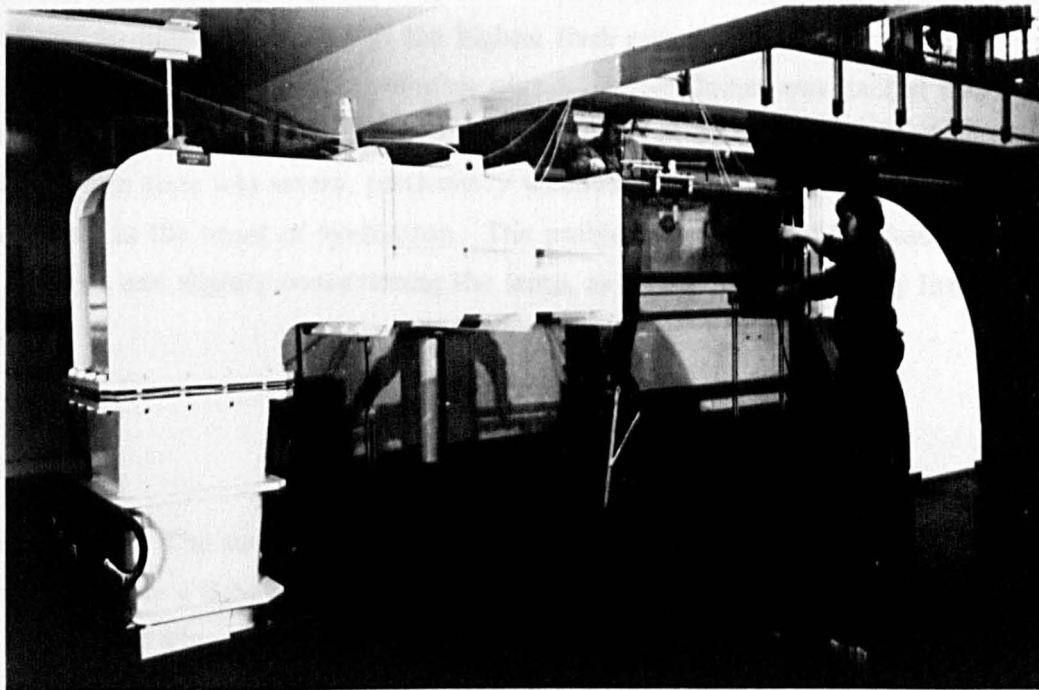
Figure 6.1b – Photograph of Working Section of High Speed Channel.

were present, but the tests in the High Speed Channel produced ventilation angles that were 3 to 4 degrees higher than would have been expected. For the case of rough models, the ventilation angles in the High Speed Channel were somewhat lower than in the Recirculating Channel, indicating that the less uniform flow in the High Speed Channel interacting with the roughness tended to overshadow the delaying effect on ventilation that the blockage apparently had on the smooth model. While the effects of blockage were undoubtedly significant, the point of the experiment was to identify trends and mechanisms, rather than produce numerical results that could be directly applied to full scale. The ability to achieve higher velocities necessitated the sacrifice of more ideal conditions in other respects.

Cine Camera and Strobe Light. To photograph the inception of ventilation in the hopes of revealing some more details of the mechanism and the effects of high speed and roughness, a Hitachi HIMAC 16 mm motion picture camera was used, synchronised with an Ernest Turner stroboscopic flash unit. The HIMAC camera was equipped with a 50 mm Macro Nikkor lens which gave excellent resolution and great depth of field. In order to reduce blur and to have a sufficient number of frames for analysis with, for example, the same bubble or perturbation visible for several frames, it was necessary to use a frame rate of at least 4000/s, and even this was not sufficiently fast for really good detail. Because the HIMAC utilised a rotating prism and a slit type shutter, it was decided to use the Stroboscopic flash unit to ensure a sharper image than would have been obtained with incandescent lighting. The combination of camera and flash unit together were capable of frame rates of 10 000/s, but the light intensity was reduced to impractical levels at the highest flash rate. Because of the high energy level per flash, (1 to 3 joules) the total number of consecutive flashes was limited to 2000, before it was necessary to allow the lamp to cool. Obviously, at 10 000 frames/s, the limitation imposed on run time was severe, particularly when trying to capture something as relatively unpredictable as the onset of ventilation. The problem was resolved by shooting most runs at 4000 frames/s and slightly overstressing the lamp, as well as throwing away literally miles of film.

PROCEDURE

Synchronisation. The strobe light was synchronised to the camera shutter by means of a pulse generated by a light sensitive electronic element in the camera which sensed the position of an illuminated wheel with two through holes drilled at right angles to each other and the axis of rotation and coupled to the 4-sided prism drive. This was found to be highly sensitive

to blockage by scraps of film debris, and a magnetic pickup is recommended for future work. The signal from the photocell was fed to a line driver, and thence to a pulse shaper. This signal drove the strobe unit through a time limit device to protect the lamp from over firing. A time code generator was also used which had to be synchronised with the light and camera. Each element of the system had a different delay time to start – the camera had to accelerate to speed before the light could be fired, the light had a delay time between the time it received the "fire" signal and the first flash, and the time code generator could not be fired until an appropriate amount of film had run through the camera, since each reel had to be exposed twice – once at the beginning and then at the end, to get maximum use of the camera acceleration overlap. Each delay was dependent upon frame rate, which varied according to the channel velocity – unnecessarily high frame rates reduced run time and wasted film. Under certain conditions, it became necessary to sacrifice the advantages of stroboscopic lighting and revert to incandescent lights to achieve longer duration of the filming. In the end, representative ventilation inceptions were filmed over the entire range of velocities tested for the smooth foil, but only one photograph of inception with roughness was obtained, due to the extremely erratic nature of the onset. The first attempt at cine photography was extremely lucky. Ventilation inception was captured at 62 ft/s (19 m/s). No positive results were again achieved until some time later, after modifications had been made to the piping system of the channel to service other laboratory apparatus. The photographic quality of the water was never again as good during the rest of the experiment, in spite of nearly constant operation of the filtering system.

Yaw Rotation. Rotation of the strut to the required incidence angles was accomplished by mounting the model above the working section, attached firmly to the shaft of a 1000:1 TASC unit driven by a synchronous motor with electirc clutch and brake (Figure 6.3). The apparatus was originally designed to test the dependence of ventilation angle on the rate of increase of the sideslip angle during runs at constant speed. The control system of the device allowed the ventilation angle to be approached at a constant rate of 1 degree/s, previously established by Wright et al[6.2] to give consistent results for the NACA 0012 shape. Because the run duration was only about 45 seconds at the highest speeds, a rate of 2 degrees/s was used to traverse from port to starboard after inception had been recorded on the port side, thus enabling data from both points to be established during the same run. The yaw rate was reduced to 1 degree/s significantly before ventilation inception.
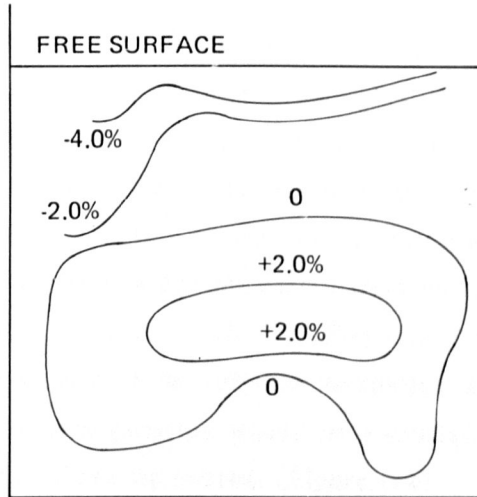
Figure 6.2 – Velocity Distribution in Channel Working Section at 15 ft/s (4.5 m/s). Figures Are Percentage Variations from Mean Velocity. From Hunter et al[6.1].
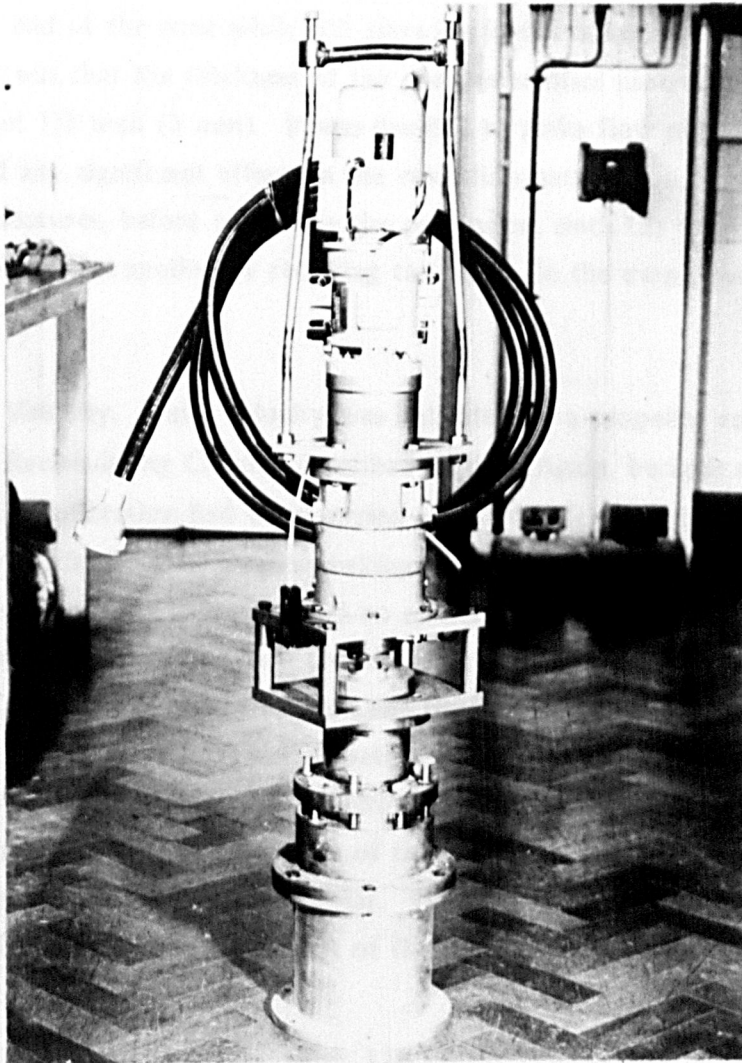
Figure 6.3 – Photograph of Rotation and Mounting Mechanism

Mounting of Model. In preliminary tests, the model was mounted in the same way that it was in the Recirculating Channel, suspended vertically piercing the surface to a depth of about 2 chords. As noted previously, this resulted in many cases of premature ventilation via the tip vortex, which became aerated in the exit of the working section to the sump. This mechanism was not available in the fully closed Recirculating Channel. Besides the tip vortex problem, observations of bending of the strut during the preliminary test spurred calculations then being undertaken of the potential loads and bending to be expected at the highest speeds. Since the tip of the strut as originally mounted was quite close to the bottom of the channel (0.2 chord), conservative estimates of the effective aspect ratio led to the conclusion that at 62 ft/s (19 m/s), there would be unacceptable bending and the possibility of complete structural failure. Recomputation of the relevant parameters assuming the strut supported at both ends indicated that this configuration would be a satisfactory solution from all stand-points, including elimination of the tip vortex. (Figure 6.4)

Therefore a circular disc was fabricated and attached to the lower end of the strut. This disc was allowed to rotate within a concentric disc fixed to the channel bottom, effectively fixing the lower end of the strut while still allowing free rotation. The only disadvantage of the arrangement was that the thickness of the concentric discs protruded above the floor of the channel about 1/8 inch (3 mm). It was decided to make flow observations to determine whether this had any significant effect on the cavitation patterns on the strut or other noticeable flow features, before correcting the protrusion, since the transparent floor of the channel would have been spoiled by recessing the discs. In the event, the disturbance proved to be negligible.

Measurement of Velocity. Water velocity was indicated by a propellor anemometer similar to that used in the Recirculating Channel described earlier. Again, because of the blockage effects, once initial calibration had been carried out, it was felt that the best indication of velocity with the model installed in the working section was the velocity which would have obtained with the same valve geometry and no model present. The pneumatic control valve was found to repeat its setting within a few thousandths of an inch – the major error being the coarseness of the pressure gauge used on the pneumatic system. The high speed cine film system was used to photograph the anemometer propellor to obtain an accurate calibration of that instrument. Velocity fluctuations were then estimated from the films by tracking bubble paths. Polaroid pictures were taken of the trace over the face of an oscilloscope screen of the pulse output of the anemometer. The variations in period of the pulse were then measured. Fluctuations of 10 percent of the nominal velocity were observed at the
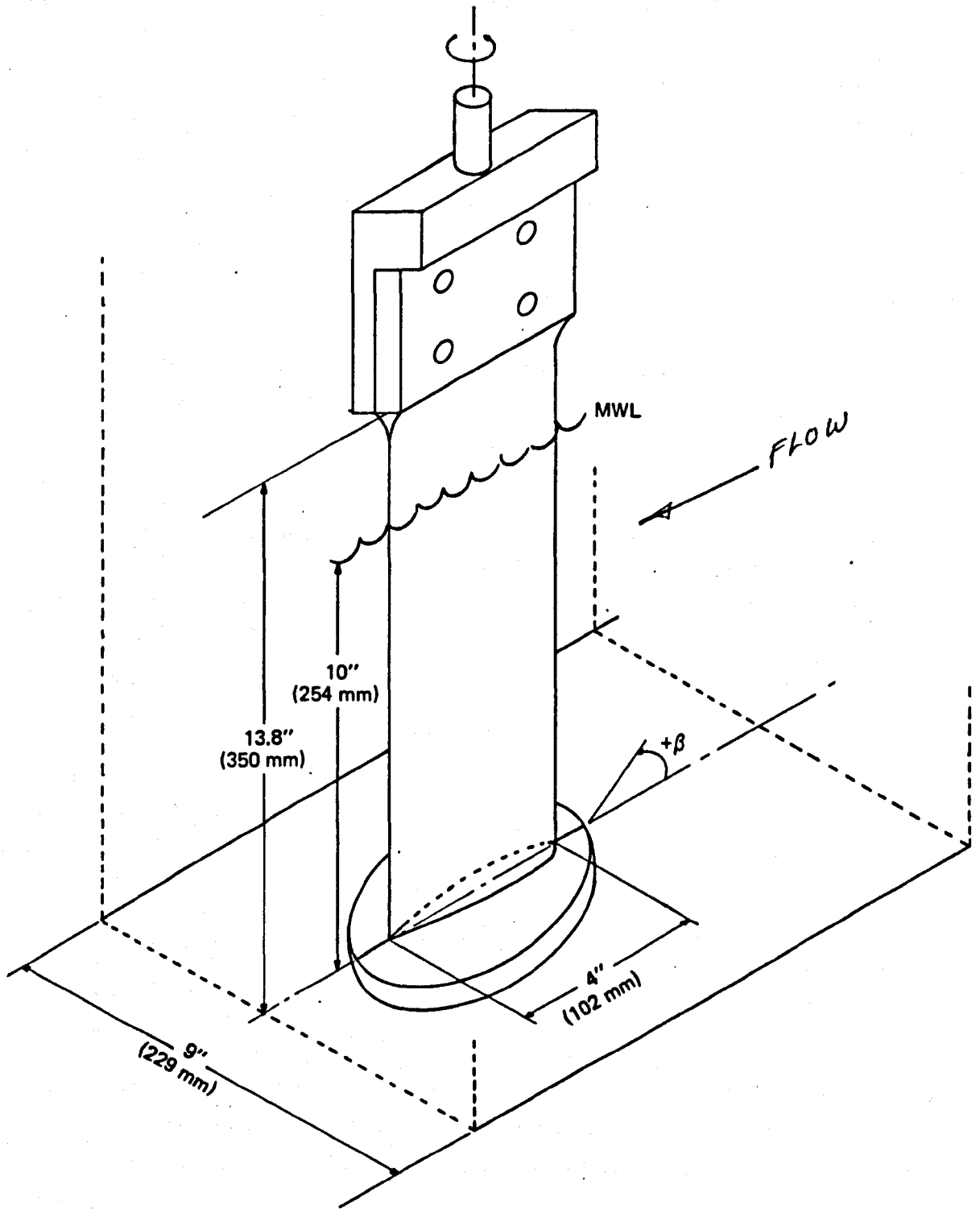
Figure 6.4 — Sketch of Method of Mounting NACA 0012 Mk II Strut
Showing Principal Dimensions.

higher speeds. The uncertainty of the effective mean velocity and the fluctuations are not thought to affect the experimental results, or the conclusions, which are mostly qualitative.

Roughness Application. The grade 10 roughness was selected for application to the strut for the high speed test, because it was thought that the limit of maximum effect might be reached. It was not possible to conduct tests on a full range of roughnesses. The application procedure was the same as described in the prededing chapter.

<div align="center">

RESULTS AND DISCUSSION

</div>

Inception Angles. The ventilation inception angles recorded for the 0012 strut without and with roughness are shown in Figures 6.5 and 6.6, respectively. Also shown on the figures is the boundary for cavitation inception. The curve of the cavitation inception boundary was derived on the assumptions that

(a) The minimum pressure is a linear function of the sideslip angle – that is, the minimum pressure behaves similarly to the overall lift coefficient.

(b) The minimum pressure at zero incidence is small (in absolute value) compared to the minimum pressure at two degrees

Then a cavitation boundary is defined by

$$\sigma_i(\beta) = \sigma_i(2°)(\beta/2° - 1)$$

where $\sigma_i = (P_A - P_V)/\frac{1}{2}\rho U_i^2$

P_A = the ambient pressure

P_V = the vapour pressure of water

ρ = the mass density of water

U_i = the velocity far upstream of the strut at inception of cavitation

β = the sideslip angle or angle of incidence

The observed inception points fit this curve rather well. Since no sophisticated means of detecting inception were used, and it is a notoriously subjective decision as to when inception occurs, the calculated boundary was considered adequate for comparison with the ventilation boundary.

The percent figures on the graphs represent the percentage of chord of turbulent tail separation measured by Wright et al,[6.2] on the NACA 0012 strut at the indicated angle and velocity. 0% marks the "inception" of tail separation.

<div align="center">

112

</div>
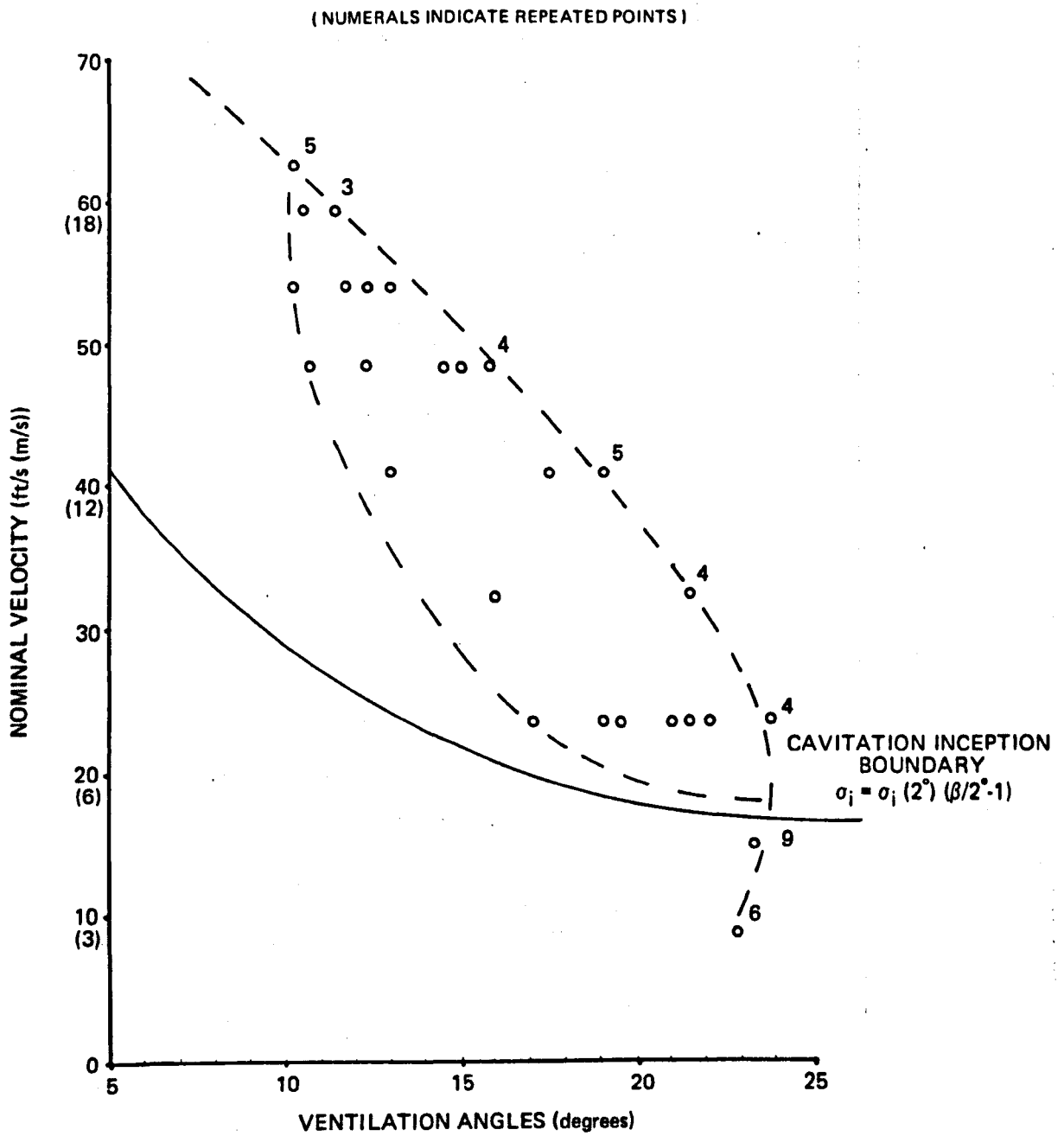
Figure 6.5 — Ventilation Angles vs Velocity NACA 0012 Foil.

KEY

o STBD

+ PORT

NOMINAL VELOCITY (ft/s (m/s))

60
(18)

50
(15)

40
(12)

30
(9)

20
(6)

10
(3)

0

CAVITATION INCEPTION BOUNDARY
CURVE $\sigma_i(\beta) = \sigma_i (2°) (\beta/2°-1)$

30% TAIL SEPARATION,
10 and 15 ft/s

TAIL SEPARATION
"INCEPTION" @ 10 ft/s

5% TAIL SEPARATION,
10 AND 15 ft/s

0   2   4   6   8   10   12   14

VENTILATION ANGLE (degrees)

114
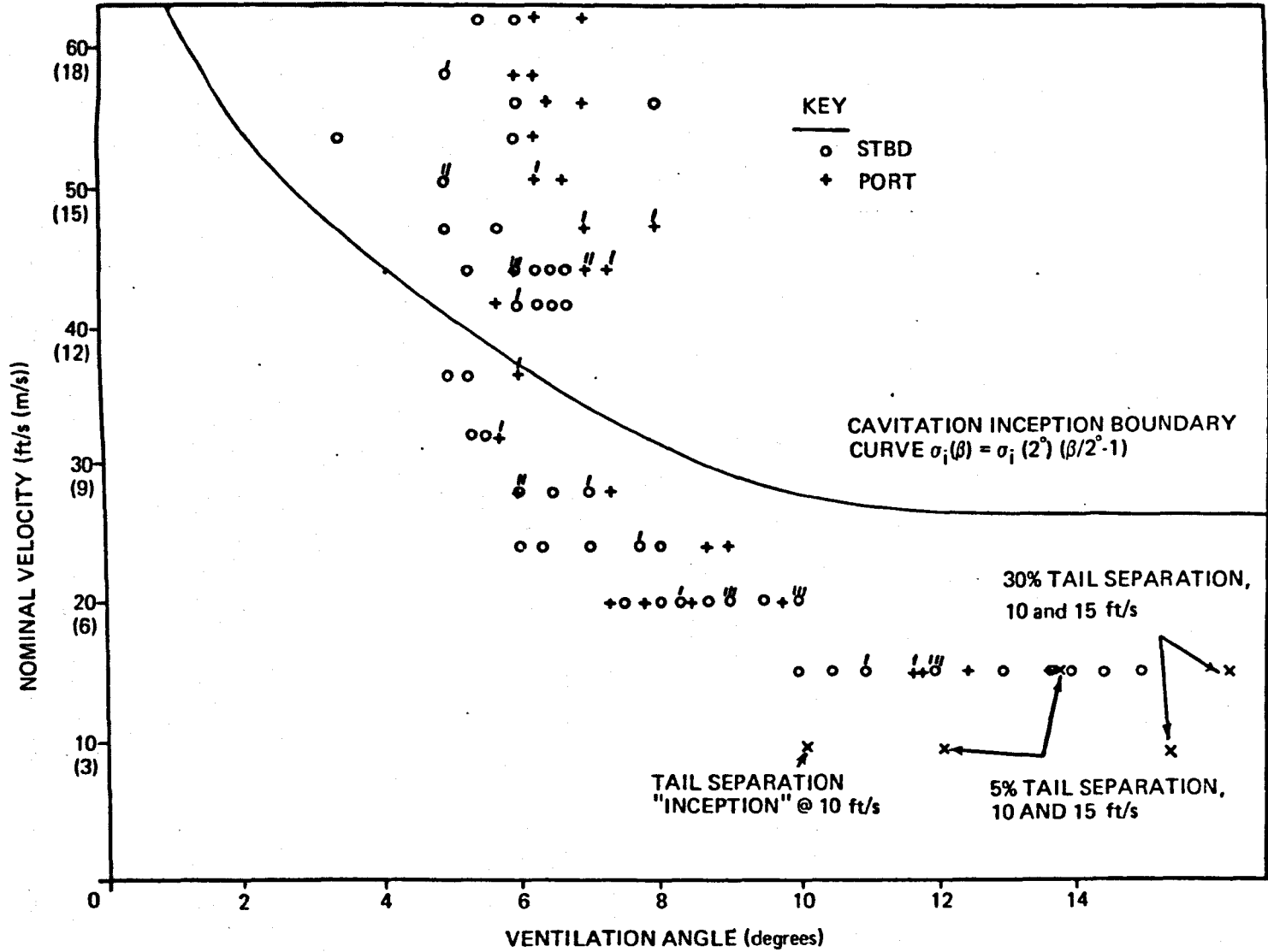
Figure 6.6 — Ventilation Angles vs Velocity, NACA 0012 Model with No. 10
Roughness. Percent Figures Indicate Extent of Tail Separation
in Smooth Case for Like Velocities and Incidence Angles.

Mode Change. The principal and most interesting result of the study without roughness was that the mode of ventilation changed from tail ventilation at low speeds to nose ventilation at moderate speeds, when a small nose cavity existed, then back to tail ventilation at the highest speeds tested. In addition, a mode of ventilation was observed which had a mixture of the characteristics of nose and tail ventilation. The high speed cine revealed some interesting behaviour of the vapour cavity associated with the smooth foil and allowed the inception mechanism to be identified. A few of the most interesting of the photographs have been reproduced.

Figures 6.7 to 6.11 are prints of some of the 16 mm frames taken with the high speed camera. The water velocity, frame rate, lighting, sideslip angle and mode of ventilation are noted on the figures. To aid in the interpretation of the still prints, notes based on the cine projection of the same films are included in the figure titles. Figures 6.7 and 6.8 taken at 62 and 50 ft/s (19 and 15 m/s) show the typical strongly pulsating cavity coupled with re-entrant flow inside cavity which periodically burst through cavity wall to roll up and be swept away as frothy vortex mass. During final oscillations preceding ventilation, a "clean" region was visible between the relatively clear expanding nose cavity and the frothy section being swept downstream, indicating a region of unseparated flow isolating the vapour cavity from the separated region. The characteristic elongation of perturbations are also apparent as they feed separated region in foil wake. These "false strikes" are typical of tail ventilation. At 40 ft/s (12 m/s) the nose cavity is shortened. Also the forward striking "fingers" of aerated water in tail separated region "reaching" for the nose vapour cavity may be seen. This is a possible mode of ventilation inception, although in this particular case the mode was ordinary nose ventilation.

In Figure 6.10, three distinct regions may be noted: cavitating, attached, and separation mixed with air. At 30 ft/s (9 m/s), the mode of ventilation is still the nose type. 25 ft/s (7 1/2 m/s) was the speed at which nose ventilation was most prevalent. The run photographed was anomalous in that the angle attained was much greater than was usual before ventilation occurred. Ventilation inception was due in this case to "fingers" of aerated water from the wetted separated region striking forward into the nose cavity, as shown in Figure 6.11. This mode has not been previously observed.

Description of Pulsating Cavity. The effects of high speed on the surface seal proved to be somewhat obscured by the presence of a violently pulsating vapour cavity as seen in Figures 6.7 and 6.8. The high speed cine films revealed much about the mechanism of pulsation of these cavities, particularly when interpreted in the light of experiments performed by

Figure 6.7 – High Speed Cine Films of Ventilation on NACA 0012 Strut. U = 62 ft/s (19 m/s), Synchronized Strobe Flash, 4000 frames/s 11° < β < 12°. Mode of Ventilation, Tail Type Initiated by Growth of Perturbations.

◁—— FLOW
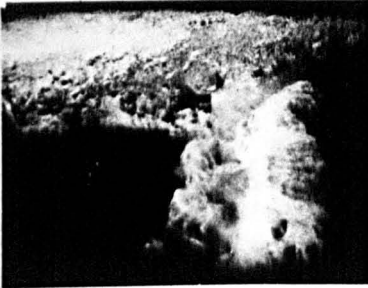
t = 0

INITIAL STAGE OF CAVITY OSCILLA-TION -- RELATIVELY CLEAR LEADING EDGE CAVITY WITH PREVIOUSLY SHED CAVITY TO THE REAR ISOLATED BY REGION OF ATTACHED FLOW
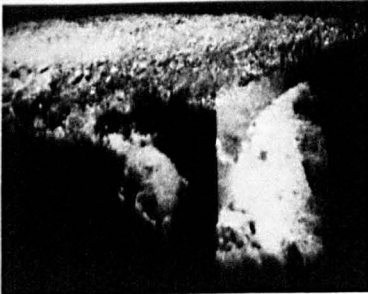
t = 2½ ms

RE-ENTRANT FLOW HAS PROGRESSED FROM THE TRAILING EDGE OF THE CAVITY TO ABOUT HALFWAY TO THE LEADING EDGE
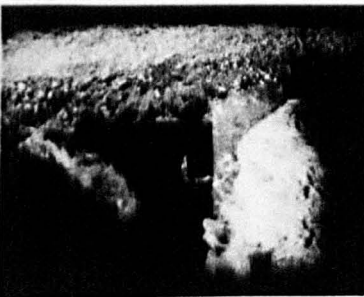
t = 4½ ms

AT MIDSPAN, THE RE-ENTRANT FLOW IS NEARLY AT THE LEADING EDGE. THE CAVITY IS STARTING TO "PUFF OUT" AS THE RE-ENTRANT FLOW PENE-TRATES THE CAVITY WALL IN PLACES
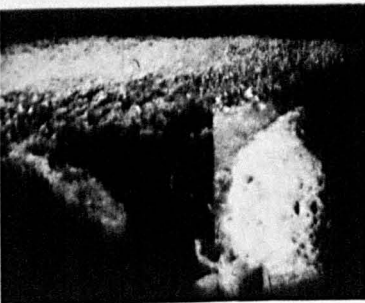
t = 5 ms

THE RE-ENTRANT FLOW HAS FULLY ARRIVED AT THE LEADING EDGE

Figure 6.7 (Continued)

t = 7 ms

THE VORTEX FORMED BY THE INTER-
ACTING OF THE PENETRATING JET
WITH THE FREE STREAM IS DISTINCTLY
BEING WASHED AWAY, AND A NEW
LEADING EDGE CAVITY IS GROWING TO
REPLACE IT

t = 10¾ ms

OLD CAVITY ABOUT TO BE WASHED
OFF, WITH RE-ENTRANT FLOW ABOUT
TO COMMENCE TO RE-START THE
CYCLE
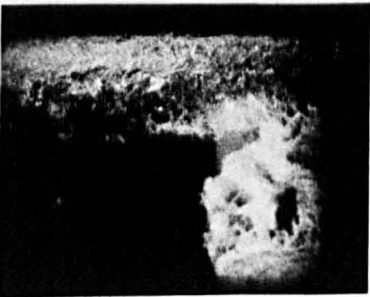
t = 128½ ms
t = 0 (resetting
clock)

VENTILATION STRIKE
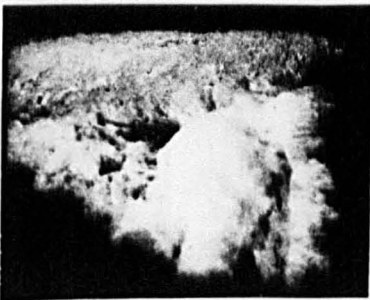
t = 9½ ms

AERATION CONTINUES

Figure 6.7 (Continued)

t = 14 ms

INITIAL STRIKE AIR MASS IS SHED, BUT MUCH AIR AND MANY AIR PATHS REMAIN

t = 24 ms

SECOND MASSIVE STRIKE ON FOLLOW-ING CYCLE
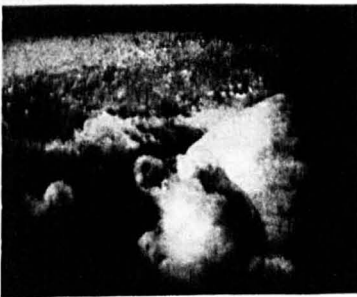
t = 27½ ms

SECOND STRIKE SHED
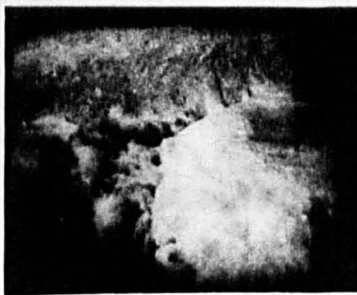
t = 42½ ms

COMPLETE BREAKDOWN OF SURFACE ON 3RD CYCLE

t = 55 ms

VENTILATION COMPLETE

Figure 6.8 – High Speed Cine Films of Ventilation on NACA 0012 Strut. U = 50 ft/s, Synchronized Strobe Flash, ~ 3000 frames/s $14° < \beta < 15°$. Mode of Ventilation – Tail Type.

← FLOW
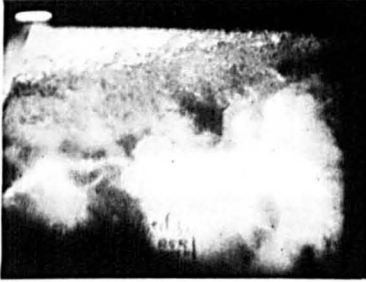
t = 0

VENTILATION "STRIKE" FROM SUR-FACE AT ABOUT MIDCHORD
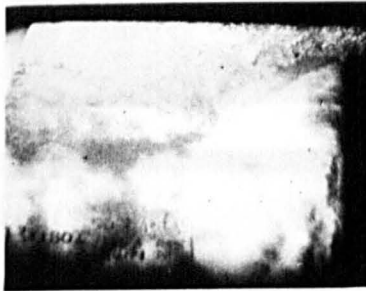
t = 4 ms

STRIKE PATH SWEPT DOWNSTREAM, FEEDING SEPARATED AND CAVITATING REGION
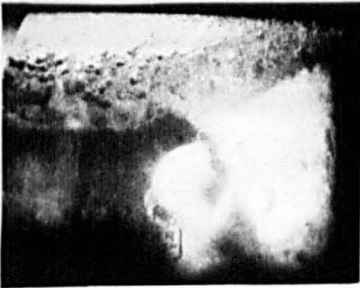
t = 7½ ms

AIR PATH ELONGATED AND SUPPLE-MENTED BY MANY SMALL PATHS FOR-WARD OF IT
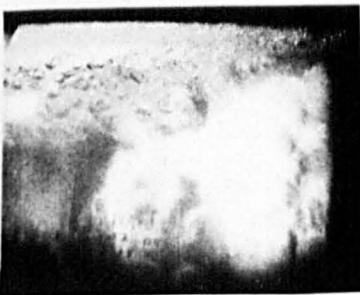
t = 12½ ms

GENERALIZED BREAKDOWN OF THE SURFACE SEAL

119

Figure 6.8 (Continued)
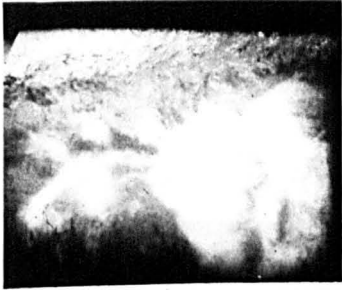
t = 15½ ms

AERATED MASS SWEPT AWAY IN CAVITY OSCILLATION, NEW CAVITY IS APPARENTLY FREE FROM VISIBLE AIR PATHS
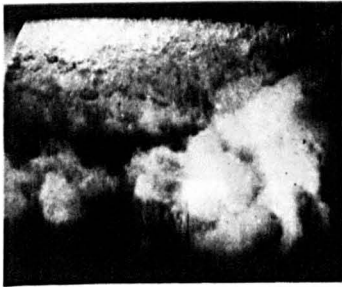
t = 30 ms

OSCILLATION PATTERN PARTIALLY RE-ESTABLISHED AFTER INITIAL STRIKE, FINAL COLLAPSE OF SURFACE IS EVIDENT HERE, ABOUT 2 CYCLES AFTER INITIAL STRIKE CYCLE

t = 34 ms

STRIKE PENETRATES DEEPER
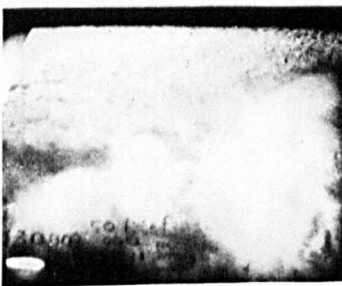
t = 44 ms

VENTILATION ABOUT 50% ESTABLISHED
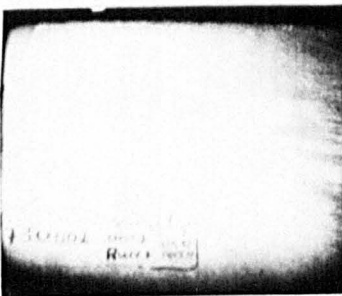
t = 71½ ms

FULL, STABLE, VENTED CAVITY ESTABLISHED

Figure 6.9 – High Speed Cine Films of Ventilation on NACA 0012 Strut. U = 40 ft/s, Synchronized Strobe Flash, 3000 frames/s $18° < \beta < 19°$. Mode of Ventilation – Nose Type.

←— FLOW

t = 0

LARGE NOSE CAVITY REFORMED. SHED CAVITY STILL VISIBLE AT ABOUT MIDCHORD
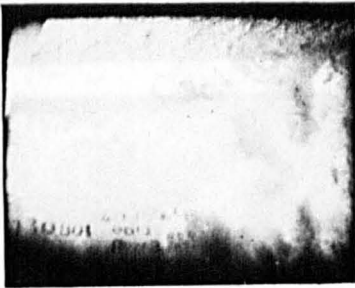
t = 26 ms

LARGE AMOUNT OF AIR IN TAIL RE-GION INTERACTING WITH SHED NOSE CAVITY
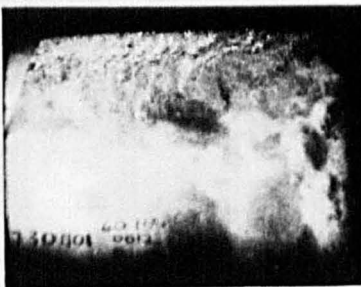
t = 82 ms

INCEPTION AT NOSE
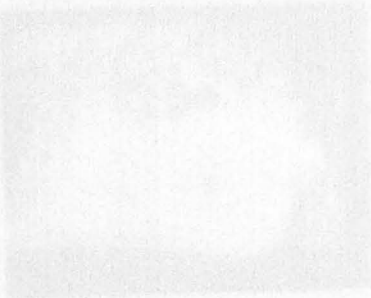
Figure 6.10 – High Speed Cine Films of Ventilation on NACA 0012 Strut. U = 30 ft/s,
Synchronized Strobe Flash, 2500 frames/s $20° < \beta < 22°$. Mode
of Ventilation – Nose Type.

FLOW
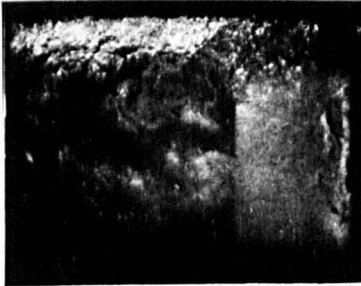
t = 0

NOSE CAVITY SHEDDING. NO INTER-
ACTION WITH SEPARATED REGION
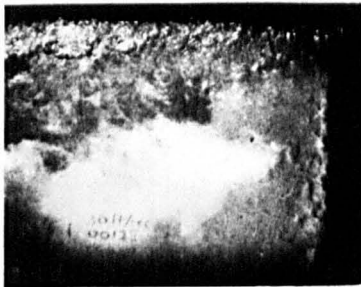
t = 435 ms

"FINGER" STRIKING FORWARD FROM
TAIL SEPARATED REGION TOWARDS
NOSE CAVITY. DISTINCT INTERACTION
BETWEEN SEPARATED AND CAVITAT-
ING REGION
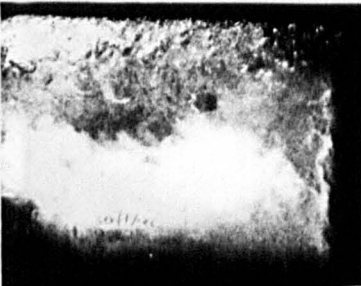
t = 562 ms

ANOTHER STRIKE
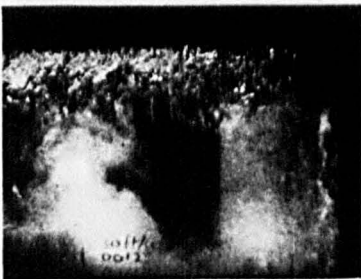
t = 872 ms

"CLEAN" INTERVAL BETWEEN TWO SUC-
CESSIVE STRIKES
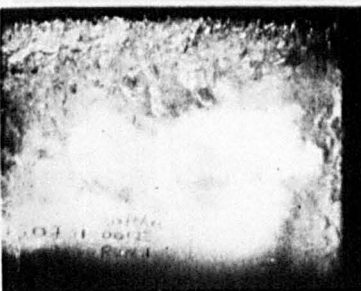
t = 1136 ms

LARGE AMOUNT OF AIR IN SEPARATED
REGION INTERACTING STRONGLY WITH
SHEDDING NOSE CAVITY

122

Figure 6.10 (Continued)
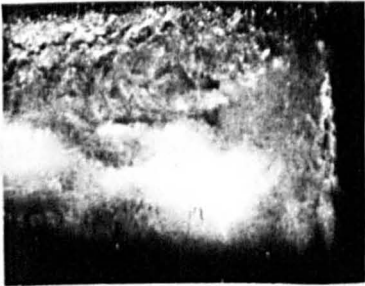
t = 1254 ms   JUST PRIOR TO INCEPTION
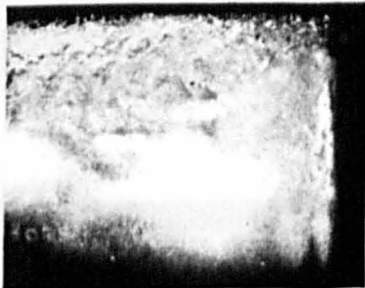
t = 1255 ms   INCEPTION DISTINCT
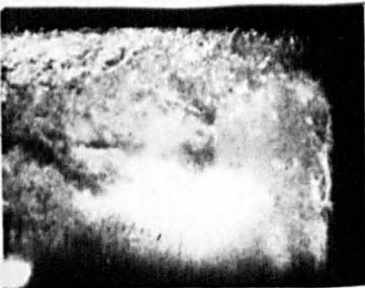
t = 1257 ms   INCEPTION PROGRESS ABOUT 5% COMPLETE
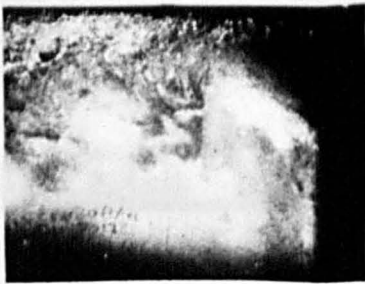
t = 1261 ms   ABOUT 20% COMPLETE

t = 1266 ms   ABOUT 50% COMPLETE

Figure 6.11 – High Speed Cine Films of Ventilation on NACA 0012 Strut. U = 25 ft/s
(7½ m/s), Incandescent Lighting ("Colortran"), 3000 frames/s
$22° < \beta < 24°$. Mode of Ventilation – Fingers of Air Striking Forward
to Intercept Nose Cavity at Midspan.
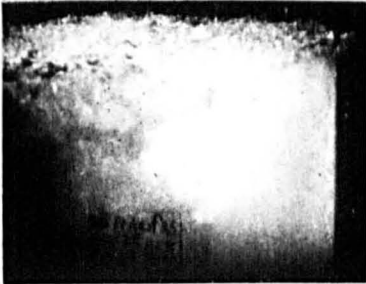
t = 0

NOSE CAVITY PRIOR TO INTERACTION
WITH SEPARTED REGION

t = 982 ms

NOSE CAVITY INTERACTING WITH AIR
BUBBLES IN TAIL SEPARATION REGION

t = 1412 ms

SEPARATED REGION PRIOR TO VENTI-
LATION

t = 1456 ms

"FINGER" REACHING FORWARD TO
NOSE CAVITY

Figure 6.11 (Continued)

t = 1461 ms   SAME 5 ms LATER
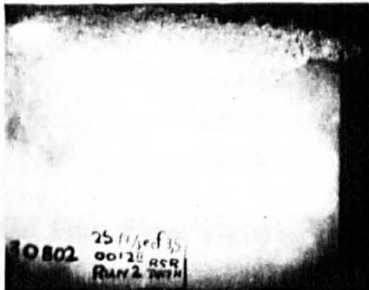
t = 1467 ms   VENTED CAVITY EXPANDING TOWARDS FREE SURFACE FROM MIDSPAN AT NOSE
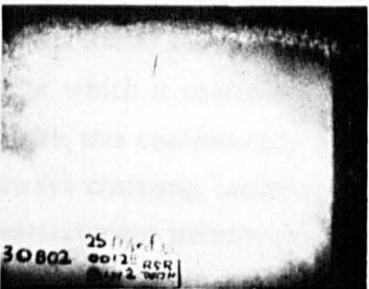
t = 1488 ms   NEARLY FULLY DEVELOPED VENTED CAVITY

t = 1568 ms   VENTED CAVITY FULLY ESTABLISHED

Swales et al[6.3] in the Recirculating Channel on the NACA Mk 1 strut at lower speed and reduced ambient pressures, using the oil film flow visualisation technique. From the high speed film, the following behaviour of the cavity was inferred prior to ventilation at speeds above 40 ft/s (12 m/s). Referring to Figure 6.12:

(i) The cavity started from the nose and grew steadily downstream with well defined boundaries. The flow behind remained attached.

(ii) A limit to cavity growth was set by the balance between inertia and pressure forces in the water and the pressure forces within the cavity.

(iii) When the cavity stopped growing the flow behind it separated. Water from this separated region was drawn into the cavity by the prevailing pressure gradient and formed a re-entrant jet or sheet over the foil surface.

(iv) As the sheet of water moved forward into the cavity, the air entrained in the jet sheet expanded and the sheet thickened.

(v) At some point the jet would intersect the cavity wall, burst through the wall, and be swept back downstream, truncating the cavity.

(vi) Contact with the mainstream travelling in the opposite direction imparted considerable vorticity to the frothy mass swept downstream, isolated from the remaining clear-walled truncated cavity by attached wet flow. The truncated cavity grew again, its downstream edge trailing the previously washed away frothy vortex, to complete the cycle. An embryonic vapour bubble was always left at the nose, although its length might be only 2 or 3 percent of chord.

Oil Film Flow Visualisation of Pulsating Cavity. Figure 6.13 is a diagrammatic reproduction of a typical oil film flow visualisation result of Swales et al. It may be interpreted as follows:

The oil accumulation near the stagnation region at the nose shows as a dark line (A). To the rear of this is a region of attached flow, of the order of 2-3 percent of chord in length, which shows as a light band (B). The line (C) gives the point at which the flow separated, after which it passed over the vapour bubble and re-attached in the region (D). Since the cavity was continuously pulsating, the exact point at which reattachment occurred was always changing, resulting in a wide region of possible reattachment with the "herringbone" reattachment pattern characteristic of steady state flow in evidence only at the spanwise boundaries. The point at which the re-entrant jet ruptured the cavity wall and ceased to flow forward is marked by the presence of a "tidal" accumulation of oil, shown as line (E), upstream of the re-attachment point. The line (E) is not well defined toward midspan, where the unsteady effects were prevalent. The reattachment region (F) is also ill defined, indicating an unsteady flow which could not establish a definite pattern in the oil film.

126
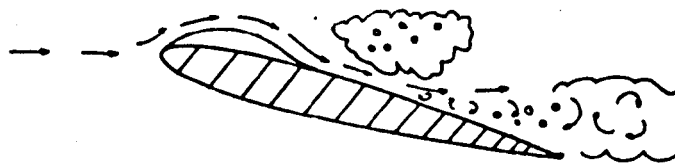
A CAVITY WITH CLEAR WALLS AND RATHER WELL DEFINED BOUNDARIES
COVERS PERHAPS THE FORWARD QUARTER OF THE STRUT.
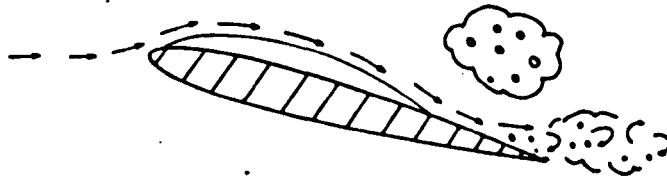
THE VAPOUR CAVITY EXPANDS DOWNSTREAM, WITH THE ATTACHED WATER
PRECEDING IT, SWEEPING AWAY THE SEPARATED REGION.
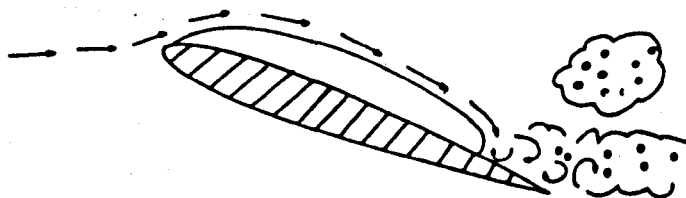
AS THE ELASTIC LIMIT OF THE CAVITY IS REACHED, THE FLOW BEHIND
THE CAVITY SLOWS AND THEN REVERSES.
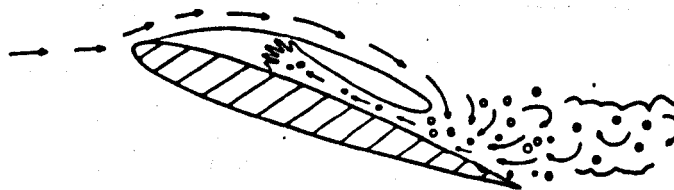
THE FROTHY RE-ENTRANT FLOW INTO THE BACK OF THE CAVITY THICKENS
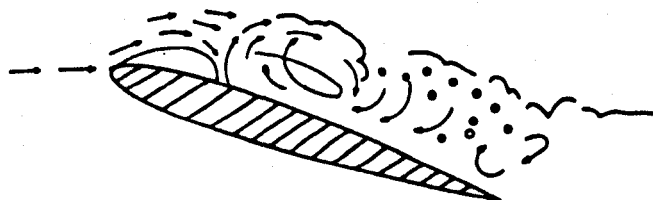
THE THICKNESS OF THE JET EXCEEDS THE CONFINES OF THE CAVITY WALL AND THE
RE-ENTRANT FLOW IS SWEPT BACKWARDS AND DOWNSTREAM.

Figure 6.12 – Pulsating Cavity Diagram.

STRUT

STAGNATION LINE
(A)

SURFACE LINE

SCRUBBED
(B)

FLOW →

SEPARATION
(C)

D, F - REATTACHMENT

RE-ENTRANT JET
TIDAL MARK
(E)

TIP VORTEX SMEAR
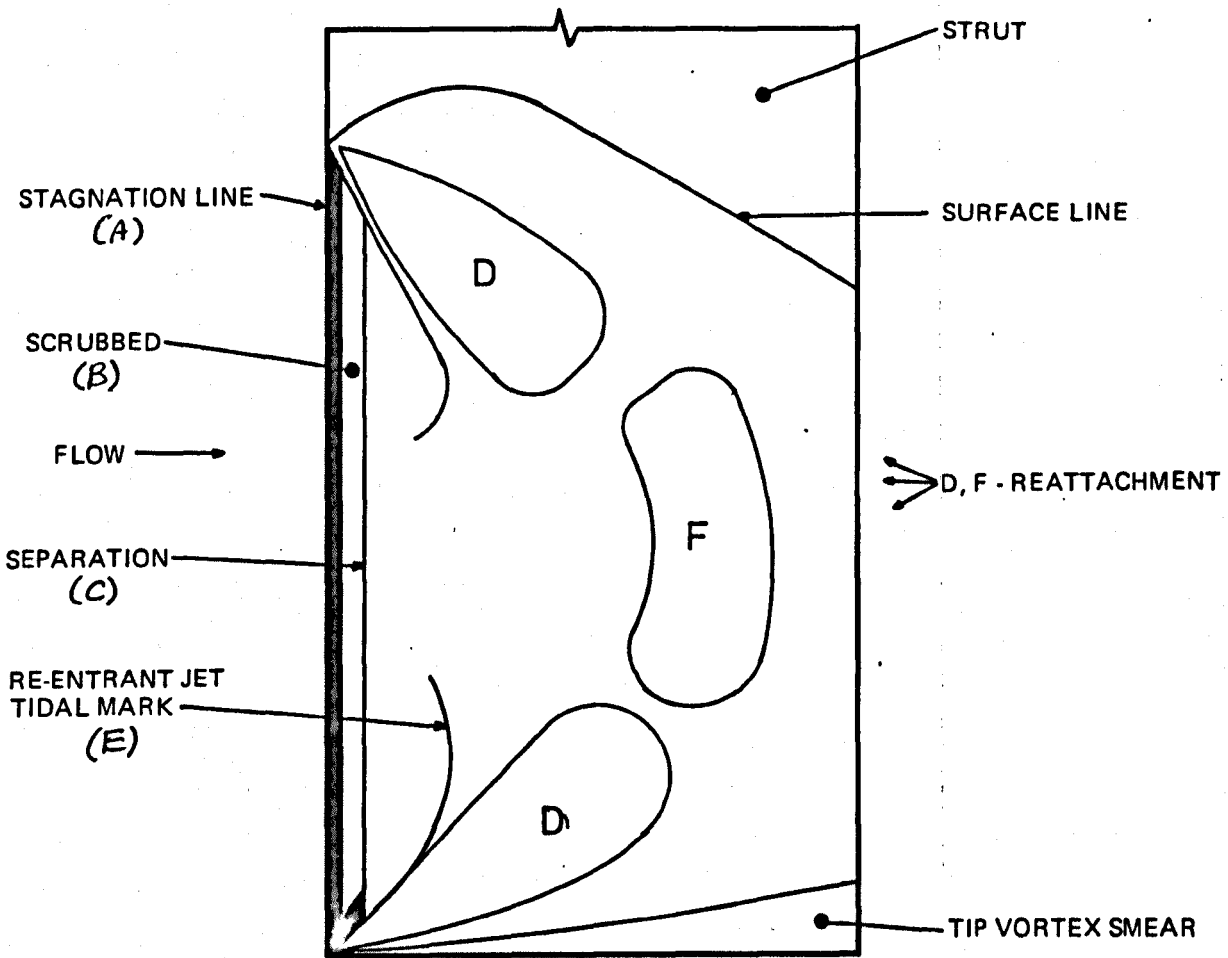
Figure 6.13 – Diagram of a Flow Visualisation Pattern.
From Swales.[6.3]

128

Similar observations to these have been made by Knapp[6.4] on axisymmetric cavitating bodies, and by Acosta[6.5] on two-dimensional, fully submerged hydrofoils. The present observations are thought to be unique in certain aspects of the mechanism which are identified, and also because of the free surface involved. Unfortunately, it was not possible to define the influence of the cavity pulsation on ventilation.

Change of Ventilation Mode. The mode of ventilation was determined by direct observation of high speed cine films for a few cases, but can also be deduced from the data displayed in Figure 6.5. As discussed in Chapter 2 on the mechanism of ventilation, nose ventilation depends upon the chance encounter with a flow disturbance which intrudes into a separated or cavitating region at the nose to trigger inception. If the type of flow disturbance which will trigger nose ventilation under particular conditions is distributed throughout the flow according to some statistical law, then the probability of encounter with the strut is a function of time. If the angle of incidence is uniformly increased with time, the distribution of disturbances will ensure that the ventilation angle recorded will be distributed over a corresponding range of angles. Therefore, a wide scatter of measured ventilation angles for a particular velocity generally indicates that inception is taking place at the nose. On the other hand, the amplification mechanism of the accelerating sheet ensures that even infinitesimal disturbances will be sufficient to provoke tail ventilation, making tail ventilation apparently independent of the existence of flow irregularities and time. Therefore, good repeatability of ventilation angle is an indication of tail ventilation.

Note that a right hand boundary of the data envelope in Figure 6.5 is distinctly formed by a conglomeration of points, the numerals denoting repeated identical measurements. This indicates the maximum angle before tail ventilation, an extremely repeatable phenomenon. The relatively scattered points to the left hand side of the distinct tail vent boundary were most likely nose ventilations. The envelope of data points is narrow at low speeds and at high speeds, indicating the predominant occurrence of repeatable tail ventilation. A gradual thickening of the envelope which reaches a maximum at 25 ft/s (7.6 m/s) indicates nose ventilation was significant at moderate speeds, and less so at higher speeds, until at 62 ft/s (19 m/s) nose ventilation was not observed at all, in spite of the long established presence of a nose vapour cavity. This can be observed by comparing the ventilation boundary with the nose cavitation inception boundary.

Correlation with Towing Tank Results. These results provide a valuable clue as to why nose ventilation was apparently not observed in high speed towing tank tests at the

129

David W. Taylor Center. It was previously thought that the lack of ambient disturbances precluded the occurrence of nose ventilation in towing tanks and, in fact, several investigators observed that artificial disturbances ahead of a strut in a towing tank reduced the ventilation inception angle. However, it has never been demonstrated that the reduction in vent angle was actually due to a change in mode from tail to nose ventilation. Furthermore, the characteristic scatter in the vent angle associated with nose ventilation was not observed.

Water Surface Disturbances. In August 1973, a test was conducted at the Taylor Center in a rotating arm facility using a one foot (0.3 m) chord NACA 16-012 strut.* Even though the strut was towed through its own wake many times and the water surface was consequently very disturbed, no anomalous scatter was observed in the ventilation angle boundaries at speeds between 35 and 50 knots (18 and 26 m/s). Ordinarily, ventilation would not have been expected below these speeds at the maximum incidence angle of 15 degrees allowed by the test apparatus. However, when the strut was towed at 15 degrees at 15 knots (8 m/s), time dependent vents did occur, after 7 minutes, 9 minutes, and one after 10 seconds. Spontaneous closure also occurred after these vents.

Effect of Waves. The results of unpublished work by Pattison at the Taylor Center, in which the same models tested by Kramer[6.6] at Lockheed were towed at high speeds in waves, indicated that the effect of waves diminished with increasing speed. The Center tests revealed no significant differences in the ventilation boundaries in head seas of any model except a sharp-nosed biogive, even though irregular, breaking waves were generated, as well as sinusoidal ones. Because of the limitation of the model rotation device, the maximum sideslip angle that could be tested was 15 degrees. This meant that ventilation did not occur for any of the family of struts tested at less than 35 knots (18 m/s) in calm water or waves. Therefore, all the ventilation boundaries recorded must be considered high speed boundaries. Kramer, at Lockheed's reduced pressure towing tank facility, towed the identical models at lower speeds and reduced ambient pressure, simulating the higher speeds in respect to the vapour cavitation characteristics only. He found that both head and following seas significantly affected ventilation boundaries, and that the boundary points became extremely scattered.

These results imply that there may be a speed limit on nose ventilation. They also suggest an explanation of the difficulty encountered in provoking ventilation in high speed experiments, described in Chapter 2.

---

*This test was conducted at the request of the author, and was unreported.

Decreased Effect of Disturbances at High Speeds: Cavitating Case. The stability of the surface seal at the nose, as at the tail of a surface piercing strut, depends on the thickness and velocity of the sealing layer, the pressure differential between the separated region and the atmosphere, and the streamwise extent of the separated region. This was more fully discussed in Chapter 4 on Scaling and Chapter 2 on the Mechanism. In the case where the low pressure region is cavitating, the pressure differential between a vapour cavity and the atmosphere does not increase with increasing speed. If there is a limit to how nearly the vapour cavity can approach the free surface, the thickness of the surface seal may not change appreciably with speed. However, its momentum must increase with speed. Hence the net effect of increasing speed is stabilising providing the chordwise growth of the cavity is not too great. Apparently, by the time the chordwise extent of the cavity is great enough to be destablising, tail ventilation becomes re-established as the dominant mode.

Case of Wetted Separation. The same arguments apply, with perhaps more force, to the case where the nose region is occupied by a wetted separated region. Laminar nose separation "bubbles" can shrink and even disappear with increasing speed, thus eliminating the qualification that the growth in extent of the separated region may offset the stablising effect of higher momentum of the sureface seal. In fact, nose ventilation has never been observed to occur with a shrinking separation "bubble".[6.7] Since transition to turbulence causes the reattachment of both shrinking and growing nose "bubbles", it would be reasonable to assume that with increasing speed the growing bubble type of separation would also recede from the surface. Therefore, the surface seal would tend to become stronger at the nose in every case so far observed. As already discussed, larger sizes and higher speeds encourage turbulence in the surface seal which would be expected to have the most pronounced effect towards the tail, thus encouraging tail ventilation.

High Speed Inception Point. The cine films show, too, that as speeds become higher, the distinction between nose and tail ventilation becomes more nebulous. The path which air takes to enter the separated (cavitating) region moves forward even though the mechanism of surface seal breakdown still resembles the characteristic Taylor amplification associated with tail ventilation. It is certainly possible that this is also the effect of boundary layer turbulence weakening the surface seal, although the effect of increased speed on the boundary layer is somewhat ambiguous with respect to ventilation. Although the turbulence and mixing grow with speed, the physical extent of the layer becomes smaller and the momentum loss a smaller proportion of total momentum flux, if the flow is initially turbulent. If the flow is

initially laminar, and speed is increased to transition, the flow close to the strut has more momentum, although the total momentum loss is greater.

Roughness: Scatter and Asymptotic Behaviour. The result of combining a roughened foil with high speed flow was to produce a form of ventilation unlike any previously observed by the author in the laboratory. Figure 6.6 tells part of the story in the immense and apparently incoherent scatter of the boundary points. Two features are evident in spite of the scatter. The most obvious is that the inception angles were much lower for a given velocity than for the smooth foil. Less evident is the suggestion that a lower bound on the vent angle has been reached by the roughened foil at a relatively low speed. It would not be difficult to imagine that the boundary for the smooth foil was approaching the same asymptote. However, tests at the Center towing tank with larger models at speeds up to 93 ft/s (28 m/s) did not reveal an asymptotic behaviour. The most plausible conclusion is that the roughened and smooth models would approach the same behaviour at sufficiently high speed.

Partial Vents. Part of the reason for the considerable scatter of Figure 6.6 is that it was difficult to define when complete ventilation had occurred. A regularly observed phenomenon was inception over 95 percent of the submerged area in runs to port side, with the final bit ventilating significantly later. During a run, partial vents opened and collapsed, occasionally leaving sub-surface vented cavities behind. Washout angles were extremely erratic as well. Typically, one or more pockets or ventilation would persist to zero or negative angles. Whether they would have persisted indefinitely could not be determined because of the inherently limited run time of the facility, but it seems unlikely. Because of the low angles at which ventilation occurred, cavitation was not observed even at 62 ft/s, (19 m/s) the highest speed tested.

Roughness and Surface Seal. The behaviour of the flow around the roughened strut was compatible with a ventilation mechanism in which the surface seal was much weaker than that observed with smooth models. The surface seal ordinarily would prevent atmospheric air from rushing in to displace low momentum fluid in a region of separated flow at lower than atmospheric pressure. If the surface seal had less restraining effect, atmospheric air would tend to immediately displace the separated low pressure fluid as soon as such a region was created. The rather large flow fluctuations normally present in the high speed channel would cause regions of separation to appear in a somewhat erratic manner. The changes in the depth of the ventilated cavity may have corresponded to the sudden appearance of separated regions.

132

Ventilation and Separation. In the last chapter it was noted that for the grade 20 roughness, ventilation of the NACA 0012 foil occurred at 20 ft/s (6 m/s) at an angle at which separation had not been detected in flow visualisation studies of the same foil in the smooth condition at 15 ft/s (4 1/2 m/s). Although it could not be said positively that there was no separation present, the effect of roughness in many cases was apparently to decrease the requirement for the extent of separation. Figure 6.6 raises the same question. Ventilation is seen to occur before cavitation inception and at far smaller angles than turbulent tail separation would be expected in the smooth case. No visual observation could be made of cavitation prior to ventilation until speeds of 40 ft/s (12 m/s) were tested. This was corroborated by the empirical curve fit boundary for cavitation inception based on the smooth foil. No positive conclusions can be drawn, because no flow visualisation techniques were used, and no means of detection of microscopic cavitation were employed. However, some weight is lent to the argument that the requirement of a low momentum region may be satisfied by a sufficiently thickened boundary layer, in this case induced by roughness.

Implications for Full Scale Performance. The ventilated cavities observed in the roughness experiment were very reminiscent of cine films of ventilation taken on full scale craft with surface piercing struts.

It is possible that at prototype speeds and sizes, the surface seal is weakened relative to the other factors influencing ventilation in a similar manner to the weakening effect of the roughness on relatively lower speed models. The larger size, coarser surface finish and greater ambient flow disturbances in the prototype case act to produce thicker boundary layers with consequent greater vorticity, greater mixing and longer "residence" times in the accelerating region of the flow. Enough information is not now available to say quantitatively how ventilation boundaries will be affected when extrapolated from model scale tests. The results of the present study indicate that model results must be used with caution. In particular, the role of the surface seal may be modified in the mechanism of ventilation as it occurs on full scale craft. Also, some doubt is cast on the role of separation as being required to furnish the low momentum region necessary for ventilation inception. This question is explored further in Chapters 8 and 9.

It may be possible to ensure more accurate prediction of full scale performance by the rational application of roughness to models.

CONCLUSIONS

The mode of inception of ventilation on the NACA 0012 strut changed from tail to nose to tail with increasing speed and the occurrence of vapour cavitation. The inception point of tail ventilation moved forward with increasing speed. This correlates with increased boundary layer turbulence and momentum loss with increased speed. At intermediate speed, a new mode of ventilation was observed, in which aerated water in a tail separated region interacted with a pulsating vapour cavity at the nose, the point of inception of the ventilated cavity being submerged, at about midspan.

Comparison with towing tank data suggests nose ventilation becomes less likely to occur at high speeds. Disturbances to the oncoming flow including waves are not as significant in triggering ventilation at high speed. This may be due to the increased momentum of the surface seal and a reduction or lack of growth of the separated region with speed.

The effect of roughness was to introduce scatter and asymptotic behaviour with increasing speed. The necessity for large regions of separation was reduced or possibly eliminated by roughness. The behaviour of the roughened foil was reminiscent of full scale observations, and compatible with a physical model in which the surface seal is weakened by boundary layer growth, turbulence and mixing action. Accurate modeling of prototype performance will probably require the inclusion of controlled roughness on the model.

Chapter 6 References

6.1   Hunter, B., Swales, P.D., Cole, B.N., *"A High Speed Short Duration Water Channel,"* Jour. Physics E, Vol. 6, No. 3, pp. 145-146, 1973.

6.2   Wright, A.J., McGregor, R.C., and Swales, P.D., *"Time Dependency of Ventilation,"* Hovering Craft and Hydrofoils, Vol. 12, No. 9, 1973.

6.3   Swales, P.D., McGregor, R.C., Foster, J.L., Rothblum, R.S., and Cole, B.N., *"DREA Hydrofoil Project. Report on half year, 1st October 1973 – 31st March, 1974,"* University of Leeds Dept. of Mech. Eng. Res. Rept. TP/DREA/13, March 1974.

6.4   Knapp, R.T., Daily, J.W., Hammitt, F.G., *"Cavitation,"* McGraw-Hill, New York, 1970.

6.5   Acosta, A.J., *"Hydrofoils and Hydrofoil Craft,"* J. Ship Res., Vol.   , No.   , pp. 161-184, 1973.

6.6   Kramer, Ray L., *"An Experimental Study of the Effects of Waves on the Ventilation of Surface-Piercing Struts,"* Lockheed Missiles & Space Co. DO29678, Nov. 1970.

6.7   Swales, P.D., Wright, A.J., McGregor, R.C., and Cole, B.N., *"Separation and Ventilation Interaction Studies,"* Hovering Craft and Hydrofoil, Vol. 13, No. 3, pp. 8-12, 1973.

CHAPTER 7
SEPARATION AS IT RELATES TO VENTILATION

SEPARATION THEORY

As mentioned in preceding chapters, a prerequisite for the inception of ventilation on a surface piercing strut or hydrofoil is a region of separated flow of sufficiently low pressure and low momentum that it can be displaced by atmospheric gases after initiation of a triggering mechanism. It has been convincingly shown that viscous separation of the boundary layer around a fully wetted surface piercing hydrofoil or strut provides such a region. It is the purpose of this chapter to briefly discuss the phenomenon of boundary layer separation, to assess the most current techniques for predicting or preventing separation, and to extend these methods where possible to the case of surface piercing hydrofoils and struts.

Limitations of Theory. First, a disclaimer should be made. There is no adequate method for treating three dimensional flow with separation. In fact, there is no agreed definition of three dimensional separation. Furthermore, nearly all work on separation has been done in air, so the interaction between boundary layer separation and cavitation is not generally known. Therefore, the designer who does not wish to break new theoretical ground must rely on techniques which are, strictly speaking, applicable only to two dimensional airfoils. This restriction is not as serious as it might be. Finite aspect ratio and the presence of the free water surface result in a pressure gradient which is not as severe as that which would be predicted by two dimensional theory. This means that a two dimensional design to avoid separation will be conservative, with certain reservations. Furthermore, the criterion for avoidance of cavitation—avoidance of large negative pressures—is compatible with the (simplified) criterion for avoidance of boundary layer separation—avoidance of large positive pressure gradients.

Mathematical Definition of 2-D Separation. Separation in two dimensions is usually defined as having occurred when the slope of the velocity parallel to the body surface with respect to the perpendicular distance from the body, evaluated at the body surface, is zero. That is—

$$\frac{du}{dy}\bigg|_{wall} = 0$$

This is also the condition for zero skin friction.

Physical Description of Separation. Separation occurs when the momentum of the main, or free stream, flow can no longer be transmitted by viscosity to the flow near a wall (solid boundary) at a sufficient rate to overcome the retarding effect of friction at the boundary in a region of

increasing pressure. At the inception point of separation, the flow close to the wall slows down until it becomes zero, the same as the velocity of the fluid at the wall. If the adverse pressure gradient continues downstream, the flow near the wall reverses its direction and begins to flow upstream. At the same time, the region of the flow which is being slowed by the viscous drag at the wall, the boundary layer, becomes greatly enlarged which causes the streamlines to separate from the wall, leaving a "stagnant" region of low momentum fluid adjacent to the wall (Fig. 7.1). It is this region of stagnant fluid which is then susceptible to replacement by air if a path is provided to the atmosphere by a triggering mechanism.

Types of Separation. Two dimensional separation of flow around an airfoil may be divided into somewhat arbitrary categories which are not universally agreed upon. The categories chosen here correspond to the two types of ventilation observed in the Leeds studies; nose initiated and tail initiated. Nose initiated ventilation is associated with a laminar separation "bubble" at the leading edge of the foil, whereas tail ventilation is associated with fully turbulent separation from a point which originates on the after portion of the strut and which progresses forward with increasing incidence angle. Figure 7.2 (after Barr[7.1]) shows the types of separation pertinent to hydrofoils.

Long and Short "Bubbles". Nose separation can be further categorised depending on whether it is of the long or short bubble type. The short bubble type is typically of 1 percent or less chord length although it may be larger at its inception. It moves forward and shrinks with increasing incidence angle and changes immediately to full leading edge stall once a critical incidence has been attained. The long bubble type, when it appears, may be more of the order of 3 percent of the chord length and grows with increasing incidence in a fairly regular manner. This is the type of separation associated with ventilation in the University of Leeds studies. Figure 7.3 shows the growth of a long separation bubble with incidence angle. (After Barr[7.1] and McCullough[7.2])

Significance of Turbulence to Separation. The occurrence of a separation bubble is a consequence of the fact that fully turbulent flow is less likely to separate than laminar flow. The physical reason for this is that there is greater mixing and effective friction away from the wall in turbulent flow. Thus, momentum is more readily transferred to the flow close to the wall to enable it to overcome wall friction in an adverse pressure gradient. Stratford[7.3] gives an excellent discussion of the physics of the boundary layer.

A separation bubble occurs when a laminar boundary layer separates, undergoes transition to turbulence and consequently reattaches itself. Thus, leading edge separation will be associated with laminar incident flow. The Reynolds numbers and surface finish associated with present
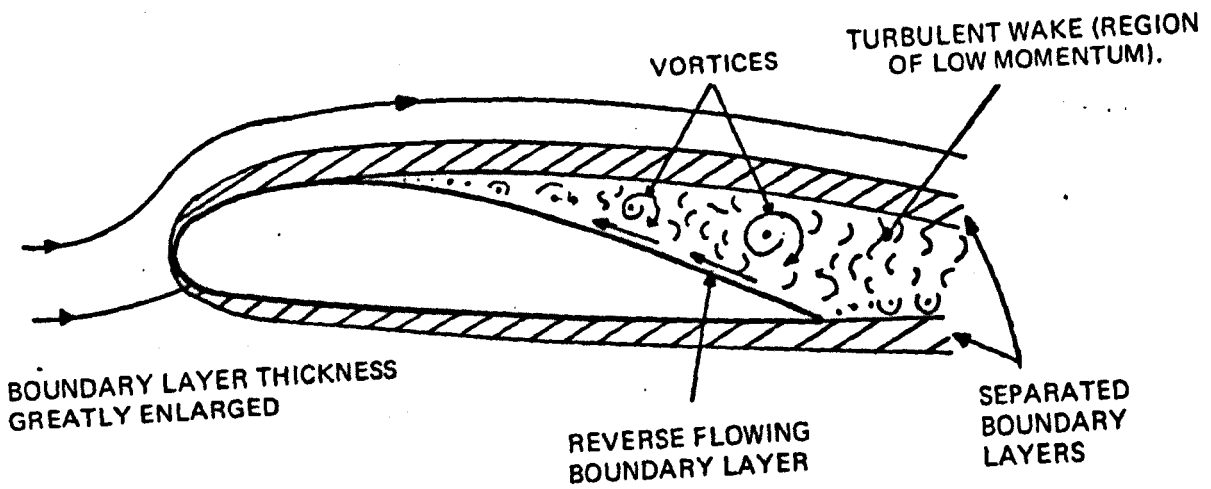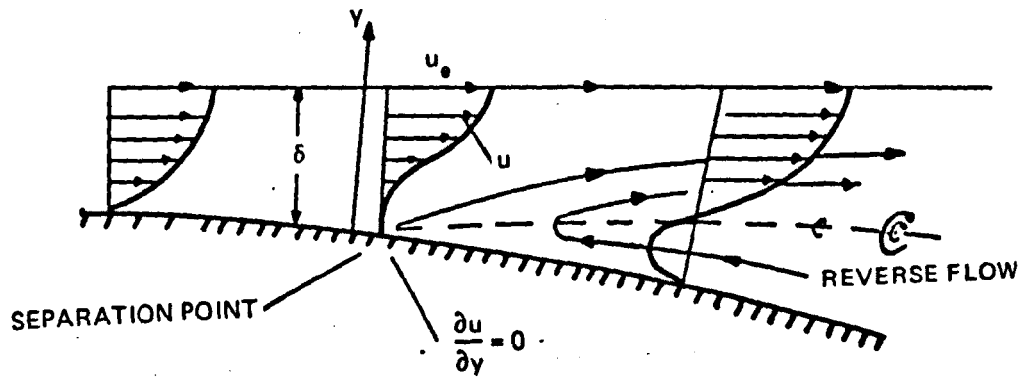
Figure 7.1 — Velocity Profiles and Physical Diagram of Separation on an Aerofoil. From Barr.[7.1]

Figure 7.2 – Illustration of the Various Types of Separation Observed on Foils.
After Barr.[7.1]

NO SEPARATION
$\alpha = 0$

SEPARATION BUBBLE

SEPARATION BUBBLE

SEPARATION BUBBLE

V

A.

V
α
B.

V
α
C.

V
α
D.
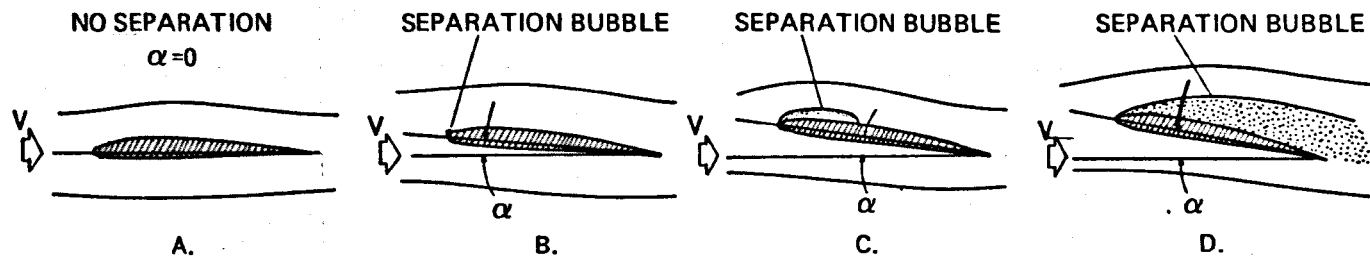
Figure 7.2a – Long, or Growing, Bubble (Thin Airfoil) Type Separation.
This Type Occurs on Very Thin Sections.

NO SEPARATION

SEPARATION BUBBLE

SEPARATION BUBBLE

SEPARATION BUBBLE

V

A.

V
α
B.

V
α
C.

V
α
D.
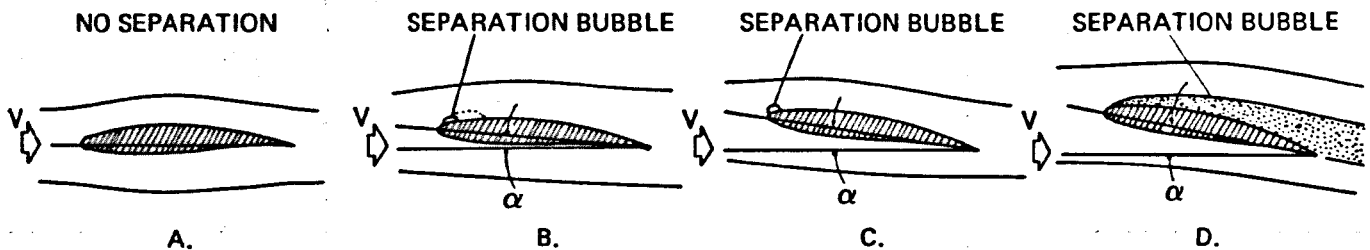
Figure 7.2b – Leading Edge Stall (Short or Shrinking Bubble).
This Type Occurs on Sections of Moderate Thickness.

NO SEPARATION
$\alpha = 0^\circ$

SEPARATED REGION.

A.

V
α
B.

V
α
C.

V
α
D.
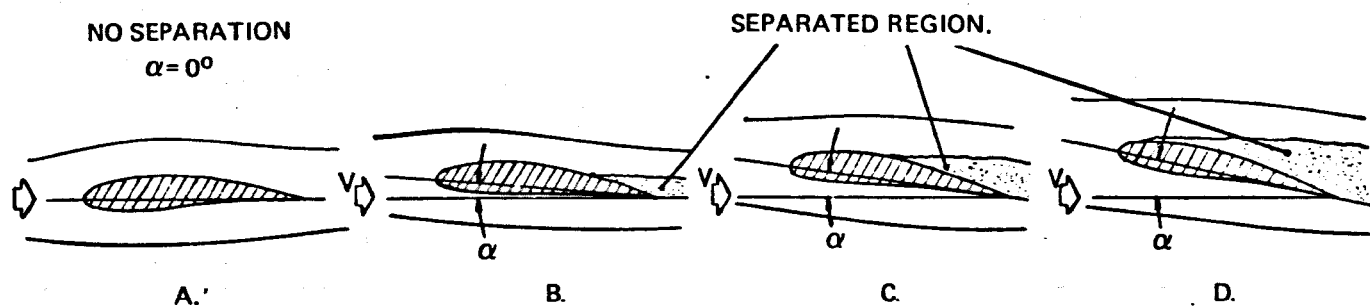
Figure 7.2c – Trailing Edge Stall (Turbulent Tail Separation).
This Type Occurs on Very Thick Sections.
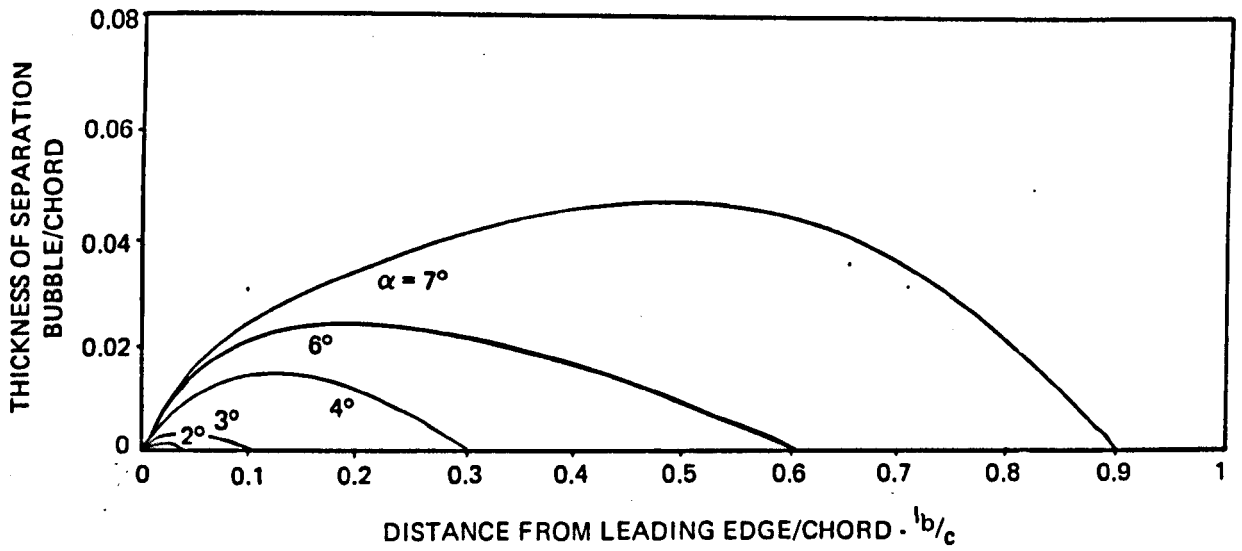
Figure 7.3a — Size of Separation Bubbles for Double Wedge Section for Various Angles of Attack
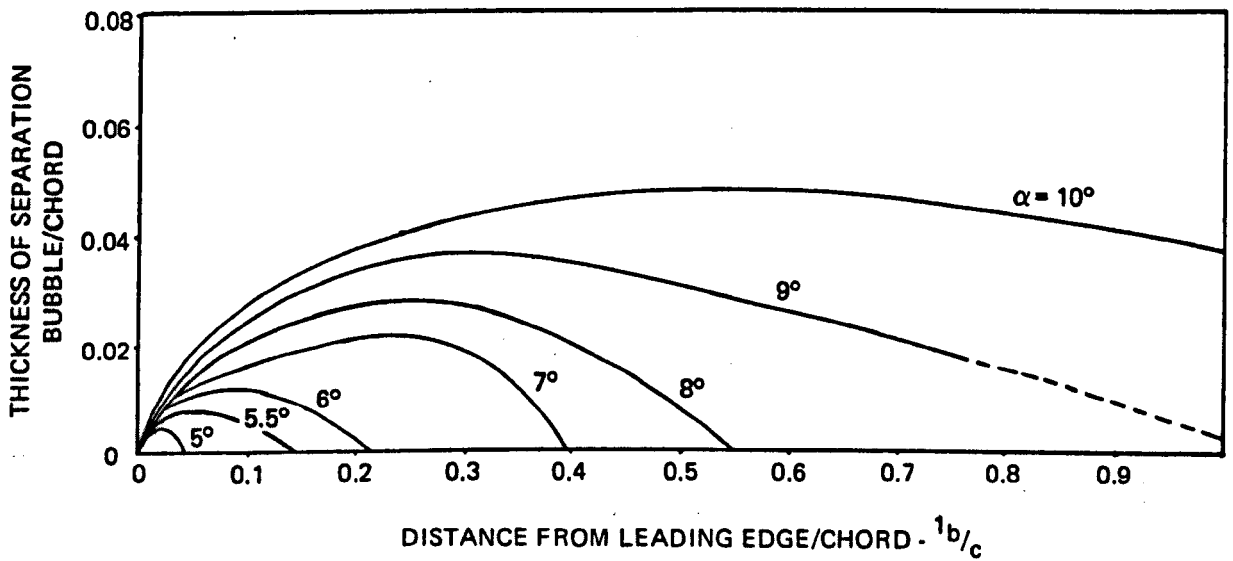
Figure 7.3b — Size of Separation Bubbles for NACA 64A006 Section for Various Angles of Attack. From Barr[7.1], and McCullough[7.2].

military and large sized civil hydrofoils and struts would make laminar flow unlikely to occur for more than an inch aft of the leading edge, although the specific conditions would have to be considered. Generally, if excessive section fineness and sharpness is avoided, a laminar separation bubble will not occur. For a very sharp leading edge, such as a wedge shape, separation will occur at the leading edge on the low pressure face at infinitesimally small incidence angles, independent of Reynolds number. It is best to avoid this shape unless it is desired to provoke separation or cavitation.

Effect of Viscosity on the Pressure Distribution Around an Aerofoil. The pressure distribution which is a characteristic of all aerofoils at angles of incidence consists of a high peak pressure at the leading edge corresponding to the stagnation point. After that, the flow near the foil "upper" surface is quickly accelerated to its peak velocity and hence, minimum pressure just aft of the leading edge. This is followed by a region of deceleration and rising pressure. If it were not for the effect of viscosity, full stagnation pressure would be recovered at the aerofoil trailing edge. But because of friction and insufficient momentum transfer, the velocity near the foil boundary falls to zero before the trailing edge is reached, and separation occurs. Fig. 7.4 (Riegels[7.4]) shows the pressure calculated by inviscid theory on the NACA 4412 foil for various lift coefficients, C_L,

where
$$C_L = L/(\tfrac{1}{2}\rho\,U_\infty^2)$$
L = lift force
ρ = fluid density
U_∞ = stream velocity far upstream

Figure 7.5 shows the influence of viscosity on the measured pressure distribution for various angles of incidence (α). Note that for α = 16 percent, for the lowest Reynolds numbers, R,

where
$$R = cU_\infty/\nu$$
c = chord length
ν = kinematic viscosity

the suction peak on the upper surface is greatly reduced. This is due to laminar separation near the leading edge. As R increases, the flow near the leading edge becomes turbulent and remains attached, greatly increasing the height and sharpness of the suction peak. At higher angles of incidence, the pressure towards the trailing edge recovers less and less of the stagnation pressure. The sudden fall to zero indicates turbulent separation. Because of the thickening effect of the boundary layer, the foil effectively is no longer a closed body, so stagnation pressure is not recovered at the trailing edge even in the most favourable case.

143 ...
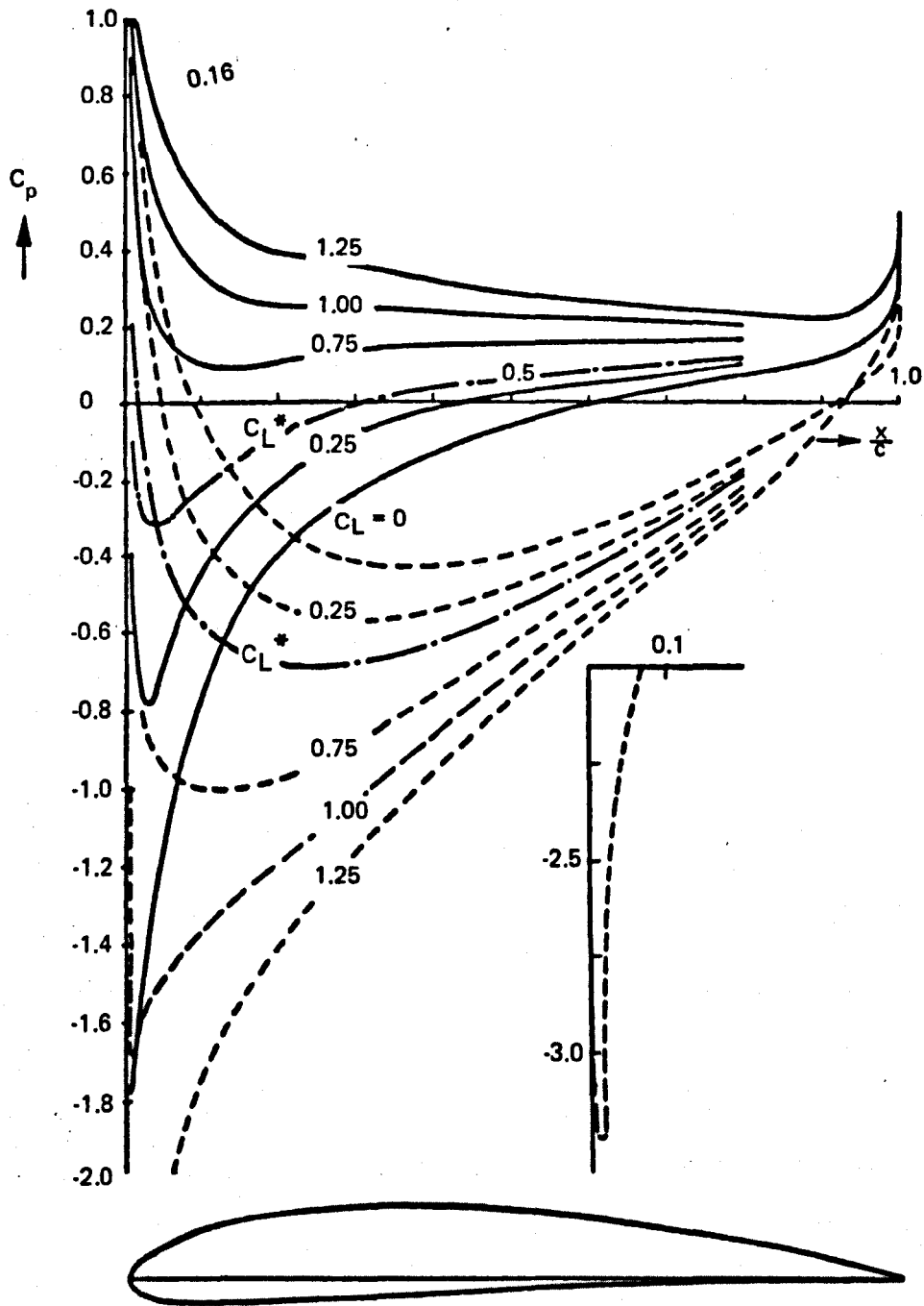
Figure 7.4 – Change of Pressure Distribution with Angle of Attack
(Change in Lift Coefficient). From Riegels[7.4].
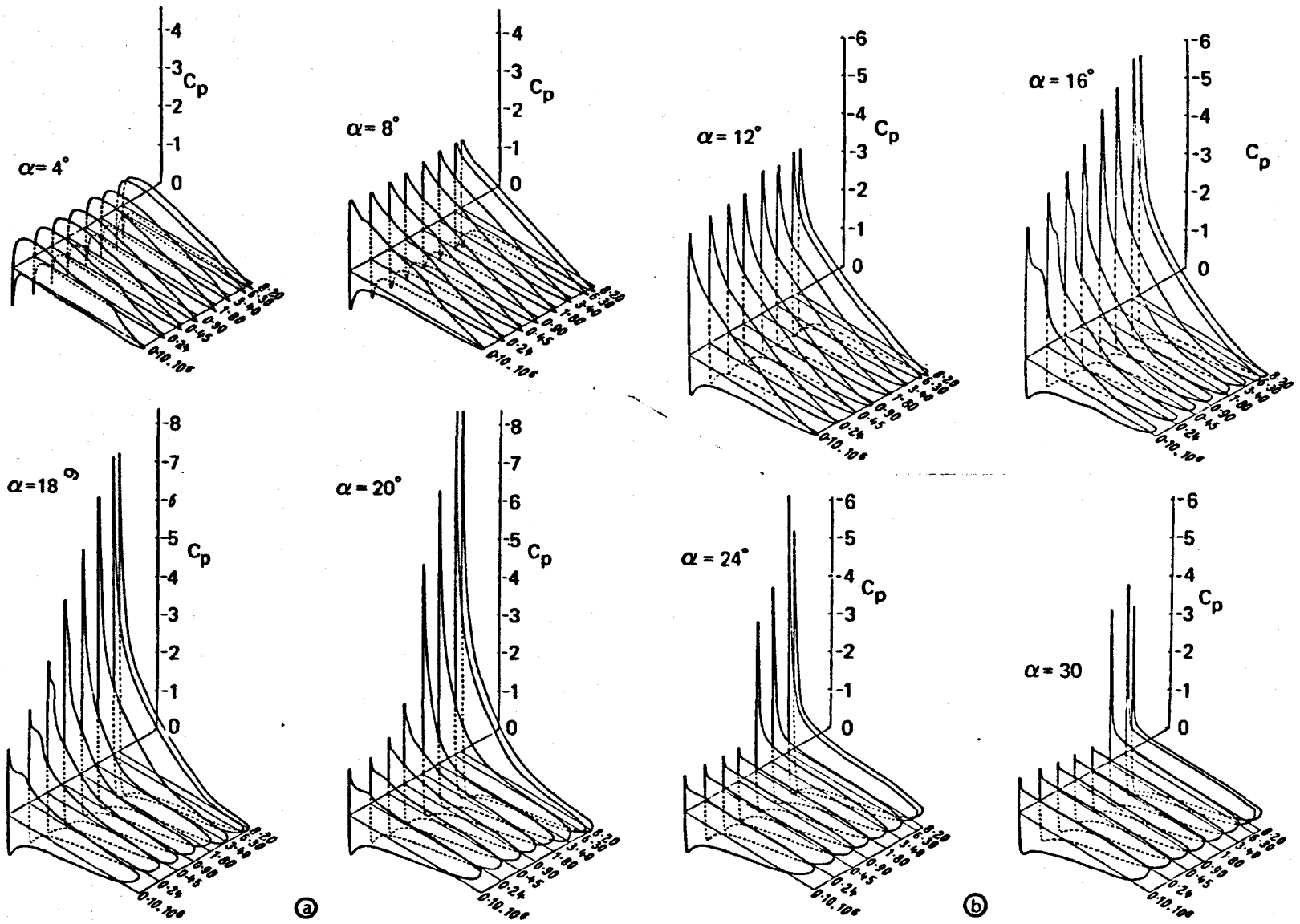
Figure 7.5 — Influence of Reynolds Number on the Pressure Distribution. Profile: 4412. VDT [R 613]. From Riegels[7.4].

Problems Created by Different Possible Flow Patterns. The changing pressure distribution of Figure 7.5 illustrates the problems facing the designer trying to avoid or minimise separation. He must decide whether the flow is laminar or turbulent before the adverse (rising) pressure gradient begins after the suction peak. If the flow is laminar, he must determine whether laminar separation will take place. If the flow is turbulent for leading edge shapes other than sharp wedges, separation will not take place. For practical purposes, once the flow has passed the suction peak, it may be assumed to be fully turbulent. Then the conditions under which turbulent "trailing edge" separation will occur must be determined.

Available Techniques for Solving Boundary Layer Flow Problems. Fortunately, theoretical methods which are virtually exact exist for solving all of the aforementioned problems, at least for two dimensional aerofoils in incompressible flow. Methods for the prediction of transition may correspond somewhat less to reality, but for design purposes, an estimate is usually sufficient. Computer programs for calculating the complete viscous flow around arbitrary two dimensional aerofoils are widely available. Gentry and Oliver[7.5] have collected and compared the most useful of these programs. They have also linked them together into "one giant aerofoil evaluation program". The basic components of that program were then extracted to form the Airfoil Analysis Program which has been published as Volume II of Reference 7.5.

R.M. James[7.6] has developed and programmed an exact method of transforming a specified trailing edge angle and velocity (pressure) distribution into a closed aerofoil shape. This program has been used by Liebeck[7.7] to design a high performance airfoil by using Stratford's criterion[7.3] for separation (which depends only upon the pressure distribution) to specify an afterbody pressure distribution, which is everywhere at incipient separation, hence zero friction. Pick and Lien of the David W. Taylor Naval Ship Research and Development Center (unpublished) have also used this method, developed by Liebeck and Ormsbee[7.8], and the James Program to design an aerofoil with an experimentally measured maximum lift to drag ratio of 160.

The uses and constraints of these methods and programs will be discussed more fully in the section of this chapter on Trailing Edge Separation. However, it will not always be appropriate or possible to use the full arsenal of analytic tools which, in principle, might be available.

Firstly, the exact mathematics of the two dimensional continuum may bear little resemblence to three-dimensional wet reality. Second, the scope of the problem may be such that the effort of obtaining and running elaborate computer programs is not justified. Lastly, other than hydrodynamic considerations may determine the basic shape parameters of struts and foils. Therefore, methods and references are given in the section on Nose Separation which amount to rules of thumb and easy approximations. In the following section, the Stratford method[7.3] of predicting

tail separation is presented. A method of predicting transition due to Michel and Smith is also presented.

Corrections for three-dimensional and free surface effects naturally depend very strongly upon the way in which the surface piercing elements are terminated below the surface. Fig. 7.5 (Rothblum and Mayer)[7.9] compares several theoretical corrections for aspect ratio with experimental force coefficients for surface piercing symetric struts with and without endplate. A first approximation to a corrected pressure distribution would be to assume an elliptic spanwise distribution of the two-dimensional pressure (depending upon termination conditions) and an aspect ratio correction to total lift from Fig. 7.6. For more accurate pressure distributions, Widnall's[7.10] computer program based on three-dimensional theory including free surface, which was used for some of the points in Fig. 7.6, is available at the David W. Taylor Naval Ship R&D Center. The Douglas Neumann program[7.11] is fully three-dimensional but does not include the free surface. Flow observations at high speeds reveal striking symmetry between the flow near the surface and flow at the tip of a surface piercing symmetric strut without end plate. This suggests that a surface piercing strut or foil element might be adequately represented in the Douglas Neumann Program by ignoring the free surface and simply terminating the element where it would normally pass through the surface. A method of correction for aspect ratio and free surface effects based on measured pressure and separation patterns is applied to the Stratford Criterion in Chapter 8, where boundary layer suction is applied to prevent ventilation.

In order to prevent separation for most cases it is probably not necessary to know the flow pattern close to the surface where three-dimensional and surface effects are most pronounced. The separation prediction criteria can be applied well below the free water surface where two dimensional analysis can be most easily corrected for three dimensional effects. As the surface is approached, the pressure relief provided by the surface will be forgiving. Indeed, this is the explanation for the existence of the surface seal discussed in Chapter 2.

LAMINAR NOSE SEPARATION

When laminar flow at the rounded nose of an aerofoil encounters the steep adverse pressure gradient associated with incidence angles (Figures 7.4 and 7.5) the flow is likely to separate. Unless the Reynolds number is impractically low, the flow will become turbulent. If the incidence angle is not too large, the flow will re-attach to the foil, forming a laminar separation bubble. (Turbulent separation then may occur further aft). As mentioned earlier, the types of bubbles may be classified as long or short, depending on their behaviour. The long bubble (Figure 7.2) typically starts out with a length of 2-3 percent of chord and grows with increasing incidence
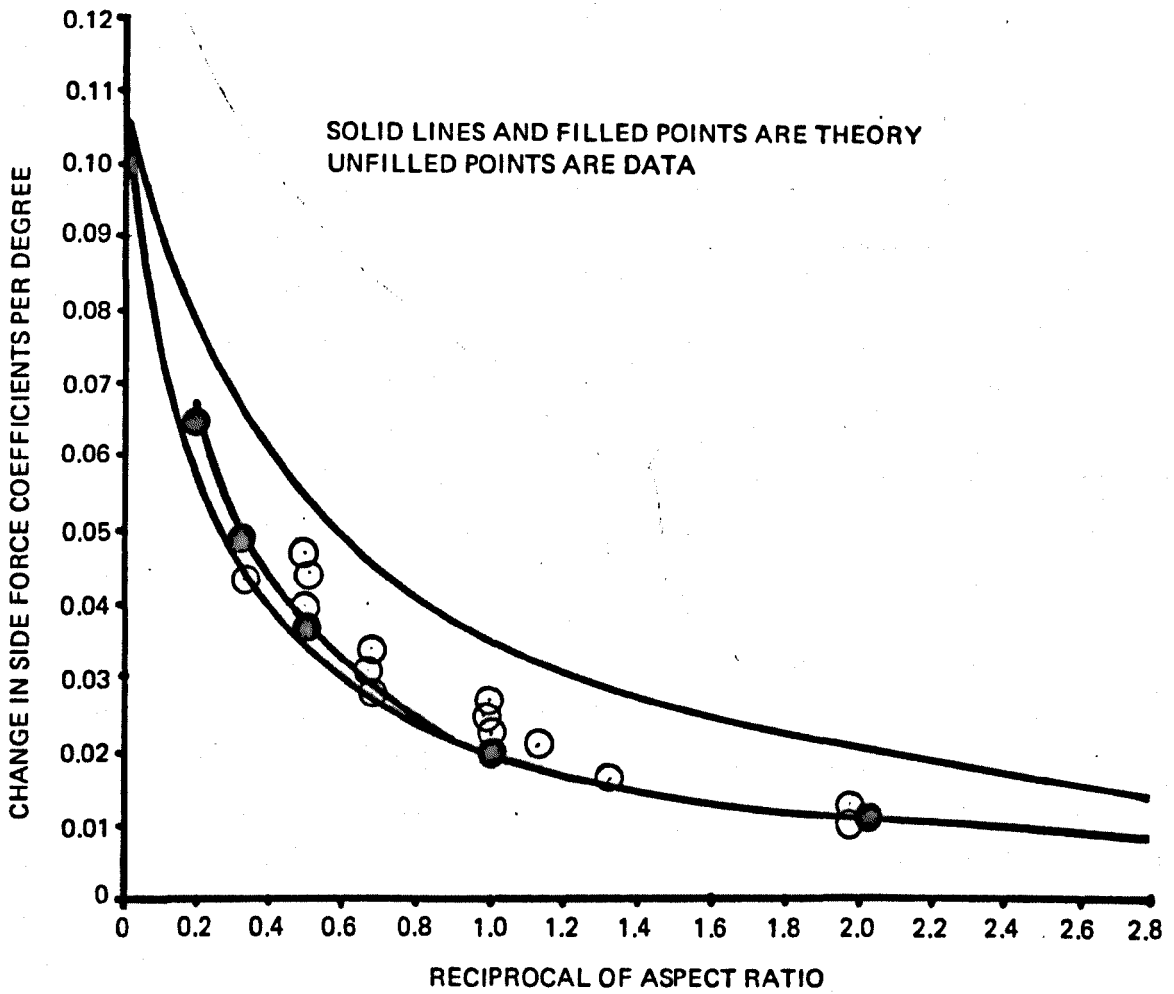
Figure 7.6 — Sideforce Coefficient Slope Versus Reciprocal of Aspect Ratio. From Rothblum, Mayer and Wilburn[7.9].

angle until full leading edge stall occurs. Referring to the same figure, the short bubble appears with a length of only one percent of chord or less. It moves forward with increasing incidence and may shrink, until a critical incidence is reached, at which point it bursts into full leading edge stall. In the flow visualisation work at Leeds the principal distinction between the long and "short" bubbles was found to be their lengthening or shrinking behaviour, rather than their size. The lift coefficient versus incidence curves (C_L vs α) are shown in Fig. 7.7 (after Chappell[7.12]) for the two types of bubbles as well as for trailing edge stall and mixed bubble and trailing edge stall.

Nose ventilation has been observed which was associated with long bubble (growing) separation. However, it is possible that the short (shrinking) bubble, may under certain conditions provide the requirement for a separated region. Furthermore, in prediction, no distinction is usually made between the two types.

Of course, for the hydrofoil designer who wishes to avoid leading edge ventilation, the problem is prevention as well as prediction. The general rule is: thicker shapes, rounded leading edges and higher Reynolds numbers mitigate against leading edge separation. Unfortunately, thick shapes with blunt leading edges have higher drag and are more likely to stall at the trailing edge. Therefore, a criterion is needed which allows the thinnest and sharpest shape for a given Reynolds number.

First Approximation to Transition Prediction. A rule of thumb to determine whether or not a bubble might occur in a particular application is to consider the flow around a two dimensional cylinder (Chang[7.13]). At a Reynolds number of 80 000 (based on diameter), transition does not occur until the separation point. At $R = 10^6$ transition occurs before the laminar separation point. Therefore, if the Reynolds number, based on local foil thickness, is 1 000 000 or more before an adverse pressure gradient is expected on the particular foil at design conditions, fully turbulent flow can be assumed and laminar separation disregarded.

Transition Prediction Based on Boundary Layer Thickness. A more sensitive test depending on the Reynolds number based on boundary layer thickness, is given by Gentry and Oliver,[7.5] attributed to Crabtree.

If $R_{\delta*}$ is defined as
$$\frac{u_e \, \delta^*}{\nu}$$

where
$$\delta^* = \int_0^\infty \left(1 - \frac{u}{u_e}\right) dy, \text{ the displacement thickness}$$

(A) SHORT BUBBLE STALL   (B) LONG BUBBLE STALL   (C) TRAILING EDGE STALL

(D) COMBINED STALL
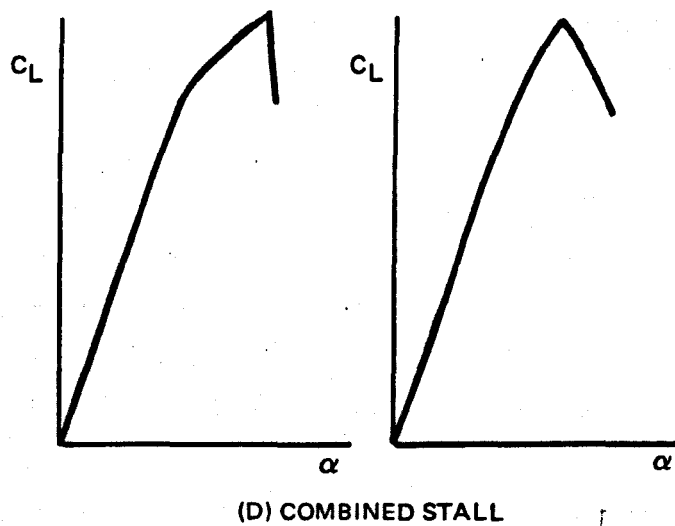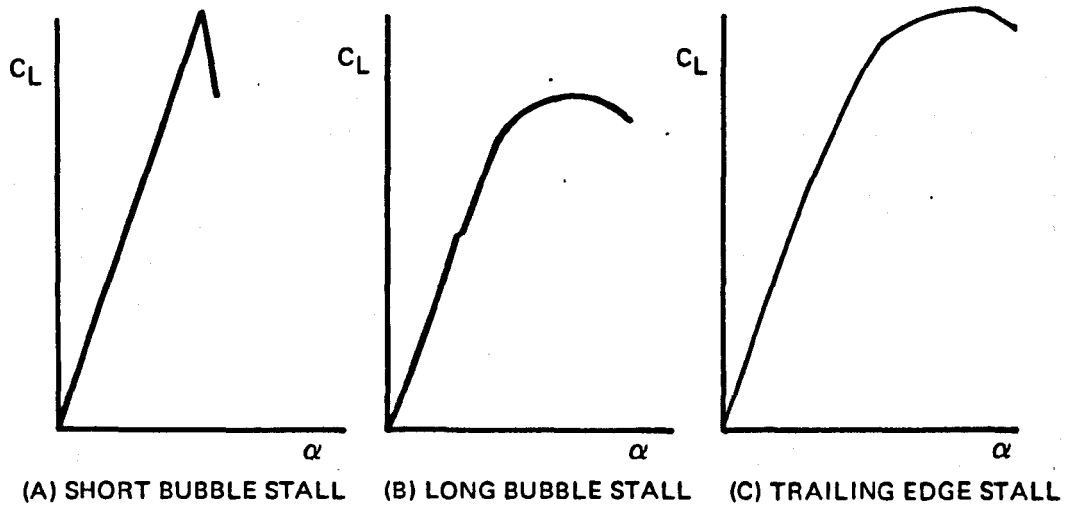
Figure 7.7 — Aerofoil Stall Classification.
After Chappell[7.12].

U = local velocity parallel to foil surface

e = denotes external to boundary layer, usually calculated by inviscid theory

ν = kinematic viscosity

and if $400 < R_{\delta*} < 450$ based on experimental pressure distribution, or $450 < R_{\delta*} < 550$ based on theoretical pressure distribution, then a short nose bubble may be formed. For $R_{\delta*}$ less than the above range, the long bubble or full stall will occur. For $R_{\delta*}$ greater then the range, the flow is likely to be turbulent.

An estimate of $\delta*$ may be obtained without resorting to detailed calculations by using the formulas due to Young and Winterbottom, quoted by Rosenhead[7.14]

$$\theta^2 = 0.45 \, \frac{\nu}{u_e^6} \int_o^x u_e^5 \, dx$$

and $\delta*/\theta \equiv H = 2.56$ for favourable pressure gradient. The constant 0.45 becomes 0.44 in a derivation based on energy rather than momentum balance. Since the Crabtree criterion is not meant to be exact, there is no point in computing the entire inviscid flow just to evaluate $\delta*$. A first approximation would be flat plate flow in which u_e = constant. The next step would be to look for simple potential flows similar to the shape in question.

If the inviscid flow is known, and there is still doubt as to whether the flow is laminar or turbulent, a method of calculating the transition point is given in the section on Turbulent Tail Separation.

Laminar Separation Prediction Methods. Once it has been determined that the flow is laminar up to the point of minimum pressure at the nose—that is, up to the point at which the adverse gradient begins—the next problem is to determine whether laminar separation occurs.

Chang[7.13] enumerates 12 methods for calculating the separation point. The simplest are those due to Stratford and Curle and Skan. They are, respectively

$$\left\{ \bar{x}^2 \, \bar{C}_p \left(\frac{d\bar{C}_p}{dx} \right)^2 \right\}_s \begin{array}{l} = 0.0076 \text{ (Stratford)} \\ = 0.0104 \text{ (Curle \& Skan)} \end{array}$$

Where x = streamwise distance downstream from leading edge

$\bar{x}$ = $x_{eq} + x_o$

o   denotes at point of minimum pressure

s   denotes at separation

$\bar{C}_p = 1 - u_e^2/u_{eo}^2$

U_∞ = flow velocity far upstream

$$x_{eq} = \int_0^{x_0} \left(\frac{u_e}{u_{eo}}\right)^3 dx,$$ the Stratford equivelent flat plate distance which corresponds to the length of flow over a flat plate which would give the same momentum thickness as laminar flow in a favourable pressure gradient.

If the first and second x derivatives of u_e are known, another simple criterion for laminar separation given by Chang and due to Prandtl is

$$\frac{u_e u_e''}{(u_e')^2} > 11$$

Chang also compares the accuracy of the twelve methods with experiment (Chang and Dunham) and with exact solutions.

Curle and Skan seem to agree with the exact methods better than Stratford.

There is some disagreement on equivalent flat plate distances. Rosenhead prefers Thwaits:

$$x_{eq} = \int_0^x \left(\frac{u_e}{u_{eo}}\right)^5 dx$$

Comparison with Experiment on Surface Piercing Strut. McGregor[7.15] calculated the separation point of the blunt nosed biogive surface piercing strut tested at Leeds and found the predicted separation point to be virtually at the leading edge for a pressure distribution based on two-dimensional potential theory. The actual separation point was found experimentally to be at about x/c = 0.03. The discrepancy was probably due to the lowered pressure gradient associate with the submergence aspect ratios of only 2.0. This serves to illustrate that computations based on the two dimensional theory will be conservative.

Empirical Prediction Methods for Laminar Separation. Perhaps the best estimate, including three dimensional effects, of whether or not leading edge separation will occur can be made by a comparison with accumulated experimental data. This has the advantage of eliminating computations altogether.

Since the flow near the leading edge of an aerofoil depends primarily on the leading edge radius, McCullough and Gault established an empirical correlation between the different types of stall, Reynolds number and the half thickness based on chord at 1.25 percent chord ($z_{1.25}/c$).

This correlation is presented as Figure 7.8, taken from Chappell.[7.12] For wings of finite aspect ratio Chappell was able to establish that the important parameter was a Reynolds number based on streamwise chord length at the wing tip, with a minor correction for sweep and taper. This is shown in Fig. 7.9 as $(R_{ct})_n$ vs $(z_{1.25}/c)_n$. The subscript n indicates measurement normal to the leading edge for swept wings. Subscript t indicates measurement at the wing tip. Figure 7.10 shows Chappell's correlation for the maximum incidence angle before initial leading edge separation occurs (α_κ). The term $\cos\Lambda_0$ is a correction for leading edge sweep. Note that in this case an additional parameter is necessary, namely $(t/c)_s$

where

t = max section thickness

c = chord length

s denotes streamwise measurement

The abscissa is a Reynolds number, $(R_{\rho t})_n = \dfrac{\rho U_\infty}{\nu}$ for untapered, unswept wings,

where

U_∞ = the stream velocity far upstream

ρ = the leading edge radius

t indicates measurement at the wingtip

n indicates measurement normal to the leading edge

ν = kinematic viscosity

The more general definition of $(R_{\rho t})_n$ is somewhat complex, and the interested reader should refer to Chappell.

An area that deserves a comment is the model testing of prototype shapes. Because of the higher Reynolds numbers associated with prototype size and speed, the prototype may not experience laminar separation, but geometrically similar but smaller models, tested at slower speeds, will. In order to eliminate these discrepancies in airfoil and ship model testing, turbulence stimulators, such as sandpaper roughness, are often used. The height of sandpaper type roughness necessary to stimulate turbulence corresponds to a roughness height Reynolds number of

$$R_k \equiv \frac{u_k k}{\nu} > 600$$

where

k = the maximum height of roughness
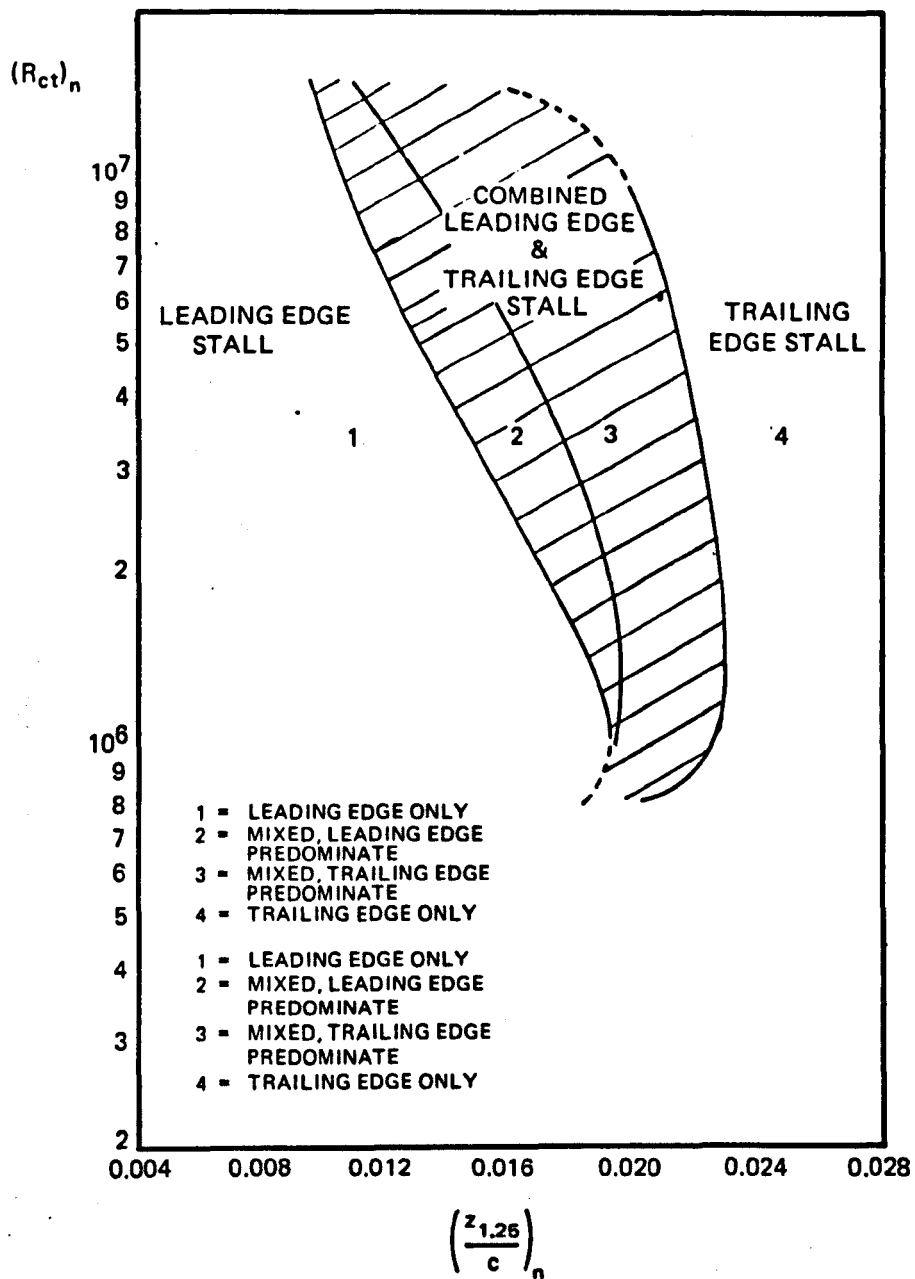
Figure 7.9 — Initial Separation Characteristics of Three-Dimensional
Plane Wings with Constant Symmetrical Sections.
(Chappell[7.12])

155
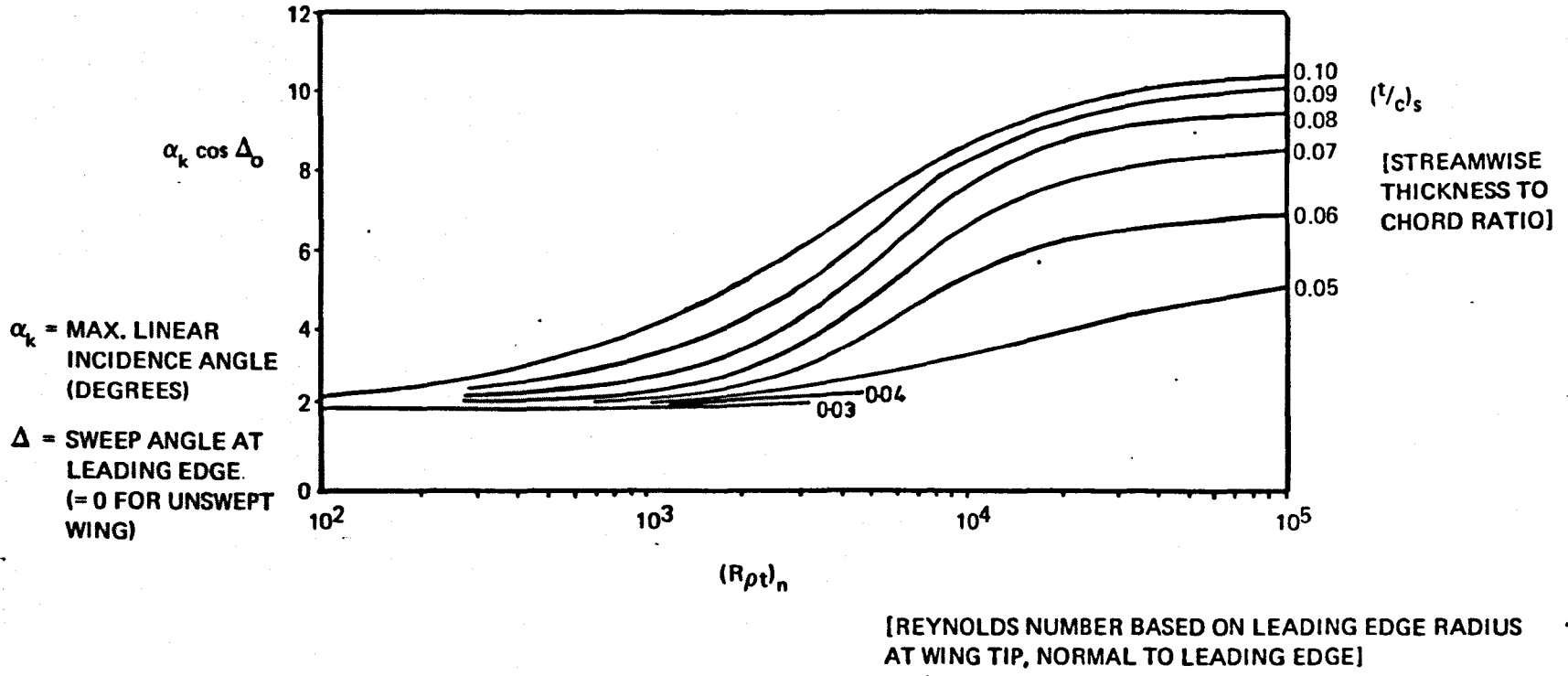
Figure 7.10 — Leading Edge Initial Separation Boundaries for Plane Wings
with Constant Symmetrical Sections. (Chappell[7.10])

$$u_k = \text{the local velocity at the roughness height.}$$

If $R_k < 200$, the roughness will not initiate turbulence. (Dommet[7.16]).

A simple estimate for u_k may be made using the Young–Winterbottom assumption, quoted by Rosenhead

$$\frac{\delta}{\theta} = 8.51$$

Where θ is as before and δ is the effective thickness of the boundary layer. Then by assuming that u/u_e has the form approximating (flat plate profile)

$$\frac{u}{u_e} = \frac{3}{2}\frac{y}{\delta} - \frac{1}{2}\left(\frac{y}{\delta}\right)^3 \quad (\text{Schlichting}[7.17])$$

u_k is calculated by substituting $u_k = u$, $y = k$.

$$u_k = u_e \left\{\frac{3}{2}\frac{k}{\delta} - \frac{1}{2}\left(\frac{k}{\delta}\right)^3\right\}$$

$$\delta = \frac{5.7}{u_e^3}\left\{\nu \int_0^x u_e^5 \, dx\right\}^{1/2}$$

TURBULENT TAIL SEPARATION

Relation of Tail Separation to Ventilation. Once laminar separation at the nose has been avoided, the ventilation design problem then becomes one of avoiding turbulent separation on the after portion of the foil. It is not known whether there is a correlation between the location on the body of turbulent separation and occurence of ventilation. A separation point which is farther forward will create a larger region of separated flow, but, on the other hand, the surface drawdown will not be as great because of reduced pressure differential. The rule then, is simply to avoid separation under design conditions. If this is impossible, other considerations, such as maximum linearity of lift forces, will favour a separation point as far aft as possible.

Methods of Prediction of Tail Separation. There are many good methods for calculating the properties of turbulent boundary layers, including the separation points. A recent comparison of four of the more convenient methods representative of the principal approaches to the problem as applied to aerofoils is given by Cebici, Mosinskis and Smith[7.18]. The methods of Douglas,

Head, Goldschmied, and Stratford are used to calculate separation points on two aerofoils and the results are compared with experimental pressure distributions. The method of Stratford, by far the most simple, is in fairly close agreement with experimental values and with the two most consistent but computationally more involved methods of Douglas and Head. The Stratford method predicts a somewhat earlier separation.

Stratford Criterion. The Stratford criterion for separation depends only upon the velocity distribution and its derivatives outside the boundary layer. Therefore, a velocity distribution is implied which recovers a given pressure difference in the least distance while preventing separation. This result was utilised by Stratford[7.3] to build a surface in a wind tunnel with nearly zero shear stress in an adverse pressure gradient. The zero shear stress resulted from the condition of incipient separation over the entire surface in the adverse pressure gradient.

The same principle was used by Liebeck and Ormsbee[7.8] to design an airfoil with maximum lift without separation. A second order theory (Weber) was used to relate a particular airfoil shape to the specified velocity distribution, which incorporated Stratford's criterion to achieve the maximum suction peak which could be recovered from without separation.

More recently Liebeck[7.8] used the "exact" method of James[7.6] to derive a class of high lift airfoil shapes from the Stratford velocity distribution. Pick and Lien at the U.S. Naval Ship Research and Development Center designed and experimentally tested an airfoil, using the James method and Stratford's criterion, whose measured lift to drag ratio was greater than 100 at design lift, and was as high as 160. (Internal publication).

Derivation of the Stratford Criterion: Physical Argument. Because the Stratford method of predicting separation is so useful and easy to apply, it is the one presented here as a design aid. In essence, the boundary layer is considered to consist of two regions; an inner region dominated by viscosity and an outer region dominated by inertial forces. In the outer region, flow along a streamline loses inertia to balance a rising static pressure in an adverse gradient. The shear forces are relatively unimportant in this layer. In the inner region, the fluid inertia is too low to balance the pressure forces. In fact, at the wall, the inertia is zero. Therefore, the pressure forces must be balanced entirely by shear forces. Specifically, the flow in the outer region is assumed to be exactly that over a flat plate, except that the velocity along each "streamline" is reduced by an amount $\Delta u^2 \propto \Delta p$. The term "streamline" does not strictly apply, since the flow is assumed turbulent.

(1)
$$\tfrac{1}{2}\rho u^2 (x, \psi) = \tfrac{1}{2}\rho u^2 (x, \psi) - (p - p_0), \psi \geq \psi_i$$

where

ρ = mass density

x = distance from start of initial conditions

ψ = stream function = $\int_0^y u\,dy$

u = local streamwise velocity

p_o = pressure initially

p = local pressure

u' = flat plate comparison velocity

i — denotes inner layer

The shape of the comparison profile is taken to be

(2a)
$$\frac{u'}{U_o} = \left(\frac{y'}{\delta'}\right)^{1/n},$$

(2b)
$$\delta' = \frac{(n+1)(n+2)(0.036)\,x}{nR_x^{1/5}}$$

where U_o = the initial velocity or the velocity far upstream

n = an integer varying with R but close to 7 for practical purposes

δ' = the boundary layer thickness of the comparison profile

y' = the perpendicular distance from the boundary in the comparison profile

R_x = the Reynolds number, xU_o/ν

ν = kinematic viscosity

Stratford references Goldstein and Schlichting as the source of this form of the flat plate comparison profile. It appears in roughly this form in basic fluid mechanics texts.

By differentiating (1) with respect to ψ and replacing $u\left(\frac{\partial}{\partial\psi}\right)$ by $\frac{\partial}{\partial y}$, it can be shown that

(3)
$$\left|\frac{\partial u}{\partial y}\right|_{(x,\psi)} = \left|\frac{\partial u'}{\partial y'}\right|_{(x,\psi)} \quad (\psi \geq \psi_i).$$

Since the chain rule for partial diffentiation states that $\frac{\partial}{\partial y} = u\frac{\partial}{\partial\psi} + \left(\frac{\partial x}{\partial y}\right)_{\psi\,=\,const}\partial x$, Equation (3) does not seem justified on mathematical grounds, or at least the step from (1) to (3) is non-trival. However, the physical interpretation of (3) that the shape of the outer layer profile is the same as the comparison profile for the same values of x and ψ, (along the same "streamline") may be accepted as a reasonable starting assumption. Arguing from mixing length theory and dimensional considerations, Stratford hypothesises that the inner layer, at the point of incipient

separation (wall shear stress $\tau_0 = 0$) has the form

(4)
$$u^2 = \frac{A^2}{\rho} \frac{\partial p}{\partial x} \, y, \quad y \le y_i$$

where A is a constant to be determined later but which includes the Karman mixing length.

Outline of the Mathematical Argument. The crux of Stratford's argument is that at incipient separation, the inner boundary layer is parabolic (e.g. (4)) and the outer layer obeys a power law (eqs. (1) and (2)). The shape of the inner layer depends on $\frac{dp}{dx}$, and the shape of the outer layer on $\frac{dp}{dx}$, x and slightly on R. (n is a function of R). As it happens, the requirement that the inner and outer layers meet for some value of ψ, u and $\frac{\partial u}{\partial y}$, uniquely determines an x which depends only upon $\bar{C}_p$, $d\bar{C}_p/dx$ and R,

$$\left(\bar{C}_p \equiv 1 - \left(\frac{u_e}{U_o}\right)^2 \right)$$

where u_e denotes streamwise velocity calculated <u>outside</u> the boundary layer (e.g. from potential flow). The following equations represent the functional relationship between the above variables, with some slight changes in notation which reflect that the point of minimum pressure and maximum velocity may not occur at the leading edge, as assumed in the derivation.

(5a)
$$(2\bar{C}_p)^{1/4}(n-2)\left(x\frac{d\bar{C}_p}{dx}\right)^{1/2} = 1.06\beta \, (10^{-6} R_x, u_{eo})^{1/10}, \quad \bar{C}_p \le \frac{n-2}{n+1}$$

(5b)
$$\beta = 0.66, \quad \bar{C}_p \le \frac{n-2}{n+1}$$

(5c)
$$n = \log_{10} R_s$$

where
$$R_s \equiv \frac{x_s u_{eo}}{\nu}, \quad R_x, u_{eo} \equiv \frac{x u_{eo}}{\nu}, \quad \bar{C}_p \equiv 1 - \left(\frac{u_e}{u_{eo}}\right)^2$$

o denotes "at the point of minimum pressure" in the general case where the adverse pressure gradient may be preceded by a favourable one.

e denotes (e.g. velocity) evaluated just outside the boundary layer, from the calculated inviscid flow at the solid boundary

s denotes separation

Simplified Stratford Criterion. For Reynolds numbers of about 10^6, a simplified form of equations 5a, b, c is

(6)
$$\bar{C}_p \, (xd\bar{C}_p/dx)^{1/2} = 0.39 \, (10^{-6} \, R_s)^{1/10}$$

After a comparison with some experimental results, Stratford found that for $d^2p/dx^2 \geqslant 0$, he got better result using $\beta = 0.73$. This correction reflects the essentially empirical nature of the derivation of the criterion. (In equation (6) $\beta = 0.73$ changes the factor 0.39 to 0.35). To clarify the use of equations (5) or (6) an example is given by Stratford of the case of a linear pressure rise starting at the leading edge.

$$\bar{C}_p = \frac{x}{c}$$

For simplicity in solving equation (6) the Reynolds number R_s (at separation) is assumed to be 10^6. Since $d^2p/dx^2 = 0$, $\beta = 0.73$. Then

$$\left| (x/c)^{3/2} \right|_s = 0.39$$

$$x_s/c = \bar{C}_{p,s} = 0.53$$

$$u_{es}/U_o = 0.68$$

Equivalent Flat Plate Distance. Because equations (5) are based on flat plate velocity profiles as an initial condition, their validity is limited to the case of an adverse pressure gradient arising after an initial length of constant pressure, turbulent flow. On the typical hydro-aero-foil there will be an initial favourable pressure gradient in which flow may be either laminar or turbulent. If this is the case, the distance from the leading edge to the point of minimum pressure must be replaced by an equivalent distance, x_{eq}, which is the distance over which the turbulent boundary layer on a flat plate would have to progress to have a momentum thickness equal to the actual momentum thickness at x_o, with a freestream velocity $U_\infty = u_o$.

Cebici et al [7.18] use a slightly different, and more recent formulation for x_{eq} than Stratford, based on an analysis by Thwaites. It is this version which is presented since it has been compared with airfoil results with a reasonable degree of success. For struts and most moderately cambered airfoils, the point at which the adverse pressure gradient begins is rather far forward, so any corrections to the distance from the leading edge to the point of minimum pressure will not have much

effect and, in fact, can be ignored as a first approximation.

$$(7) \qquad x_{eq} = 58 \frac{\nu}{U_o} \left[\frac{u_{tr}}{\nu} \int_0^{x_{tr}} \left(\frac{u_e}{u_{eo}} \right)^5 dx \right]^{3/5} + \int_{x_{tr}}^{x_o} \left(\frac{u_e}{u_{eo}} \right)^4 dx$$

where $_{tr}$ denotes transition from laminar to turbulent flow.

Liebeck and Ormsbee[7.8] used the integrated Stratford criterion for separation to get an expression for the pressure recovery which is the greatest possible in a given distance without provoking separation. It should be quite useful to a designer:

$$(8) \qquad \overline{C}_p (x/x_o) = 0.49 \{ (R_{x, u_o})^{1/5} \ [(x/x_o)^{1/5} - 1] \}^{1/3}, \qquad \overline{C}_p \le 4/7$$

$$(9) \qquad \overline{C}_p (x/x_o) = 1 - \{ a/[x/x_o + b]^{1/2} \}, \qquad \overline{C}_p > 4/7$$

where a and b are constants chosen to match the value and slope of the C_p curve for $C_p < 4/7$ at $C_p = 4/7$.

Equation (5) was derived from the Stratford n = 6 case, that is, $R \sim 10^6$. For this case, (1) assumes the simpler form given in equation (6). Stratford gives a more general integration of (1) for $\beta = 0.66$, the value which he found to obtain for surfaces of zero shear: :

$$(10) \qquad \overline{C}_p = 0.645 \left(0.435 \, R_o^{1/5} \left[(x/x_o)^{1/5} - 1 \right] \right)^{2/n}, \qquad \overline{C}_p \le \frac{n-2}{n+1}$$

For $R_o \sim 10^6$, this simplifies to

$$(11) \qquad \overline{C}_p = 1.23 \left[(x/x_o)^{1/5} - 1 \right]^{1/3}, \qquad \overline{C}_p \le 4/7$$

Equation (9) can also be used to extend the range of $\overline{C}_p$ to $\overline{C}_p > 4/7$ in (11) by choosing a and b to match the slope of the $\overline{C}_p$ curve in (11).

Calculation of Transition Point. To utilise equation (7) to calculate x_{eq}, it will be noted that the position of transition from laminar to turbulent flow must be known. In general, it is usually sufficient to assume that the flow from the leading edge to the point of minimum pressure, x_o, is either fully turbulent or fully laminar using the criteria of the section on Laminar Nose Separation. If the case arises, and the "exact" location must be found, Cebici et al[7.18] found that

Granville's method[7.19] gave good agreement with experimental values of transition. A second method due to Michel[7.20] and Smith did not agree so well at low Reynolds numbers but did better at the higher ones. Because the Michel-Smith method is vastly more simple, it will be presented.

Figure 7.11 shows R_θ plotted against R_x for transition values,

where
$$R_\theta = \frac{u_e \theta}{\nu}$$

and

$$\theta = \int_0^\infty \frac{u}{u_e} \left(1 - \frac{u}{u_e}\right) dy, \text{ the boundary layer momentum thickness.}$$

Approximate values of θ can be calculated from the formula presented earlier.

$$\theta = \left(0.45 \, \nu u_e^{-6} \int_0^x u_e^5 \, dx\right)^{1/2}$$

After determining R_θ and R_x for several values of x, the intersection with the correlation curve gives the transition "point".

In any case, prediction of transition is not as accurate as prediction of other boundary layer properties. For one thing, transition is not instantaneous, but takes place over a non-zero length. Gentry and Oliver,[7.5] in the Airfoil Analysis Program (AAP) assembled at Douglas Aircraft Company, account for this length by a slow activation of eddy transport coefficients (Cebici-Smith) or by an empirical delay distance (Granville).

An Iterative Method for Designing Separation-Free Foils. Not only does the AAP account for nearly all the fine points that hand calculated predictions must ignore, but when coupled with the program of James' inverse airfoil method[7.6] it makes possible an iterative design procedure of great power. Specifically, the AAP calculates all the viscous properties of two dimensional flows about aerofoils. The James program calculates an aerofoil shape from a given velocity distribution. The required velocity distribution to avoid separation is given by Stratford[7.2]. Liebeck and Ormsbee proposed velocity distributions for laminar and turbulent nose flows and high lift coefficients. These criteria and any other which can be reduced to a velocity distribution may then be used as input to the James program. The tail angle may be specified to avoid the impractically fine tail which results from first and second order inverse airfoil theories (e.g. Richardson[7.21]). The James program provides as output the closed airfoil shape which most

163
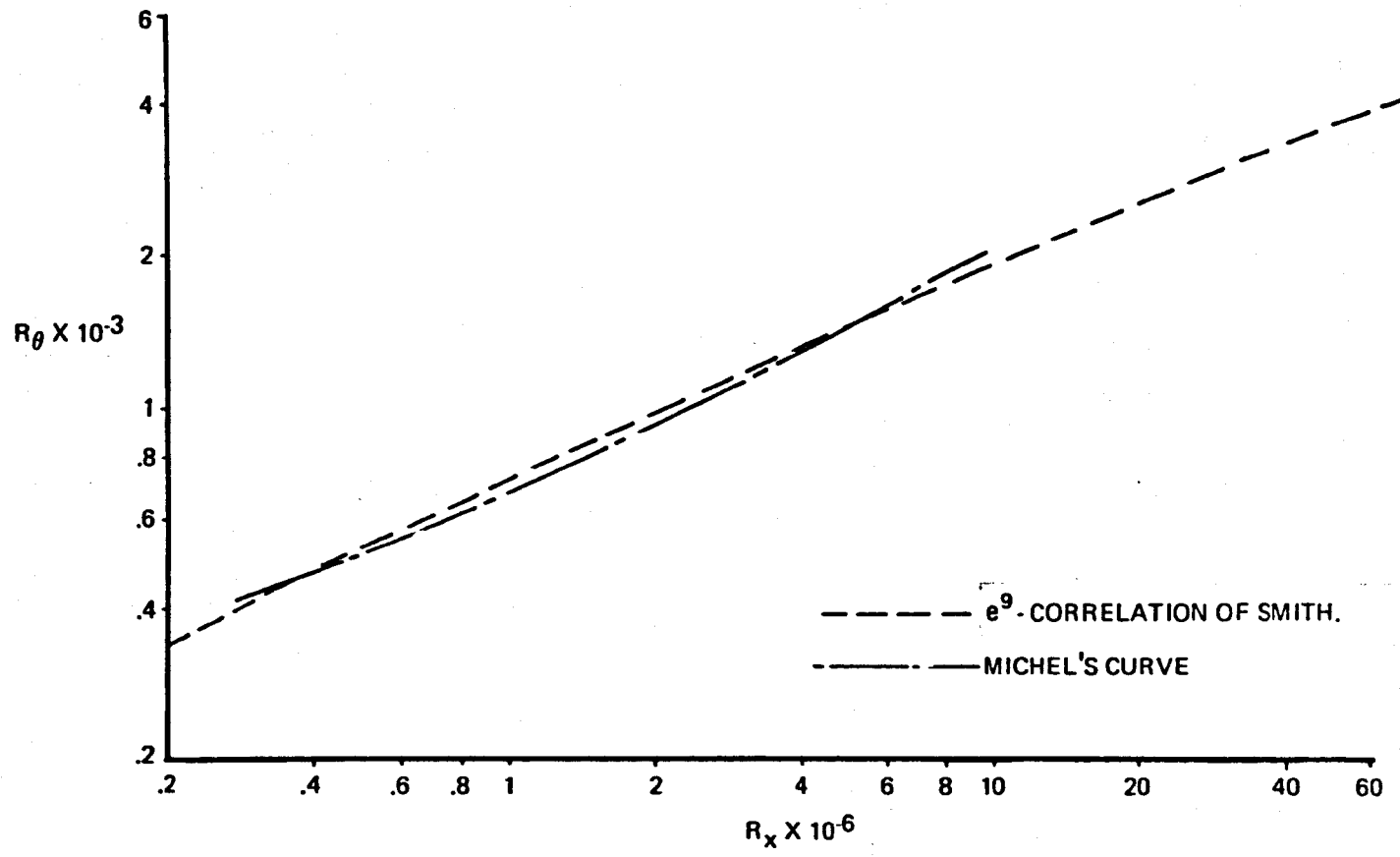
Figure 7.11 — Transition-Correlation Curves of Michel and Smith[7.15].

closely approximates the input distribution, as well as giving the final velocity distributions of the output shape. When the designer is satisfied that he has achieved as much of his goal as possible he can then use the AAP to calculate the viscous properties of his new shape to ensure they are as anticipated. He may then use the viscous results to further refine his shape.

Application of Separation Prediction Methods. The actual design of a strut or foil using the techniques described in this chapter is beyond the scope of the thesis. However, use of the laminar and turbulent separation criteria is demonstrated in Chapters Eight and Nine, including the necessary modifications due to finite length and the presence of the free water surface.

7.1   Barr, R.A. and Vermeulen, J.C., *"Hydrodynamics of Hydrofoil Craft: Sub-Cavitating Hydrofoil Systems,"* Hydronautics Incorporated Technical Report 463-1, 1964.

7.2   McCullough, G.B. and Gault, D.E., *"Examples of Three Representative Types of Airfoil – Section Stall at Low Speeds,"* NACA TN 3505, Sept 1955.

7.3   Stratford, B.S., *"The Prediction of Separation of the Turbulent Boundary Layer,"* Journal of Fluid Mechanics, Vol. 5, p. 16, 1959.

7.4   Riegels, F.W., *"Aerofoil Sections,"* London Butterworths, 1961.

7.5   Gentry, A.E. and Oliver, W.R., *"Investigation of Aerodynamic Analysis Problems in Transonic Maneuvering,"* Report No. MDC-J5264-31, Office of Naval Research, Department of the Navy, 1971.

7.6   James, R.M., *"A New Look at Two Dimensional Incompressible Airfoil Theory,"* Report No. MDC-J0918/01, Douglas Aircraft Company, 1971.

7.7   Liebeck, R.H., *"A Class of Airfoils Designed for High Lift,"* AIAA 73-86, Jan 1973.

7.8   Liebeck, R.H. and Ormsbee, A.I., *"Optimisation of Airfoils for Maximum Lift,"* Journal of Aircraft, Vol. 7, No. 5, pp. 409-415.

7.9   Rothblum, Richard S., Mayer, Dennis A., and Wilburn, Gene M., *"Ventilation, Cavitation and Other Characteristics of High Speed Surface Piercing Struts,"* Naval Ship R & D Center Rept. No. 3023, 1969.

7.10   Ashley, H. et al, *"New Direction in Lifting Surface Theory,"* AIAA Journal, Vol. 3, No. 1, pp. 3-16, 1955.

7.11   Smith, A.M.O. and Pierce, J., *"Exact Solution of the Neumann Problem. Calculation of Plane and Axially Symmetric Flows About or Within Arbitrary Boundaries,"* Douglas Aircraft Company Report ES 26988, April 1958.

7.12   Chappell, P.D., *"Flow Separation and Stall Characteristics of Plane, Constant-Section Wings in Subcritical Flow,"* The Aeronautical Journal, Vol. 72(1), pp. 82-90, Jan 1968.

7.13   Chang, P.K., *"Separation of Flow,"* Pergamon Press, 1970.

7.14   Rosenhead, L., *"Laminar Boundary Layers,"* Oxford, Clarendon Press, 1963.

7.15   McGregor, R.C., *"Quasi Separation Bubble,"* Interim Report TP/DREA/6, 1972.

7.16   Dommet, R.L., Journal Royal Aeronautical Society, Vol. 63, p. 722, 1970.

7.17   Schlichting, Hermann, *"Boundary Layer Theory,"* 4th Ed., McGraw-Hill, 1960.

7.18   Cebici, T., Mosinskis, G.J. and Smith, A.M.O., *"Calculation of Viscous Drag and Turbulent Boundary Layer Separation on Two Dimensional and Axisymmetric Bodies in Incompressible Flows,"* Report No. M.I.C. J0973-01 Douglas Aircraft Company, 1970.

7.19 Granville, P.S., *"The Calculation of the Viscous Drag of Bodies of Revolution,"* David Taylor Model Basin Report 849, July 1953.

7.20 Michel, R., *"Etude de la transition sur les profiles d'aile; etablissement d'un critere de determination du point de transition et calcul de la trainee de profile incompressible,"* O.N.E.R.A. Report 1/1578A, July 1951.

7.21 Richardson, J.R., *"Studies of the Nose Shape of Hydrofoil Profiles Which Have a Wide Non-Cavitating Incidence Range,"* Engineering Research Associates Report 53/2.

CHAPTER 8
SUPPRESSION OF VENTILATION BY ELIMINATING
THE SEPARATED REGION BY SUCTION

OBJECT OF THE EXPERIMENT

Necessity of Separation. It was noted in Chapter 2 that separation had been associated with ventilation at least since 1940. Based on the mechanism of ventilation postulated in Chapter 2, it is plausible that separation or cavitation is necessary to provide a region which could be displaced by atmospheric air. In Chapter 3 elimination of the region of separation was suggested as a method of ventilation suppression. However, this has never previously been accomplished in a direct and unequivocal manner. Von Schertel solved the problem of ventilation on his surface-piercing hydrofoils by using a combination of section design, taper, twist and dihedral as discussed in Chapter 3. This may have eliminated regions of separation which existed on earlier, unsuccessful versions of his foil systems, but so many parameters were changed, elimination of separation may not have been the critical factor.

Because of the ambiguity of available information, it was felt important to the formulation of the ventilation mechanism to conduct an experiment in which ventilation was suppressed by the elimination of a previously existing region of separation, while changing all other parameters as little as possible. By doing this, the role of separation in the mechanism of ventilation would be firmly established, and a technique of suppression would be verified.

EXPERIMENTAL APPROACH

Use of Suction. The requirement to eliminate a region of separation without changing any of the relevant geometric characteristics of a surface-piercing foil suggested the technique of boundary layer suction, mentioned in Chapter 3. The use of the suction technique required only the addition of a fine slot near the nose of a symmetric, surface-piercing strut. The entire geometry of the experiment was then nearly constant. In particular, there was no change in nose radius, thickness, camber, roughness, immersion depth, and angle of attack, which have all been shown to influence the onset of ventilation.

Choice of Model. For the suction experiment, a symmetric surface-piercing strut was chosen which had a section shape that was known to favour predominately nose ventilation, due to a small region of laminar separation at the nose. It was felt that this small region of separation, associated with a laminar separation "bubble", could be more easily eliminated than massive separation observed on other section shapes prior to ventilation. Also, if it were true that ventilation could be precipitated in the absence of separation, it was most likely that

this would be possible in a situation for which very little separation ordinarily occurred prior to ventilation.

A strut with a modified bi-ogival section had been previously tested extensively at Leeds.[8.1, 8.2, 8.3] Its ventilation characteristics were well-known, as was its separation pattern. A calculated pressure distribution was available, as well as an experimental verification of the pressure at certain points. The biogive is one of the most extensively tested section shapes in ventilation research, so there was a relatively large basis for comparison in the literature.

The particular biogival section chosen was symmetric, with maximum thickness equal to 10 percent of chord, the thickness distribution being described by arcs of a circle, as shown in Figure 8.1. The sharp nose of the pure ogival section shape was modified by blunting the leading edge to a radius of 1/10 chord. The chord length of the model chosen was about 120mm. Further details of the model's physical characteristics will be found in the section of this Chapter on Experimental Procedure.

The previous Leeds studies had established that the blunt-nosed biogive was particularly prone to nose ventilation at a speed of 6m/s. At this speed, the maximum sideslip angle that could be sustained for more than a few seconds was 10 degrees. This low ventilation angle ensured that extraneous tail separation associated with higher sideslip angles would not cloud the test results.

THEORETICAL CONSIDERATIONS

Boundary Layer Theory. In order to understand the effects of suction, it is necessary to review the fundamental equations of the boundary layer. The notation will be as in Figure 8.2. The two-dimensional boundary layer equations may be derived from the Navier-Stokes equations by assuming that, in the region near a solid boundary of the fluid, certain quantities are small compared to others. Without going into great detail, the basic assumptions are that the flow is well-described by inviscid theory everywhere except for a narrow region near the fluid boundary of thickness δ. Following Schlichting,[8.4] the Navier-Stokes equations may be non-dimensionalized by referring all velocities to the free stream velocity, U_∞, and all lengths to length L which is chosen such that $\frac{\partial u}{\partial x} < 1$ in the boundary layer. Pressures are referred to ρU_∞^2, and time to L/U_∞. The Reynolds number is as perviously defined

$$R = \frac{U_\infty L \rho}{\mu} = \frac{U_\infty L}{\nu}$$

171
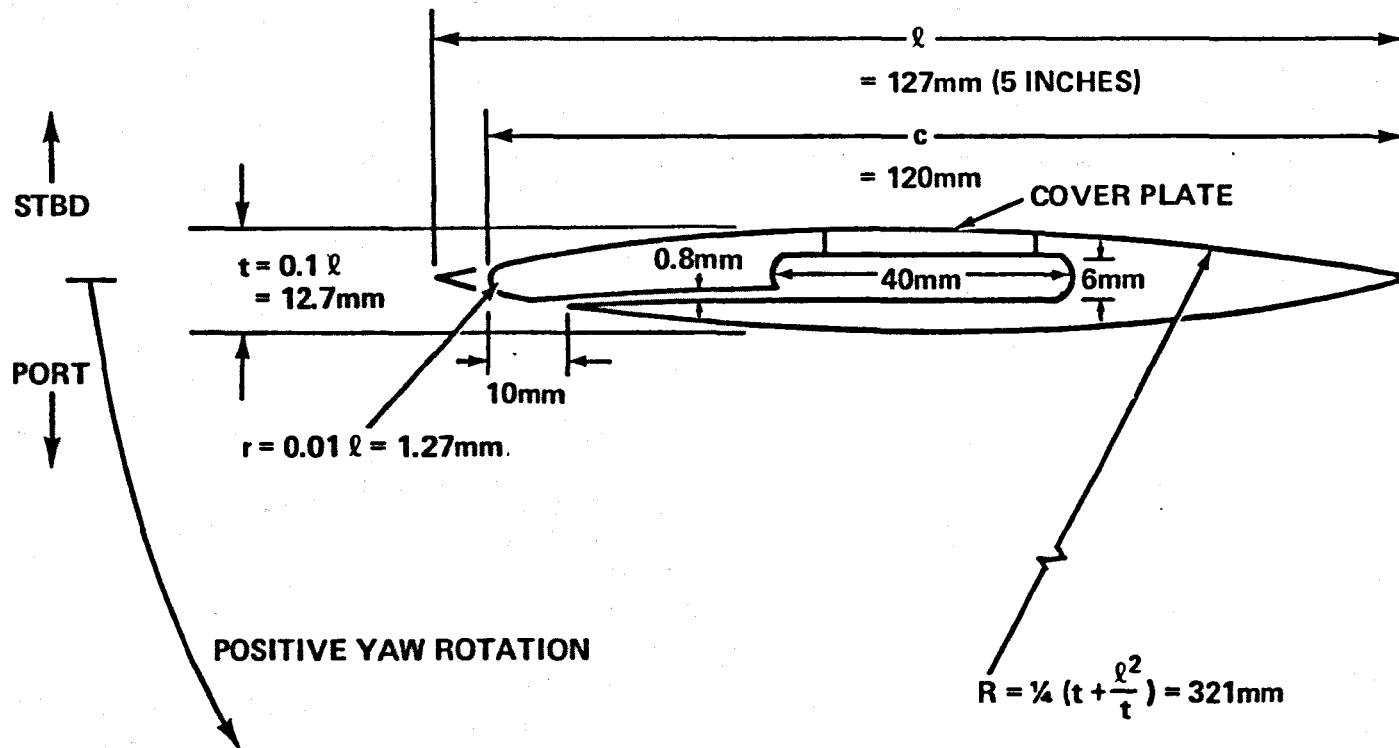
Figure 8.1 — Section of Blunt-Nosed Biogive Showing Principal Dimensions

y (DISTANCE ⊥ TO BOUNDARY)

U_∞ (VELOCITY FOR UPSTREAM)

u_e (EXTERNAL VELOCITY)

OUTER EDGE OF BOUNDARY LAYER

v (VELOCITY ⊥ TO BOUNDARY WITHIN BOUNDARY LAYER — POSITIVE SENSE IS TOWARDS BOUNDARY)

u

δ (BOUNDARY LAYER THICKNESS)

x (DISTANCE ALONG BOUNDARY)

BOUNDARY

v_0 (SUCTION VELOCITY)

(VELOCITY PARALLEL TO BOUNDARY WITHIN BOUNDARY LAYER)

P IS PRESSURE AT A POINT REFERRED TO ρU_∞^2, WHERE ρ IS DENSITY

τ_0 IS SHEAR AT THE BOUNDARY

Figure 8.2 – Notation Used in Boundary Layer Theory

and is assumed to be very large. The steady state Navier-Stokes equations (for two-dimensional flow) may then be written

1)
$$u \frac{\partial u}{\partial x} + v \frac{\partial u}{\partial y} = - \frac{\partial p}{\partial x} + \frac{1}{R} \left(\frac{\partial^2 u}{\partial x^2} + \frac{\partial^2 u}{\partial y^2} \right)$$

(x-direction)

2)
$$u \frac{\partial v}{\partial x} + v \frac{\partial v}{\partial y} = - \frac{\partial p}{\partial y} + \frac{1}{R} \left(\frac{\partial^2 v}{\partial x^2} + \frac{\partial^2 v}{\partial y^2} \right)$$

(y-direction)

3)
$$\frac{\partial u}{\partial x} + \frac{\partial v}{\partial y} = 0 \quad \text{(continuity)}$$

A mathematical argument is presented by Schlichting, which demonstrates which of the quantities may be ignored in comparison to others. A brief physical argument will be given here.

Because of the no-slip condition at the wall and the condition that the velocities in the outer part of the boundary layer must match the inviscid flow outside the boundary layer, there is a large change in u over a small distance, δ. This means that the viscous forces in the x-direction corresponding to the change in the rate of shearing, $\frac{\partial^2 u}{\partial x^2}$, will be large. On the other hand, the term $\frac{\partial^2 u}{\partial x^2}$, which corresponds to viscous forces arising from a change in the rate of elongation of the fluid elements in the x-direction, will be small in comparison with the $\frac{\partial^2 u}{\partial y^2}$ term. Therefore, $\frac{\partial^2 u}{\partial x^2}$ is neglected in the sum, $\left(\frac{\partial^2 u}{\partial x^2} + \frac{\partial^2 u}{\partial y^2} \right)$, in the x-direction equation (Equation 1). In the y-direction, the constraint that v = 0 near the solid boundary and that v be small at y = δ implies that the inertial and viscous forces in the y-direction in the boundary layer are small. This leads to the deduction, from Equation 2, that $- \frac{\partial p}{\partial y}$ is small and hence that the pressure in the boundary layer is nearly constant across the layer. Therefore, the pressure in the outer flow, outside the boundary layer, determines the pressure in the boundary layer.

Because the flow at the outer edge of the boundary layer flow matches the inviscid flow, Equation 1 (x-direction) becomes

1')
$$u_e \frac{\partial u}{\partial x} = - \frac{1}{\rho} \frac{\partial p}{\partial x}$$

(The subscript $_e$ denotes flow external to the boundary layer)

or, since p and u_e vary only with x,

1'')
$$u_e \frac{du}{dx} = -\frac{1}{\rho} \frac{dp}{dx}$$

and

1''')
$$p + \frac{1}{2} \rho u_e^2 = \text{constant}$$

The basic steady state boundary layer equations are then

4)
$$\underbrace{u \frac{\partial u}{\partial x} + v \frac{\partial u}{\partial y}}_{\substack{\text{acceleration} \\ \text{along the} \\ \text{boundary}}} = \underbrace{-\frac{1}{\rho} \frac{dp}{dx}}_{\substack{\text{force per unit} \\ \text{mass due to} \\ \text{external pres-} \\ \text{sure gradient}}} + \underbrace{\nu \frac{\partial^2 u}{\partial y^2}}_{\substack{\text{viscous force per} \\ \text{unit mass due to} \\ \text{change in tangential} \\ \text{shear with normal} \\ \text{distance from} \\ \text{boundary}}}$$

5)
$$\frac{\partial u}{\partial x} + \frac{\partial v}{\partial y} = 0 \qquad \text{(continuity as before)}$$

with the boundary conditions

$$\text{at } y = 0, u = v = 0$$

$$\text{at } y = \infty, u = u_e$$

In the foregoing argument, curvature of the boundary and the pressure gradient normal to the boundary resulting from curved flow were neglected. If the radius of curvature of the boundary is large compared to δ, then the centrifugal forces will be small compared to the quantities in equations 4 and 5 and properly may be neglected. This can be demonstrated by writing the Navier-Stokes in curvilinear coordinates and estimating the magnitudes of the various components.[84] In the case of curved boundaries, the pressure gradient normal to the boundary is no longer negligible, but is of the order of the free stream dynamic pressure. However, the pressure change within the boundary layer compared to the dynamic pressure is of the order of δ and can still be assumed negligible. That is, the pressure across the boundary layer is a constant for radius of curvature large compared to δ.

Modification of Boundary Layer Theory Due to Suction. If suction is applied at the boundary, and is not so great as to make the previous assumptions about the relative magnitude of quantities in the Navier-Stokes equations invalid, then the analysis of the boundary layer is the same except that the velocity normal to the boundary at the boundary is $v = v_0$ instead of $v = 0$.

Substituting the equality (1″) for the pressure term in equation (4) and noting that (5), the equation of continuity, implies that

$$\int_0^y \frac{\partial u}{\partial x} \, dy = v_0 - v$$

and then integrating over the boundary layer, the result is

$$\int_0^h \left(u \frac{\partial u}{\partial x} + v \frac{\partial u}{\partial y} - u_e \frac{du_e}{dx} \right) dy = v \int_0^h \frac{\partial^2 u}{\partial y^2} \, dy$$

$$v_0 - \int_0^y \frac{\partial u}{\partial x} \, dy$$

The right hand side is just

$$- \frac{\tau_0}{\rho}$$

since

$$\frac{\partial u}{\partial y} = 0 \text{ at } y = h$$

Recalling from Chapter 7 the definitions of the boundary layer momentum thickness, θ, and displacement thickness, δ^*, the following can be written:

$$u_e^2 \, \theta = \int_0^\infty u \, (u_e - u) \, dy \quad \text{(by definition)}$$

$$\frac{\partial}{\partial x} u_e^2 \, \theta = \int_0^\infty u \left(\frac{\partial u_e}{\partial x} - \frac{\partial u}{\partial x} \right) + \frac{\partial u}{\partial x} (u_e - u) \, dy$$

and

$$u_e \, \delta^* = \int_0^\infty (u_e - u) \, dy \text{ (by definition). Then } \frac{\partial u}{\partial x} u_e \, \delta^* = \int_0^\infty \frac{\partial u_e}{\partial x} (u_e - u) \, dy$$

combining the above identities,

$$\frac{\partial}{\partial x} u_e^2 \theta + \frac{\partial u_e}{\partial x} + \frac{\partial u_e}{\partial x} u_e \delta^* =$$

$$\int_0^\infty u \left(\frac{\partial u_e}{\partial x} - \frac{\partial u}{\partial x} \right) + \frac{\partial u}{\partial x} (u_e - u) + \frac{\partial u_e}{\partial x} (u_e - u) \, dy$$

$$= u \frac{\partial u_e}{\partial x} - u \frac{\partial u}{\partial x} + u_e \frac{\partial u}{\partial x} - u \frac{\partial u}{\partial x} + u_e \frac{\partial u_e}{\partial x} - u \frac{\partial u_e}{\partial x}$$

$$= -2u \frac{\partial u}{\partial x} + u_e \left(\frac{\partial u}{\partial x} + \frac{\partial u_e}{\partial x} \right)$$

Comparing the above with (7), the result is

$$u_e v_0 - \frac{\partial}{\partial x}(u_e^2 \theta) - u_e \frac{du_e}{dx} \delta^* = -\frac{\tau_0}{\rho}$$

Changing signs and combining terms, noting that $\dfrac{\partial}{\partial x}$ can be changed to $\dfrac{d}{dx}$ when referring to θ and u_e,

$$8) \qquad u_e^2 \frac{d\theta}{dx} + (2\theta + \delta^*) u_e \frac{du_e}{dx} = -v_0 u_e = \frac{\tau_0}{\rho}$$

A solution to (8) may be found by assuming a velocity distribution in the form of a polynomial of the fourth order

$$9) \qquad \frac{u}{u_e} = f(\eta) = a\eta + b\eta^2 + c\eta^3 + d\eta^4$$

where $\eta = y/\delta$. In this case δ is a function of x such that the family of curves $f(\eta)$ is similar and independent of x. It may be considered to be the thickness of the boundary layer. In fact, it does not enter into the calculation of physical quantities. The function $f(\eta)$ (9) is substituted into the following boundary conditions:

10) $\qquad$ at $y = 0$, (a) $u = 0$ and (b) $\nu \dfrac{\partial^2 u}{\partial x^2} = -\dfrac{1}{\rho}\dfrac{dP}{dx} = -u_e \dfrac{du_e}{dx}$

$\underbrace{\phantom{\nu \dfrac{\partial^2 u}{\partial x^2} = -\dfrac{1}{\rho}\dfrac{dP}{dx} = -u_e \dfrac{du_e}{dx}}}$
because $u = 0$, the pressure force
is balanced by the viscous force
only.

at $y = \delta$, (c) $u = u_e$, (d) $\dfrac{\partial u}{\partial y} = 0$, and (e) $\dfrac{\partial^2 u}{\partial x^2} = 0$

The condition (10a) is satisfied identically by the polynomial form. If the four coefficients, a, b, c, and d, are chosen to satisfy the remaining four conditions, a one-parameter family of curves results:

$$\frac{u}{u_e} = F(\eta) + \Lambda\, G(\eta)$$

where $\Lambda = \dfrac{\delta^2}{\nu}\dfrac{du_e}{dx}$ is a shape factor. By setting $\left.\dfrac{\partial u}{\partial y}\right|_0 = 0$ it is found that the condition for separation is that $\Lambda = -12$.

To calculate the laminar boundary layer without suction, it is necessary to continue by substituting the function $F(\eta) + \Lambda G(\eta)$ back into the differential equation for the boundary layer and solving numerically for the shape factor. However, a very simple result is obtainable for the boundary layer with uniform suction. If it is wished to determine the amount of suction which will just prevent separation, then a value for Λ may be assumed greater than -12, say $\Lambda = -10$. Just prior to separation, the shear force at the wall is zero. A further simplification arises if a solution is sought for which the boundary layer thickness does not increase with x. Then (in this case, for constant shape factor) $\dfrac{d\theta}{dx} = 0$, the expression for $\dfrac{u}{u_e}$ which arises from satisfying the boundary conditions (10) is as follows, according to Schlichting: [8.4]

11) $\qquad u = u_e \left\{ 6\left(\dfrac{y}{\delta}\right)^2 - 8\left(\dfrac{y}{\delta}\right)^3 + 3\left(\dfrac{y}{\delta}\right)^4 \right\}$

The displacement and momentum thickness can then be calculated from their definitions with the result

$$\delta^* = \frac{2}{3}\delta\ ,\quad \theta = \frac{4}{35}\delta$$

178

Substituting these values into the differential equation (8) and noting that $\frac{d\theta}{dx} = 0$, the result for the suction velocity is

$$12) \qquad v_o = \frac{22}{35} \, \delta \, \frac{du_e}{dx}$$

The value of δ can be determined by considering equation (4) at the boundary, where $\frac{du}{dy}\bigg|_o = 0$;

$$4') \qquad \nu \left(\frac{\partial^2 u}{\partial y^2} \right)_o = - u_e \frac{du_e}{dx} \cdot$$

From (11)

$$\frac{\partial^2 u}{\partial x^2} \bigg|_o = 12 u_e / \delta$$

Substituting into (4') and solving:

$$\delta = \sqrt{\frac{12\nu}{-\dfrac{du_e}{dx}}}$$

It then follows from (12) that

$$13) \qquad v_o = -2.18 \sqrt{-\nu \, \frac{du_e}{dx}}$$

Calculation of Suction Required in Present Case. McGregor[8.5] has calculated the two-dimensional inviscid pressure and velocity distribution on the blunt biogive using the method of Theodorsen. He compared his calculations with experimental measurements, and found very

good agreement at mid-span under conditions of no separation. The experimental conditions were similar to those of the present work.

McGregor's computed velocities for the case of 10-degree angle of attack on the lower pressure side of the strut are shown in Figure 8.3 plotted against $\bar{x}$, arc length along the strut non-dimensionalised in terms of chord length, with zero at the point of maximum velocity. Because the suction equation and separation criteria depend upon derivatives of the velocity and pressure coefficient, it was necessary to express the numerical values as an easily differentiable function.

To do this, a parabolic distribution was matched to the negative pressure peak and an expotentially decaying function fitted to the numerical values in the pressure recovery region. The mating requirement that the two functions be continuous through the first derivative as well as conform to the required calculated pressure values at the join resulted in a set of simultaneous non-linear equations which were solved numerically to yield

$$
14) \qquad \frac{u_e}{U_\infty} = \begin{cases} 16\ 300\,\bar{x}^2 + 3.3, & 0 \leq \bar{x} \leq 0.0025 \\ \\ 1.58 + 1.62e^{-50\,(\bar{x} - 2.62 \times 10^{-3})}, & 0.0025 \leq \bar{x} \leq 0.1 \end{cases}
$$

where $\bar{x}$ is the arc length non-dimensionalised by the chord. As may be seen from Figure 8.3, the fit was extremely close.

The blunt biogive had been previously found to experience nose ventilation consistently at a side slip angle, β, of 10 degrees at a speed of 20 ft/s (6 m/s). Therefore, this was the speed and geometry selected to attempt to prevent ventilation by eliminating the nose separation region.

Besides an expression for the minimum suction velocity required to prevent separation, it was also necessary to know over what portion of the strut to apply suction. The experimental evidence of separation on previous tests [8.6] of a similar blunt biogive section indicated that re-attachment occurred no further aft than 10-percent chord at the given conditions.

Using the criterion of Curle and Skan [8.7] presented in Chapter 7, separation will not occur if

$$
15) \qquad \left| \bar{x}^2\, \bar{C}_p \left(\frac{d\bar{C}_p}{d\bar{x}} \right)^2 \right| < 0.0104
$$

$$\frac{u_e}{U_\infty} = \begin{cases} -16\ 300\ \bar{x}^2 + 3.3,\ 0 \leqslant \bar{x} \leqslant .0025 \\ 1.58 + 1.62\ e^{-50(\bar{x}-2.62\times10^{-3})}, \\ \qquad .0025 \leqslant \bar{x} \leqslant .1 \end{cases}$$

(x̄ IN TERMS OF CHORD)

KEY △ POINTS CALCULATED BY McGREGOR
— — CURVE FIT ACCORDING TO ABOVE FORMULA

x̄ ARC LENGTH IN PERCENT CHORD, ZERO AT MAXIMUM VELOCITY
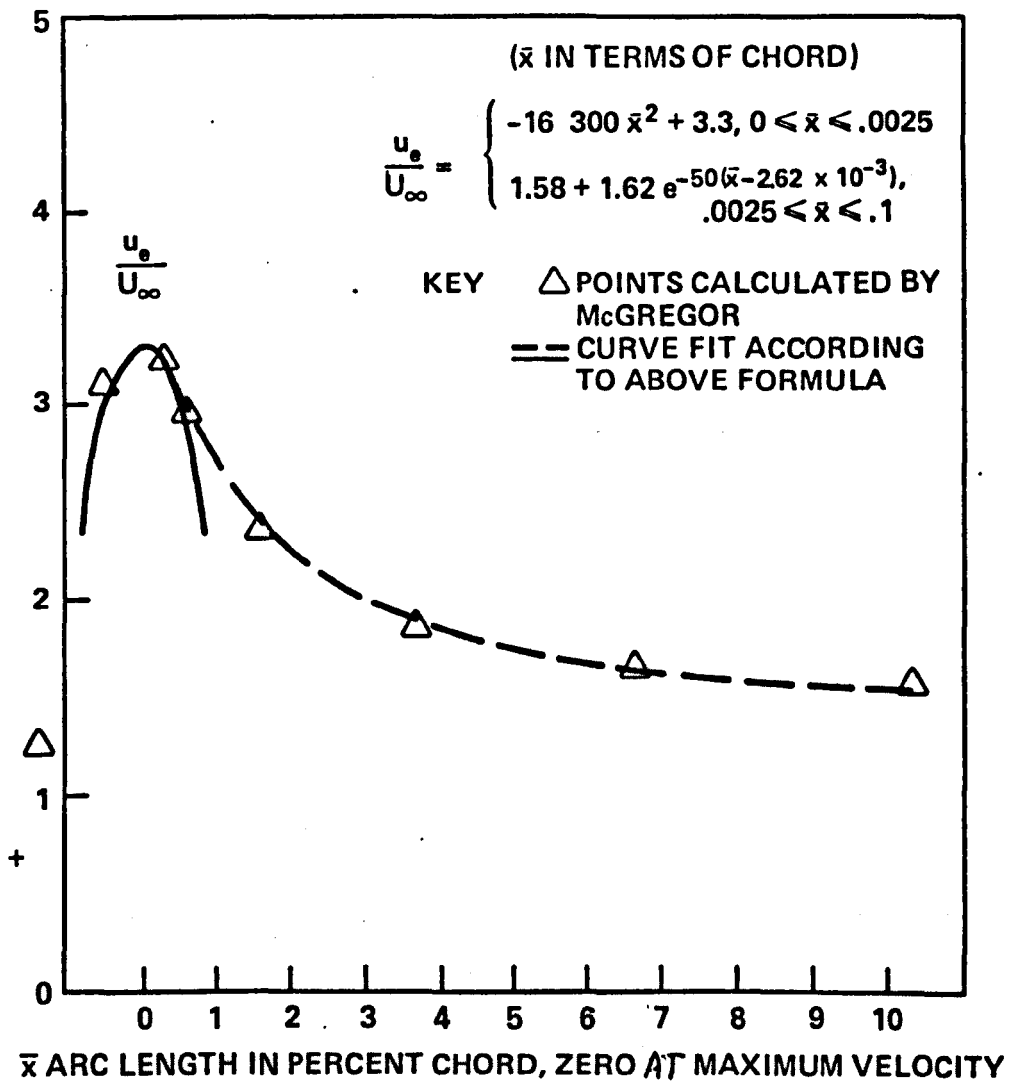
Figure 8.3 — Velocity Distribution Near Nose of Blunt Biogive as a Function of Arc Length from Point of Maximum Velocity.

where $\overline{C}_p$ is the pressure coefficient based on the maximum rather than free stream velocity:

$$16) \qquad \overline{C}_p = 1 - \left(\frac{u_e}{u_{e_{max}}}\right)^2$$

The empirical expression for u_e given in (14) was used to evaluate the left-hand side of (15). The result of the calculation is shown in Figure 8.4. It can be seen that separation will occur at $\overline{x} = 0.006$ and that after $\overline{x} > \sim 0.05$ the boundary layer is stable with respect to separation. Therefore, the region over which suction must be applied is $0.006 \le x \le 0.05$.

By differentiating the expression for the external velocity (14) and substituting the result into (13), the Prandtl suction velocity formula, it is found that the maximum value of $\left| v_o \right|$ occurs at $x_o = 0.0025$ when $\frac{1}{U_\infty} \frac{du_e}{d\overline{x}} = 81.5$. Then

$$v_o = -4.65 \times 10^{-1} \text{ ft/s} (-1.41 \times 10^{-1} \text{ m/s})$$

The volume rate of flow which corresponds to this value of v_o integrated from $\overline{x} = 0.006$ to $\overline{x} = 0.05$ is

$$17a) \qquad Q = 3.54 \times 10^{-3} \text{ ft}^3/\text{s} (1.25 \times 10^{-4} \text{ m}^3/\text{s})$$

In fact, because of mechanical considerations the suction slot was placed 10mm aft of the leading edge, corresponding to $\overline{x} = 7.6 \times 10^{-2}$. To provide a suction velocity equal to the maximum required to prevent separation from $x = 0$ to $x = 7.6 \times 10^{-2}$ would imply

$$17b) \qquad Q \approx 5.9 \times 10^{-3} \text{ ft}^3/\text{s} (2.08 \times 10^{-4} \text{ m}^3/\text{s})$$

Calculation of Minimum Pressure. The expression (17a) represents the minimum suction velocity, which, if uniformly applied over the indicated region, would just prevent separation. Because of the changing pressure distribution in the region where suction must be applied, merely establishing a pressure difference across a porous surface would not suffice to provide a uniform suction velocity. If the pressure on the inside of the strut were uniform, the suction velocity across the porous
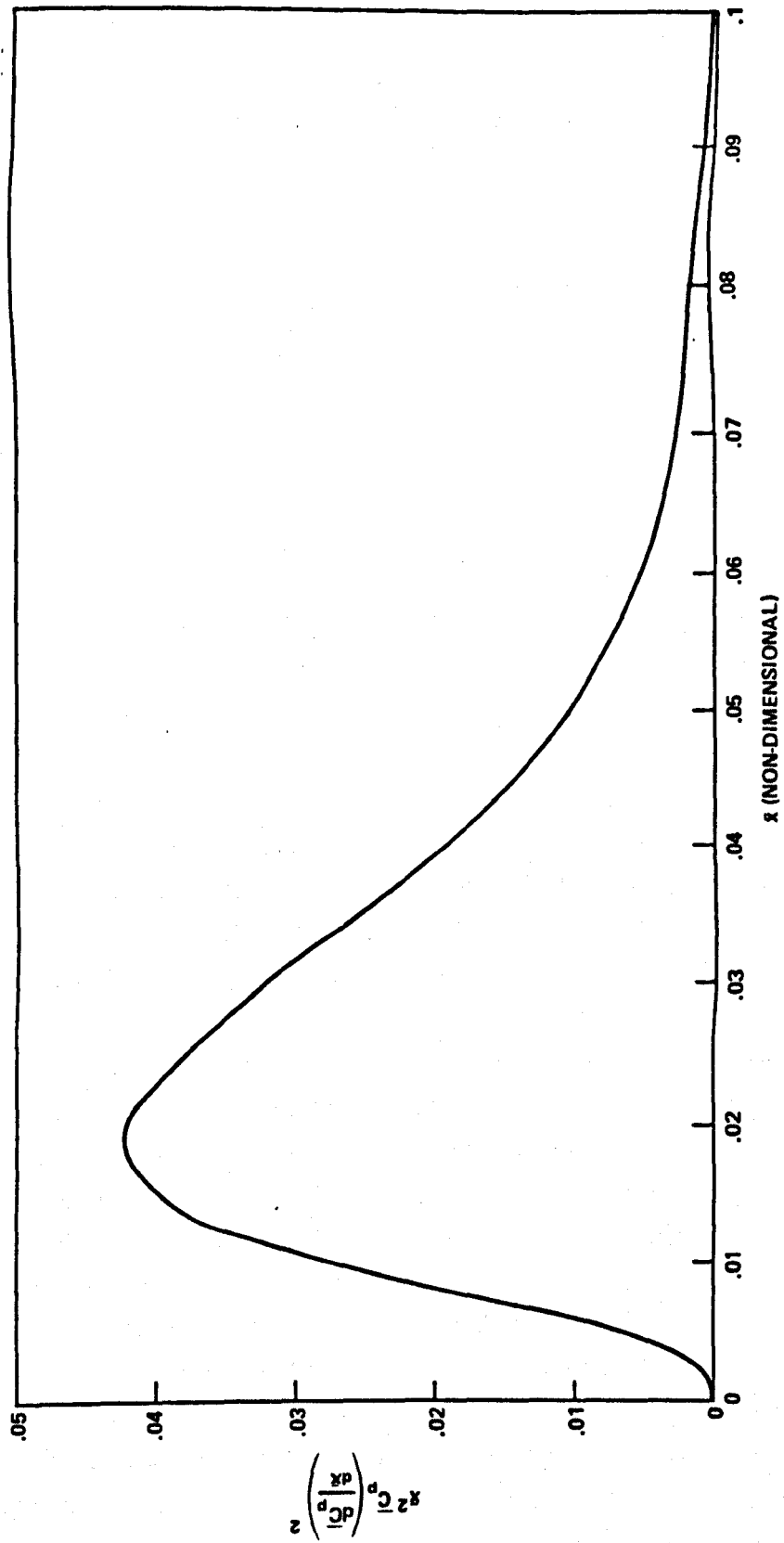
Figure 8.4 – Separation Criterion $\bar{x}^2\, \bar{C}_p \left(\dfrac{d\overline{C}_p}{d\overline{X}}\right)^2$ vs. $\bar{x}$

183

surface would be the least in the region of lowest external pressure, near the point where the theory requires the greatest suction velocity. A further consideration is revealed by an examination of the two-dimensional pressure distribution. From (14) the maximum value of the velocity around the blunt biogive is

$$\left(\frac{u_e}{U_\infty}\right)_{max} \cong 3.3 \text{ at } \overline{x} = 0$$

at 20 ft/s (6 m/s). The pressure at x = 0 is then

18)
$$p - p_o = \left[1 - \left(\frac{u_{eo}}{U_\infty}\right)^2\right] \frac{1}{2} \rho \, U_\infty^2 \cong -27\frac{1}{2} \text{ lbf/in}^2 \, (1.9 \times 10^5 \text{ Pa})$$

Therefore, for $p_o \sim$ atmospheric pressure, suction to prevent separation would be impossible where the two-dimensional results apply. Fortunately for the experiment, the theoretical two-dimensional pressures are not attained in the region of the free water surface. The results of an experimental pressure survey of the blunt biogive by Swales et al[8.3] suggested an empirical correction to the two-dimensional calculations which proved quite useful.

The most simple correction would have been to reduce the two-dimensional chordwise pressure by a factor which decreased to zero as the mean free was approached. Indeed, the experimental data shown in Figure 8.5 suggested that an elliptical spanwise distribution symmetric about the midspan chordline would have been reasonable. However, this procedure would not have accounted for the distortion of the actual free surface in the vicinity of the strut, particularly at sideslip angles of 10 degrees and greater. The region of the free surface was especially important, because that was where the significant effects were thought to be.

The problem of distortion of the free surface was solved by defining an effective free surface as the locus of points at which the extrapolated measured spanwise pressure fell to zero (local atmospheric pressure). Because of the sparseness of the experimental data and the confusing effects of separation and ventilation, a rather elaborate rationale was applied to achieve what was felt to be a reasonable extrapolation. The details of this argument have been relegated to an appendix of this chapter.

184
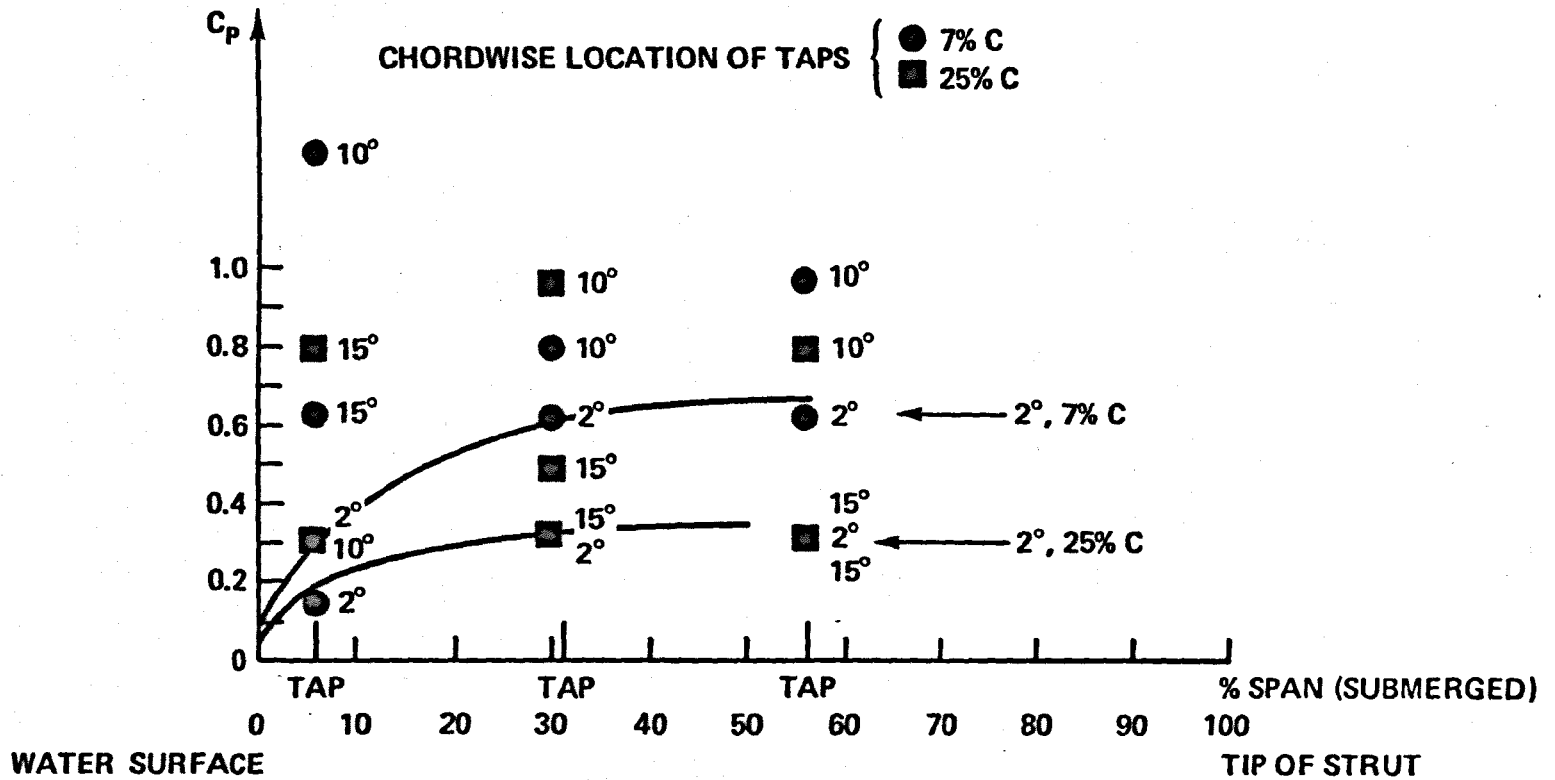
Figure 8.5 – Experimental Pressure Coefficient versus Span, 5ft/s, (1.5m/s), β = 2 Degrees, 10 Degrees and 15 Degrees Blunt-Nosed Biogive. Data From Reference 8.3, Taken at 0.07C and 0.25C.

185

Briefly, the effective free surface near the strut nose was described as a flat plane, identical to the undisturbed mean free surface for $\beta = 0$ degrees, linearly increasing (absolute) slope and height near the nose with increasing β to match the empirically projected effective free surface when $\beta = \beta_0 = 10$ degrees. Mathematically,

$$19) \qquad \bar{z}(\bar{x}, \beta) = 1 - \frac{4}{3}\frac{\beta}{\beta_0}\bar{x} + 0.293\frac{\beta}{\beta_0}, \qquad 0 < x < 0.25 \text{ (approximate range of validity)}$$

where $\bar{z}$ is the distance above midspan, nondimensionalised by chordlength. Then, using the assumptions of elliptical loading, symmetry about midspan and zero pressure at the effective free surface, the modified pressure distribution became

$$20a) \qquad \bar{C}_p(\bar{x}, \bar{z}, \beta) = \bar{C}_p(\bar{x}, 0, \beta)\sqrt{1 - \frac{\bar{z}^2}{\left(1 - \frac{4}{3}\frac{\beta}{\beta_0}\bar{x} + 0.293\frac{\beta}{\beta_0}\right)^2}}$$

$$0 < \bar{x} < 0.25, \qquad \bar{z}^2 \leq (1.293 - \frac{4}{3}\bar{x})^2$$

at $\beta = 10$ degrees, (20a) became

$$20b) \qquad \bar{C}_p(\bar{x}, \bar{z}, \beta_0) = \underbrace{\bar{C}_p(\bar{x}, 0, \beta_0)}_{\substack{\text{2-D pressure} \\ \text{distribution}}}\underbrace{\sqrt{1 - \underbrace{\frac{\bar{z}^2}{(1.293 - \frac{4}{3}\bar{x})^2}}_{\substack{\text{free surface modification} \\ \text{factor}}}}}_{\text{elliptical loading factor.}}$$

Equation (20b), together with the expression for the two-dimensional velocity near the nose (14) and the definition (16) completely describe the pressure in the vicinity of the intersection of the free surface and the forward part of the strut at a sideslip angle of 10 degrees.

Estimate of the Thickness of the Surface Seal. If a factor

$$21) \qquad k(\bar{z}) = \frac{\bar{C}_p(\bar{x}, 0)}{\bar{C}_p(\bar{x}, \bar{z})}$$

is defined, then the separation criterion given by Equation (15) and Figure 8.4 can be re-written to account for three-dimensional variation as follows:

$$22) \qquad k^3\bar{x}^2\,\bar{C}_p(\bar{x}, 0)\left(\frac{dC_p(\bar{x}, 0)}{d\bar{x}}\right)^2 < 0.0104 \text{ (no separation)}$$

If it is noted from Figure 8.4 that the maximum value of the left hand side of (22) is 0.0423 and occurs at $\bar{x} = 0.0195 \equiv \bar{x}_s$, then the separation criterion becomes

$$23) \qquad [k(\bar{z})]^3 < \frac{0.0104}{0.0423} \equiv k_s^3 = 0.246$$

The criterion no longer depends upon $\bar{x}$ since it has been assumed that separation will appear first at $\bar{x} = \bar{x}_s$.

The height of the effective free surface at $\bar{x}_s$ is given by (19) as $\bar{z}_{ss} = 1.27$. Using (20) and (21), the definition of $k(\bar{z})$ can be inverted to restate the separation criterion in terms of z:

$$24) \qquad \sqrt{1 - \left(\frac{\bar{z}}{\bar{z}_{ss}}\right)^2} = k < k_s \text{ (no separation)}$$

$$\bar{z} > \bar{z}_{ss}\sqrt{1 - k_s^2} \quad \text{(no separation)}$$

$$\bar{z} > 0.99 \quad \text{(no separation)}$$

$$\text{(at separation } z = z_s = 0.99)$$

This implied that no separation would take place in the flow above the mean free surface. The non-dimensional height of the effective free surface at $\bar{x}_s, \bar{z}_{ss}$, was calculated to be 1.27. Therefore the thickness of the surface seal above the point of inception of separation was $\bar{z}_{ss} - \bar{z}_s$, or approximately 0.28 c. This was in good agreement with photographs taken of the oil smear patterns.

Effect of Suction near the Mean Free Surface. It has been shown that suction to prevent separation on the blunt-nosed biogive at a sideslip angle of 10 degrees and a speed of 20 ft/s (6 m/s) is impossible where the two-dimensional calculated values of pressure occur, since the minimum pressure would then be 27.5 psi (1.9×10^5 Pa) below ambient. However, in the presence of the free surface local pressures are required to go to zero. Therefore, there is a depth above which suction would be effective, which can be calculated similarly to the depth of separation inception, using (14), (18) and (20b), and noting that the vacuum pump available for the nose suction experiment had the capability of maintaining a reservoir at a pressure corresponding to $-C_p = 5.2$. After performing the calculations, it was found that the minimum pressure on the strut would not exceed the minimum reservoir pressure except at points higher than 0.09 c above the mean free surface. It was previously established that the pressure relief provided by the

free surface would be sufficient to suppress separation, in any case, above points at the height of the mean free surface.

However, this does not mean that suction would have no effect below the mean free surface. As the effective surface is approached, the predicted point of separation moves aft, away from the point of minimum pressure. This can be seen from the graph of the separation criterion, Figure 8.4. The point of separation moves from $\bar{x} = 0.006$ to $\bar{x} = 0.02$ as the pressure coefficient decreases due to proximity of the free surface. At $\bar{x} = 0.02$, $-C_p = 4.1$ at midspan according to (14) and (18). This corresponds to a higher pressure than the pump inlet pressure which was equivalent to $-C_p = 5.2$. Therefore, in the vicinity of the mean free surface, the application of suction is possible. Furthermore, it would be likely to retard or prevent the onset of separation by reducing the steepness of, or eliminating, the adverse pressure gradient aft of the point of minimum pressure, while sucking away a substantial amount of low momentum fluid in the boundary layer.

Near midspan, unlike the region near the mean free surface, the most which could be expected of suction would be that the extent of the separated region would be reduced. The results of the theoretical calculations based on the assumed pressure distribution show that the overall effect of leading edge suction on the blunt biogive should be to increase the thickness of the surface seal while reducing the extent of the deeply submerged region of separation. Ideally, to establish conclusively the object of the experiment, it would be necessary to completely eliminate the separated region. The calculations have shown that this is not possible for the case considered. The best that could be expected would be a decrease in the chordwise extent of the region of separation, coupled with the elimination of separation near the free surface, resulting in a thickening of the surface seal. If the suction should eliminate ventilation under these conditions, it would be a strong argument in favor of the proposition that separation near the free surface is a necessary condition for ventilation.

DESCRIPTION OF THE MODEL, EXPERIMENTAL
APPARATUS AND TECHNIQUE

The Model. The overall dimensions of the strut model used in the nose suction experiment and shown in Figure 8.1 have already been discussed. The model was cast in aluminum and then a plenum chamber was hollowed out by milling an undercut slot the length of the span on the starboard side. A cover plate was affixed to the starboard side. Since the model was generally tested yawed to port, all discontinuities in the model surface except for the suction slot were on the less critical high pressure side. The suction slot was 1/32-inch (0.8mm) wide slot formed by a saw cut through the port side and parallel to the model plan of symmetry. The aft edge of the slot was about 10-mm behind the strut leading edge. To encourage uniformity of suction, the slot thickness was selected so that the pressure drop due to flow inside the strut would be negligible compared to the pressure drop of the slot flow. The model was spray painted matte black with acrylic lacquer. For the initial tests, the intersection of the forward edge of the slot with the original section contour was not broken (smoothed).

Modifications to the Model. After initial tests, the original sharp edged contour ahead of the slot was faired into the forward slot edge, so that the flow into the slot around the leading edge would be smooth. Preliminary tests were conducted with waterproof tape covering various sections of the slot to determine which configuration was most effective. Figure 8.7 is an example of the model with waterproof tape covering part of the leading edge slot. The tape had the effect of somewhat altering the contours of the original blunt biogive, partly because of its tendency to collapse into the slot recess somewhat. Also, the thickness of the tape created a slight ridge between the taped and untaped areas. Because of this, after promising configurations were identified, the tape was removed and the slot was then filled with beeswax faired to the original contours. Then, the runs were repeated to ensure that spurious results had not been generated by the tape.

Because turbulent boundary layers are more likely to remain attached than laminar ones, roughness was added to the model leading edge to stimulate transition ahead of the suction slot for certain conditions. The grade 11 glass spheres used in the roughness experiment were applied in the manner described in Chapter 5. Figure 8.9 is an example of a configuration with leading edge roughness.
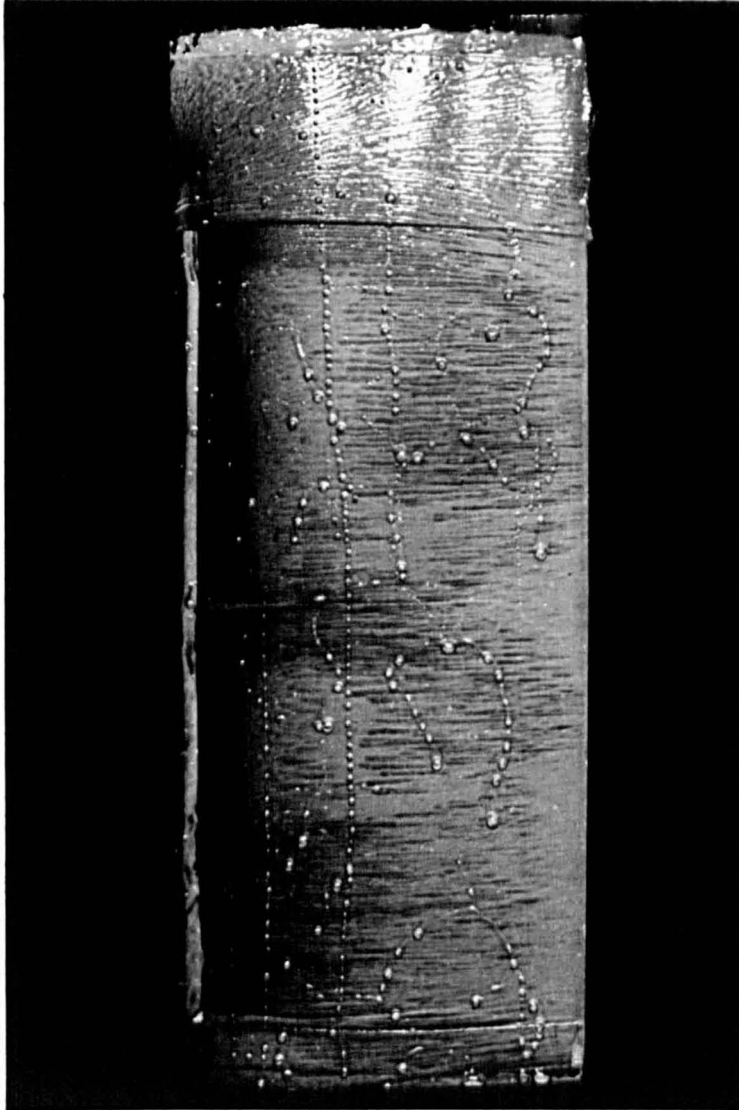
Figure 8.6 – Blunt Biogive with Tape on Upper and Lower
Part of Slot and Smoothed Leading Edge.
20 ft/s (6m/s), β = 0 Degrees, Maximum
Suction.

Figure 8.7 – Blunt Biogive with Tape on Upper and Lower Part of Slot
and Smoothed Leading Edge. 20 ft/s (6m/s) β = 12 Degrees,
Maximum Suction.

Figure 8.8 – Blunt Biogive with Slot Partially Filled with Wax –
20 ft/s (6m/s), β = 12 Degrees, Maximum Suction
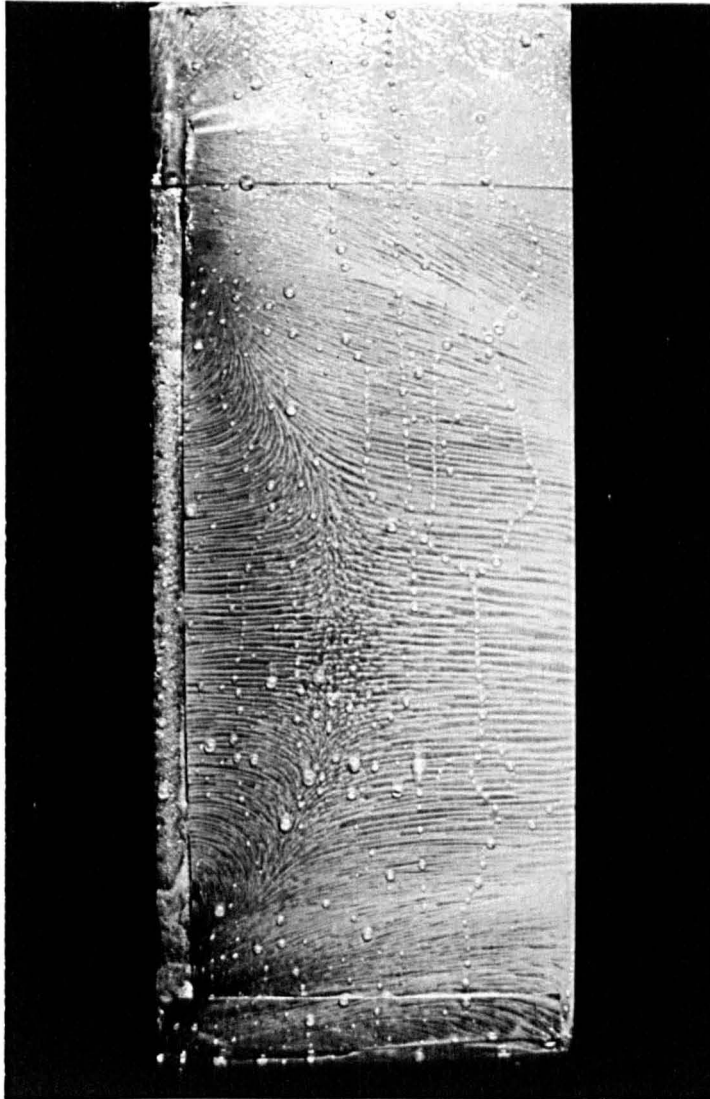
Figure 8.9 – Blunt Biogive with Roughened Leading Edge. 20 ft/s
(6m/s) β = 13 Degrees, Maximum Suction

General Experimental Apparatus. Figure 8.10 is a photograph of the general experimental setup. The University of Leeds Variable Pressure Free Surface Water Channel[8] provided the required flow conditions. The test section was 14 x 14 inches square (355mm) and 9 ft long (2750mm). A complete discussion of this channel was given in Chapter 5 and the references therein, including surface quality, air content, velocity cross section, velocity calibration, and wall interference and blockage effects.

Suction System. Figure 8.11 shows a schematic diagram of the suction system. A high speed vacuum pump was used to evacuate a pressure vessel connected to the model suction slot by a combination of copper pipe and flexible hose. The vacuum pump was that normally used to lower the ambient pressure in the channel and hence had more than adequate capacity to maintain the reduced pressure in the pressure vessel reservoir during a run. The pump had the capability of maintaining the reservoir pressure at about 29 inches Hg (98 kPa) differential pressure. The volume of the reservoir was approximately 0.11 m^3. Generally, this allowed a filling time of about 225 seconds. Wright et al[2] using a model geometrically similar to the present study, but of 4/5 the chord length, found that at 20 ft/s (6 m/s) and for sideslip angles greater than 10 degrees, with one exception out of 19 events, ventilation occurred no longer than 45 seconds after initial immersion. Thus the 225 second filling time for the suction reservoir provided adequate time to assure that ventilation was probably not going to occur if it had not occurred during a run.

The flexible hose allowed the strut to be raised and lowered into the streaming water. This was accomplished by means of a pneumatically driven ram, which provided sufficiently rapid movement into and out of the water to allow accurate interpretation of oil smear flow visualization patterns on the strut.

Mounting, Yawing Mechanism and Alignment. The pneumatic ram was attached to a platform guided by cylindrical rails. The strut was mounted in a bearing on the platform so that the strut was free to rotate about a vertical axis (yaw). The friction in the bearing was adjustable and was increased until the model could just be turned with a purpose-made wrench to a preset sideslip angle once it had been immersed. Preset stops enabled the chosen sideslip angle to be acquired quickly and accurately.

Close attention was paid to the mechanical alignment of the strut with the stream. As in previously described tests, runs were made to both port and starboard to verify correctness of alignment by hydrodynamic symmetry. Of course, the strut was symmetric only for those cases in which the suction slot was completely filled with beeswax.

194
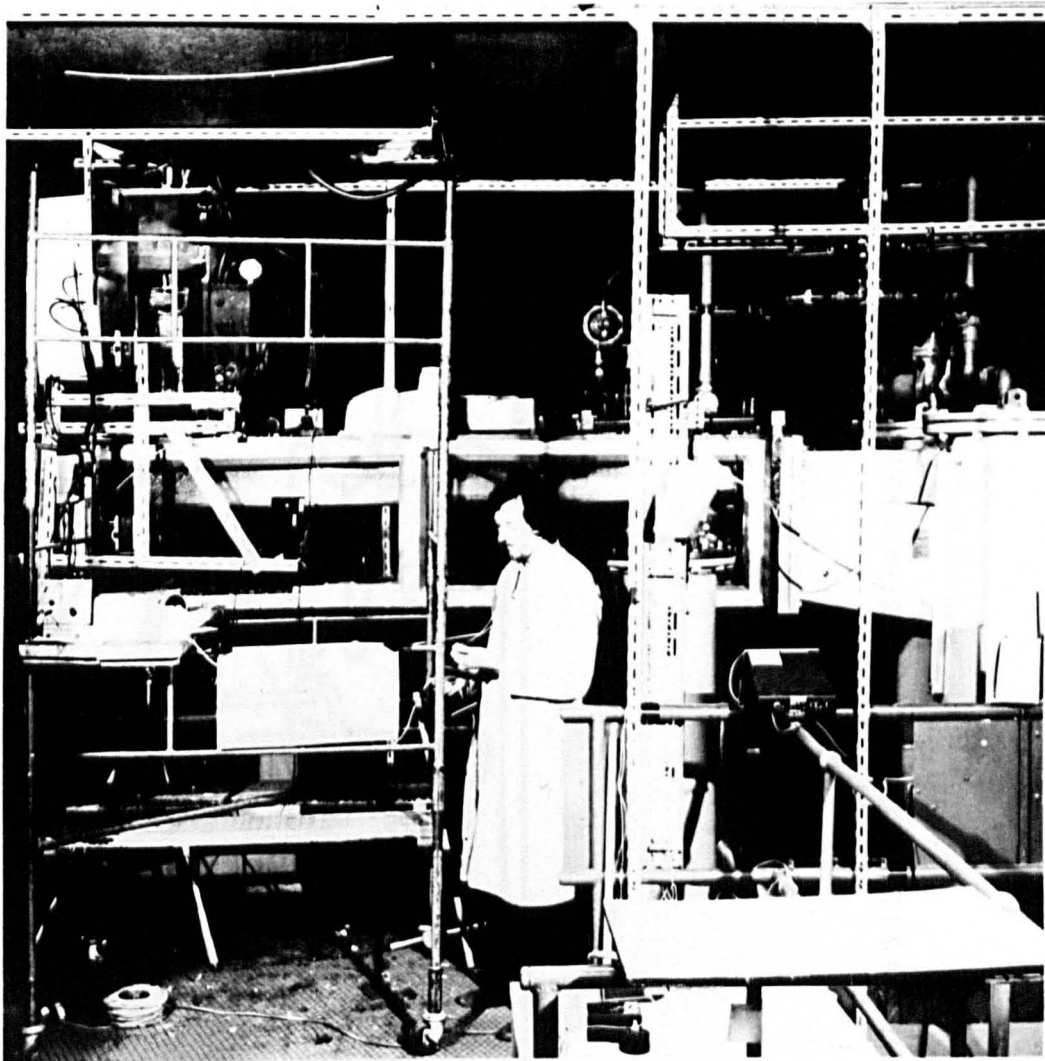
Figure 8.10 – Flow Visualisation Apparatus As Used With Blunt Biogive Suction Model In Free Surface Water Channel
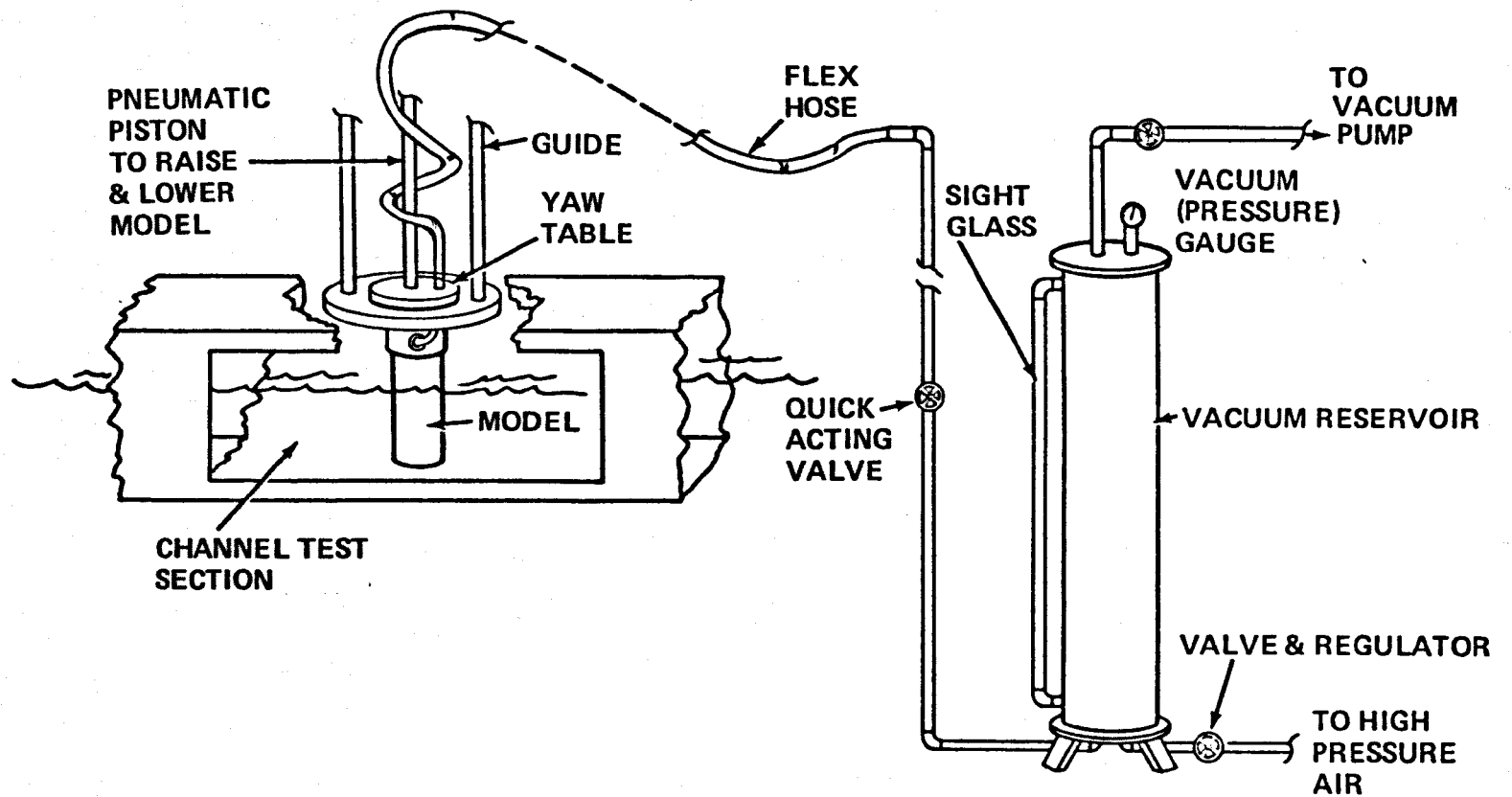
Figure 8.11 — Suction System and General Arrangement of Yawing and Immersion Apparatus

After initial alignment, yaw angles different from zero were read directly from an engine-divided engraved brass scale. The accuracy of the measurement of relative angular position was limited by the ability of the experimenter to judge the coincidence of two scribed lines and was correct to within a small fraction of a degree. The absolute angular position was probably correct within a half degree. This was difficult to determine because the reference surface on the model was not accessible once the model was in position in the channel. The absolute position was deemed not important, since the principal objective of the experiment was to compare the ventilation characteristics of two essentially identical geometric configurations, rather than to establish a general relationship between sideslip angle, suction, and ventilation.

The Photographic Oil Smear Flow Visualisation Technique. A technique developed for wind tunnel flow visualisation by Loving,[8.9] and applied to use in water by Breslin[8.10] and adapted to the Leeds facilities by Swales[8.1] was used to determine the flow patterns on the experimental model. In particular, the technique is valuable for revealing flow separation.

A viscous automobile gear oil was mixed with an oil-soluble pigment which had the property of fluorescence when irradiated by ultraviolet light. While the model was out of the water, the oil mixture was applied with a paint brush in a thin, uniform film. Care was taken to ensure that previous patterns had been obliterated by first wiping the model clean from the previous test and then brushing in two perpendicular directions, ending with vertical striations remaining from the brush strokes. The model was then immersed at 0-degree sideslip angle and quickly rotated to the run angle determined by preset stops.

In regions of high shear, relatively complete scouring of the oil film occurred. High shear could be associated with either attached flow or strong reverse flow. In regions of low shear, oil would either accumulate, or the original pattern applied to the dry model would be scarcely disturbed. Generally, oil accumulation occurred in laminar flow regions prior to transition to turbulent flow. The transition region could be identified by a ragged edge of thick oil film from which streamers of thick film extended into a scoured region. Figure 8.12 is a photograph showing a transition oil film pattern. In areas of massive tail separation, the pattern tended to be undisturbed because of the absence of either attached or reverse flow in the separated region (Figure 8.13). Where separation and subsequent reattachment occurred near the nose, a characteristic "herringbone" pattern would be observed at the reattachment point. This was due to split flow scouring in opposite directions at the reattachment point, where part of the boundary layer flow was carried upstream due to the adverse pressure gradient in the region of separation while the remaining flow joined the principal external flow in the downstream direction. Figure 8.14 shows a typical herringbone pattern.
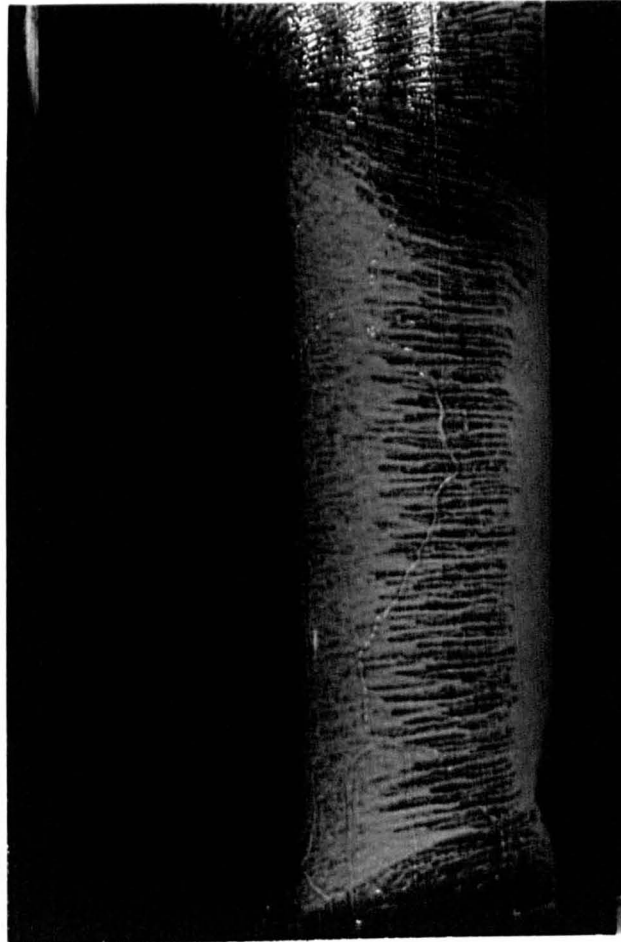
Figure 8.12 – A Typical Oil Smear Pattern Showing Transition from Laminar to Turbulent Flow. The Fully Turbulent Region is Scoured by High Shear Stresses.

Figure 8.13 – The Vertical Striations of the Oil Pattern as Originally Applied are Unchanged in the Region of Tail Separation. Evidence of Re-entrant Flow Can Be Seen at the Trailing Edge.

Figure 8.14 – Characteristic "Herringbone" Pattern Caused by Separation and
Re-attachment.

At the point of separation and just behind, a particularly thick accumulation of oil could be observed. This was due to the depositing of oil by the reverse flow in the region of zero or low shear at the initiation point of the separation.

Other flow features were also evident in the oil smear patterns, such as the tip vortex and the high water mark which indicated the maximum height of the spray sheet which clung to the low pressure face of the strut model.

After immersion, the model was observed with ordinary incandescent light to determine the degree of development of the oil smear pattern. When the flow features were deemed to have become sufficiently defined, and before too much oil had been removed by the scouring action of the water, the model was quickly removed from the flow using a pneumatic ram. The incandescent lights were turned off and a bank of ultraviolet lights were lowered to excite the phosphorescent pigment in the oil. A 35-mm black and white photograph was then taken of the pattern before it deteriorated. Photogrammetric analysis was subsequently performed on the flow patterns to determine the extent and type of separation on the model. At first, the strut was photographed at the same angle as that at which it had been run. It was then necessary to correct the photographic measurements to compensate for the skewed optical axis, relative to the vertical plane of symmetry of the model. Later, additional stops were installed in the rotational mechanism so that the model could be quickly returned to zero angle after withdrawal, without loss of detail in the oil pattern. Then, the camera optical axis was normal to the plane of symmetry of the model, and no correction was necessary.

OUTLINE OF THE EXPERIMENT - PROCEDURE
AND CONDITIONS TESTED

Test Series. The blunt-nosed biogive model with leading edge slot suction was tested in four configurations in the Free Surface Water Channel. The flow speed was 20 ft/s (6 m/s) for all conditions tested.

In all cases, the maximum possible suction was applied—approximately 28 inches of mercury differential pressure. The flow rate was nearly constant for all configurations tested, whether partially filled or full span slots. In all cases, $Q \sim 4.9 \times 10^{-4} \, m^3/s$. This number is not considered to be significant since flow in the slot must have been nonuniform due to the spanwise external pressure variation.

Preliminary runs were performed to establish the range of test parameters and geometry, such as total slot length and immersion. Then each series of geometric configurations was tested to

determine the largest angle for which attached flow could be sustained.

After the initial exploration, a detailed survey of the growth of the region of separation would be made using photographs of the oil smear. The separation patterns were then plotted and superimposed to show the development of the patterns and the influence of suction and the various geometries.

First Series: Full Span Leading Edge Slot. The leading edge slot as initially constructed was a simple parallel-sided slit as shown in Figure 8.1 The top of the slot extended considerably above the mean water line. In order to determine the maximum height of the slot which could be used for suction without drawing air into the suction system, the top of the slot was blocked with waterproof tape as shown in the photograph of Figure 8.7. It was found that the slot could be left open a distance of 5-10mm above the mean free surface without sucking air. The immersion depth initially tested was 238mm from the mean free surface to the tip of the strut.

A survey of the separation pattern and ventilation angles was performed. During the flow visualisation runs, it was noted that oil tended to accumulate aft of the inside or forwardmost lip of the suction slot. It was felt that this could be attributed to separation within the slot caused by flow over the abrupt break in contour of the inner, or leading, lip. Therefore, before proceeding with more detailed tests, the lip of the slot was smoothed so that no break in the contour of the model was apparent to the eye. Then the slot sides formed a converging channel.

The waterproof tape was removed, and the section of the slot formerly covered by the tape was filled with beeswax, molded to the contours of the unmodified blunt biogive section. This was to ensure that the results were not affected by discontinuities caused by the thickness of the tape, or the tendency of the tape to collapse into the slot, spoiling the contour of the strut section.

Second Series: Full Span Leading Edge Slot (Faired). With the leading edge entrance to the slot faired, a flow visualisation sequence of runs was performed, in which sideslip angle was varied from 0 to 18 degrees. Depth of immersion was 298mm, as before. No attempt was made to maintain the angles for longer than was necessary for the shear stress patterns in the oil to become fully developed, which typically took from 20 to 60 seconds. It was noted that oil accumulation still occurred at the entrance to the slot, as had happened previously with the sharp contour break caused by the unfaired slit.

During the flow visualisation sequence, vents occurred at β = 14 degrees without suction. Thereafter, ventilation occurred during every run up to 18 degrees, both with and without suction. Generally, enough time elapsed before ventilation for a reasonable shear pattern to develop in the oil so that the flow prior to ventilation could be interpreted from the photographs. The exceptions

were for β = 17 degrees without suction and β = 18 degrees with suction. In these cases, ventilation was virtually instantaneous once the run angle had been acquired.

Third Series: Roughened Leading Edge. After the completion of the test series using the faired slot, the leading edge of the strut ahead of the slot was roughened with number 11 grade glass spheres, as described previously. In this case, the top of the slot was sealed with waterproof tape, rather than beeswax. The model was tested at the same immersion, 238mm, as the foregoing series. However, it was possible to perform flow visualisation photography to only 15 degrees of sideslip angle because of the increased tendency of this roughened leading edge configuration to ventilate.

Fourth Series: Shortened Slot Near Mean Free Surface. During the first three test series, it was noted that, as predicted by the theory, the suction did not completely eliminate the separated region at the nose, but only reduced its extent. The fourth series of tests was designed to concentrate the suction near the mean free surface, where it would be most effective in preventing separation. Of course, the area below the suction was expected to be little affected.

The suction slot was nearly completely filled with beeswax, except for a 75mm segment which was about 45mm below the mean free surface at a tip submergence of 238mm, the submergence used in the previous series. The slot extended from a point 120mm above the tip to a point about 195mm above the tip.

Exploratory runs were conducted at various tip submergences to determine the best submergence for the slot with respect to the mean free surface. This was somewhat difficult to do because of the erratic time-dependent nature of nose ventilation which was a characteristic of the blunt-nose biogive section.

A further factor which appeared to influence the onset of ventilation under the circumstances of that test was the presence in the water channel of large air bubbles due to a fault in the air removal system. After a few minutes of running time during which ventilation had taken place, the removal system would be taxed beyond its capacity. When this happened, an increase in the number of seemingly anomalous vents could be observed. Because the objective of the experiment was the complete elimination of ventilation under rather particular circumstances, no procedure had been developed to deal with the possibility of an additonal mechanism of ventilation inception which might have been introduced by the presence in the flow of large air bubbles.

Therefore, when it appeared as though the bubble content of the water was affecting the test results, the flow was stopped and the air was allowed to dissipate before the experiment was resumed.

After the exploratory study of the effect of slot submergence was complete, three submergences were selected for flow visualisation photogrammetry—corresponding to tip submergences of 238mm, 206mm, and 181mm. Thus the slot was tested well below the mean free surface (~45mm), just below the mean free surface (~10mm) and just above the mean free surface (~12mm). Flow visualisation photographs were taken at sideslip angles of 10, 12, and in the case of the 206mm tip submergence, at 14 degrees.

RESULTS AND DISCUSSION

Effect of Slot on Ventilation Characteristics. One of the most interesting results of the series of tests of the blunt biogive with a leading edge slot was that there was no pronounced difference in the ventilation behaviour of the strut whether or not suction was applied to the slot. The maximum angle that could be sustained without ventilation occurring immediately was in every case only a degree or two greater with suction than without. However, when compared with previous tests of the same strut without slots and with another strut of 4/5 the chord length but with a geometrically similar section, it is evident that a significant improvement in resistance to ventilation resulted from the slots.

This improvement in ventilation resistance associated simply with the presence of the slot is explainable in terms of the postulated mechanism of ventilation and the pressure distribution inferred earlier in this chapter. The slot was at a chordwise position where the two-dimensional pressure was calculated to be below vapour pressure. Because of the presence of leading edge separation, the pressure did not actually attain the low, calculated value. But, pressure measurements made within the separation bubble indicate that, near midsubmergence, the value was still low compared with the static pressure variation due to increasing depth. It was not established that the elliptical pressure distribution applied to regions within the separation bubble. However, it was undoubtedly true that the pressure within the bubble tended to zero at the effective free surface. This established a pressure gradient from the surface downward.

Under ordinary circumstances, the strong secondary flow within the separated nose bubble would limit the spanwise flow which could take place in response to this pressure gradient. The presence of the slot probably inhibited the secondary flow close to the strut surface, and allowed a spanwise current to be established, bringing flow into the slot near the surface and expelling the flow in the lowest pressure region of the separation bubble near midsubmergence. This secondary flow functioned in the same way as the imposed suction from the external suction pump. Therefore, the chordwise and spanwise extent of the separated region was reduced in the vicinity of

the effective free surface. The chordwise extent of the separation bubble increased somewhat in the midspan region, although this was not unequivocally evident.

An examination of the results of the individual test series supports this hypothesis. Figure 8.15 shows the nose bubble reattachment lines on the blunt biogive, taken from measurements of unpublished photographs of the previous Leeds University test of the unmodified model. Note that it was not possible to obtain data for sideslip angles greater than 9°. Comparing Figure 8.15 with Figure 8.16, which shows the results of the second test series of the present experiment, it can be seen that the reattachment lines for 9, 10, 11 and perhaps 12 degrees in the case of applied suction, disappear substantially deeper below the mean waterline than the 9-degree reattachment line for the unmodified strut. For the cases in which suction was applied to the slot, the re-attachment lines for 9, 10, and 11 degrees were nearly the same as for the unmodified case at 9 degrees. This shows that the suction did not have much effect near midsubmergence, except that the separated region did not continue to grow with increasing sideslip angle from 9 to 10 degrees.

The effect of the suction slot can be more clearly seen in those cases from the fourth series in which the suction was concentrated near the surface in a restricted span slot. The results of flow visualisation photogrammetry are shown in Figure 8.17 for these cases. There, the 10-degree sideslip separation line below the slot is in good agreement with the 9-degree line from the unmodified strut test of Figure 8.15. In the cases of no suction, the reattachment line balloons aftwards at the bottom of the open slot, but moves forward as the top of the slot is approached, and disappears farther from the mean free surface than in the unmodified case, for the 9-degree reattachment line. In cases where suction was applied, the reattachment points immediately move forward as soon as the height of the suction slot is attained, and disappear significantly further below the free surface than does the corresponding 9-degree reattachment line in the unmodified case or the cases without suction.

It would be pleasant to be able to state that the evidence in support of the proposed mechanism of ventilation suppression by the suction slot was definite and incontrovertible. Unfortunately, the flow visualisation patterns near the free surface and ahead of the suction slot were ambiguous. The characteristic herringbone pattern indicating reattachment was seldom observed ahead of the suction slot, even when other evidence—such as the existence of an oil tidal mark near the leading edge—indicated that separation was definitely present. Therefore, in deciding the height to which the separation bubble extended, it was necessary to weigh factors such as the location at which the herringbone pattern disappeared, the extent of scouring ahead of the slot, and the direction indicated by the centerline of the herringbone pattern before it disappeared. However, the trend in the data appears to be firmly established and consistent.
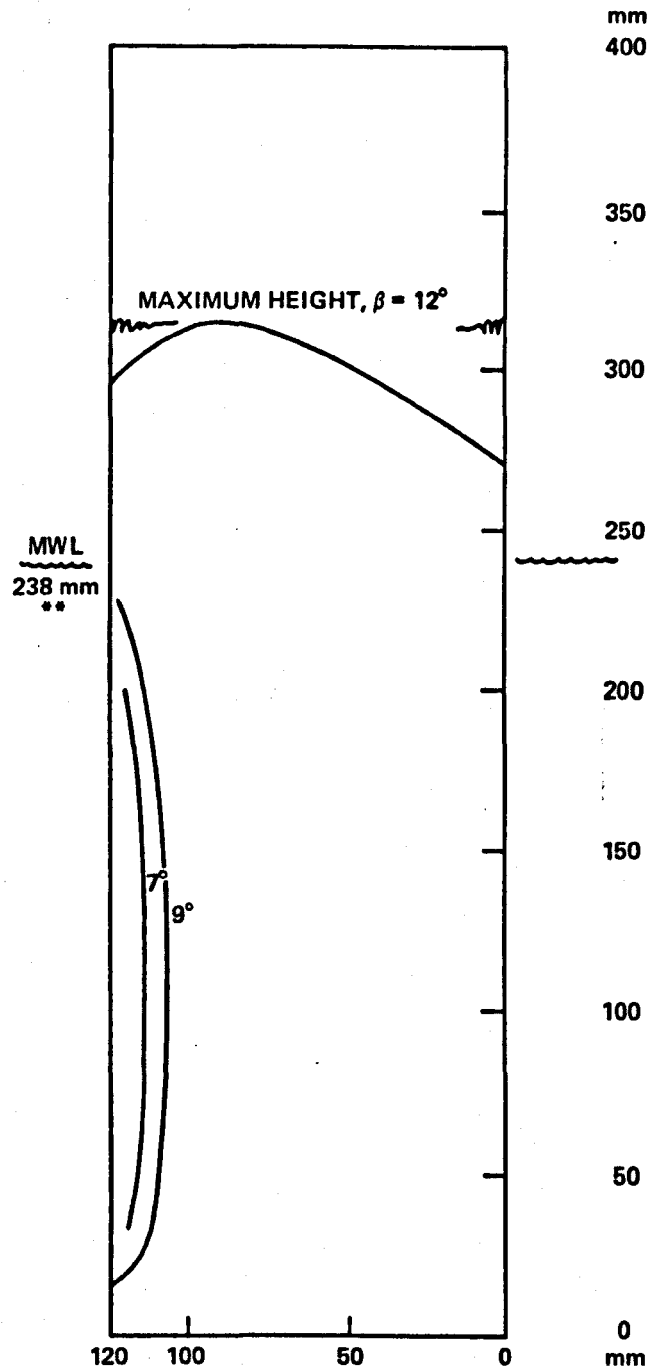
Figure 8.15 — Reattachment Lines, Leeds Blunt Biogive, 20 ft/s
(6m/s), $7° \leqslant \beta \leqslant 9°$, Bare Strut.

206

Figure 8.16 — Re-attachment Lines, Blunt Biogive, 20 ft/s (6m/s).

207
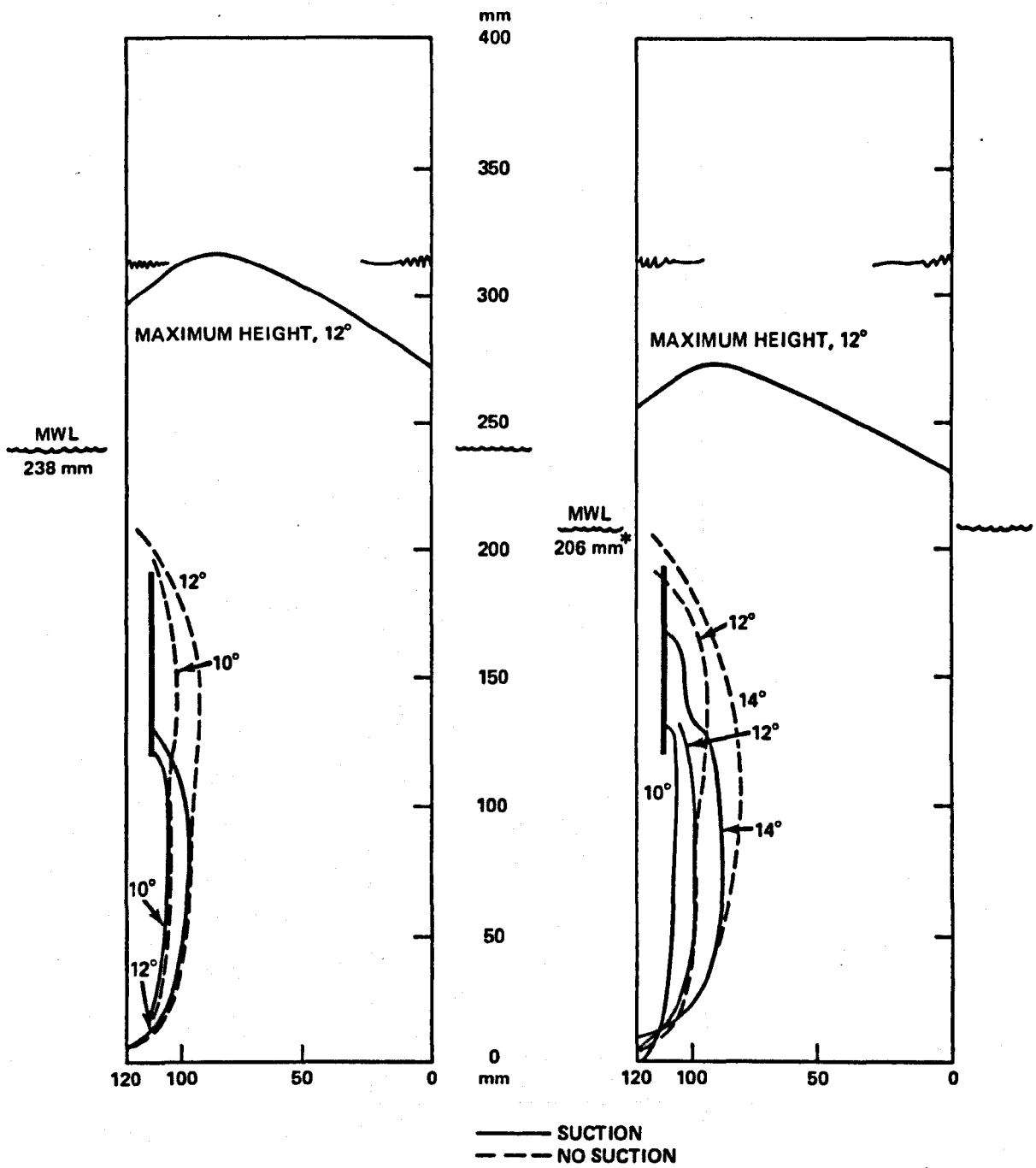
Figure 8.17 – Re-attachment Lines, Blunt Biogive, 20 ft/s (6m/s), Short Slot Below Surface.

208
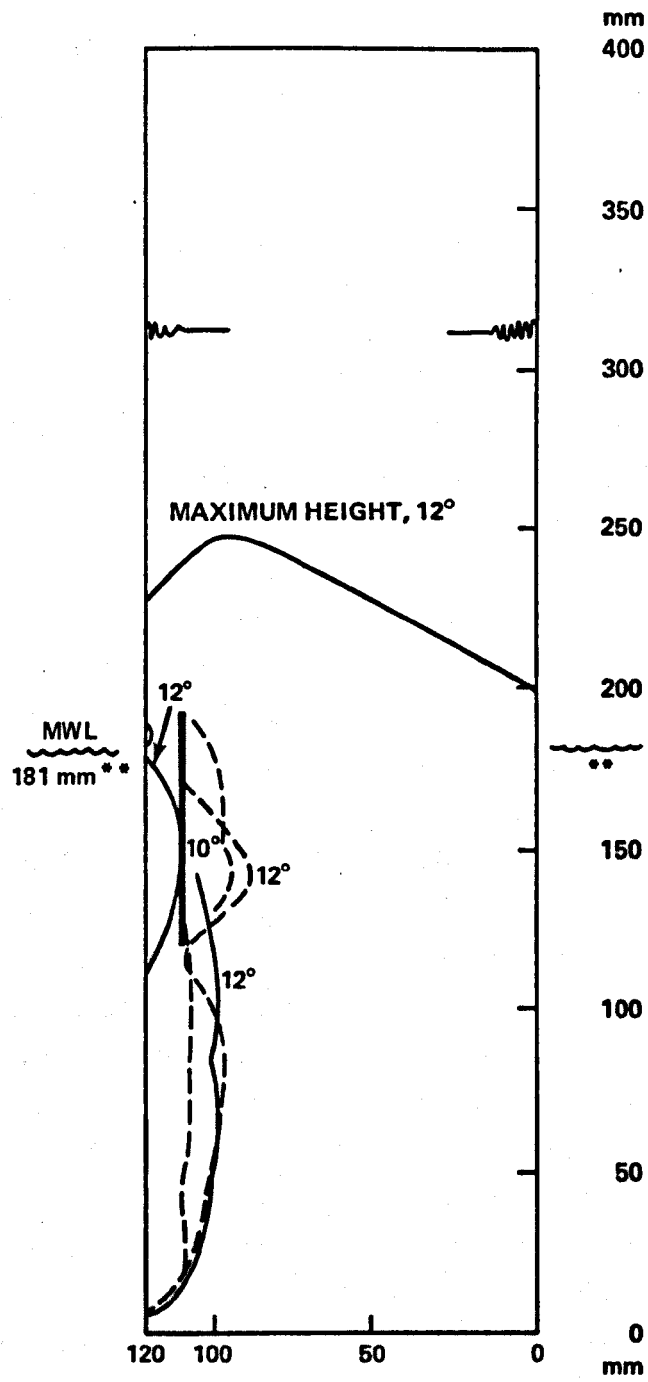
Figure 8.17 (Continued)

Demonstration of Prevention of Ventilation by Control of the Separated Region. As stated in the beginning of this chapter, the primary objective of the experiment as originally conceived was to establish that separation is a necessary condition which must precede ventilation. This was to be done by eliminating separation, and observing the change in ventilation characteristics while changing as few other parameters as possible. It was decided that suction was the ideal way to accomplish this goal. In the section of this chapter on theory, it was shown that the region of separation on the blunt biogive strut would be impossible to remove completely under the chosen circumstances. The most that could be accomplished by suction would be the reduction of the extent of the separated region, particularly in the region of the free water surface. It was felt that if ventilation could be prevented by the reduction in extent of a separated region, this would serve nearly as well to establish separation as a precondition for ventilation.

Previous tests of the unmodified blunt biogive fitted with a slot for this test established that a sideslip angle of 10 degrees could not be maintained long enough to develop an oil smear pattern for flow visualisation purposes. Exactly how long angles of 10 degrees or greater could be maintained was not an objective of the previous test and was not established. However, Wright et al,[2] working with a geometrically similar model of 4/5 the chord length of the present model, did a careful study of the time dependence of the ventilation event as a function of angle. The same submergence ratio and the same facility was used as the present test. The test technique was somewhat different in that the strut was immersed after the run angle was acquired, and timing then began immediately. This was judged irrelevant except for those cases where ventilation occurred immediately, which did not happen regularly below a sideslip angle of 15 degrees. Using a statistical analysis on their data, Wright et al determined that the expected time to ventilation at 10 degrees was about 15 seconds, falling linearly to about 8 seconds for 14 degrees. Virtually all vents at sideslip angles of 6 degrees or more occurred at times of immersion substantially less than 90 seconds. Therefore, the 225 second maximum run time of the present experiment was long enough to establish the absence of ventilation.

For the second series of tests described in this chapter, with the full span faired slot, no systematic attempt was made to measure exactly the time to ventilation, but an approximate time was noted if, during the flow visualisation runs, vents occurred. No vents occurred below 12 degrees with suction or below 10 degrees without suction with the following exceptions: at 8 degrees of sideslip angle, a vent occurred after about 30 seconds during suction, and then again during a suction run at 11 degrees after about 20 seconds; a vent was noted at 9 degrees, with suction off, after about 15 seconds.

The fact that even an anomalous vent occurred with suction at 8 degrees meant that the evidence collected with the full span slot had failed to establish the required objective of positive

prevention of ventilation. There is no doubt, however, that on a statistical basis, the presence of the slot, with and without suction, represented an improvement over the plain biogive tested by Wright, et al. It is not so clear that the application of suction was beneficial compared to the slot with no suction applied, since no vent was noted without suction to 14 degrees of sideslip angle. It is true that a larger (by one degree) angle was possible before immediate ventilation with suction than without. It was also true that suction delayed the aftward spread of the separation bubble by a degree or two compared with the case of a slot with no suction. No data exist for the case of the unmodified blunt biogive, but extrapolation and the experience of other cases indicate that the growth of the separation pattern was slowed by the presence of suction.

On balance, the experiment with the full span slot produced no conclusive evidence on the role of separation, although it was strongly indicative that reducing the separation reduced the tendency to ventilate.

The fourth series, in which suction was concentrated 45mm below the mean free surface. 12mm below the mean free surface and 12mm above the mean free surface, was more conclusive, both in its effects on the separation pattern, as previously noted, and on the ventilation characteristics.

With the top of the slot 12mm below the mean free surface, the model was run at 15 degrees sideslip angle for the time it took to fill the suction reservoir (about 225 seconds) without ventilation. This performance was repeated at 10, 12, and 14 degrees, and then again for flow visualisation photographs. With the top of the slot 12mm above the mean free surface, 225 second runs were achieved without ventilation at 10 and 12 degrees sideslip angle. In the flow visualisation sequence of runs performed to take photographs, no vents were observed under the foregoing conditions, nor were any observed for the 45mm immersion. This immersion was not tested as extensively as the $\pm$ 12mm case, since it did not appear as promising in the preliminary survey. This was in agreement with the theoretical prediction of the early part of this chapter that to be effective, suction would have to be concentrated near the mean free surface.

The principal results from this series of suction experiments was that the surface seal thickness could be influenced by suction, and was directly related to the ventilation resistance of a strut with a nose separation bubble.

Combining Leading Edge Roughness with Suction: Effect on Separation and Ventilation. The inspiration for the roughness/suction experiment came during the preliminary runs with the full span slot. There, it was observed that small roughnesses ahead of the slot were correlated to patches of attached flow downstream. It seemed theoretically plausible that the earlier transition to turbulence was adding more energy to the boundary layer and thus adding to the effect of the

suction. The effect of the number 11 grade glass sphere roughness applied can be seen in Figure 8.18. In fact, a possibly beneficial effect can be noted in the separation pattern near the mean free surface compared to the smooth full span slot case, but the separation pattern is patchy. A vent was noted at 10 degrees sideslip angle during the intial flow visualisation runs, which discouraged a full-run-time survey. Although no further vents were noted until 14 degrees, both with and without suction, the maximum angle which could be achieved without immediate vent was 14 degrees, with and without suction. Because this was significantly worse than the smooth case, and because of the lack of differences between the suction and non-suction cases, this configuration was not investigated more thoroughly.

CONCLUSIONS OF THE SUCTION EXPERIMENT

- Partial suction slots concentrated near the free surface were effective in preventing nose ventilation.
- Complete elimination of separation was not possible with full span slots and so the conclusion that separation is a necessary precondition for ventilation could not be drawn.
- A reduction in the extent of separation reduced the tendency to ventilation.
- The theoretical approach adopted for predicting the effect of suction is valid.
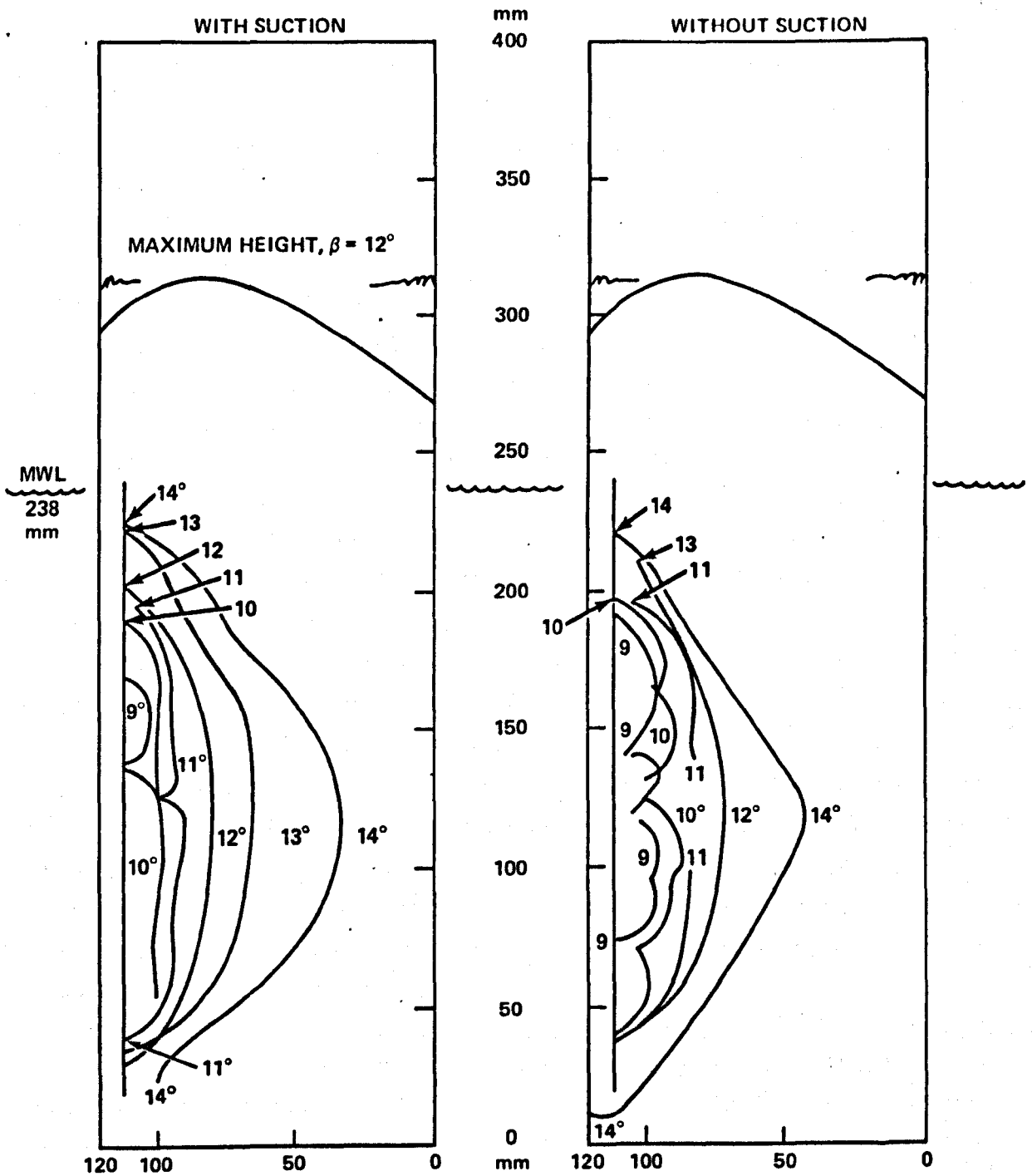
Figure 8.18 — Re-attachment Lines With Roughness; Blunt Biogive, 20 ft/s (6m/s).

213

Effect of Proximity to Free Surface on Measured Pressure. Figure 8.5 shows the values of pressure experimentally determined for various locations on the blunt biogive by Swales et al.[3] The locations of the pressure taps are also shown in the figure. The conditions displayed in the figure were chosen because of their closeness to the configuration of interest. Experimental data for β = 10 degrees and V_∞ = 20 ft/s (6 m/s) were not available, probably because of the tendency of the strut to ventilate after a short time under these conditions. The cases which seemed to provide the most insight were those for which β = 2 degrees, 10 and 15 degrees at 5 ft/s (1½ m/s). Shown in the figure are the experimental pressures recorded for these conditions at 0.7 c and 0.25 c, at immersions of 6, 31, and 56 percent of mean submergence, which was equal to 2 chord lengths. The blunt biogive used in the pressure measurements had a 2.81-inch (71 mm) chord. From the figure it can be seen that, for β = 2 degrees, the spanwise pressure distribution was roughly elliptical, as nearly as can be inferred, with a maximum (of $-C_p$) at midspan and approaching zero at the mean free surface. Furthermore, the experimental value of lift coefficient at midspan closely matched the two-dimensional theoretical prediction. This would be expected considering the slight surface distortion and the absence of separation at the low sideslip angle (β) of 2 degrees. For β = 10 degrees, the value of $-C_p$ at midspan and 0.25 c was reduced somewhat from the theoretical. Closer to the surface, $-C_p$ rose nearly to the theoretical value of 1.0. Very near the surface, $-C_p$ fell, apparently towards zero. The rising and falling of the spanwise distribution of $-C_p$ was a consequence of a region of separation which, flow-visualisation studies showed, started at the leading edge, just below the mean free surface, and extended nearly to the submerged tip. The chordwise extent of the separated region was greatest at midspan, and shrank to nothing at the tip and near the mean free surface. Therefore, the maximum influence of the separated region was manifested at the midspan pressure taps. The relatively smooth spanwise behaviour of the pressure distribution at 0.25c and β = 10 degrees indicates that, although the pressure at the midspan tap was influenced by the separation, the tap was not within the separated region.

The rapid variation with span of the measured pressures at 0.7 c for β = 10 degrees and at 0.25 c for β = 15 degrees implies that the taps below the mean free surface at 31 and 56 percent of total submergence were indeed within the region of separation. The high values of $-C_p$ at points only 0.07 c below the mean free surface in these latter two cases indicate that the flow in this region was fully attached. Furthermore, for the pressures measured there to have been so far from zero (relative to ambient pressure at the mean free surface far upstream) implies that the effective free surface — where the pressure actually fell to zero — was probably somewhat

above the mean free surface. This hypothesis corresponds to observations of the surface distortion in the flow around partially submerged struts.

Estimate of Height of Effective Free Surface. The experimentally measured values of pressure under conditions where separation did not occur suggest that
  (a) the midspan pressures corresponded to two-dimensional theory,
  (b) the spanwise variation of pressure was elliptical.

It may be hypothesised that similar circumstances obtain when separation is present:
  (a) the spanwise variation of pressure is elliptical except for regions aft of or within a region of separation,
  (b) the locus of the ellipse, where applicable, may be determined by fitting an elliptical distribution to points outside of, but not aft of the separation region, and including the theoretical two-dimensional value of $-C_p$ as an "imaginary" point at midspan.

For example, in the experimental pressure distribution cited, for $\beta = 10$ degrees, $U_\infty = 5$ ft/s (1½ m/s), at $x = 0.07$ c, $-C_p = 1.3$ at $y/h = 0.06$. The theoretical value of $-C_p$ at the same chordwise position is 1.77. Fitting an ellipse (symmetric about midspan) to these two points, it is found that the effective free surface ($-C_p = 0$) occurs about 0.20 c higher than the mean free surface at $x = 0.07$ c.

In the second useful case with $\beta = 10$ degrees, $U_\infty = 5$ ft/s (1½ m/s), $x = 0.25$ c, $-C_p = 0.3$ at $y/h = 0.06$, and $-C_p$ (theory) $= 1.0$. Fitting an ellipse to these points indicates that at $x = 0.25$ c, the effective free surface is about 0.04 c below the mean free surface. This estimate of the height of the effective free surface provided the basis for Equation (19).

Chapter 8 References

8.1 Swales, P.D., Wright, A.J., McGregor, R.C., Cole, B.N., *"Pressure, Flow Visualisation and Ventilation,"* Hovering Craft and Hydrofoil, Vol. 13, No. 1, pp. 11-16, 1973.

8.2 Wright, A.J., McGregor, R.C., and Swales, P.D., *"Time Dependency of Ventilation,"* Hovering Craft and Hydrofoils, Vol. 12, No. 9, 1973.

8.3 Swales, P.D., Wright, A.J., McGregor, R.C., Cole, B.N., *"First Interim Report on DREA Hydrofoil Ventilation Problems,"* University of Leeds Dept. of Mech. E. Research Rept. TP/DREA/1, Jan 1971.

8.4 Schlichting, Hermann, *"Boundary Layer Theory,"* McGraw-Hill, 1960.

8.5 McGregor, R.C., Calculations partly published in Reference 8.1.

8.6 Wright, A.J., and McGregor, R.C., *"DREA Hydrofoil Project Interim Report,"* University of Leeds Dept. of Mech. E. Research Rept. TP/DREA/4, Mar 1972.

8.7 Chang, P.K., *"Separation of Flow,"* Pergamon Press, 1970.

8.8 Hunter, B., Swales, P.D., Cole, B.N., *"Variable Pressure Water Channel,"* The Engineer, Vol. 225, pp. 515-519, Mar 1968.

8.9 Loving, Donald L. and Katzoff, S., *"The Fluorescent - Oil Film Method and Other Techniques for Boundary Layer Flow Visualization,"* NACA memo 3-17-59L, Mar 1959.

8.10 Breslin, John P. and Skalak, Richard, *"Exploratory Study of Ventilated Flows about Yawed Surface Piercing Struts,"* NASA memo 2-23-59W, Apr 1959.

CHAPTER 9

SUPPRESSION OF VENTILATION BY
ELIMINATING A SEPARATED REGION BY BLOWING

OBJECT OF THE EXPERIMENT

Suppression of Tail Ventilation as a Sequel to Nose Suction Experiment. In the previous Chapter, suction was used to eliminate part of a region of nose separation near the intersection of a surface-piercing hydrofoil strut with the free water surface. Elimination of the separation was found to suppress the nose ventilation characteristically associated with the "blunt" nosed biogive, a thin, relatively sharp-nosed body. It seemed natural after the suction experiment to try to extend the same principle to a strut section known to be susceptible to tail separation and ventilation.

Exploration of the Interaction of Separation and Ventilation. One experimental objective was much the same as for the suction experiment: to explore the mechanism of ventilation as postulated in Chapter 3 — particularly to ascertain whether separation is a necessary precondition to ventilation. As before, it was desired to change as few hydrodynamic and geometric parameters as possible while eliminating a region of separation. Boundary layer blowing shares with boundary layer suction the property of preventing separation while changing only slightly the geometric boundaries, thus providing the most direct comparison of the effects of the presence or absence of separation.

Blowing as a Practical Means of Ventilation Suppression. It was known from the inception of the suction experiment that suction was not suitable for full scale application in water. Generally, hydrofoils operate in a speed regime where vapour cavitation is incipient, if not fully established. It would be difficult or impossible to apply suction under these circumstances. Even at lower, sub-cavitating speeds, where some lift enhancement might be achievable at takeoff by using suction to allow larger foil attack angles, the problem of protecting suction slots from fouling under open water conditions would be insurmountable. Boundary layer blowing does not suffer from either cavitation or fouling defects, so far as is known. For craft with waterjet propulsion, the availability of high pressure water as a byproduct of the primary motive system makes blowing even more attractive. Therefore, a further objective of the experiment was the evaluation of this technique as a practical means of suppressing ventilation.

METHOD AND APPROACH

Choice of Section. The principal constraint on the experimental approach was compatibility with the capabilities of the Variable Pressure Free Surface Water Channel and with the ancilliary

equipment associated with the suction experiment. The size of the test section and blockage effects as discussed in Chapter 5 determined the model chord length of 127mm and the nominal submergence of two chord lengths. Apart from these considerations, a section was desired which had:

1. Well behaved and defined ventilation characteristics
2. Tail separation and tail mode ventilation only
3. Enough thickness to permit rearward-facing slots and a plenum
4. Applicability to full scale craft

The section which satisfied these requirements was the NACA 16-021. It had previously been tested[9.1] at Leeds University and its ventilation and separation characteristics had been defined. It was known to develop tail separation on the low pressure side at low sideslip angles, and was observed to undergo ventilation in the tail mode with good predictability, with little or no dependence on time of immersion. This was in contrast to the markedly time dependent behaviour of the blunt biogive used in the suction experiment. The variation in angle of ventilation observed for the NACA 16-021 strut was also quite small — only $\pm$ ½ degree in eight measurements at a channel speed of three metres per second, according to Wright[9.2] et al.

The section thickness was 21 per cent of chord, which was convenient for machining the interior to provide blowing passages, but which might be considered excessively thick for full scale practical application to very high speed craft.

The 16-series section is widely applied to existing hydrofoil craft. In fact, the section was developed by the National Advisory Council on Aeronautics (NACA) specifically for hydrofoils.[9.3] The flat pressure distribution was intended to provide maximum lift with the least cavitation. The maximum thickness at midchord has structural advantages in handling the higher stress levels of lifting surfaces in water, and is well suited for struts which must enclose pipes and machinery such as propeller transmission shafts. The basic 16-021 section is shown in Figure 9.1

Choice of Test Speed. Three primary factors governed the choice of speed to be used for the test. First, as low a speed as practical would reduce the requirements of jet velocity and jet momentum from the blowing slots. Second, predictable and repeatible ventilation behaviour was required. Third, the flow regime had to be similar to the turbulent flow expected under full scale conditions.

According to the Wright et al study[9.2] the NACA 16-021 strut displayed the least time-dependent behaviour at a channel speed of three metres per second. Experience gained earlier in the present study showed that full ventilation to the tip of similar struts did not occur at speeds less than two metres per second, so speeds of significantly less than three metres per second would not demonstrate the phenomenon to be studied.

219

NACA 16-021 PROFILE

TABLE OF OFFSETS
(INCHES)

X	Y
0.	0.
0.0625	0.1130
0.1250	0.1580
0.2500	0.2196
0.3750	0.2653
0.5000	0.3025
0.7500	0.3618
1.0000	0.4081
1.5000	0.4740
2.0000	0.5123
2.5000	0.5250
3.0000	0.5106
3.5000	0.4610
4.0000	0.3674
4.5000	0.2202
4.750	0.1238
5.000	0.0105

y

R = 0.216c

2.4c

0.3c

0.6c

0.9c 1.0c

(127mm)

A 35°

15°

3 SLITS. 1/32 INCH WIDE (0.8mm)
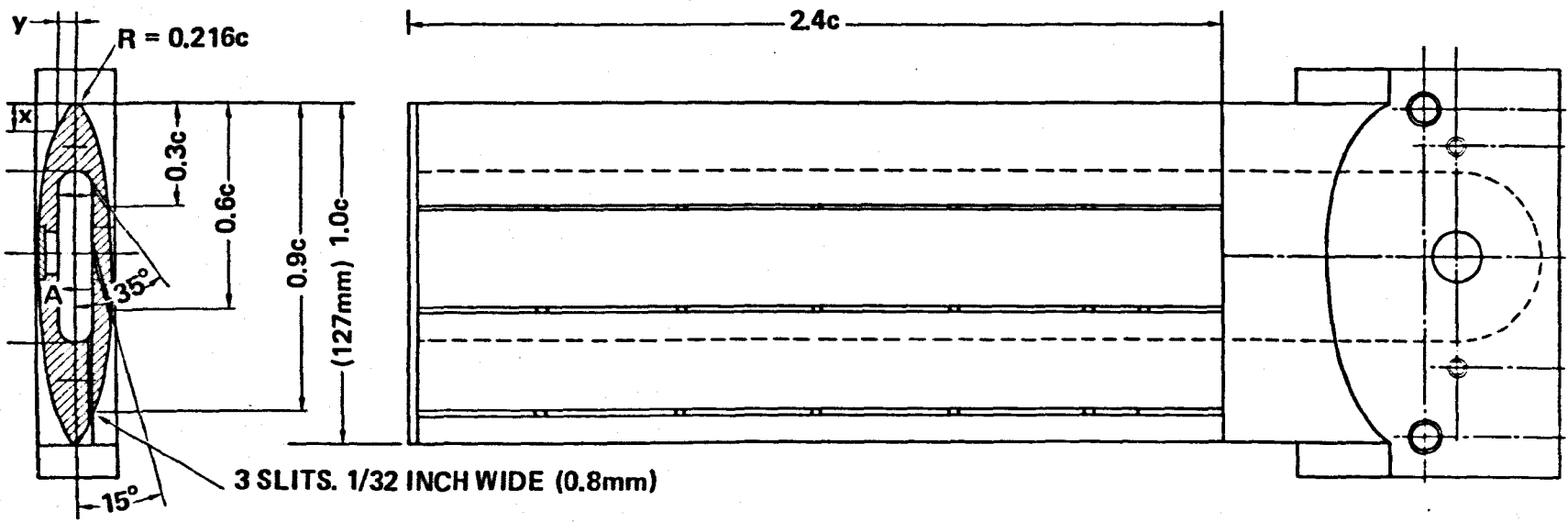
Figure 9.1 – NACA 16 021 Section Shape and Planform as Modified for Blowing.
Chordlength 127mm, Design Submergence, 2c.

The Wright tests did not reveal any anomaly in the pattern of separation attributable to a too low velocity. No laminar separation bubble appeared at the nose, and transition to turbulent flow could be clearly observed in the oil smear pattern before tail separation occurred. Evidently, the speed was not so low that an artificial separation pattern was generated which might make the results inapplicable to higher speeds or larger scales.

Additionally, the Water Channel handled air removal more easily at three metres per second than at the higher speeds, thus reducing the necessity of excessive shutdown time to clear air.

Therefore, three metres per second was chosen as the primary speed at which the investigation was performed. Certain runs were made at six and nine metres per second to ensure, within the limits of the Channel capability, that no significant extraneous effect was introduced by the choice of speed. The addition of a controlled roughness in the latter part of the blowing experiment introduced a speed dependence. During the tests in which a dependence on speed was noted in the results, the complete speed range was used.

Flow Visualisation and Photography. The oil smear flow visualisation technique described in the previous chapter was used to determine the extent of tail separation and other flow features. As before, a 35mm format photograph was taken of the oil smear pattern which was caused to flouresce by ultraviolet illumination. In addition, a second, nearly simultaneous photograph of the flow while the strut was immersed, was taken to aid in the interpretation of the oil smear pattern. For this purpose a second camera was added to the experimental equipment, synchronised with three stroboscopic flash units to capture as much as possible of the flow appearance during the runs.

Roughness. In Chapter 5, it was suggested that the addition of a controlled roughness would simulate the effect of higher speeds and larger sizes encountered in prototype applications. The experimental evidence of that Chapter demonstrated that roughness introduced a speed dependence, and generally lowered the ventilation angles. Both of these phenomena have been observed under prototype conditions. To add this dimension to the experiment, the NACA 16-021 strut selected was also tested with glass microsphere roughness applied in the manner developed in the Chapter 5 experiments.

PREDICTION OF BLOWING REQUIRED TO PREVENT SEPARATION

Before proceeding with the experiment, and in particular the design of the blowing aspects of the model and apparatus, it was necessary to estimate the amount of blowing which would be required

to eliminate the anticipated separation. This calculation would also have a bearing upon the possible practical usefulness of a device employing the proposed technique.

Gartshore-Newman-Kind Method. A search of the available literature[9.4-9.25] revealed a method for calculating the boundary layer properties of a jet blowing tangentially to a wall due to Gartshore and Newman[9.4], modified by Kind[9.5, 9.6], which could have been adapted to the present case. The method is based on plausible but unproved assumptions and empirical relationships relating to the growth and mixing properties of the wall jet. The ability of the method to predict separation of the wall jet, as shown by Kind's comparison with experiment, was poor except in the case of his own experiment. The calculation procedure was extremely complicated, and did not account for three-dimensional or free surface effects. Furthermore, the possibility of multiple slots would have strained the weakest point of the theory—the starting assumptions at the slot.

After some consideration a novel, but much simpler, theoretical approach was adopted to calculate the energisation requirements. The method is still empirically based, but deals with real situations more effectively than does Kind's method. The approach relies on an anology between aerofoil behaviour and that of an elliptical cylinder for which blowing data are known.

Similarity of Circulation Controlled Elliptical Aerofoils to Conventional Foils with Blowing. An analogy can be drawn between the flow around an elliptical cylinder with separation and an aerofoil which separates on its upper surface, forward of the trailing edge. In both cases, the lift depends upon the location of the separation points. For a blown elliptical aerofoil, as the blowing is increased, the upper surface separation point moves aft, and the circulation and lift increase linearly. A similar phenomenon occurs for a blown aerofoil, and the same linear relationship exists up to the point where the flow is completely unseparated over the upper surface. Thereafter, the excess momentum of the jet contributes to a jet flap effect, increasing the lift according to the square root of the blowing momentum[9.7].

This analogy was utilised over the regime where increase in lift coefficient is linear with increase in blowing momentum.

Prediction of Required Jet Momentum Coefficient by Analogy. Figure 9.2 shows the variation in sideforce with sideslip angle, β, for a NACA 16-021, 100mm chord strut immersed in the Leeds Channel to a depth of 1.9 chords at 3 m/s as measured by Wright et al.[9.26] Note that the sideforce had three linear ranges. Which can be defined as follows: In the first where

$$\text{I. } 0 < \beta < \beta_R \text{ ,}$$
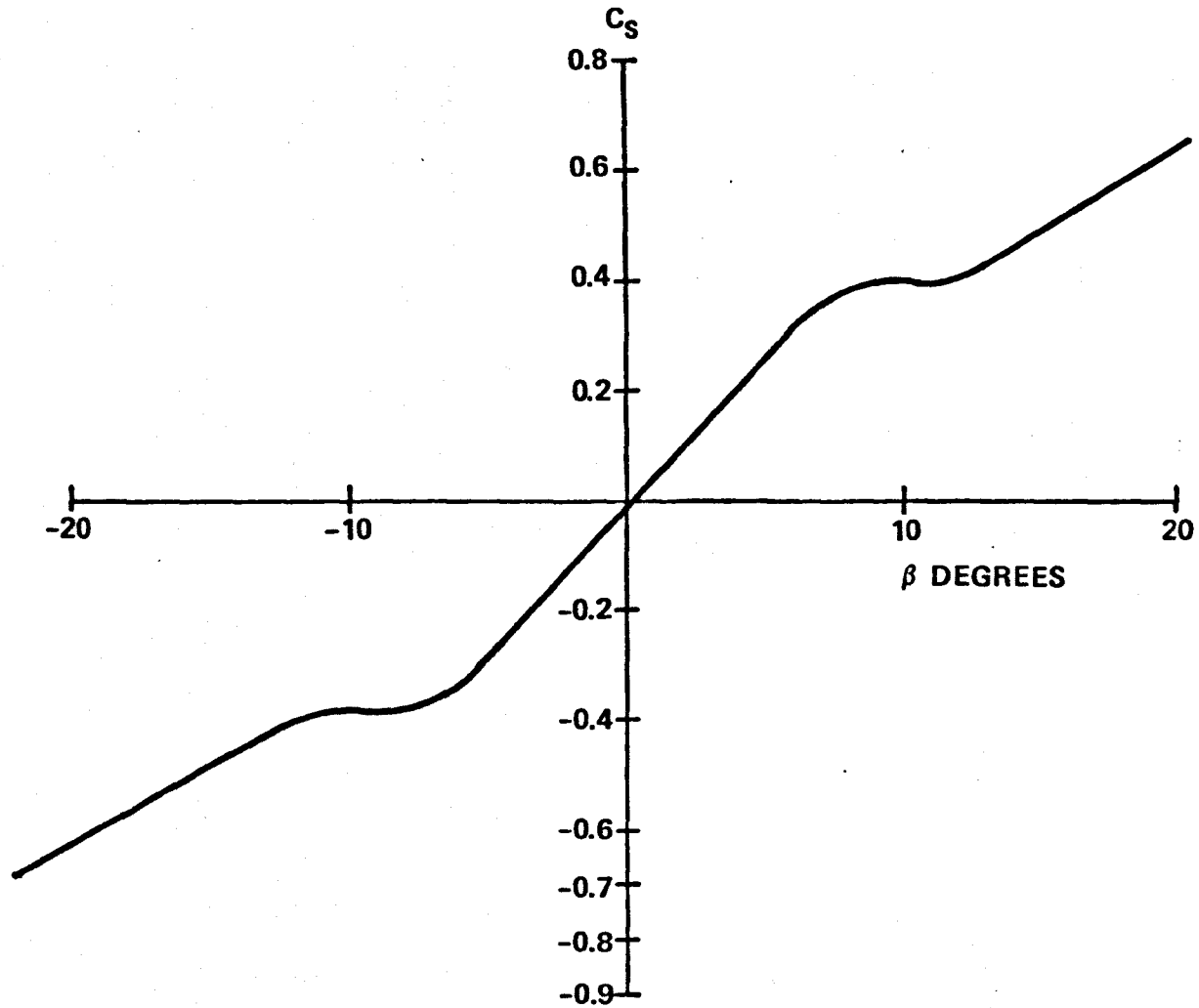
Figure 9.2 — Sideforce Coefficient Versus Sideslip Angle, β, For a NACA 16 021, 100mm Chord Strut, Immersed to 1.9c, 3m/s. From Wright, Et AL [9.26]

separation had not yet appeared. In the second range, where separation was growing rapidly,

$$\text{II.} \quad \beta_R \leqslant \beta \leqslant \beta_S .$$

Finally, there was a third linear range,

$$\text{III.} \quad \beta_S \leqslant \beta \leqslant \beta_V$$

where β_V was the ventilation inception angle.

In order to use these results it was first necessary to find a basis for comparing them with two-dimensional results. A method for doing so is illustrated graphically in Figure 9.3 with idealised sideforce slopes.

First, an efficiency factor was arrived at by dividing $\partial\beta_S/\partial\beta$ in region I by the ideal two dimensional slope, $2\pi/\text{rad}$.

$$E = \frac{\left.\dfrac{\partial C_S}{\partial \beta}\right|_I}{2\pi}$$

Then, the sideforce coefficient in each region was divided by E to arrive at a projected two-dimensional value.

The next step was to assume that in the absence of ventilation, $\left.\partial C_S/\partial\beta\right|_{III}$ would remain constant to a sufficient value of $\beta > \beta_V$, say β_{LS}, where leading edge separation might occur.

For values of $\beta > \beta_V$, there will be a μC_S "deficit," C_{SD}, where

$$C_{SD}(\beta) = C_{SD} = 2\pi\beta - \frac{1}{E}\left\{ \beta_R \left.\frac{\partial C_S}{\partial \beta}\right|_I + C_S(\beta_R) + (\beta-\beta_S)\left.\frac{\partial C_S}{\partial \beta}\right|_{III} \right\}$$

The right hand side represents the two dimensional ideal value of sideforce coefficient less the projected values from each region corrected for three dimensional losses.

For example, from the Figure if $\beta = 29$ degrees,

$$C_{SD} = 1.4$$

Elliptical Aerofoils. Williams et al[9.8] presented data for a two-dimensional, 20 percent thick elliptical aerofoil for which $\Delta C_L/\Delta C_\mu$, the change in lift coefficient with change in blowing momentum coefficient, in the linear range of interest, was about 50. C_μ is defined as

224
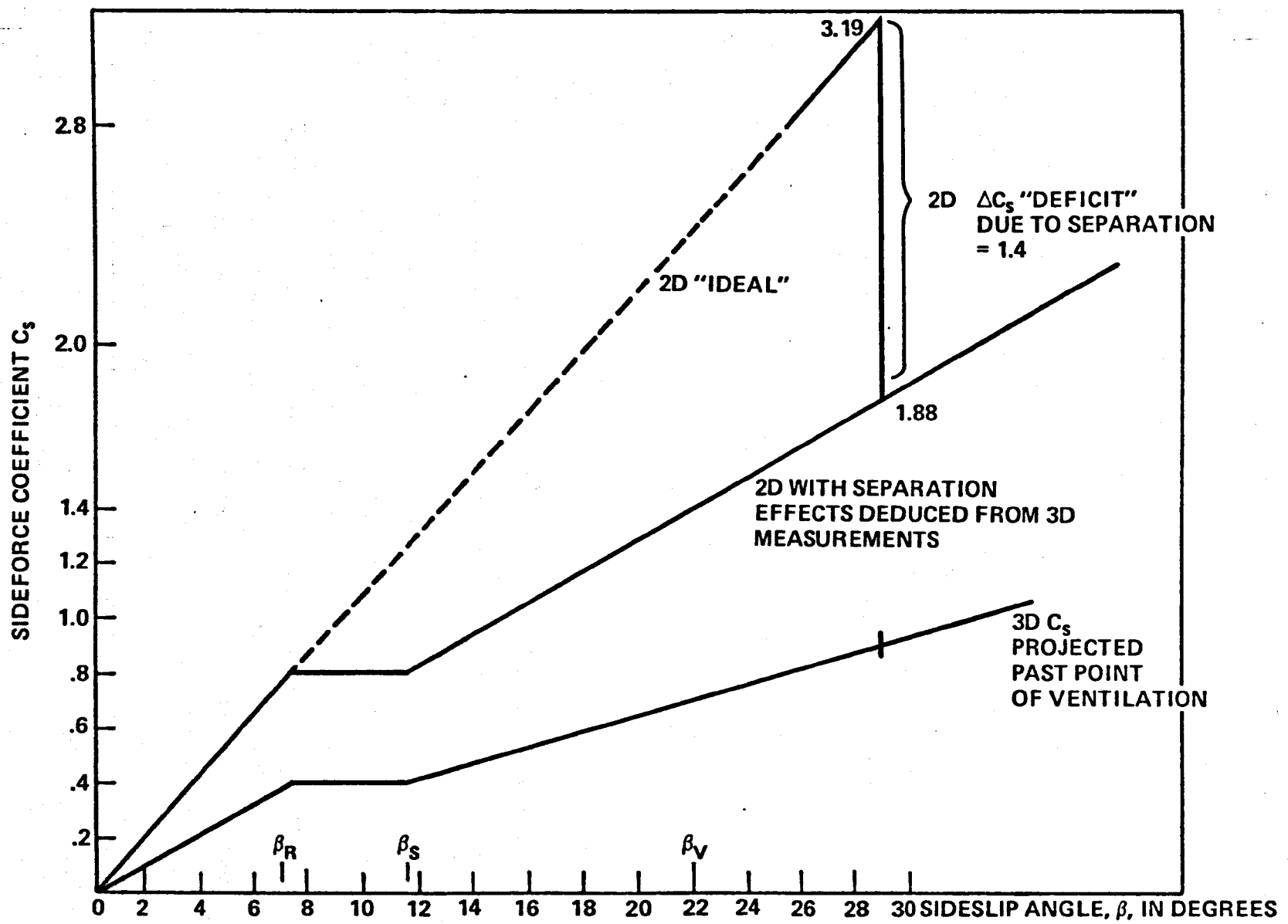
Figure 9.3 — Calculation of Sideforce "Deficit" From Idealised Force Coefficient.

225

$$\frac{V_j^2\,A_j}{\frac{1}{2}\,U_\infty^2\,A}$$

where
A = the submerged planform area

A_j = the slot crosssectional area

V_j = the jet velocity

This particular aerofoil was chosen for comparison because it is approximately the same thickness as the NACA 16–021 model. Also, it represents a very efficient experimental lifting device, which may be expected to be relatively free of deviations from ideal behaviour.

Jet Momentum Coefficient, Volume Flow Rate and Pressure Difference. Assuming the behaviour of the elliptical and conventional aerofoil sections are similar as hypothesised, the C_μ necessary to make up the sideforce deficit is

$$C_\mu = \frac{\Delta C_L}{\Delta C_\mu}\,C_{SD}$$

For the example just given, in which

$$C_{SD}\,(\beta = 29 \text{ degrees}) = 1.4$$

and using the Williams et al[9.8] value of $\Delta C_L / \Delta C_\mu = 50$, the value of C_μ necessary to make up the sideforce deficit for the NACA 16–021 model is $1.4/50 = 0.028$. This is a two–dimensional value, but, since the jet would be essentially two–dimensional, no further correction was required. Assuming a total slot crosssectional area of about $0.03A$, the volume flow rate required was about $0.02\,\text{ft}^3/\text{s}$ ($0.57 \times 10^{-3}\,\text{m}^3/\text{S}$). For a slot discharge coefficient of about 50 percent the pressure difference required to drive the jet would be around 4 psi (28 kPa), neglecting other system losses.

The value chosen for A_j represented a typical one used in the experiment. The value of V_j chosen was low for circulation control applications, but was higher than the minimum required by wall jet theory. The exact values of these parameters were not critical in the actual experimental application, as the required driving pressure was determined by losses in the piping, valves and fittings which connected the model to the pressure reservoir.

226

General. The experimental setup was basically the same as for the suction experiment of the preceding chapter, shown in Figure 8.10. The principal test facility was the University of Leeds Variable Pressure Free Surface Water Channel. The test section was 355mm x 355mm square and 2750mm long. A complete discussion of the Channel was given in Chapter 5 and the references therein, including surface quality, air content, velocity cross section, velocity calibration, and wall interference and blockage effects.

Mark I Model. The strut tested, shown in Figure 9.1, had a NACA 16-021 (symetric) section with a 127mm chord and a maximum thickness at midchord of 27mm (21 percent chord). Constructed of phosphor-bronze, the general contour of the section was milled using a shaped cutter. The shaped contour was maintained for three chord lengths along the model span, allowing one chord length of shaped contour above the mean free surface at a nominal submergence of two chord lengths, approximately the depth at which most of the experiment was performed. A plenum was milled from the starboard side of the strut in a manner similar to that used on the suction strut described in the previous chapter. Since the model was generally yawed to port during the experiment, imperfections in the surface due to the cover plate over the plenum chamber were usually on the high pressure side. There, the flow was less sensitive to disturbances due to the more favourable pressure gradient.

After the plenum had been hollowed out, backward-facing saw cuts 0.8mm wide were made in the port side of the model, along the span, extending from the tip to just below the end of the faired section contour, approximately 100mm above the mean water line. These saw cuts into the plenum chamber intersected the strut surface at approximately 30, 55 and 90 percent of chord aft of the leading edge. By taping over the slots and partially or completely closing some, eight different configurations designated P1 etc., were created for a preliminary series of tests. These configurations are shown in Figure 9.4.

Preliminary tests showed that flow through the slots was nonuniform, and an experiment was performed using a variable slot geometry in a "dummy" model to even out the flow. This indicated that the simple saw cut slots would have been satisfactory had they been smooth and uniform. The relatively sharp edge formed where the saw cut intersected the strut surface was shown to have no adverse effect on the exiting flow. The experimental slot flow adhered to the wall of the "dummy" model in spite of a similar break in contour. The difficulty appeared to be that the manufacturer of the original strut had performed the saw cuts as the last machining operation, and the weakened shell material tended to collapse inwards toward the hollowed out

227

REF.
WATER
LEVEL

NOMINAL
IMMERSION
(mm)

297

—NORMAL 265—

—• 240—

—•• 215—

—••• 190—

FLOW—

CONFIGURATION P1

CONFIGURATION P2

CONFIGURATION P3

REF.
WATER
LEVEL

NOMINAL
IMMERSION
(mm)

297

—NORMAL 265—

—• 240—

—•• 215—

—••• 190—

FLOW—

CONFIGURATION P4

CONFIGURATION P5

CONFIGURATION P6
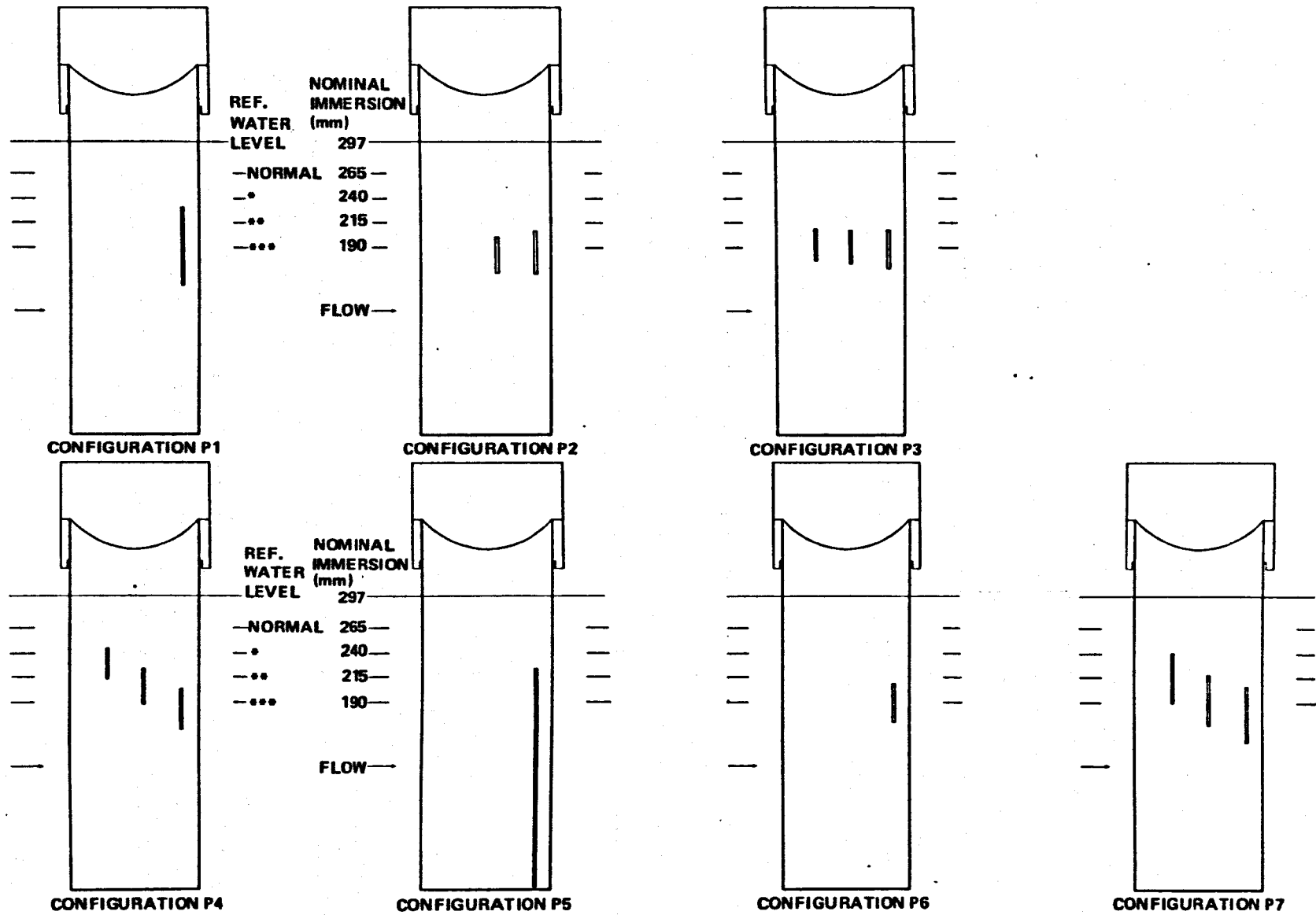
CONFIGURATION P7

Figure 9.4 – Configurations of the NACA 16 021 Vertical Slot Model Used in the Preliminary
Test Series.

portion and "grab" the saw blade. The result was that the slot interior sides were badly gouged.

After the state of the slot walls had been surmised and confirmed by probing, an initial attempt was made to improve the situation by rounding the external corners and placing baffles inside the plenum, despite the indications from the slot tests that such efforts were unnecessary. When the slot flow proved to be still unsatisfactory, a more drastic modification was applied. The material comprising the strut port side between the forward most and aft-most slots was removed by cutting horizontally across the strut. The slot walls were thus exposed and then smoothed by hand filing. Smooth plastic shims of 0.5mm thickness were then placed between the pieces of the model where the new slots were to be formed. Epoxy, reinforced with fiber-glass cloth, was used to fill in the excess space and to glue the separate pieces to the rest of the model. When the epoxy had set, the plastic shims were removed, leaving relatively smooth and uniform slots about 297mm long as shown in Figure 9.5. Several iterations were necessary to perfect this technique. The model was then faired to the original contour using a template. Besides the full length slots, two other configurations were formed by taping over first the upper sections of the slots, leaving open only the portions which were below the apparent water surface, then taping over most of the submerged portion, leaving exposed only a segment of each slot just below the apparent water surface.

After these slots were inadvertently ruined by applying too much blowing pressure, a similar technique was used to construct a third type of slot, 1.5mm thick. In this case, the slots extending from the submerged tip were terminated at the apparent free water surface, much as the previous configuration had been modified by taping the slots above the apparent water surface. This third attempt proved satisfactory, surviving the initial experiments, after which the strut was tested with grade 11 glass sphere roughness applied as described in Chapter 5.

Mk II Model. A second model was constructed, identical to the first except for the position of the blowing slots, which were nearly horizontal rather than vertical. This model was intended for a later experiment, described in the next chapter. However, it was used in the present experiment with the horizontal slots filled with beeswax to provide reference data for the plain section without slots, with and without roughness. Because the Mk I and Mk II models were made with the same milling cutter, the sections were virtually identical. This was verified by comparing shadow-graphs of the cross sections of the two models.

Blowing Apparatus. The fixtures for holding, immersing, rotating, and withdrawing the model from the Channel test section were the same as those used in the suction experiment, described in the preceding chapter. The same pressure vessel was used as a reservoir for high

Figure 9.5 — Modifications to the Slots to Encourage Uniform Flow.

pressure water as was previously used for suction. In this instance, instead of being connected to a high capacity vacuum pump, the reservoir was connected to the Departmental air supply, a virtually infinite reservoir maintained at a gauge pressure of about 175 psig (1.2×10^6 Pa). This air was fed via a regulator to the bottom of the tank, where it was guided to the top of the tank by a perforated tube as shown in Figure 9.6. The regulator was situated at the tank bottom so that the change in head as the tank emptied of water would not be sensed at the strut. The perforated pipe carried the air to the top of the reservoir without allowing excessive mixing of the air with the reservoir water.

The volume flow rate of the water was measured by timing the fall in water level over a fixed distance with a stopwatch, as in the suction experiment. A range of pressures was tested, with a corresponding variation in flow rate depending upon configuration. The flow rates versus reservoir pressure are plotted in Figure 9.7. The maximum reservoir gauge pressure was 100 psig (7×10^5 Pa).

EXPERIMENTAL PROCEDURE

General. With the Channel at the selected run speed, the blowing model was coated with oil as described in the previous chapter. If the run included blowing, blowing was started before immersion. If not, a short burst of water was blown through the model after immersion to purge air from the slots, plenum, and hose connections to the reservoir. The valve at the reservoir was then shut off. In either case, the model would be quickly rotated to the preset run sideslip angle, where it remained until the oil smear pattern had fully developed. A photograph was then taken using the lower camera and the three stroboscopic flash units. The blowing was shut off and the model pneumatically raised, rotated quickly to zero yaw angle, illuminated with ultraviolet light and photographed with the upper camera. If a vent occurred during the run it was noted. Usually, a preliminary survey was made to define the ventilation angle before proceeding with photographic flow visualisation runs.

Besides runs made with no blowing pressure, runs were frequently made with suction, since the reservoir had to be refilled anyway, and sucking water through the model speeded up the re-filling process.

Depth of Immersion. Because it was felt that the distance below the free water surface at which the boundary layer control became effective was an important parameter the depth of immersion was varied during tests of most configurations, and ranged from 302mm to 170mm (2.4c to 1.3c) below the mean free surface. In refering to the various configurations, the depth of immersion
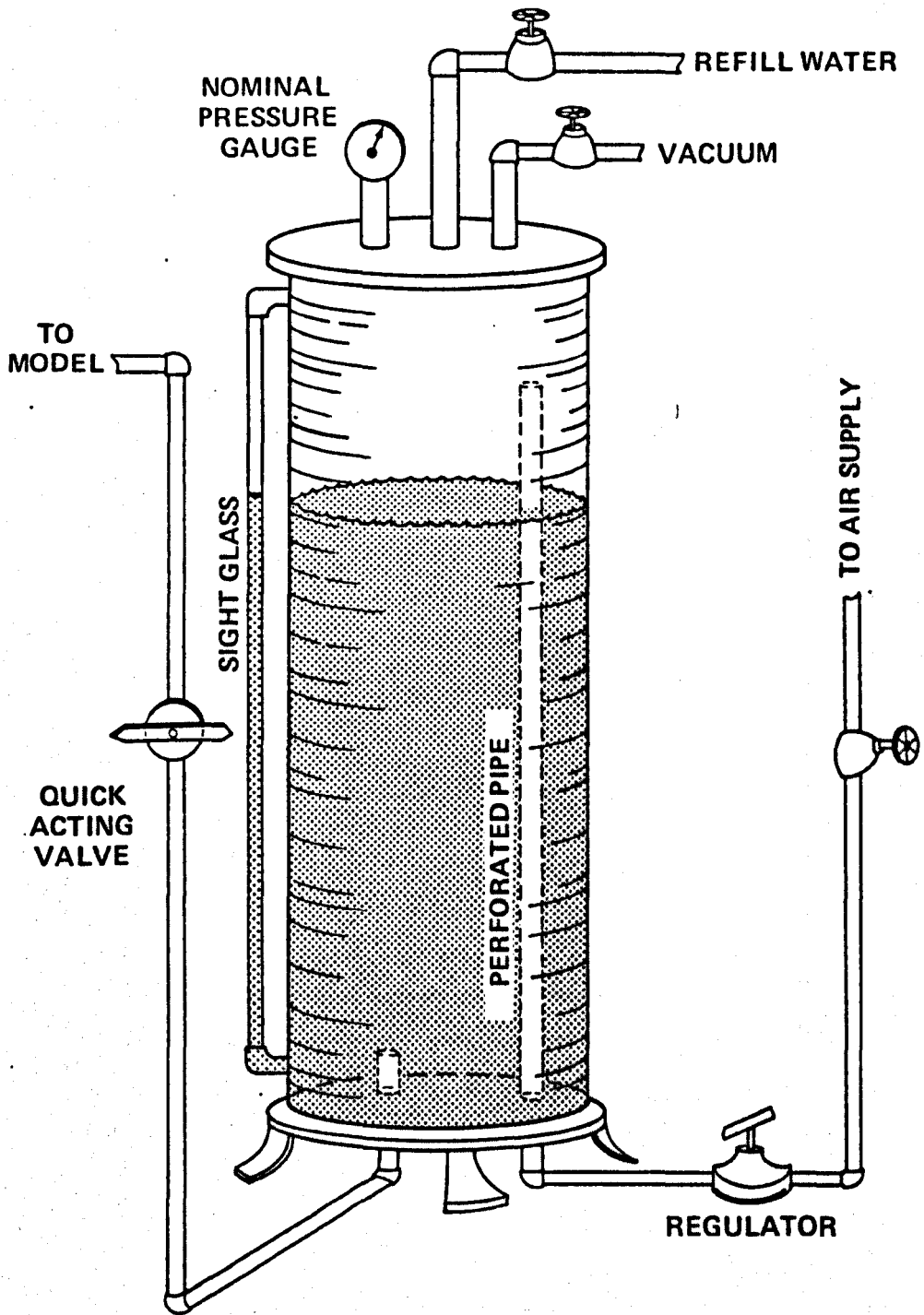
Figure 9.6 — High Pressure Water Supply for Mk I and II Models.

SOLID LINE GIVEN BY

$$\text{FLOW (ft}^3/\text{s)} = \sqrt{\frac{\text{TANK PRESS} - 2.53 \text{ PSI}}{26970}}$$

TAPED

233
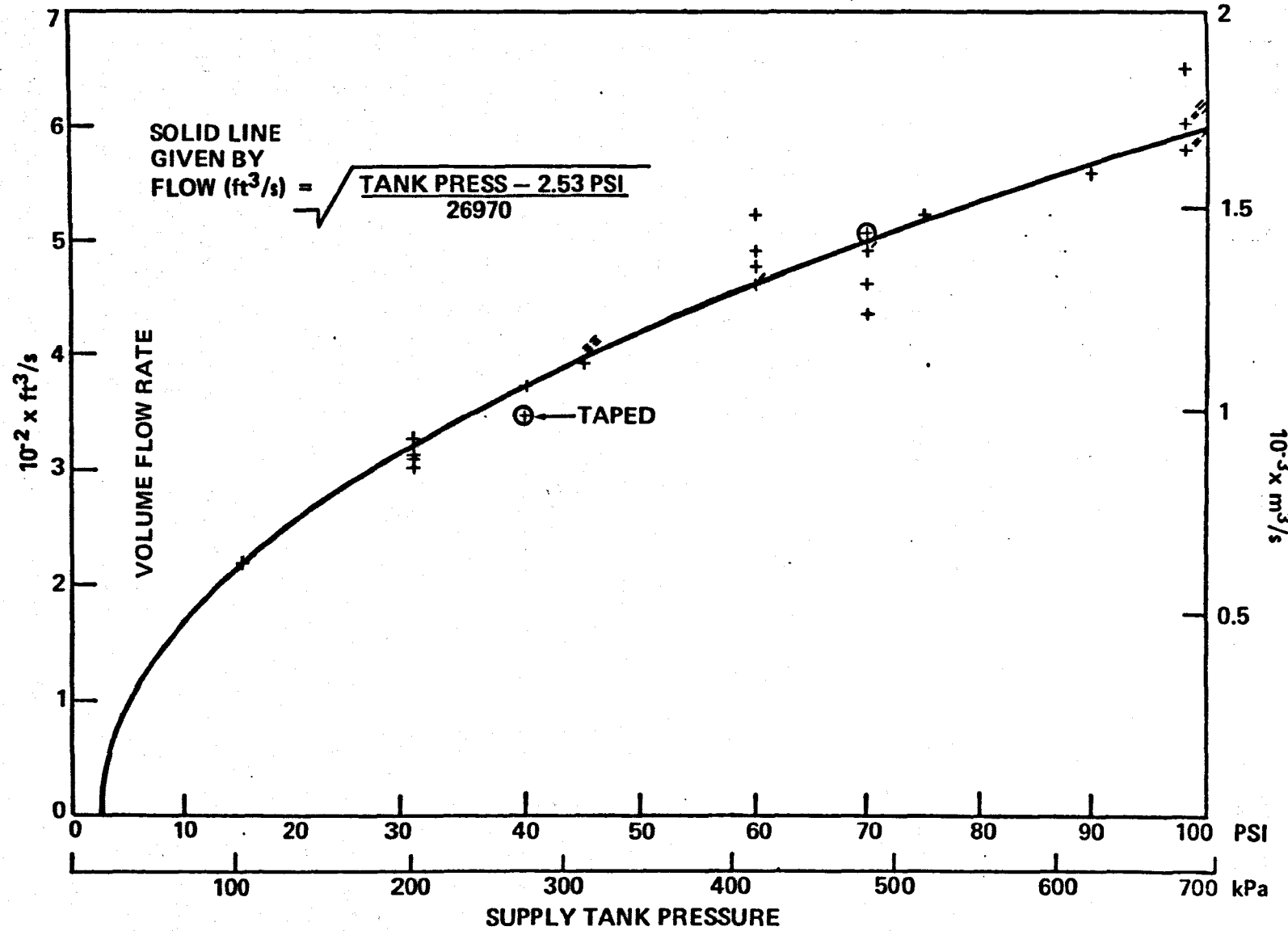
Figure 9.7 – Flow in Slots Versus Supply Pressure, Vertical Slot Model, All Configurations.

will be indicated by a superscript as follows:

Superscript	Immersion (mm)	Immersion (chord lengths)
0	302	2.4
(none)	270	2.1
*	245	1.9
**	220	1.7
***	195	1.5
****	170	1.3

The immersion depth denoted by ^{0} was a reference depth which was the deepest possible submergence. At that depth, the uncontoured span interfered with the ventilation properties of the Mk I and Mk II models, until the excessive "overhang" of unshaped metal above the leading edge was removed. After this, the ventilation behaviour was perfectly compatible with the other depths.

OUTLINE OF THE EXPERIMENT — PRELIMINARY TESTS

Preliminary Test Series. When the model as furnished by the manufacturer was first mounted in the Channel and pressurised with water, the flow from the slots was very uneven. Previously described attempts to improve the flow by rounding the inside corners of the slot or by baffling the internal flow in the plenum were only moderately successful. Cursory tests at 3 m/s with low pressure blowing and full immersion to 302mm revealed no significant differences between the blown model and the same model with the pressure off, but with water in the supply lines. If air was allowed in the supply lines with the pressure off, ventilation or partial ventilation was likely to be triggered at very low angles.

In view of the lack of promising initial results, a more extensive exploratory program was undertaken to determine whether there might be a way of concentrating the blowing to achieve more positive results, and to examine the physical details more carefully. It was decided to systematically vary the immersion and the number and length of blowing slots. The most expedient method of limiting or reducing the length and number of slots was to tape over the existing slots except for the desired open areas, creating configurations P1 through P8, as described under the section on the Mk I Model.

In order to provide a reference point for comparison of the behaviour of the taped models with and without blowing, the Mk I model was completely taped over then tested over a range of immersions at 3 m/s. This was designated Configuration P0.

In Configuration P1, only the aftermost slot was left open a short distance below the mean free surface, as shown in Figure 9.5 and the photograph of Figure 9.8. This configuration was tested with suction and neutral pressure, as well as up to 40 psig (275 kPa) of blowing pressure, again with no appreciable differences apparent.

234
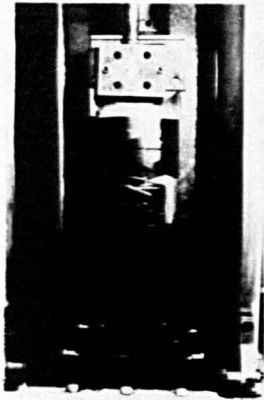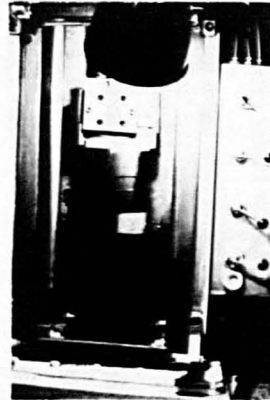
Configuration P1   Configuration P2   Configuration P3

Configuration P4   Configuration P5   Configuration P6   Configuration P7

Figure 9.8 — Photographs of Configurations of the Model Used in the
Preliminary Test Series.

In Configuration P2, shown in Figures 9.5 and 9.8, the two rearmost slots were allowed to remain open for a length of about 40mm starting at about 25mm below the mean free surface at the reference immersion of 302mm. Again, testing revealed no significant difference between blowing, non-blowing, and suction. Changing to a shallower immersion was found to have a very beneficial effect. Then, it was noticed that an overhang of uncontoured metal on the leading edge was interfering with the flow at the reference immersion. The model was removed and the offending metal filed down. Configuration P2 was then retested over a range of immersions, pressure and suction.

The tape was re-positioned to leave three slots open in a band near the mean free surface as shown in Figures 9.5 and 9.8. This was designated Configuration P3, and it was tested briefly with unpromising results.

The concept of allowing a band of slots to remain open near the mean free surface was modified by varying the depth of the open portion of the slots to more nearly conform to the free surface distortion at angles close to the ventilation point. This was the basis for Configuration P4, shown in Figures 9.5 and 9.8. This configuration was tested through a range of immersions, with varying pressures up to 80 psig (550 kPa), as well as with suction and no blowing. The results were somewhat more promising than had been achieved previously.

Configuration P5 allowed only the trailing edge slot to remain open from just below the mean free water surface to the submerged tip. A test series was conducted with blowing up to 100 psig (690 kPa), with varying immersions, suction and neutral pressure.

Encouraged by some success in improving the ventilation angle by blowing using the last two configurations described (P4 and P5) it was decided to perform a more rigorous test which would eliminate the possibility of extraneous effects due to the presence of the tape. The Mk I model slots were filled with beeswax, faired into the original contours except for a short section of the trailing edge slot near the free surface, as shown in Figures 9.5 and 9.8. This was similar to Configuration P1, even though the initial results with P1 were not especially promising. It had not had a fair trial because of the interference effect of the un-contoured overhang, and because of the low test pressures dictated by concern for the integrity of the model.

Although the beeswax interfered less with the natural flow around the model than did the tape, the technique still did not prove satisfactory. When the model was pressurised, the slots expanded and the beeswax would be lost.

While a better technique for selectively blocking slots on the Mk I 16-021 model was being developed, the Mk II 16-021 Model, described earlier, was mounted in the channel with its two nearly horizontal (10 and 20 degrees off level) slots blocked with wax, and with no blowing or suction. This was intended to provide a reference condition for a virtually unaltered 16-021

236

section. The ventilation angles were recorded over a complete range of immersions at 3 m/s, except for the 302mm immersion, which was avoided because of the earlier experience of spurious results. Following this, a complete oil smear flow visualisation series was done with the plain Mk II model, at the 265 and 215mm immersions, at sideslip angles from 0 to 24 degrees.

Meanwhile, it was found that the slots on the Mk I model could be filled with epoxy, faired, and later removed without undue damage to the model. Configuration P6 was reconstituted in this manner and retested over a range of immersions, but only to a blowing pressure of 15 psig (100 kPa), to protect the model. A flow visualisation sequence was photographed using 15 psig (100 kPa) blowing at 215mm immersion. Configuration P6 was then modified to form Configuration P7, shown in Figures 9.5 and 9.8, by opening the two forward slots just below the apparent free surface, similarly to Configuration P4. A flow visualisation study was performed with 15 psig (100 kPa) blowing, mostly at 240mm immersion. Vent angles were explored up to a pressure of 40 psig (275 kPa).

While leaving the two forward slots unchanged, the trailing edge slot was opened to approximately 40mm greater depth to form Configuration P8, which was briefly tested at 240mm immersion and 40 psig (275 kPa) blowing. This concluded the Preliminary Test Series (Series I).

RESULTS AND DISCUSSION OF THE PRELIMINARY TEST

Summary of Configurations Tested and Ventilation Angles Observed. Table 9.1 summarises the pressures tested and the ventilation angles observed for the various models and configurations. The pressures included both positive and negative values as well as zero, corresponding to blowing, suction, and neutral flow through the slots. In this series, the only channel speed used was 3 m/s. The results of testing Configuration P1 of the Mk I model were not included in the table because it was determined that the ventilation angles were influenced by the metal overhang above the shaped contour at 302mm depth of submergence, the only immersion at which this configuration had been tested.

Ventilation Boundaries. Figures 9.9, 9.10, and 9.11 are graphs of the ventilation angles versus submergence aspect ratio (ratio of depth of submergence to chord length) for the various configurations with blowing, suction and neutral pressure. Also included are the results of the Mk I fully taped configuration (all slots taped over) and the Mk II model with its slots fully blocked with beeswax. In Figures 9.6, 9.7, and 9.8, dotted lines indicate the best fit lines to these reference conditions. It is interesting to note that the dependence of ventilation angle on depth of immersion was linear for the smooth Mk II model, but for the more irregular, fully taped Mk I

MODEL	CONFIG	VEL (m/s)	PRESS (kPa)	PRESS (psi)	RUN NO	VENT ∝ (deg)
	P2	3	90	13	59	25 ½
					60	25
			276	40	26	26
					27	25 ½
	P2*		90	13	61	27
					62	26 ½
					63	26
	P2**+6mm		34	5	81	26 ¼
			69	10	82	26
					83	27
			103	15	84	28
					85	26
			138	20	86	26
			276	40	87	26
	P2**		34	5	79	26 ¼
					80	26 ¼
			90	13	64	28
			83	12	65	26 ¾
			276	40	45	28
	P2***+6mm		34	5	77	26
					78	26
			69	10	76	24
			138	20	75	26

BLOWING RUNS

MODEL	CONFIG	VEL (m/s)	PRESS (kPa)	PRESS (psi)	RUN NO	VENT ∝ (deg)
MKI	P4	3	69	10	98	27
					100	26 2/3
			138	20	99	26 2/3
			276	40	114	27 1/2
					115	28
			413	60	116	27 1/3
			552	80	117	27
	P4*		69	10	101	26 2/3
	P4**				102	28
					103	25
					104	25 2/3
					107	26 1/2
			413	80	118	28
	P4***		34	5	112	27
					113	26
			69	10	108	25 1/3
					109	26 1/2
			552	80	119	28

Table 9.1 – Summary of Preliminary Test Series Results

MODEL	CONFIG	VEL (m/s)	PRESS (kPa)	PRESS (psi)	RUN NO	VENT ∢ (deg)
MKI	P2	3	0	0	28	26
					31	26 ¼
					57	24 ½
	P2*				50	26
	P2**				47	26 ¾
					48	26
					49	25 ¾
	P2***				70	26 ½
	P3				90	25 ¾
	P3*				93	26
	P4*				96	28
	P4**				105	25
					106	28
	P4***				110	26 ½
					111	26
	P5				134	26
	P5*				122	24 ¾
					123	26 ½
					125	25
	P5**				138	25
					139	25

NEUTRAL PRESSURE RUNS

MODEL	CONFIG	VEL (m/s)	PRESS (kPa)	PRESS (psi)	RUN NO	VENT ∢ (deg)
MKI	P0	3	0	0	32	27
					36	26
					37	26
					38	26 1/3
	P0*				39	25 1/2
					40	23
					41	26 2/3
	P0**				43	27
					44	26 1/3
	P6				149	24
					150	24
	P6*				152	24
					154	24

Table 9.1 — Summary of Preliminary Test Series Results (cont'd)

MODEL	CONFIG	VEL (m/s)	PRESS (kPa)	PRESS (psi)	RUN NO	VENT ⊀ (deg)
MKI	P5	3	550	80	131	26
					132	26
					133	28
	P5*				127	29 ½
					128	NO VENT
	P5**		276	40	142	25
					143	26
			690	100	144	28
					145	27
					146	28
MKI	P6^{0-18mm}		34	5	224	24
					225	23
			69	10	226	24
					227	23 ¾
	P6*		69	10	228	24
					229	24
	P6**		103	15	230	24 ½
					231	24 ½
	P6***				232	25
MKI	P7*		103	15	239	24
			276	40	245	24 ½
	P7**		103	15	234	24 ½
					235	24 ½
			276	40	246	24

BLOWING AND NEUTRAL RUNS

MODEL	CONFIG	VEL (m/s)	PRESS (kPa)	PRESS (psi)	RUN NO	VENT ⊀ (deg)
MKII	0	3	0	0	156	23°
					157	23°
					158	23°
	0*				159	23°
					160	23 1/2
					161	23 3/4
					162	23 1/2
					163	23 3/4
	0**				164	24
					165	24
					166	24 1/4
	0***				167	25
					168	25
					169	25
	0****				170	25 3/4
					171	25 1/2
					172	25 1/2
MKI	P8*		276	40	250	24 1/2
					b	24 1/2
					c	24

Table 9.1 – Summary of Preliminary Test Series Results (cont'd)

240

SUCTION RUNS

MODEL	CONFIG	VEL (m/s)	PRESS (kPa)	PRESS (psi)	RUN NO	VENT ∝ (deg)
MKI	P2°	3	-98	-14	22	22
					25	25
	P2				55	24
					56	25
	P2*				51	26 ½
					52	26
					54	26
					55	24
					56	25
	P2**				46	26
					73	26
					74	26
	P2***				66	28
					69	26
					71	26
	P3				88	26
					89	25 ¾
	P3*				91	27
					92	25 ¾
	P4				97	27
	P4*				94	26 ½
					95	27 ¾

MODEL	CONFIG	VEL (m/s)	PRESS (kPa)	PRESS (psi)	RUN NO	VENT ∝ (deg)
MKI	P5	3	-98	-14	129	28
					130	26 2/3
					135	25
	P5*				120	28 1/3
					121	28
					124	28 1/2
					126	25
	P5**				136	27 1/2
					137	26
					140	25 1/2
	P6$^{0.18mm}$				222	24 1/2
	P6				147	24
					148	24
					223	24
	P6*				151	24 1/2
					153	24 3/4
					219	24 1/2
					220	24 1/2

Table 9.1 — Summary of Preliminary Test Series Results (cont'd)

241

KEY

○	5 psi
■	10 psi
□	13
△	15
▲	20
◇	40
▽	60
◆	80-100

242
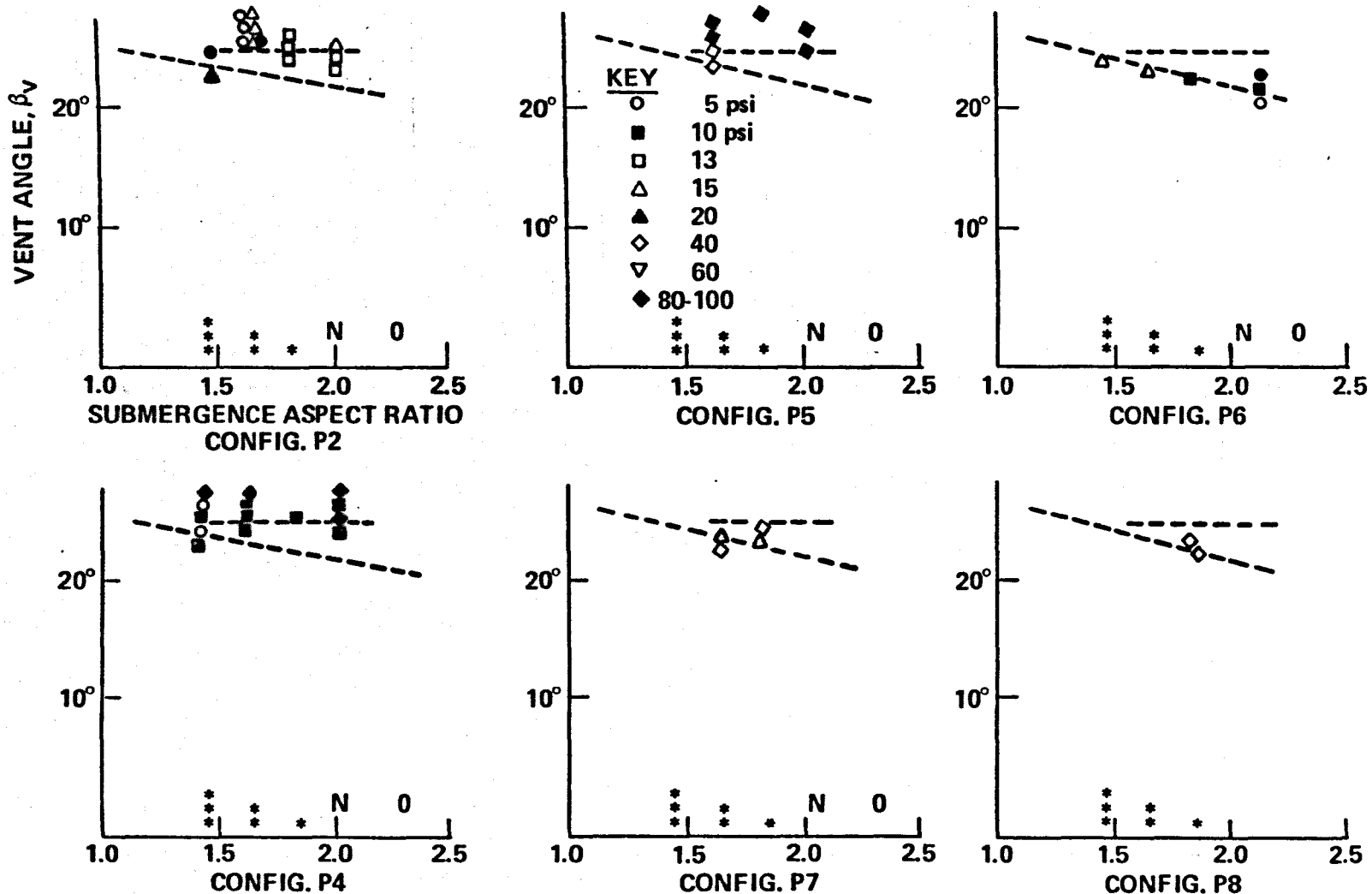
(NOTE – CONFIGS. 6, 7 AND 8 HAVE UNUSED SLOTS FILLED WITH WAX INSTEAD OF TAPE.)

Figure 9.9 – Ventilation Angles Versus Submergence Aspect Ratio For Preliminary Tests With Blowing From Vertical Slots, Mk I NACA 16 021 Model, 10 ft/s (3m/s).
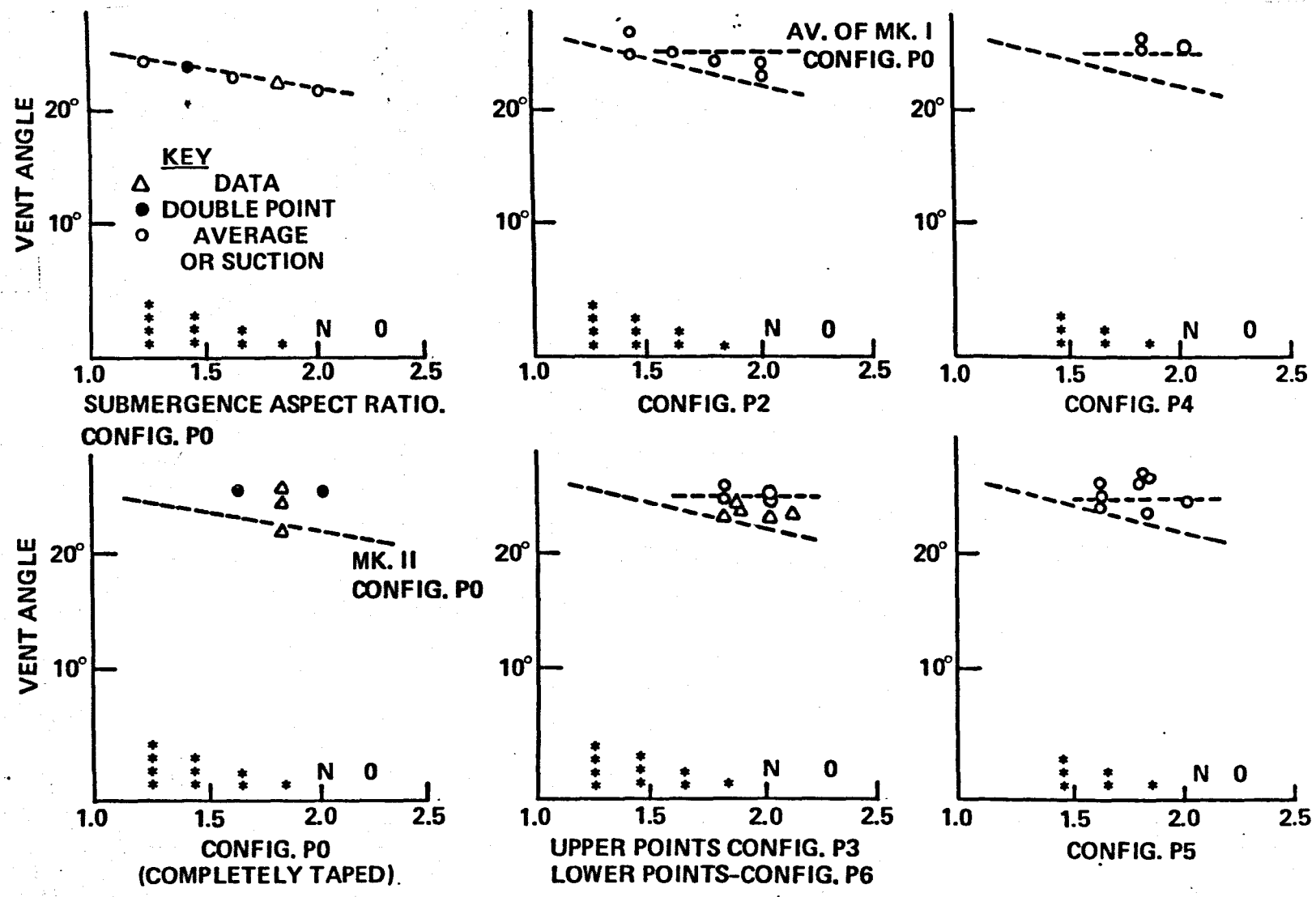
Figure 9.10 — Ventilation Angles Versus Submergence Aspect Ratio For Preliminary Tests With Suction From Vertical Slots, NACA 16 021 Model, 10 ft/s (3m/s).

243
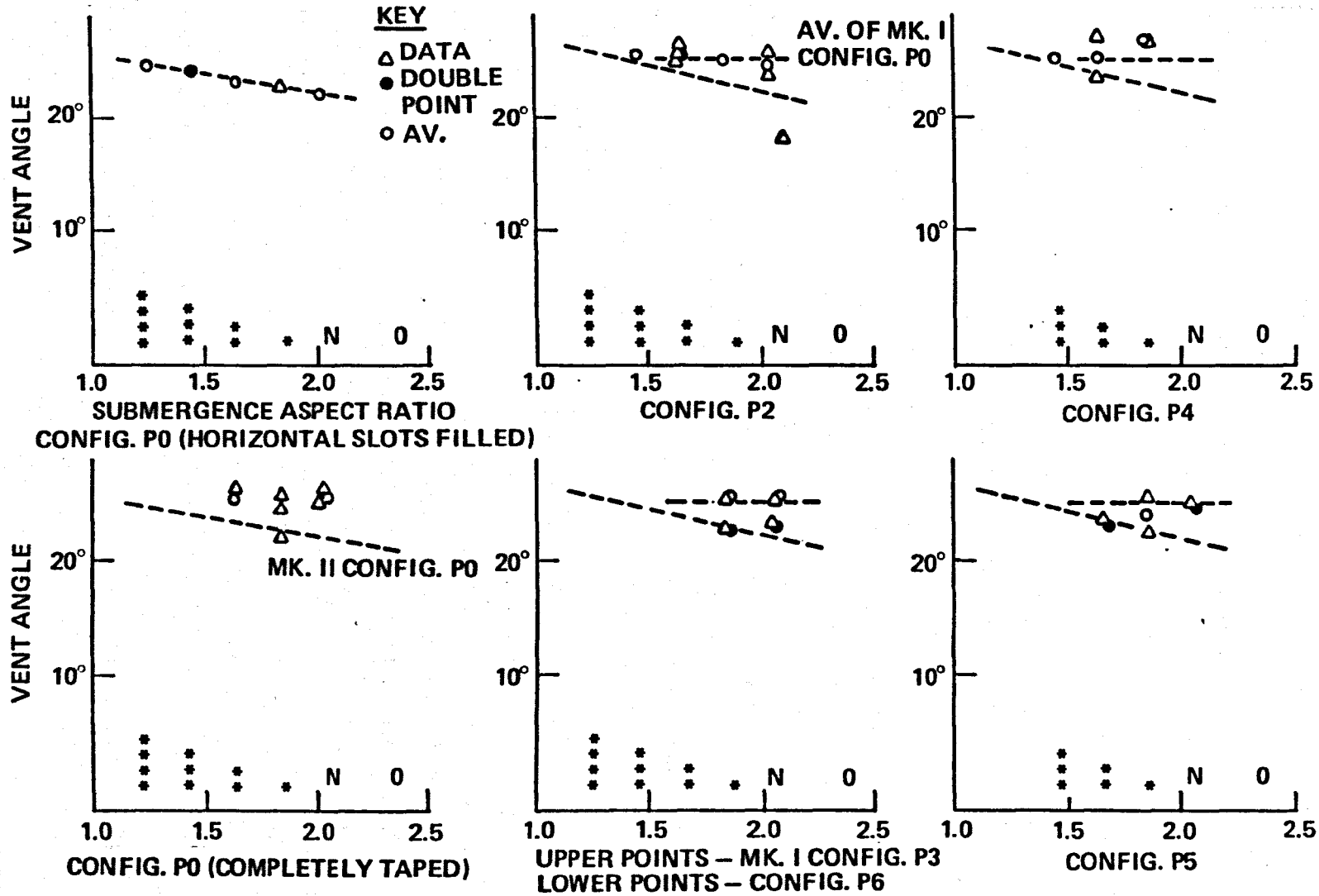
Figure 9.11 — Ventilation Angles Versus Submergence Aspect Ratio For Preliminary Tests, Neutral Pressure In Vertical Slot NACA 16 021 Model, 10 ft/s (3m/s).

244

model, the dependence on immersion was completely masked by other effects. Surprisingly, the ventilation angles were not lower for the taped Mk I model, as might have been anticipated if the effect of tape were simply similar to increased roughness as studied in Chapter 5. Greater scatter was introduced, which was consistent with the earlier roughness studies. Evidently, the tape roughness had a special character which cannot be explained in terms of equivalent spherical roughness.

In Figure 9.9, it is shown that the effect of the slots with no blowing, but purged of air, was approximately neutral. This was in contrast to the leading edge slot experiment of the preceding chapter, where without active suction, the spanwise pressure gradient (along the slot) was great enough to generate flow in and out of the slot with net beneficial effect in retarding ventilation onset.

Figure 9.10 shows that the effect of suction on the Configuration P6 ventilation boundaries was mildly helpful. There was also some small benefit of suction in Configuration P5, although this was only on average. No effect of suction can be seen for Configurations P2, P3, or P4. For Configuration P2, the use of suction seemed to re-introduce a dependence on immersion depth that had been elminated by the tape, but this trend is so tentative that it was not explored further. A possible explanation is that the suction overcame some of the tendencies introduced by the tape roughness, such as premature growth of the boundary layer.

In Figure 9.11, it can be seen that the effect of blowing was not very pronounced, but some significant and promising trends are evident. For the most successful taped configurations tested, P4 and P5, the ventilation boundaries improved with increased reservoir pressure. Thus, the blowing seemed to be having the desired influence, but may not have been strong enough to have had a pronounced effect.

Therefore, it was somewhat surprising when the beneficial effects were lost after attempting to duplicate what were thought to be the salient features of the more successful taped configurations by creating a smoother version using beeswax or epoxy to fill the unused slots. Configurations P6, P7 and P8 were essentially attempts to refine taped Configurations P4 and P5, which had demonstrated several degrees of improvement in delaying ventilation over the smooth Mk II model and the taped Mk I Configuration P0. However, the smoother configurations with blowing demonstrated little or no improvement over the smooth, unaltered Mk II, and were generally worse than the taped configuration. However, it was not possible to use as high blowing pressures with the beeswax – or epoxy-filled configurations as with the taped configurations, because the filled slots were more easily blown apart. This may have been crucial because the results with the taped models suggested that the lower blowing pressures were only marginally effective. The other aspect of the preliminary test series which may have affected the results was the poor quality of the flow

through the slots, even on the smoother versions. The non-uniformity of the slot flow led to air entrainment, hence a possible disruption of the surface seal, especially in places where the slot flow tended to break away from the model surface.

Flow Visualisation Results : Plain Mk II NACA 16-021 Model. The results of applying the oil smear flow visualisation technique to the plain Mk II NACA 16-021 strut are shown in Figures 9.12 and 9.13, for immersion depths of 270 and 215mm, respectively, for various sideslip angles up to ventilation, at a speed of 3 m/s. Figure 9.13 also includes one case of 190mm immersion for a sideslip angle of 24 degrees. This was tested unintentionally, in lieu of the maximum angle before ventilation at the 215mm immersion. It has been included for completeness of the Figure.

Some of the photographs on which the analysis was based are shown in Figures 9.14 and 9.15. Even at sideslip angles at or near zero, some tail separation was apparent at both immersions, 10 to 20mm ahead of the trailing edge. At zero degrees, transition to turbulent flow took place about 30mm aft of the leading edge. At low angles, below 10 degrees, the region of transition moved forward and became more distinct. This shear must have been quite low, but there was no evidence of the herringbone pattern of reverse flow that would have characterised full laminar separation and reattachment as it was observed in the case of the finer-nosed blunt biogive described in the preceding chapter. The region of tail separation which was noted at very low angles disappeared at the intermediate angles. Above 10 degrees, the tail separation reappeared and grew regularly with increasing angle.

At higher angles, the region of laminar flow and transition was confined strictly to the leading edge. Again, the similarity of the oil smear pattern to that induced by nose separation can be noted, but evidence of a reattachment line is lacking. In every case, this characteristic accumulation of a fine line of oil near the leading edge persisted to the maximum angles tested and was interpreted to be transition to turbulent flow. This interpretation provides an explanation for the appearance at low angles, and subsequent disappearance at intermediate angles, of tail separation. As the transition to turbulent flow moved forward, the boundary layer was more energised in spite of the greater adverse pressure gradient due to the higher sideslip angle, and was therefore less prone to trailing edge turbulent separation. Finally, above 10 degrees of sideslip angle, the adverse pressure gradient was so severe that tail separation was again manifest in spite of the fully turbulent flow.

At the highest angles before ventilation, those above 20 degrees, the region of tail separation began to shrink downward from the surface. This was because the depression of the surface caused by the increasingly low pressure associated with increasing sideslip angle brought with it the unseparated flow from the free surface. Interestingly, at 24 degrees of sideslip angle, the
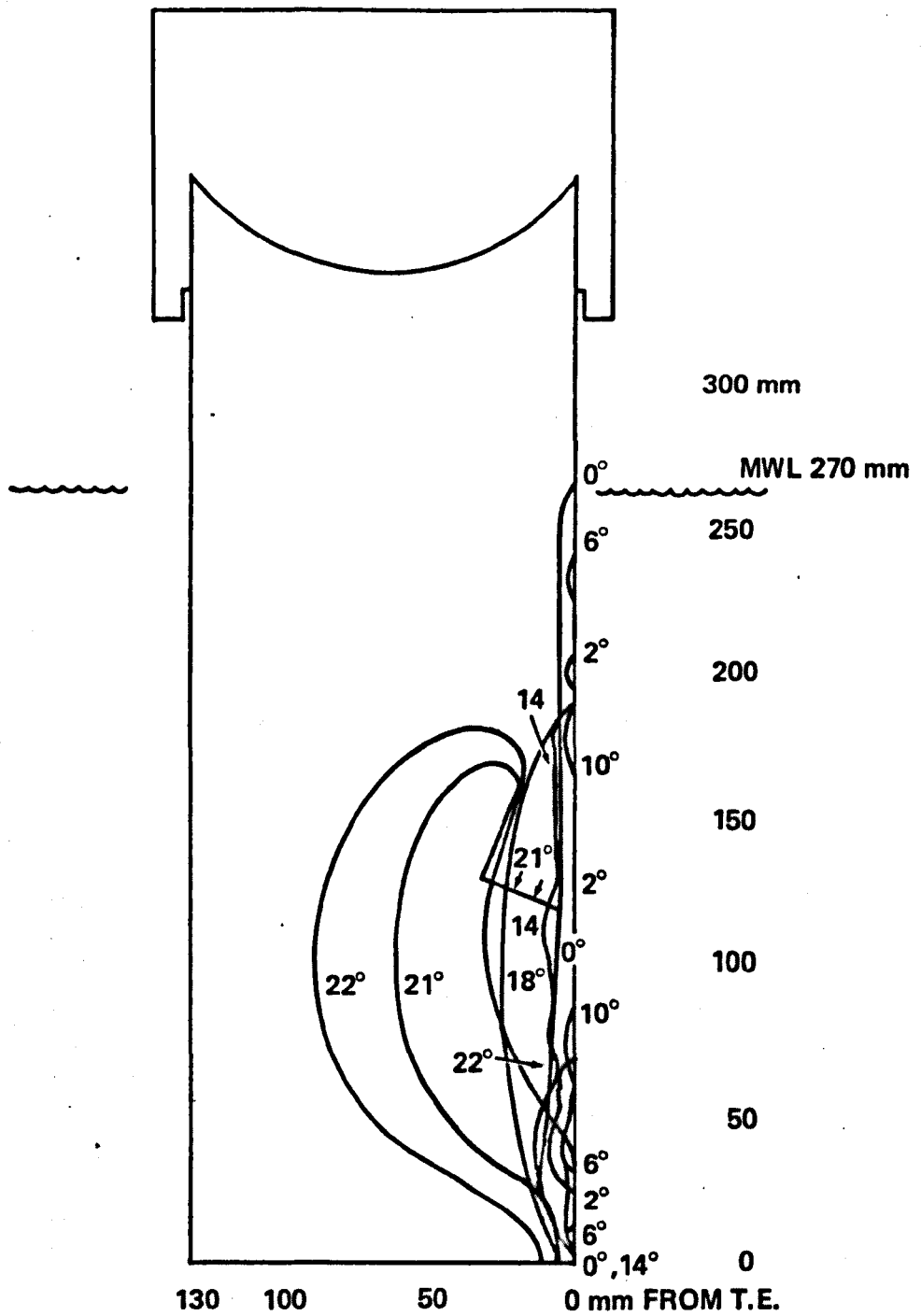
Figure 9.12 — Development of Separation on NACA 16 021 Strut, 10 ft/s (3m/s), 270mm Immersion.
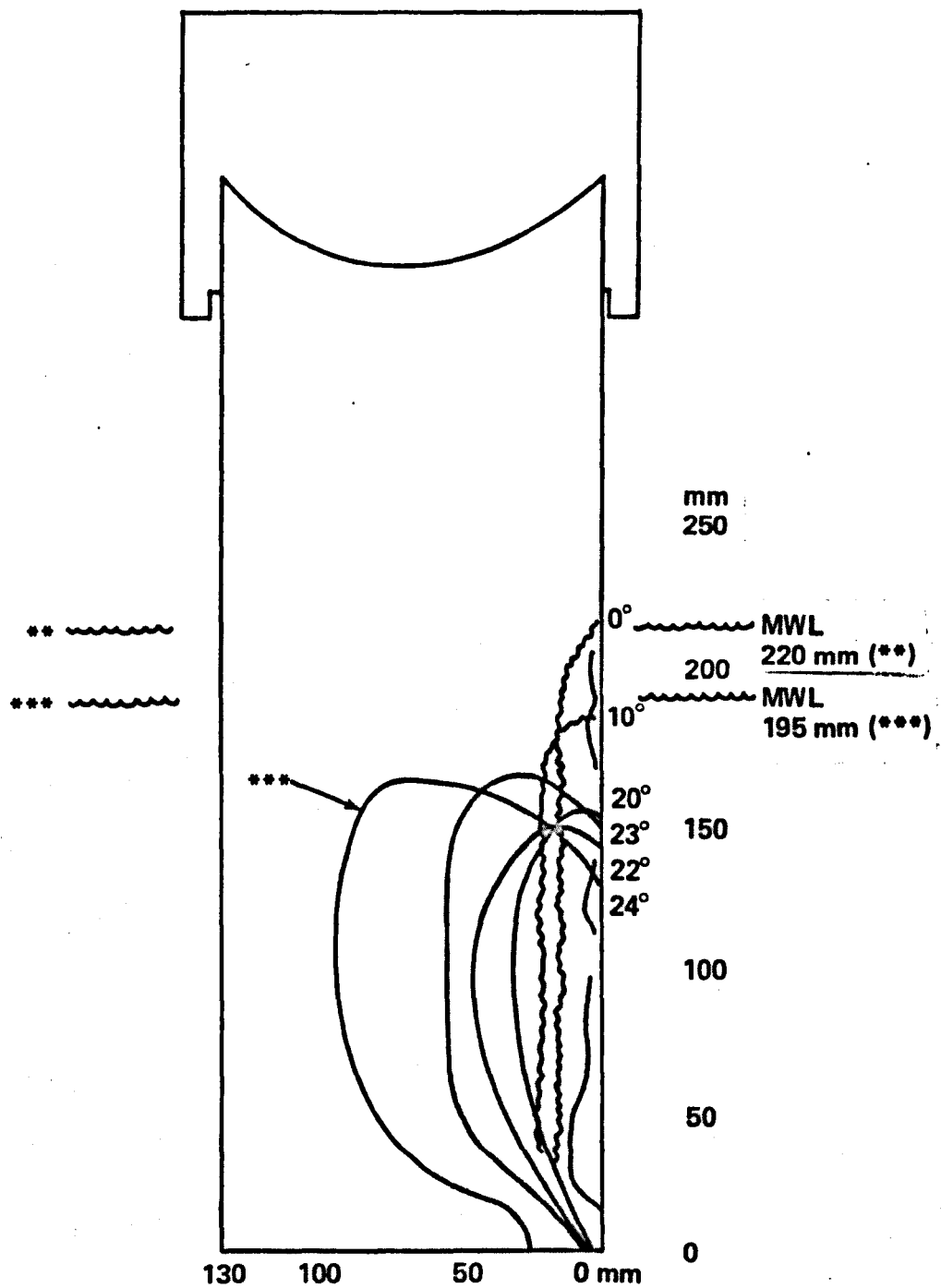
Figure 9.13 — Development of Separation on NACA 16 021 Strut, 10 ft/s (3m/s), 220mm Immersion.
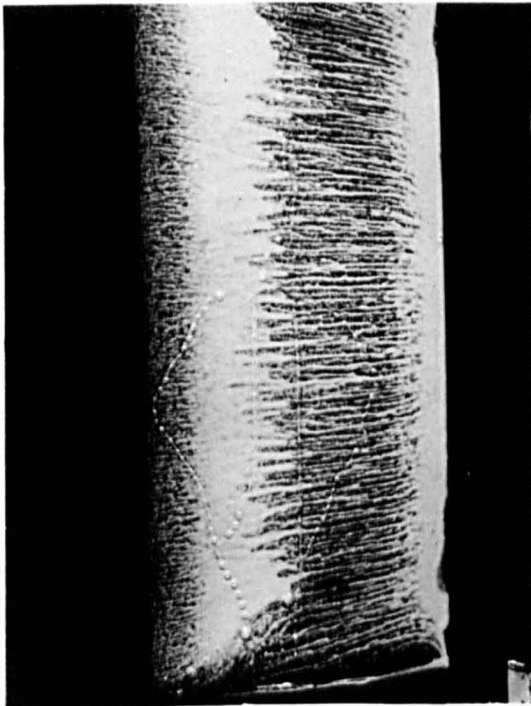
$\beta = 6$ Degrees
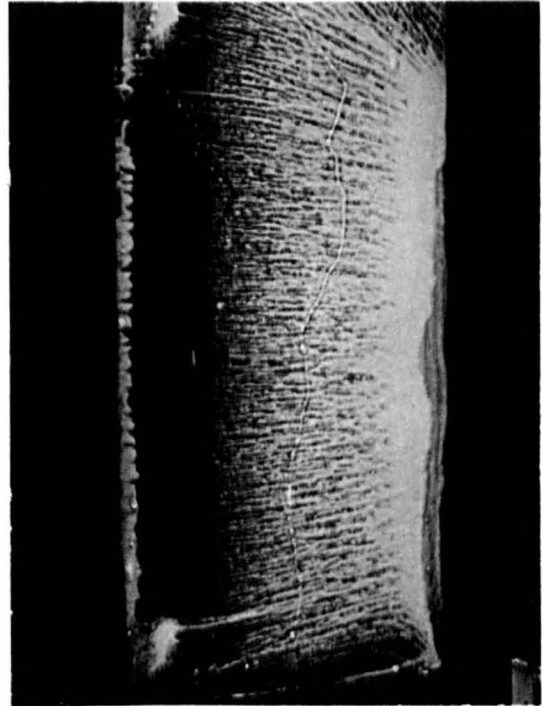
$\beta = 14$ Degrees
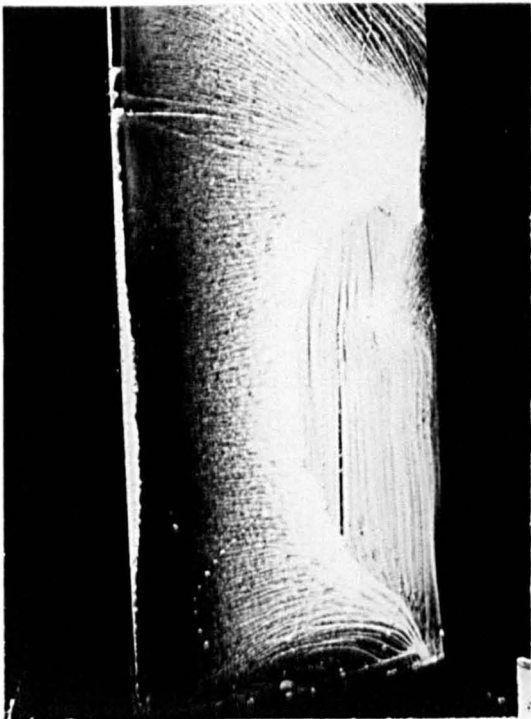
$\beta = 21$ Degrees
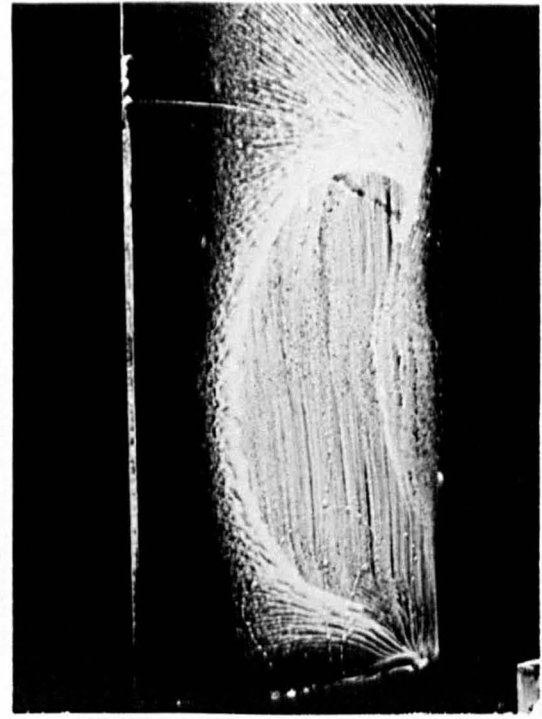
$\beta = 22$ Degrees

Figure 9.14 – Development of Separation on NACA 16 021 Strut,
10 ft/s (3m/s), 270mm Immersion.
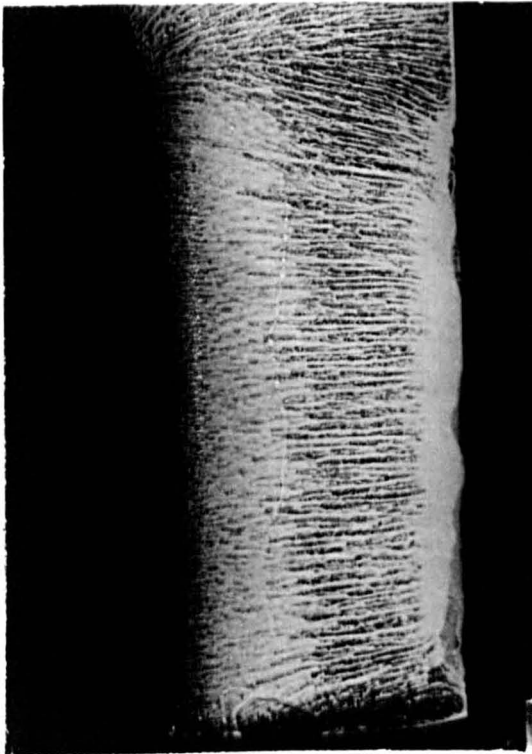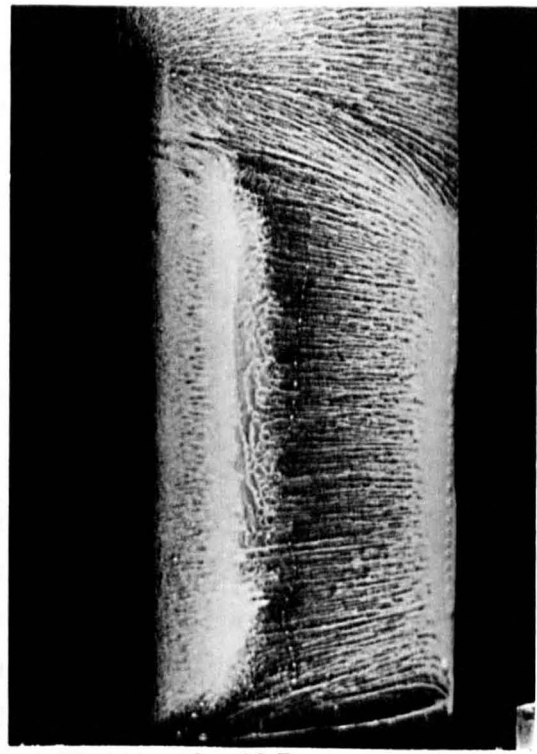
β = 0 Degrees

β = 10 Degrees
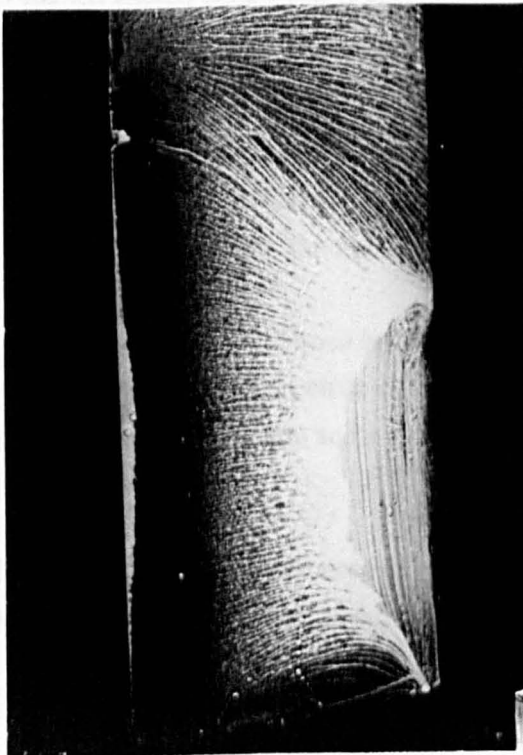
β = 22 Degrees
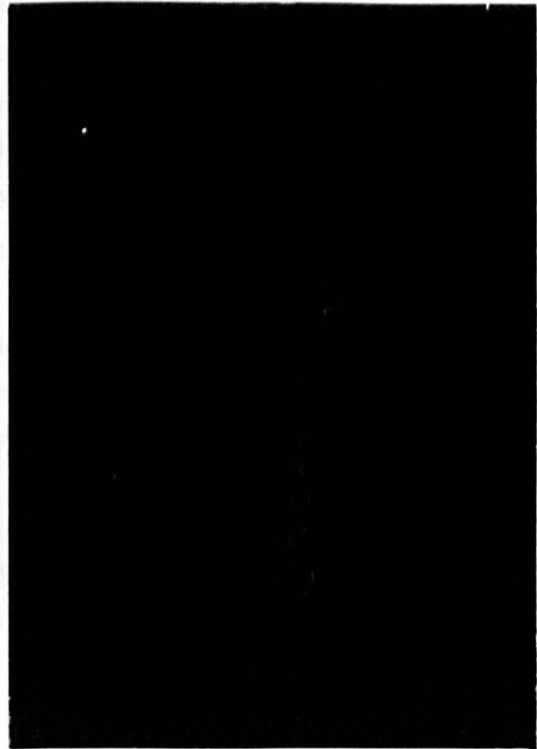
β = 23 Degrees

Figure 9.15 – Development of Separation on NACA 16 021 Strut, 10 ft/s (3m/s)
220 mm Immersion.

250

unseparated flow became nearly vertically downward, obliterating some of the low shear regions in the flow pattern by scouring away the oil. This illustrated the difficulty, mentioned in Chapter 6, of defining the onset of separation in three-dimensional flow, where the flow may fold in and around itself, with no region of low shear, and no line which could be defined as separation or reattachment.

Because this convoluted flow pattern appeared just before the onset of ventilation, it is easy to imagine that it was instrumental in carrying air to the obviously separated region well below the free surface. However, it must be remembered in interpreting oil smear patterns that the striations may not be strictly parallel to the direction of the major external flow, but only to the direction of shear exactly at the boundary. The oil smear pattern also represents a time average mean, weighted in an indeterminate manner. For example, there is no evidence in the oil smear pattern of the existence or effect of Taylor instabilities, even though they can be clearly observed in motion pictures and under stroboscopic light.

Flow Visualisation Results: Configurations P6 and P7 with Blowing. Figures 9.16, 9.17 and 9.18 are the results of analysis of the flow patterns recorded in the oil films on Configurations P6 and P7 with 15 psig (100 kPa) blowing in both cases and 40 psig (275 kPa) blowing for Configuration P7. Figures 9.19, 9.20 and 9.21 are selected photographs of the oil smear patterns of Configurations P6 and P7 under the conditions just stated. Virtually all of the remarks made concerning the behaviour of the transition region and tail separation of the plain Mk II model apply also to the smooth model blowing configurations. The scouring at the submerged tip due to the tip vortex developed regularly with sideslip angle up to 22 degrees. At 23½ degrees, the maximum angle which could be studied reliably before ventilation, the influence of the tip vortex seemed to have diminished. This is shown in Figure 9.19 for Configuration P6 at 15 psig (100 kPa) blowing pressure. Concurrently, the growth of tail separation exhibited a "burst" between 22 and 23½ degrees. At the tail it can be noted that the attached flow region actually extended deeper below the mean water line with increased sideslip angle due to the depression of the free surface.

The principal difference between the plain and the blown strut oil smear patterns was the evidence from the blown strut of irregular flow emanating from the slots. Although the oil pattern aft of the slots was highly scoured, the striations converged and diverged, indicating confused and crossed flow.

Resolution of Inconclusiveness of Preliminary Results. The weakness of the evidence of positive benefit of boundary layer blowing in retarding the inception of ventilation did not allow
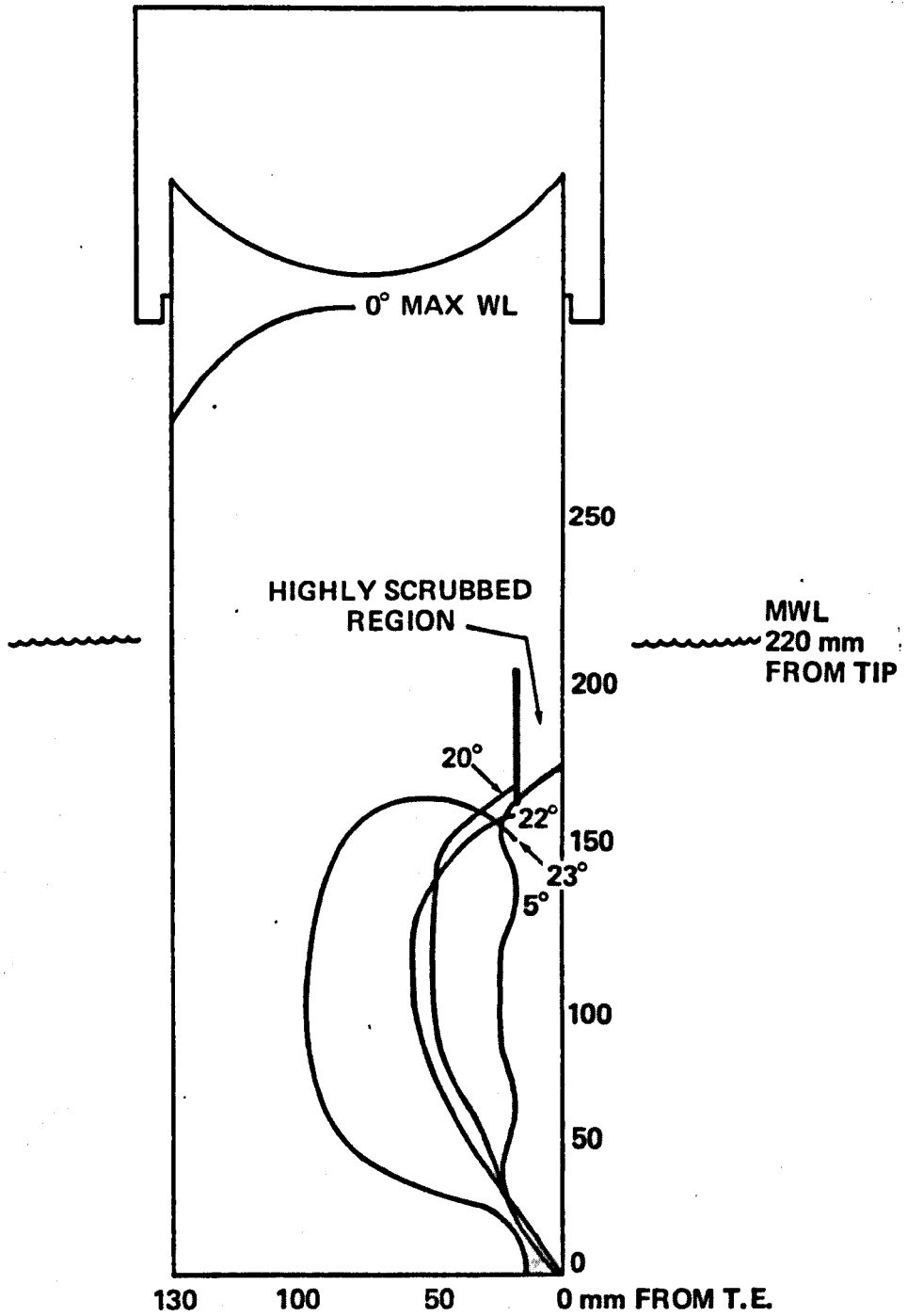
Figure 9.16 — Development of Separation on NACA 16 021 Strut, Configuration P6**,
10 ft/s (3m/s), 15 psi (100 kPa) Blowing.

252
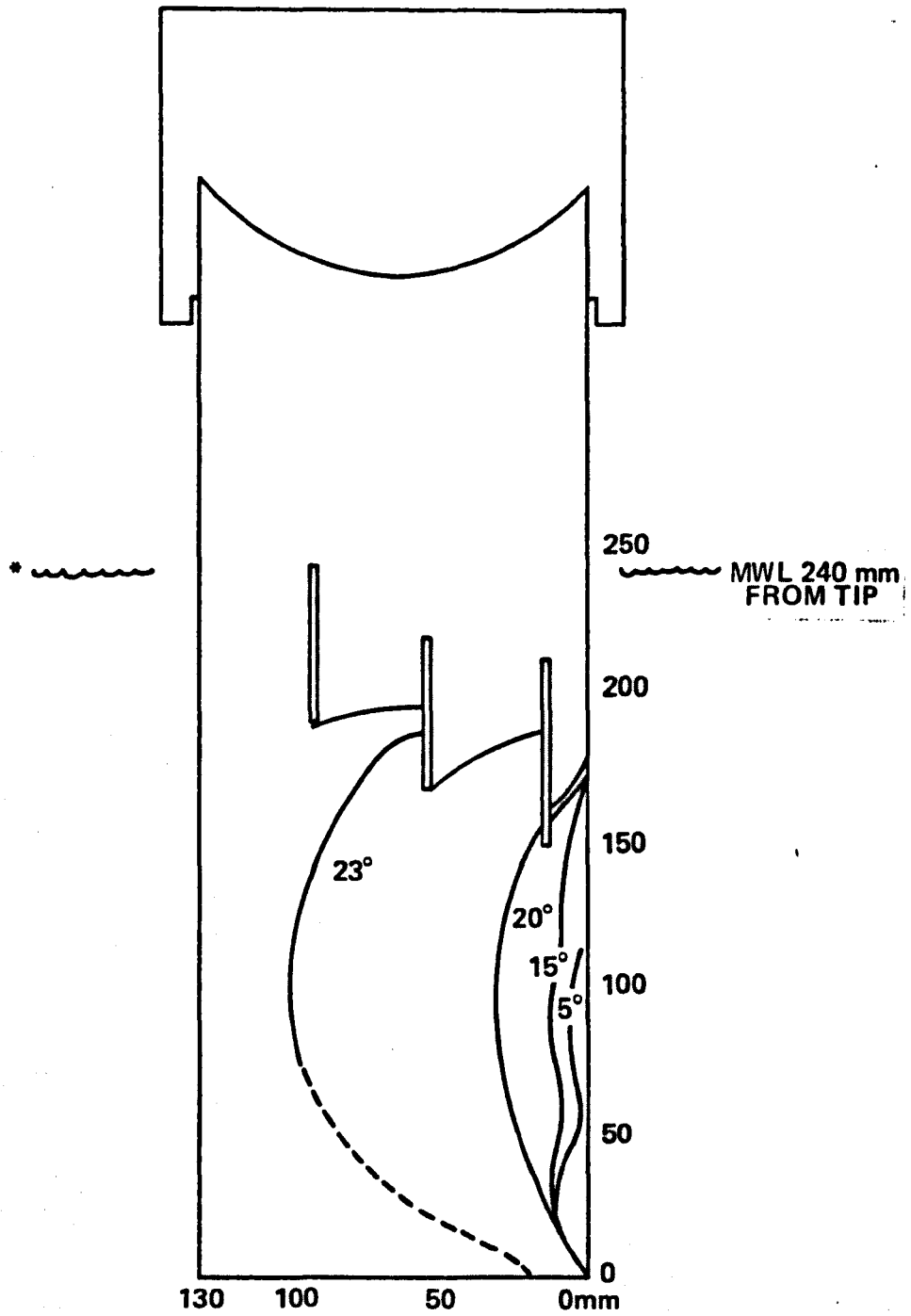
Figure 9.17 — Development of Separation on NACA 16 021 Strut, Configuration P7*, 10 ft/s (3m/s), 15 psi (100 kPa) Blowing.
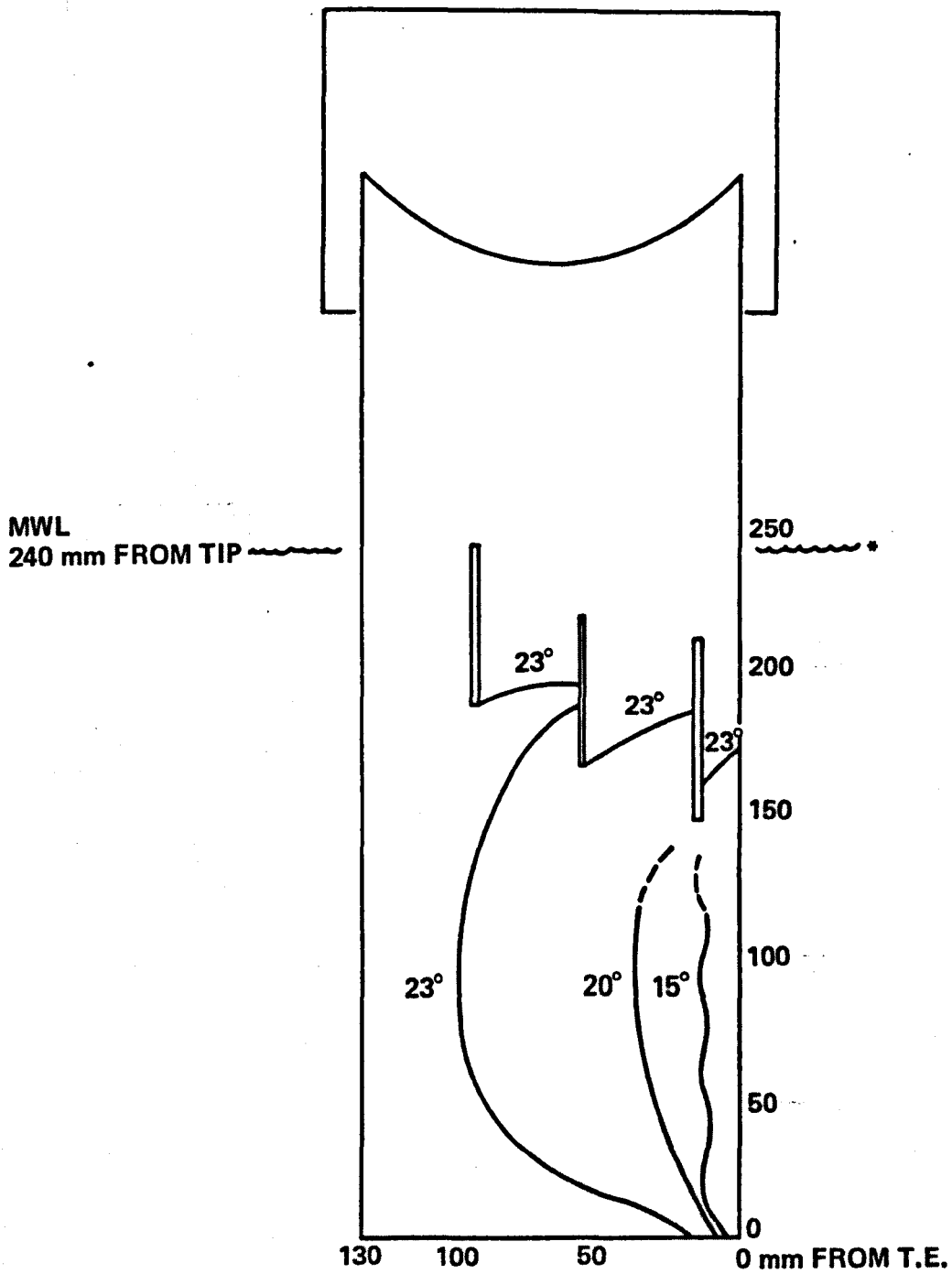
Figure 9.18 — Development of Separation on NACA 16 021 Strut, Configuration P7*, 10 ft/s (3m/s), 40 psi (275 kPa) Blowing.
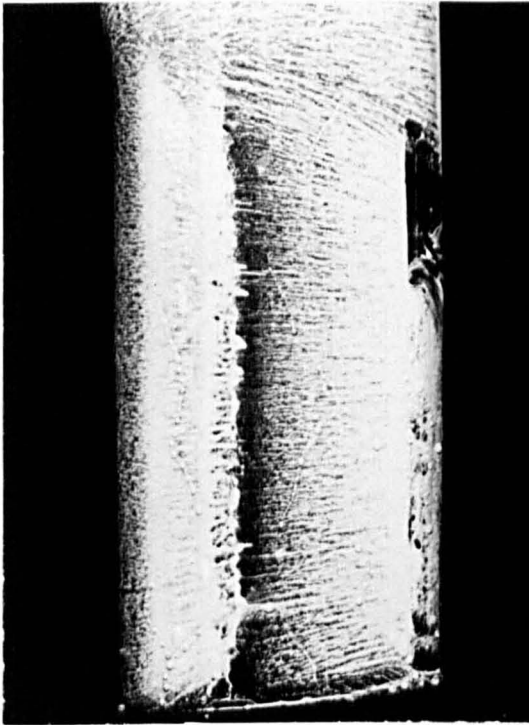
$\beta = 10$ Degrees
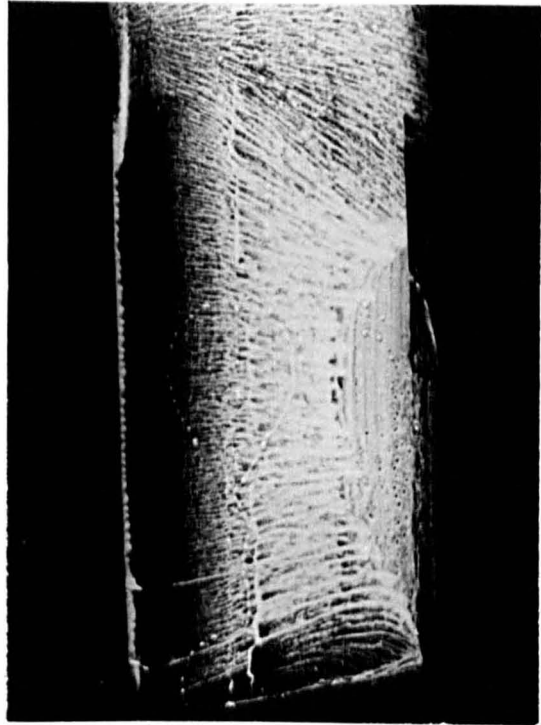
$\beta = 20$ Degrees
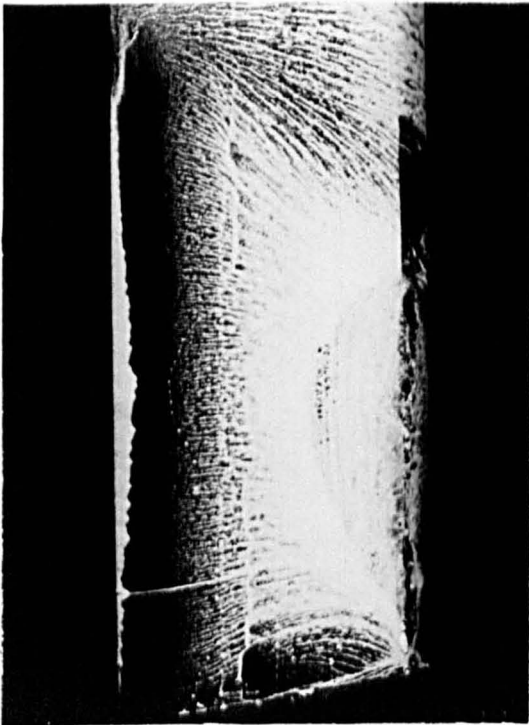
$\beta = 22$ Degrees

$\beta = 23\frac{1}{2}$ Degrees

Figure 9.19 – Development of Separation on NACA 16 021 Strut,
Configuration P6**, 10 ft/s (3m/s), 15 psi (100 kPa)
Blowing.

$\beta = $ 5 Degrees
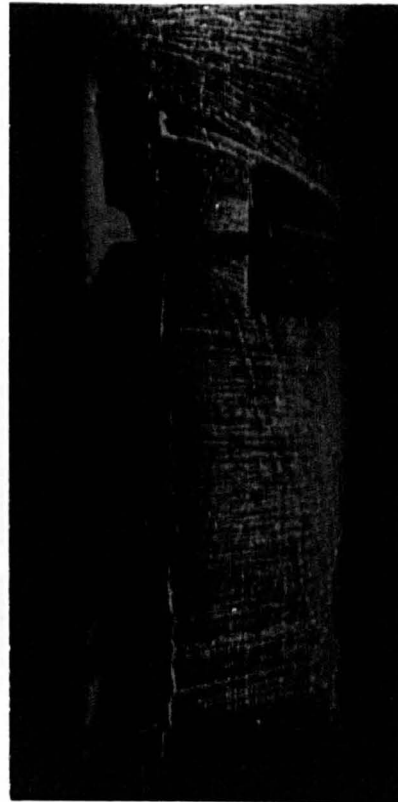
$\beta = $ 15 Degrees
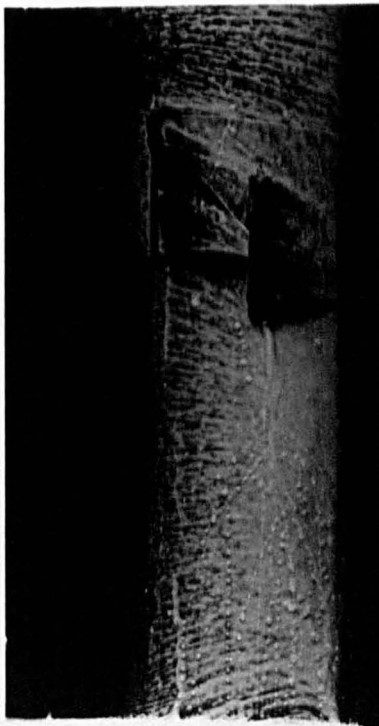
$\beta =.$20 Degrees
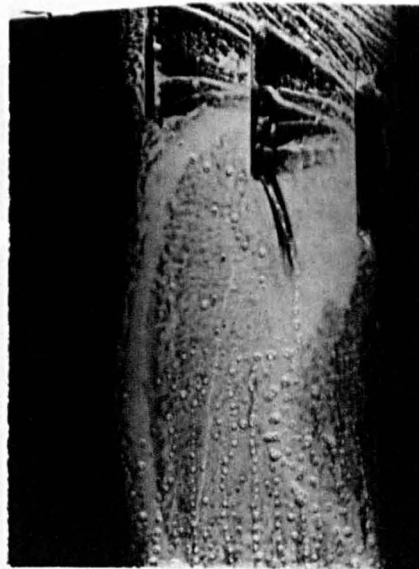
$\beta = $ 23 Degrees

Figure 9.20 – Development of Separation on NACA 16 021 Strut, Configuration
P7*, 10 ft/s (3m/s), 15 psi (100 kPa) Blowing.
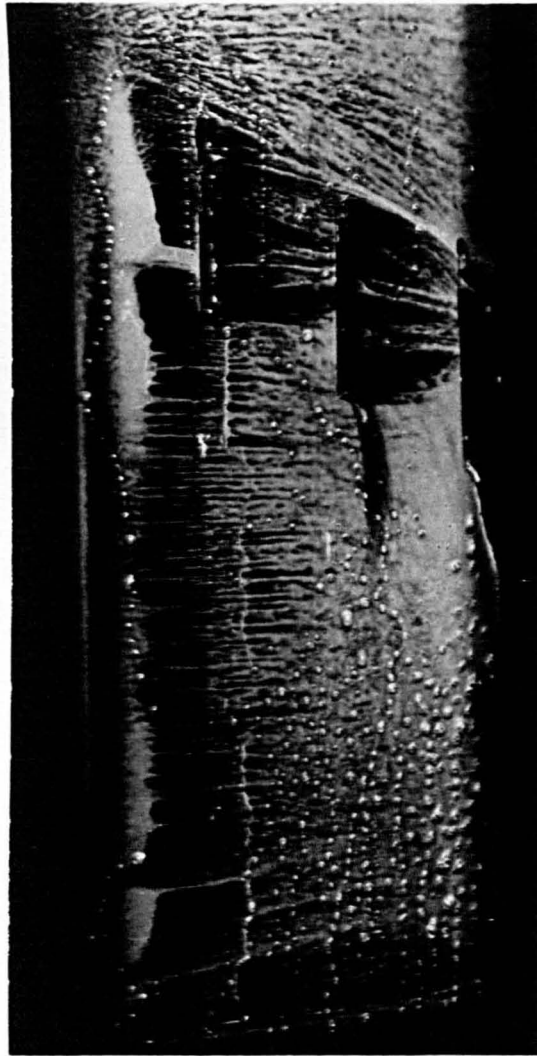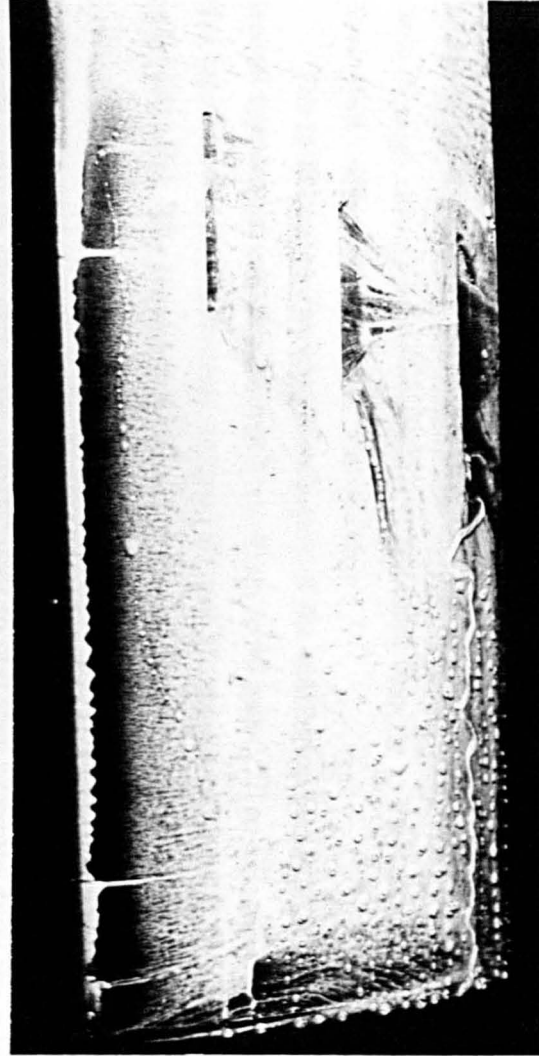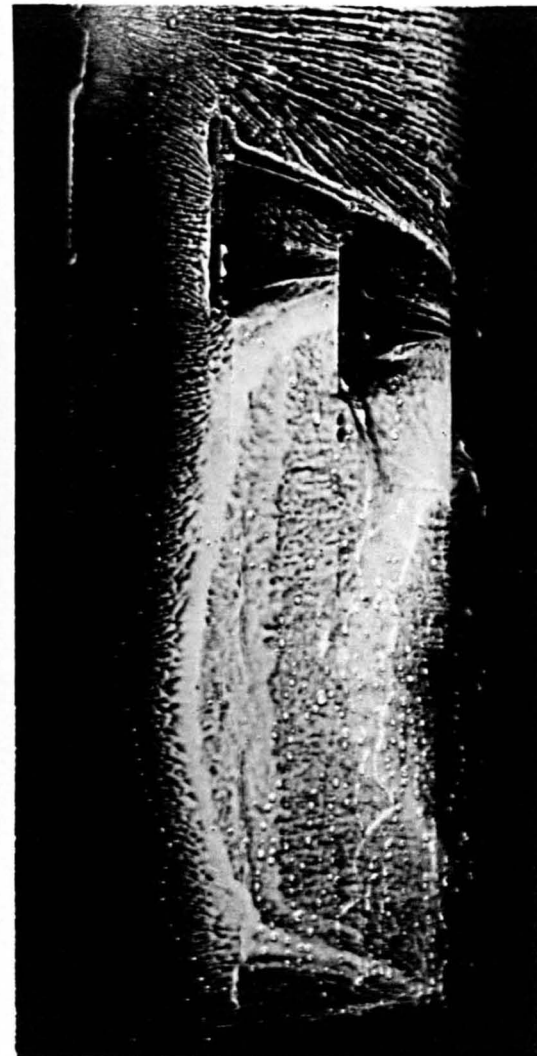
$\beta = 15$ Degrees　　　　$\beta = 20$ Degrees　　　　$\beta = 23$ Degrees

Figure 9.21 – Development of Separation on NACA 16 021 Strut,
Configuration P7**, 10 ft/s (3m/s), 40 psi (270 kPa)
Blowing.

a definite conclusion to be drawn from the preliminary experiment. It was necessary to correct the irregular flow from the slots, and strengthen the model to withstand higher pressures and greater flow rates before a rational judgment could be made.

OUTLINE OF THE EXPERIMENT · FINAL TESTS

Modifications to the Model for Smoother, More Uniform, and Faster Slot Flow. It was thought that the reason for the inconclusive results of the preliminary tests with blowing might have been due to the non-uniformity of the flow from the slots and the low jet velocity which was necessitated by the fragility of the model – its inability to withstand high internal blowing pressures without deforming or breaking up. Thus, a further series of tests were carried out with modifications to overcome this deficiency.

Mk I Model -- Long, Narrow Slots. For the final test series, the Mk I model was strengthened, smoothed, and the slots narrowed as described in the preceding section on experimental apparatus. Initial tests were made with smooth, 0.5mm wide slots each extending about 298mm (2.3c) from the submerged tip. Observations of the flow through the slots with the model out of the water showed that the internal flow baffle was no longer required to maintain the slot flow through the upper part of the slot at the same velocity as that being emitted from the lower part. After this, the baffle was omitted.

The initial survey included observation of the ventilation characteristics of the model at several immersions and at pressures from 40 up to 90 psig (270 to 620 kPa). Then the model was taped in two configurations, denoted T1 and T2, shown in Figure 9.22, and tested at 70 psig (480 kPa). The second taped configuration was also tested at 90 psig (620 kPa).

Mk I Model — Shortened Slots. Based on observations of the flow around the earlier versions of the Mk I model, the slots were reconstituted so that they extended from the submerged tip and terminated at the apparent water surface as viewed from below, with the immersion at about 170mm. Besides this, the short slot configuration was also tested at 195mm immersion, with the tops of the slots approximately 25mm submerged. Blowing pressures of 60 and 98 psig (410 and 675 kPa) were tested, as well as suction. Photographs were taken of the strut while submerged and, nearly immediately thereafter, of the oil smear pattern which resulted.
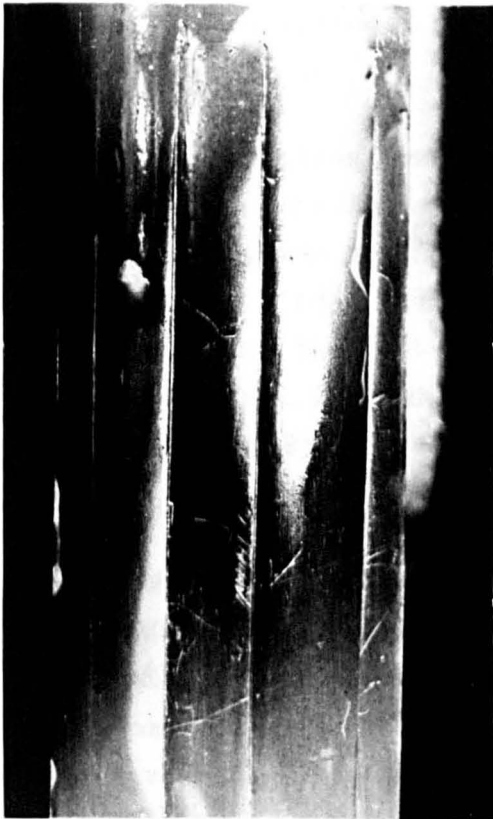
Plain

T1

T2

Figure 9.22 – NACA 16 021 Mk I Model With Long, Narrow Slots, Taped in
Configurations T1 and T2.

259

Mk I Model—Thickened and Shortened Slots. A version of the shortened slot Mk I model was tested with the slots widened from about 0.5mm to 1.5mm, at 245 and 195mm immersion. with 98 psig (675 kPa) blowing and with suction. Only a single photograph of the oil smear pattern was taken, to verify that the thickened slots still prevented separation in spite of the reduced momentum which was evident from observations of the jet flux with the model out of the water.

Mk II Model—No Slots, with Roughness. In order to provide a point of comparison for tests of the Mk I NACA 16-021 strut with roughness and blowing, the Mk II model, with its slots blocked and smoothed, was coated with glass microsphere roughness and tested at immersions of 270, 245, 220 and 195mm, at 3, 4.5 and 6 m/s. Only the ventilation boundaries were noted. No flow visualisation was attempted, because it was doubted that the oil smear technique would be effective over the roughness. During the subsequent tests of the blown model with roughness, it was found that the oil smear patterns still revealed the major flow features in spite of losing some details.

Mk I Model—Thickened and Shortened Slots, with Roughness. Following the previously described tests, the Mk I model was uniformly roughened with glass microspheres and tested for ventilation characteristics at immersion depths of 245, 195 and 170mm with 98 psig (675 kPa) blowing. Spot tests were also conducted at channel speeds of 15 and 20 m/s, in addition to the usual speed of 10 m/s. A flow visualisation sequence was photographed at the 170mm immersion, also with 98 psig (675 kPa) blowing.

RESULTS AND DISCUSSION OF THE FINAL TESTS

Mk I Model—Long, Narrow Slots. The ventilation angles versus blowing pressure for the Mk I model with full length, 0.5mm slots, are shown in Figure 9.23. Included in the Figure are the results of taping the model to form Configurations T1 and T2. The results with and without an internal baffle are also shown. The open symbols on the ordinate represent the ventilation inception angles for the plain Mk II model. The symbol to the left of the ordinate represents a suction run. Not shown is the result of a run made at 90 psig (620 kPa) and 7 ft/s (2 m/s), the lowest speed for which ventilation would occur to the full depth of the strut, immersed to 220mm (1.7c). In two trials, the ventilation inception angles were identical to those found for the 10 ft/s (3 m/s) case — 25 and 26 degrees. This showed that increasing the ratio of jet velocity to free-stream velocity had no effect.
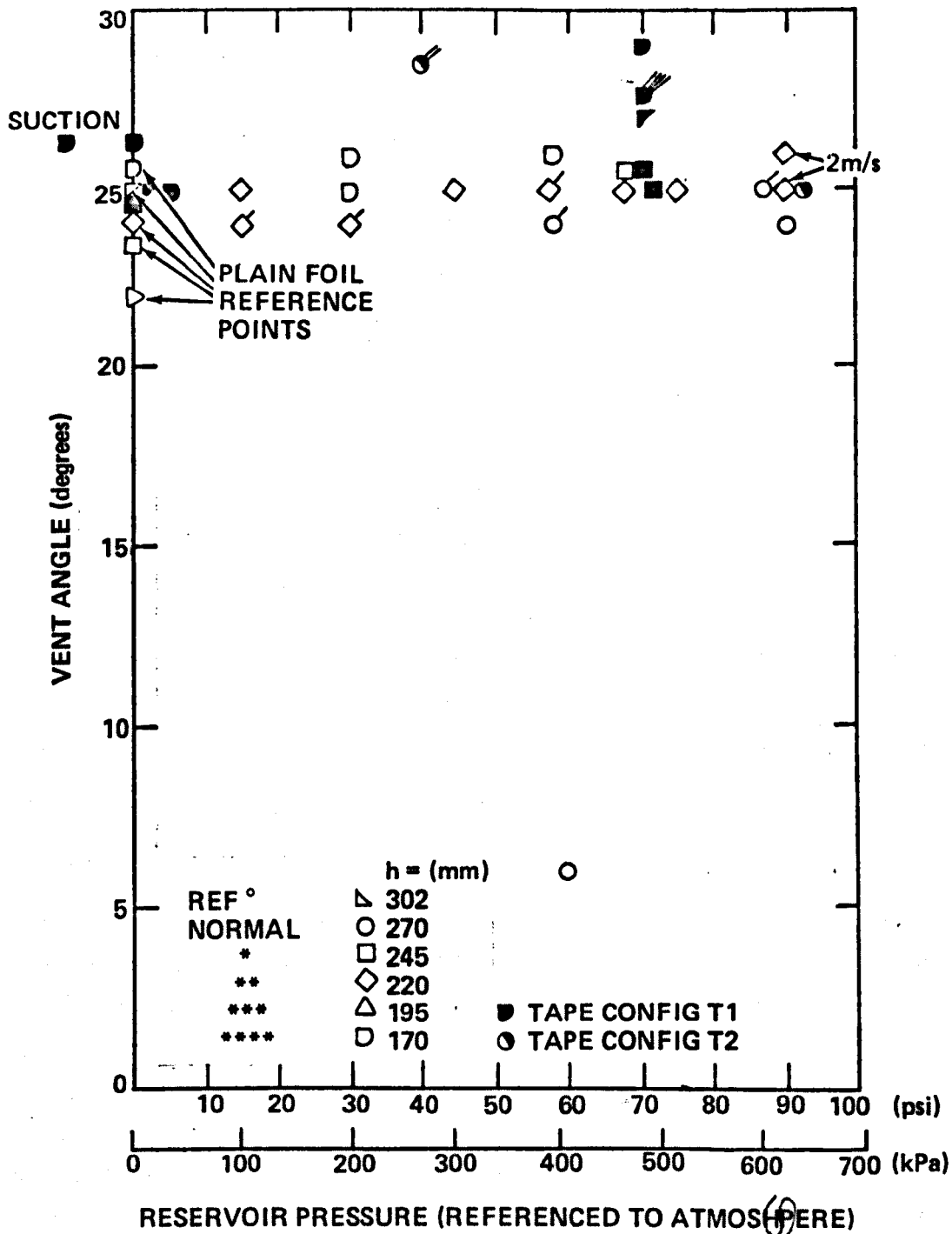
Figure 9.23 — Ventilation Angle Versus Reservoir Pressure, NACA 16 021 Foil With Long, Narrow, Vertical Slots, Plain and Taped, 10 ft/s (3m/s).

261

It was somewhat disappointing that the refined model did not produce a distinct increase in the ventilation angle. The positive results obtained by concentrating the blowing using the tape were encouraging. Interestingly, for taped Configuration T2, the ventilation inception angle fell with increased blowing pressure. This is explainable in terms of the smoothness of the flow emanating from the slots between two taped regions. With increased pressure, the slot flow became more disordered, which was apparently counter-productive.

For T1, improvement in ventilation inception angle was noted primary for a single immersion −170mm. The average inception angle at this depth for both the plain strut and the T1 configuration with no blowing was 25½ degrees. At 70 psi (480 kPa) the average improvement was 2½ degrees and the maximum was 3½ degrees. At 245mm immersion, there was no improvement, while at 195mm there was 1½ degrees. Evidently, blowing was required at or above the apparent free surface to produce the effect.

Flow Visualisation. Figures 9.24 – 9.29 are a series of photographs of the Mk I model with long, narrow slots, untaped, at blowing pressures from 15 to 90 psig (100 to 620 kPa) and at sideslip angles from 20 to 25 degrees. The upper photographs show the oil smear patterns, and the lower ones the flow during the run. The flow was made visible by the presence in the water of fine bubbles. Especially when the reservoir was nearly empty, air dispersed in the jet water which gave it a cloudy appearance much like smoke. This made it possible to verify that the flow was fully attached, rather than just attached in a micro-region below the jet, which might have resulted in a "false" scrubbed region in the oil smear pattern.

At 20 degrees, there was no decrease in the amount of separation evident as the pressure was increased from 30 to 60 psig (205 to 410 kPa). At 70 psig, (480 kPa) the separation was eliminated for all sideslip angles up to 25 degrees. The oil smear patterns taken at 24 degrees show some evidence of relatively low shear regions, indicating that separation was imminent. At the free surface, there was no apparent change in oil smear pattern with increasing blowing pressure or with increasing sideslip angle right up to the point of ventilation inception. In the flow photographs, air can be seen drawn below the free surface in the region of the trailing edge, especially just prior to ventilation inception.

A more detailed analysis of the photographs of the oil smear patterns and the flow, taken in sequence of increasing blowing pressure, gives more insight into the effect of blowing.

In Figure 9.24 taken at 20 degrees and 15 psig (100 kPa), separation is apparent just forward of the second slot, and air entrainment may be seen up to the forwardmost (upstream) slot. The shear pattern indicates weak attachment just aft of the first slot. At 24 degrees, there was separation everywhere from just forward of the leading edge slot aft to the trailing edge. Air entrainment extended to forward of the lip of the leading slot.
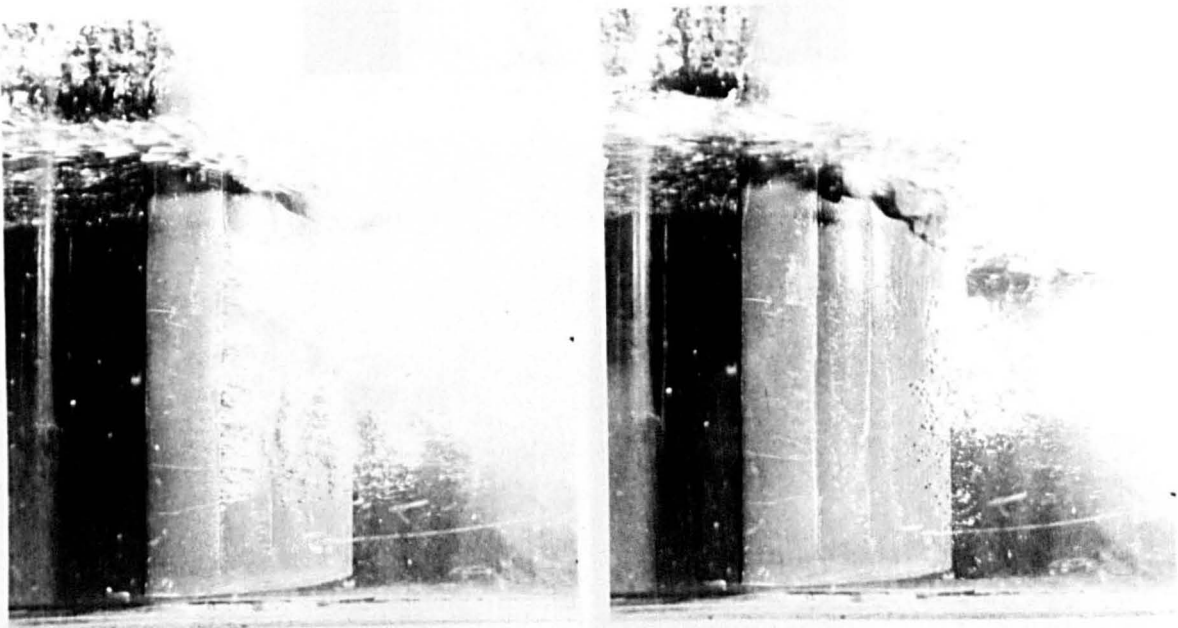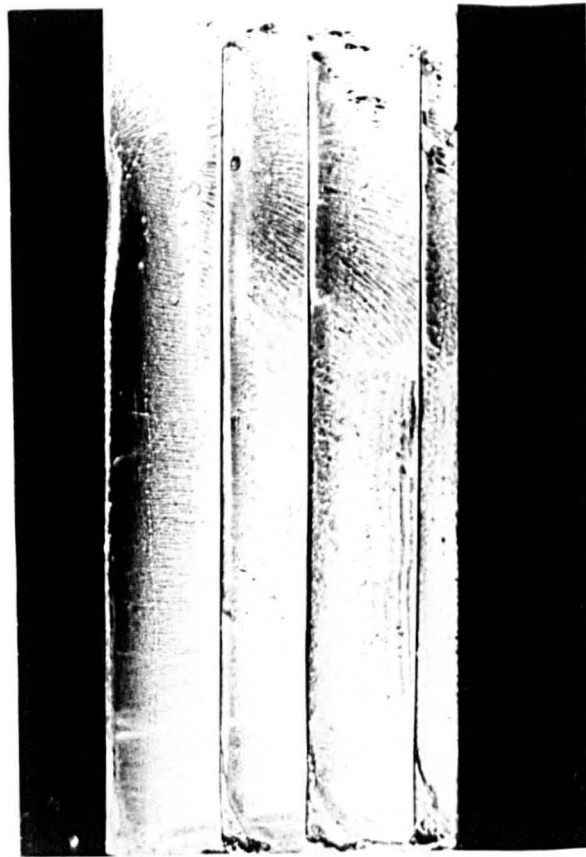
Figure 9.24a – NACA 16 021 Foil With Long, Narrow Slots, 15 psi (100 kPa) Blowing, 220 mm, Immersion, 10 ft/s (3m/s), β = 20 Degrees.
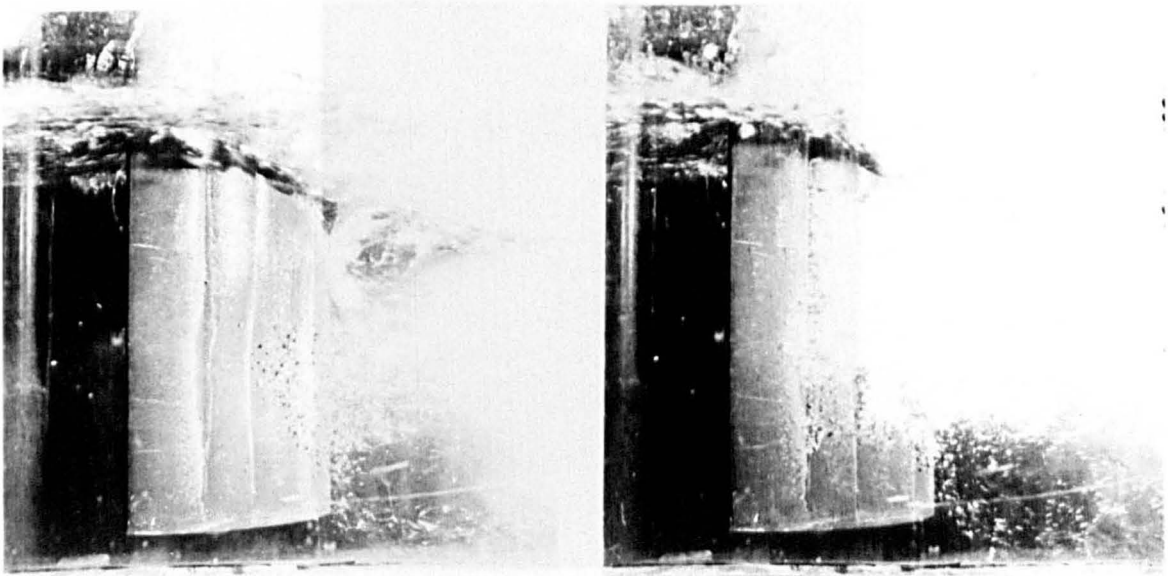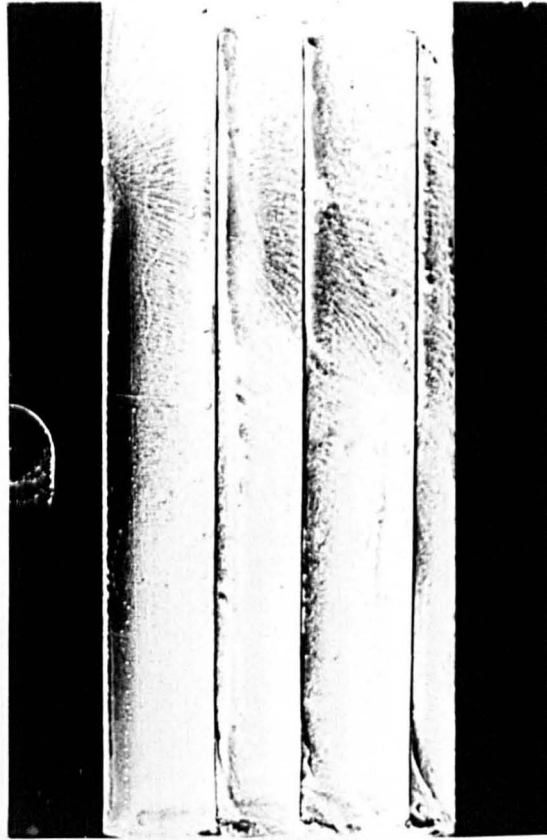
Figure 9.24b – β = 24 Degrees
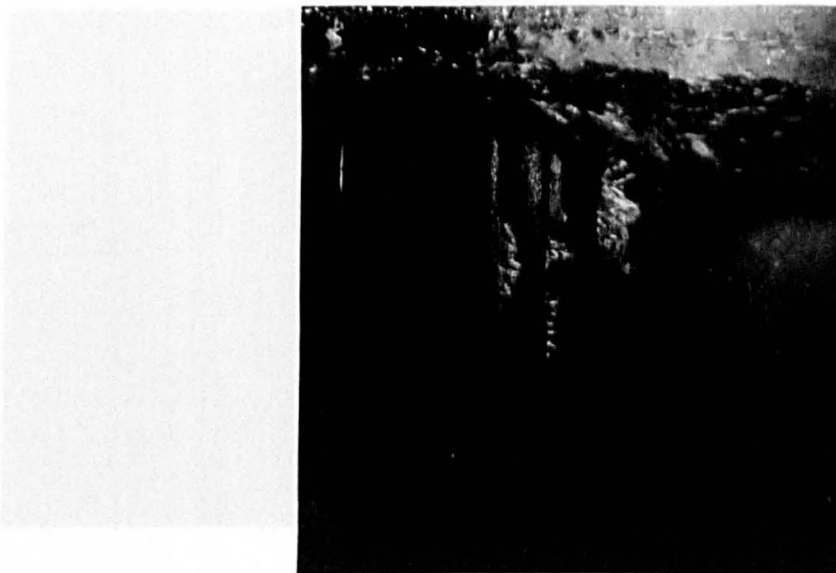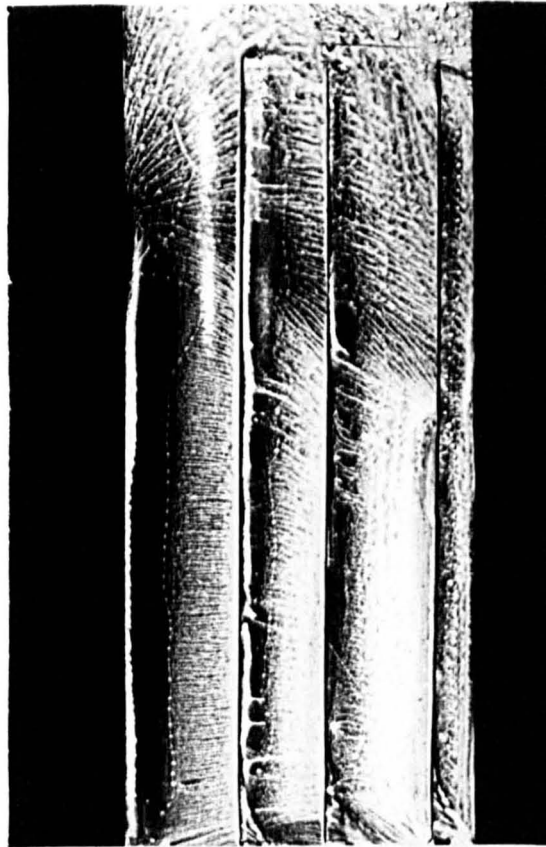
Figure 9.25a – NACA 16 021 Foil With Long, Narrow Slots, 30 psi (205 kPa) Blowing, 220mm Immersion, 10 ft/s (3m/s), β = 20 Degrees.

Figure 9.25b – β = 23 Degrees
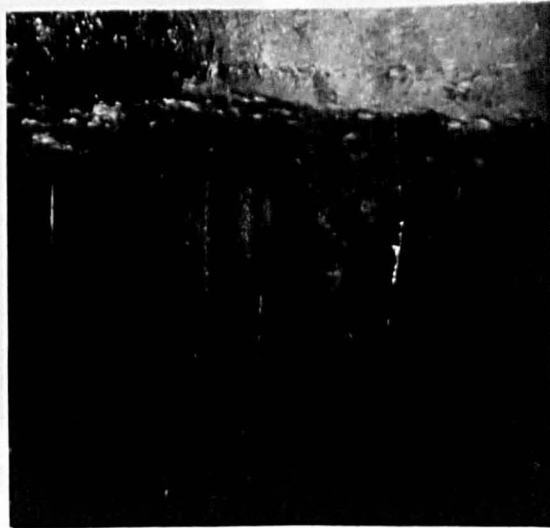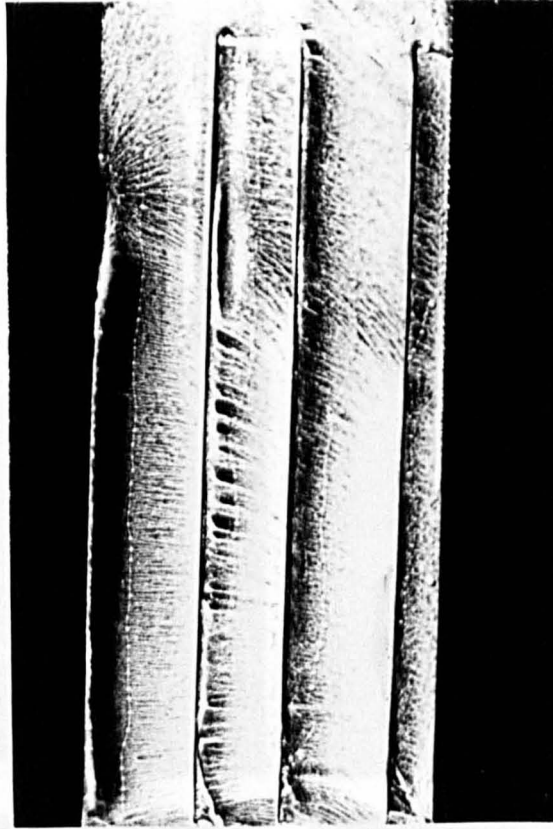
Figure 9.26a – NACA 16 021 Foil With Long, Narrow Slots, 45 psi (310 kPa) Blowing, 220mm Immersion, 10 ft/s (3m/s), β = 20 Degrees.
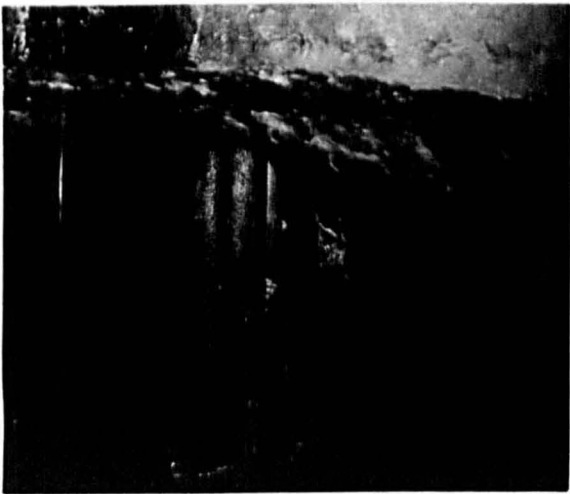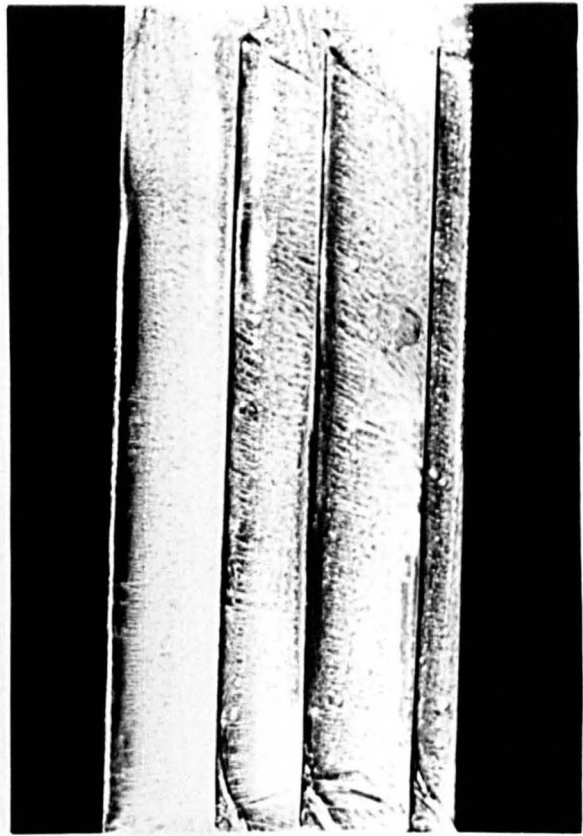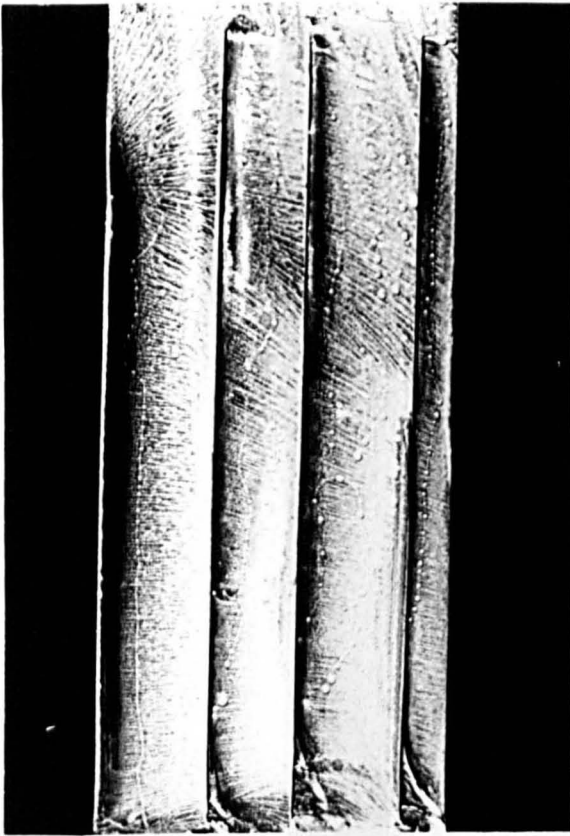
Figure 9.26b – β = 24 Degrees   Figure 9.26c – β = 25 Degrees
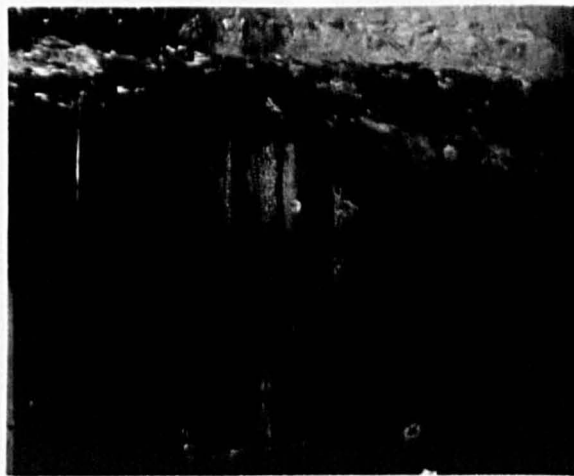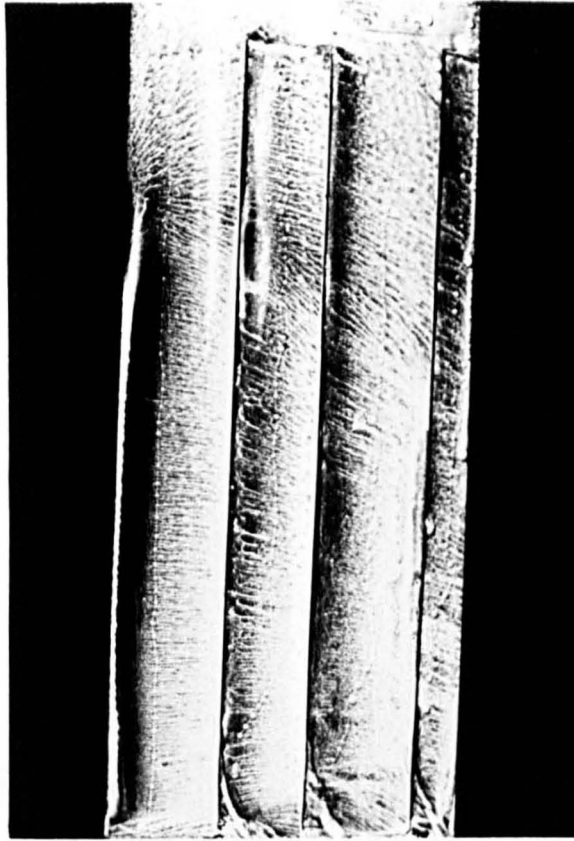
Figure 9.27a – NACA 16 021 Foil With Long, Narrow Slots, 60 psi (410 kPa) Blowing, 220mm Immersion, 10 ft/s (3m/s), β = 20 Degrees.
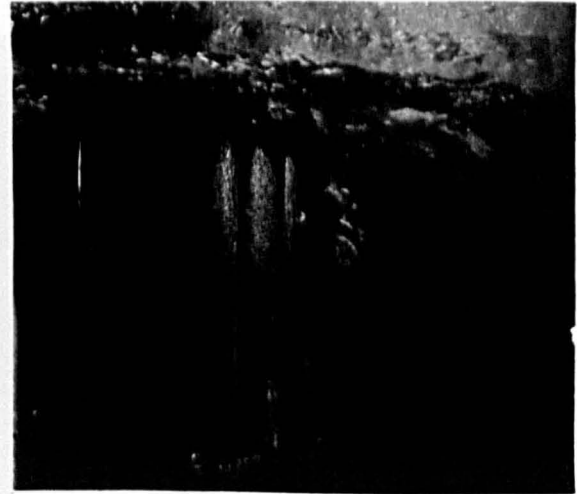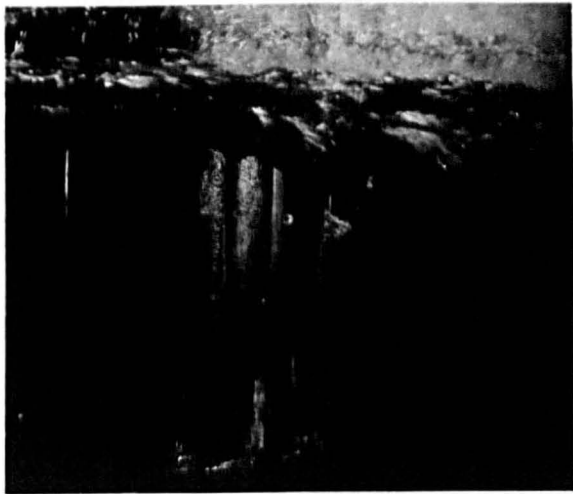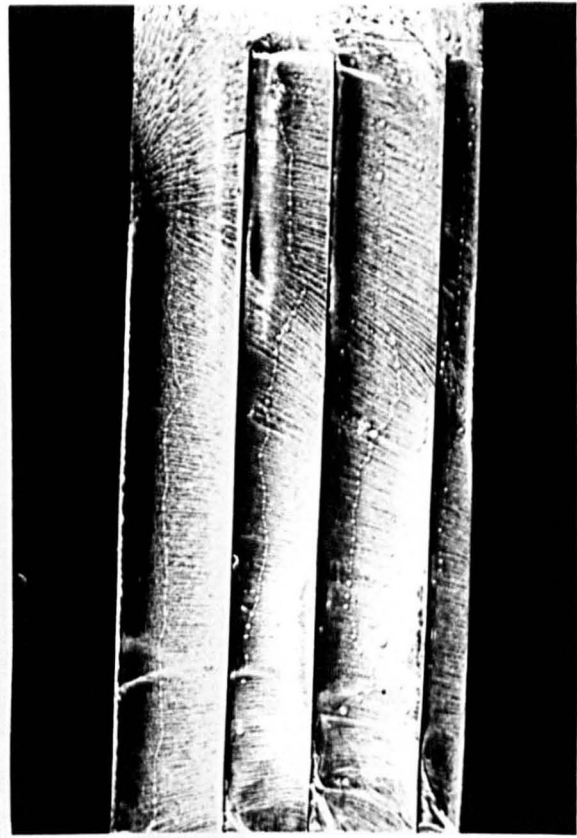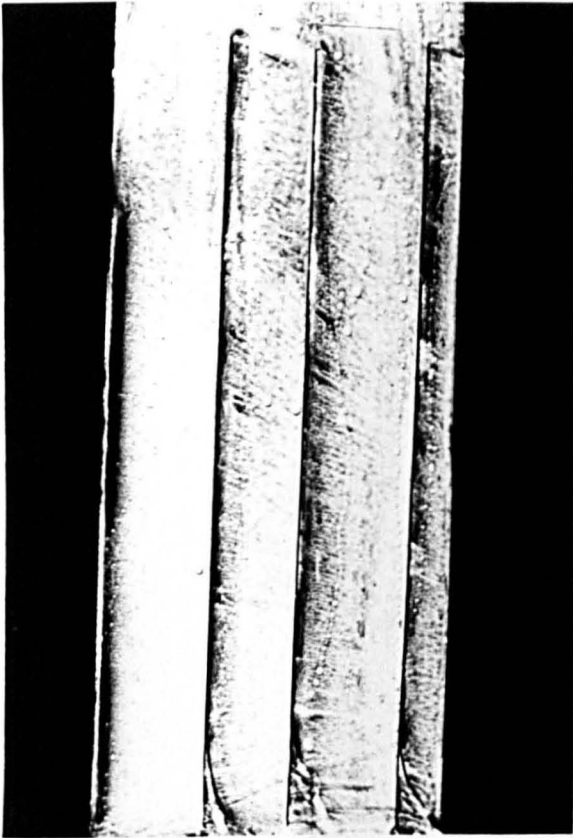
Figure 9.27b – β = 24 Degrees   Figure 9.27c – β = 25 Degrees
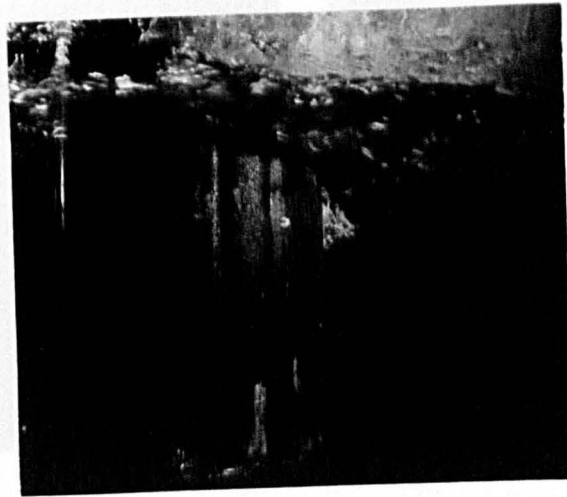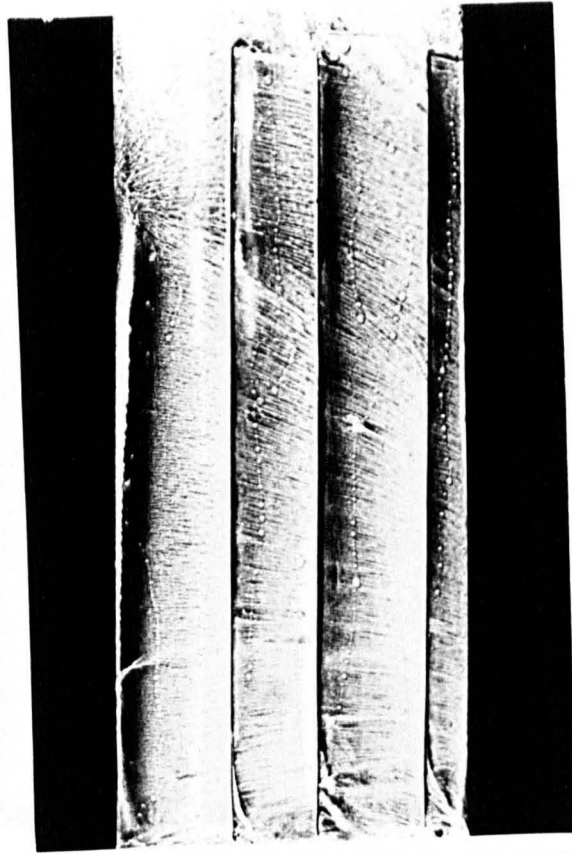
Figure 9.28a – NACA 16 021 Foil With Long, Narrow Slots, 75 psi (515 kPa) Blowing, 220mm Immersion, 10 ft/s (3m/s), β = 20 Degrees.
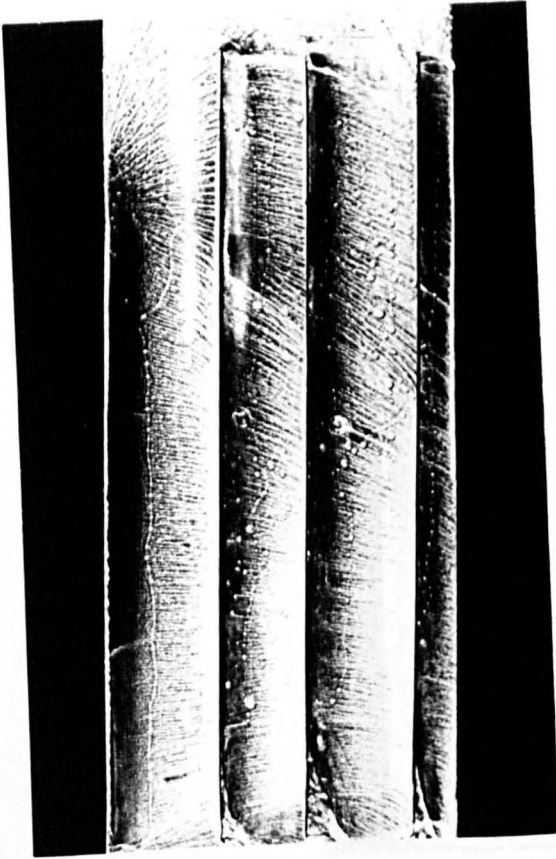
Figure 9.28b – β = 24 Degrees
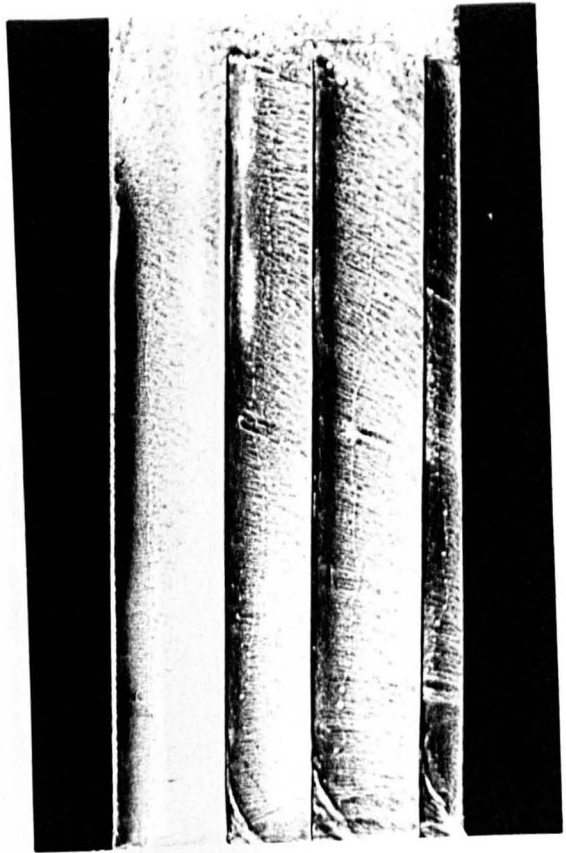
Figure 9.28c – β = 25 Degrees
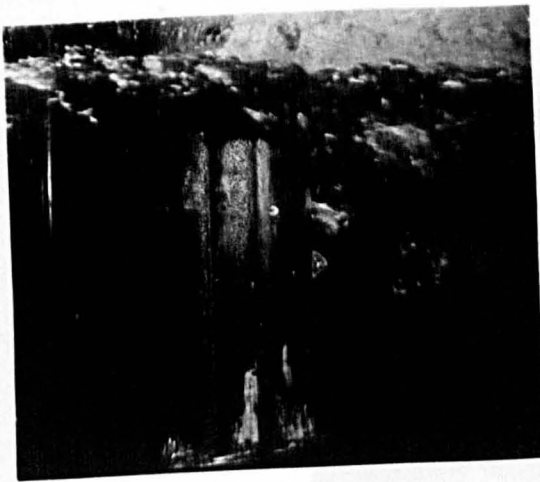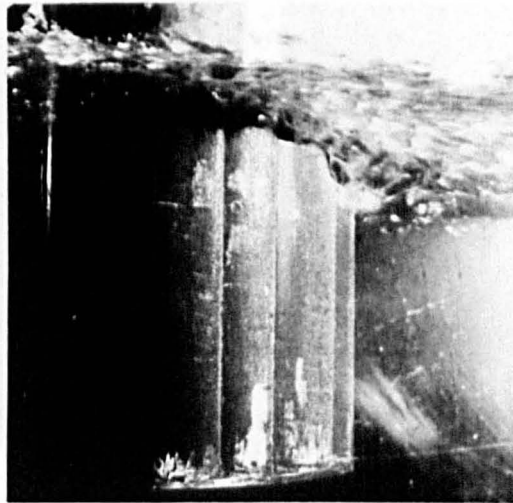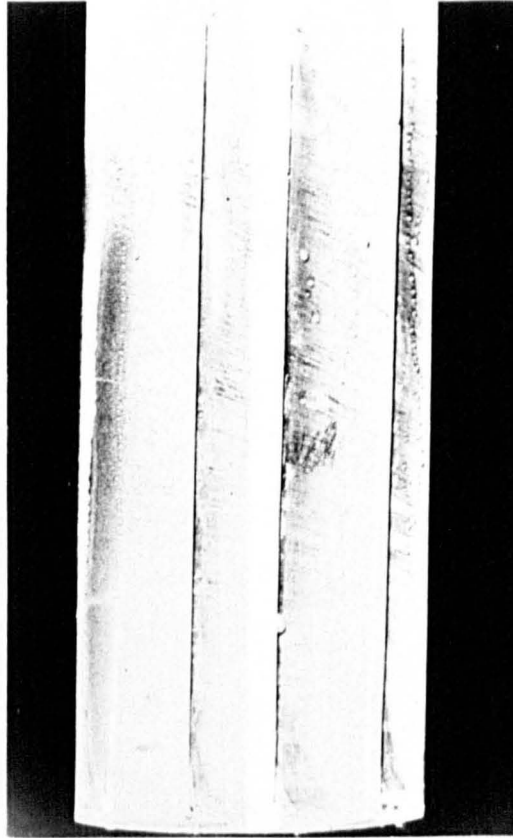
Figure 9.29a – NACA 16 021 Foil With Long, Narrow Slots, 90 psi (620 kPa) Blowing, 220mm Immersion, 10 ft/s (3m/s), β = 20 Degrees.
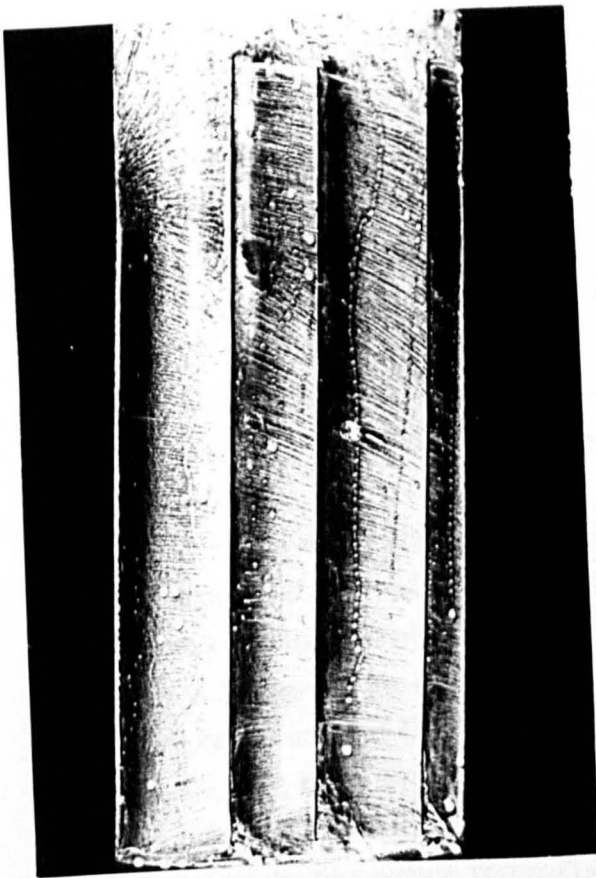
Figure 9.29b – β = 24 Degrees
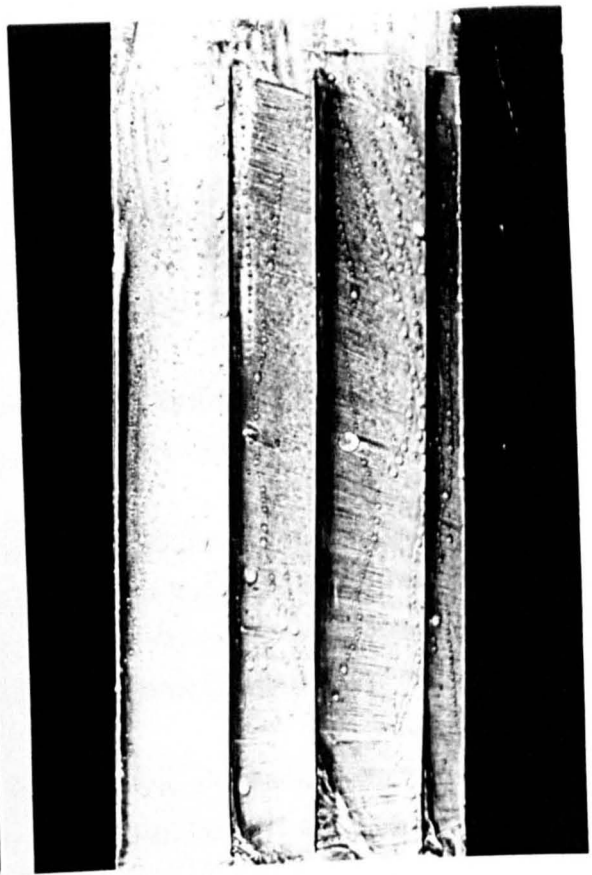
Figure 9.29c – β = 25 Degrees
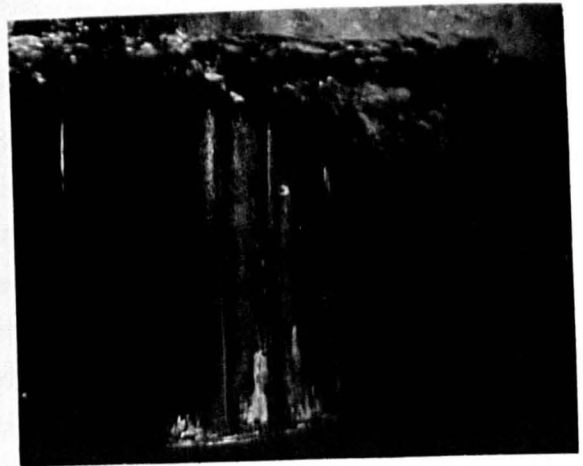
Figure 9.25, 30 psig (205 kPa), 20 degrees, shows that between the first and second slots there was weakly attached flow. Forward of the third slot, there was full separation. Between the second and third slots, air was entrained. Below the lip of the first slot, a "ridge" of oil accumulation similar to that associated with a laminar separation bubble can be noted. It is likely that the expansion of the jet was too rapid in this region, resulting in a local laminar separation. At 23 degrees, there was distinct separation between the second and third slots, weak attachment forward of the first slot, and very weak attachment forward of the second slot lip. Much air was entrained to just forward of the leading edge lip.

Figure 9.26 shows that for 45 psig (310 kPa) blowing, the flow was roughly the same as for 30 psig (205 kPa). At 25 degrees, a vent occurred. The oil smear pattern is somewhat difficult to interpret, but seems about the same as for 24 degrees at this pressure and 23 degrees at 30 psig (205 kPa).

In Figure 9.27, for 60 psig (410 kPa) blowing, the sequence of flow patterns does not differ appreciably from 30 psig (205 kPa). The laminar separation ridge below the lip of the first slot is no longer evident.

Figure 9.28 shows that for 75 psig (515 kPa) the flow pattern and air entrainment characteristics were significantly altered. The flow everywhere was well-attached, for all angles, except for some weakness just forward of the first and third slots. The weakness increased with sideslip angle, until at 25 degrees, the attachment became very weak forward of the first slot. Air entrainment can be noted at the aft slot only.

In Figure 9.29, taken with 90 psig (620 kPa) blowing, at no angle is separation apparent except for a slight oil accumulation above the forward slot lip. Air entrainment was limited to a small region near the free surface at the after slot.

Analogy with Nose Ventilation. The results of the tests of the thin-slotted model presented somewhat of a paradox in terms of the postulated mechanism of ventilation described in Chapter 2. In particular, the virtual elimination of a massive region of separation did not result in an appreciable increase in ventilation inception angle. On the other hand, concentrating the blowing near the surface and ignoring the separation below was more effective. An explanation which reconciles these seemingly contradictory results hinges upon the hypothesis that the lift coefficient must have increased proportionately to the decrease in separation. Therefore the pressure on the suction side of the strut was considerably lower than would have otherwise obtained. This combined with a minute region of separation would have created a situation similar to that of a laminar separation nose bubble on the blunt nosed biogive: a potentially explosive region which required only a disturbance to trigger transition to full ventilation.

In contrast, for the case in which blowing was concentrated near the surface, separation further below the surface was not eliminated. Therefore large negative pressures were not attained. The surface seal, or region of unseparated flow at the surface may have been enlarged, resulting in a stabilising effect. Whether or not separation is a necessary precondition for ventilation may be moot, as is the question of whether separation must exist prior to the inception of vapour cavitation. It has been shown that ventilation will occur in the presence of only minute amounts of separation. It is doubtful that separation on a microscopic scale could ever be completely eliminated, and practically ventilation is not necessarily preceded by large areas of separation.

From a practical standpoint, the ventilation inception angle is not necessarily the most important boundary. Usually, the force coefficient attainable prior to ventilation is more crucial to performance. It has been shown possible to greatly increase the force coefficient obtainable before ventilation by blowing to reduce separation. Conversly, by strengthening the surface seal by blowing near the surface only, it is possible to obtain some increase in inception angle on the model scale.

Mk I Model — Shortened Slots. Figure 9.30 shows the ventilation inception boundary for the Mk I Model after the slots above the water surface had been filled with epoxy. For comparison, the boundary points obtained for the long-slotted version and the widened-slot version are also displayed. The points to the left of the graph represent suction. The series at the 170mm immersion resulted in the greatest improvement in inception angle. A maximum of 4 degrees was measured although the average gain was about 2 degrees. At 29 degrees, ventilation occurred instantaneously. At 28 degrees, enough time elapsed before ventilation to develop a good oil smear pattern and to take a picture of the flow. At 28½ degrees, a reasonable oil smear pattern was obtained which indicated that full nose separation had occurred prior to ventilation.

It was noted that, when the model was left at 26½ degrees for about 40 seconds, ventilation occurred. Two "premature" inceptions were observed at 24 degrees. This was particularly interesting, because at this immersion, a plain strut would not ventilate regardless of the time it was left at that sideslip angle. At 24 degrees, absolutely no evidence of separation could be detected. This time dependence was more characteristic of the blunt biogive.

During these tests, a particular sensitivity of the ventilation behaviour to the air bubble content of the channel was noted. This was also more characteristic of the blunt biogive.

A change in the immersion depth from 170mm to 195mm adversely affected the ventilation boundary by about a degree. This is slightly more than would have been anticipated due to the same change in depth of the bare strut. Although the difference is not great enough to be conclusive, it indicates that blowing near the free surface is critical.
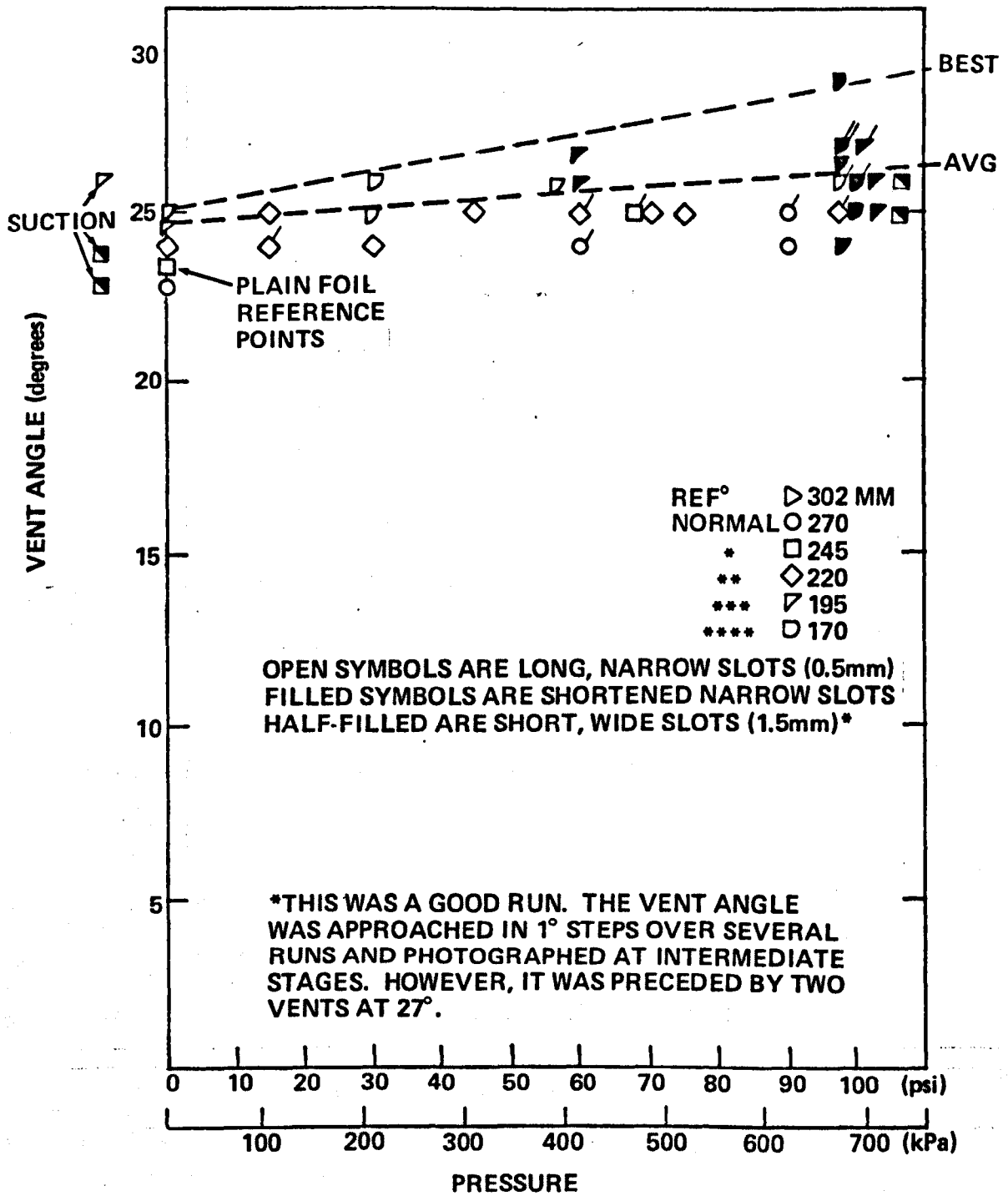
Figure 9.30 — Ventilation Angle Versus Reservoir Pressure, NACA 16 021 Foil With Long, Narrow, Vertical Slots, Shortened Slots, and Widened Slots. 10 ft/s (3m/s).

277

Flow Visualisation. Figures 9.31 through 9.34 show some of the flow and oil smear patterns which give some insight into the observed effects.

Figure 9.31 compares photographs taken of the flow through the slots at 60 and 100 psi (405 and 700 kPa), with the model raised out of the water, or with the slots discharging into a cavity already ventilated. The flow irregularities may be readily seen, especially at the forward slot. This was in spite of great pains to ensure smoothness of the slots. It is possible that the forward slot may have been damaged prior to this test by an attempt to clear it of debris.

Figure 9.32 shows a comparison between the flow and oil smear patterns taken at blowing pressures of 60 and 100 psi (405 and 700 kPa) at 25 and 26 degrees. There is no evident change or difference in flow pattern.

Figure 9.33 shows photographs of the smoke-like micro-bubbles dispersed in the flow from the slots at 26½ and 27 degrees. The flow shows no signs of separation.

Figure 9.34 was photographed during the runs at which ventilation occurred at 24 degrees on three occasions while blowing with 100 psi (700 kPa) pressure. The lower photograph shows a partial vent to the forward slot. Some air is also attached to the slot lip. The oil smear pattern shown in the upper photograph indicates weak attachment there. Under normal circumstances, without blowing, the flow would be about 75 percent separated at 24 degrees.

Effect of Suction. Figure 9.35 consists of photographs of the oil smear pattern at 22 degrees and 25 degrees with suction applied. At 22 degrees, separation was eliminated by suction except at the extreme trailing edge, and just aft of the forward slot. At 25 degrees, separation distinctly appeared, but was not so extensive as that found on the bare model at 24 degrees.

Mk I Model — Thickened and Shortened Slots. The effect of increasing the slot thickness on the jet flow was to decrease the turbulence and disorder. Unfortunately, because the jet flow rate was primarily controlled by system losses between the reservoir and the model, the jet velocity was also proportionately decreased, while the flow rate remained approximately the same. Figure 9.36 is a photograph of flow from the slots, out of the water, at a reservoir pressure of 100 psi (700 kPa). The flow from the lower slot areas is shown to be significantly greater than that at the top. This effect may have been mitigated somewhat upon submergence, when the static head difference between top and bottom was eliminated.

The reduced jet velocity probably explains why, as shown in Figure 9.30, this version of the Mk I did not demonstrate as much improvement in the ventilation inception angle as did the shortened, narrow slot configuration.
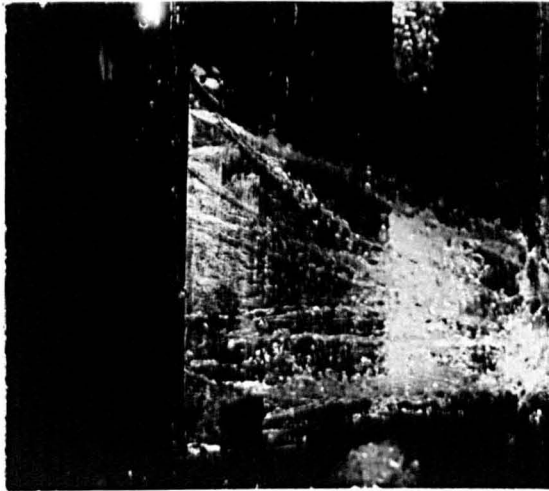
60 psi
(405 kPa)

100 psi
(700 kPa)

Figure 9.31 – Effect of Varying Supply Pressure on Flow Through Slots, NACA
16 021 Foil with Shortened, Narrow Slots.
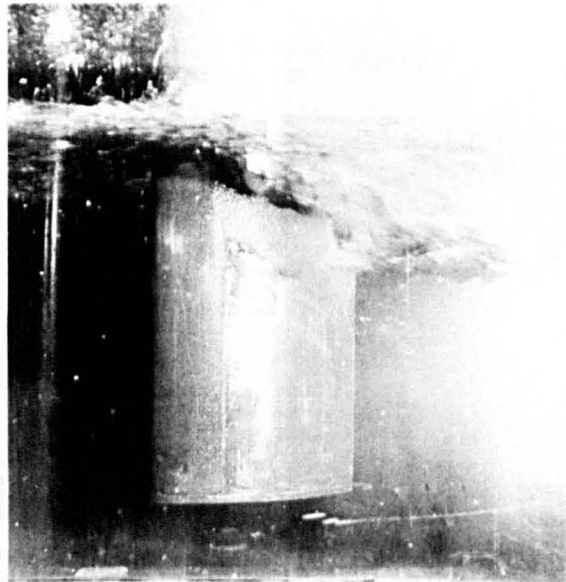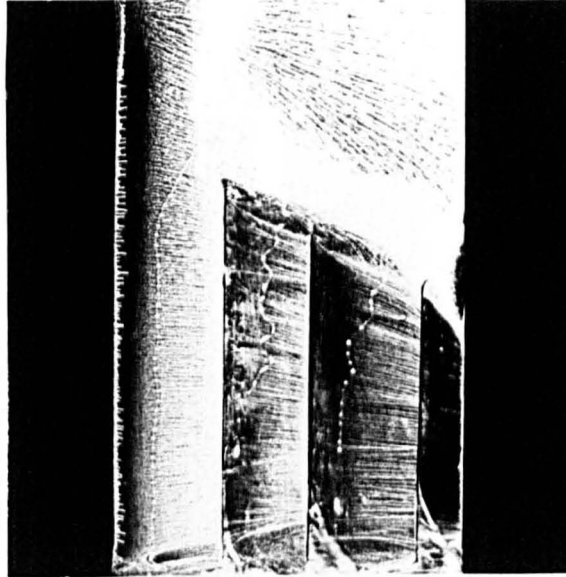
β = 25 Degrees, 60 psi (405 kPa) Blowing

Figure 9.32 – Effect of Varying Supply Pressure on Flow and Oil Smear Patterns on NACA 16 021 Foil With Shortened, Narrow Slots. Immersion 195mm, 10 ft/s (3m/s). No Differences Apparent.
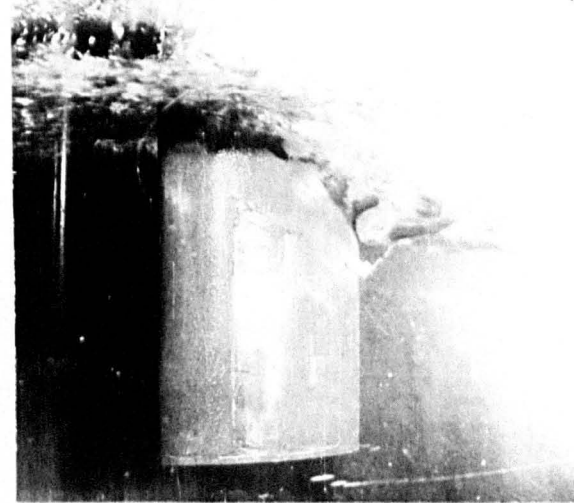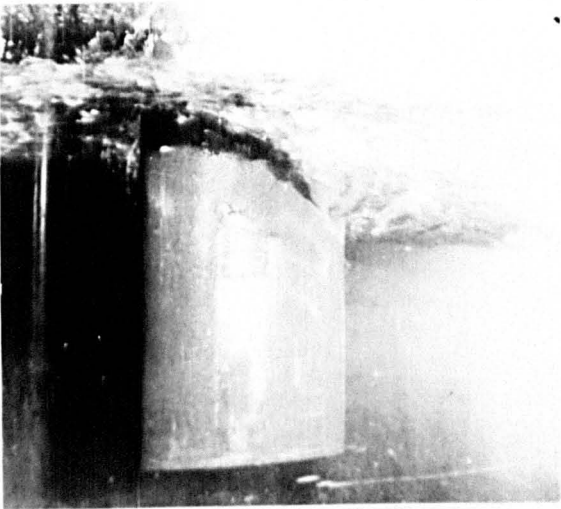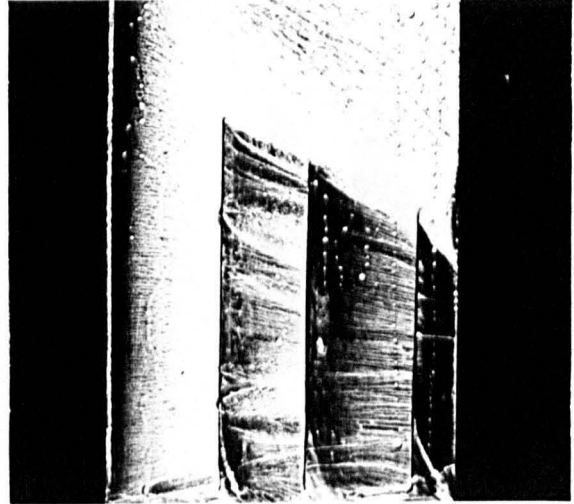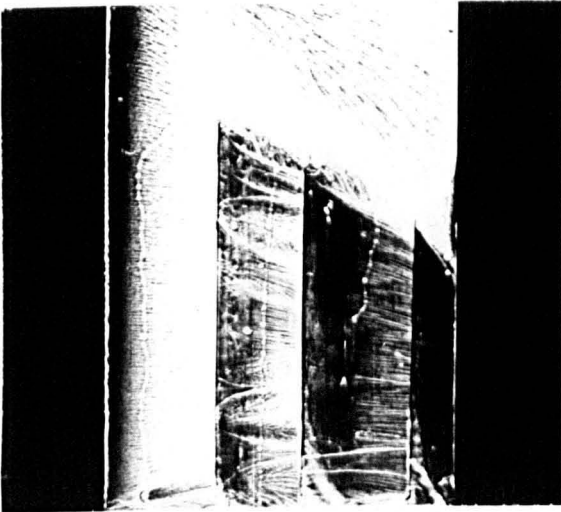
β = 25 Degrees
100 psi (700 kPa)
Blowing

β = 26 Degrees
100 psi (700 kPa)
Blowing

Figure 9.32 (Continued)
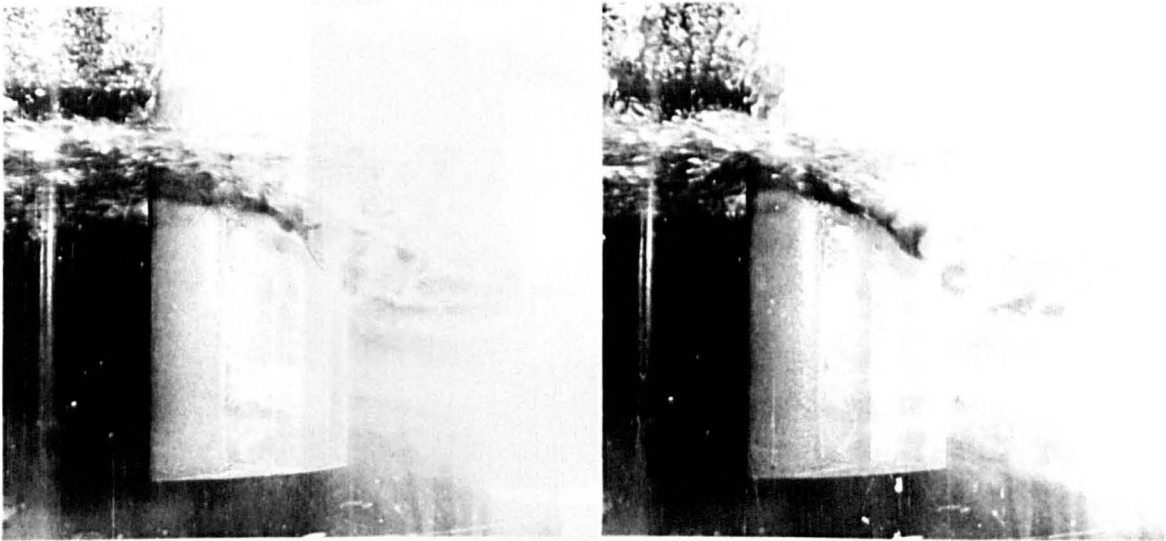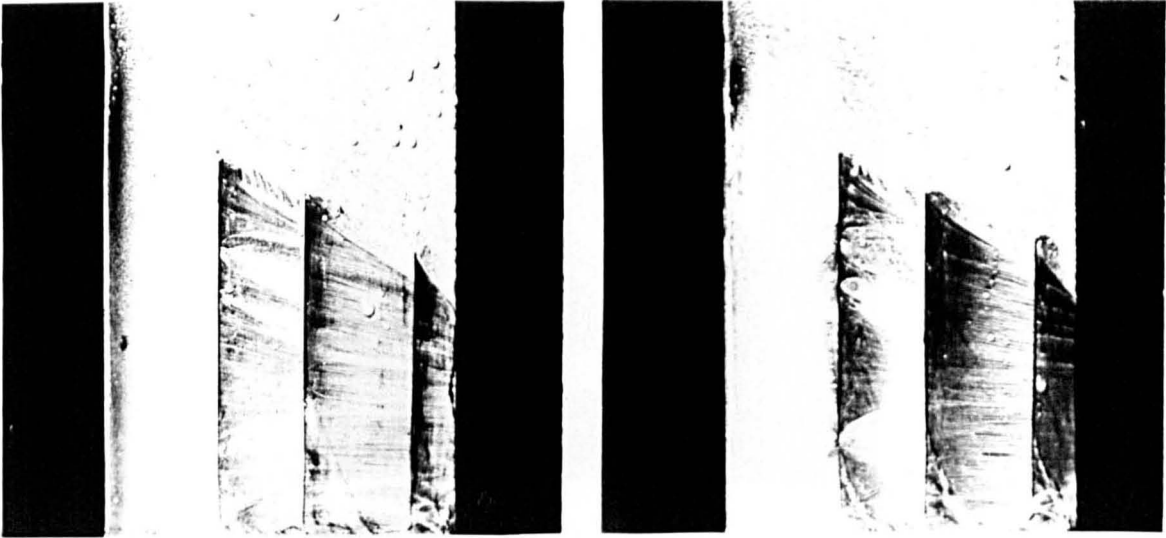
β = 26 1/2 Degrees $\qquad\qquad\qquad$ β = 27 Degrees

Figure 9.33 — NACA 16 021 Foil With Shortened, Narrow Slots, 100 psi (700 kPa) Blowing, 10 ft/s (3m/s), Immersion 170mm. Lower Photos Show Microbubbles in Flow, No Separation.
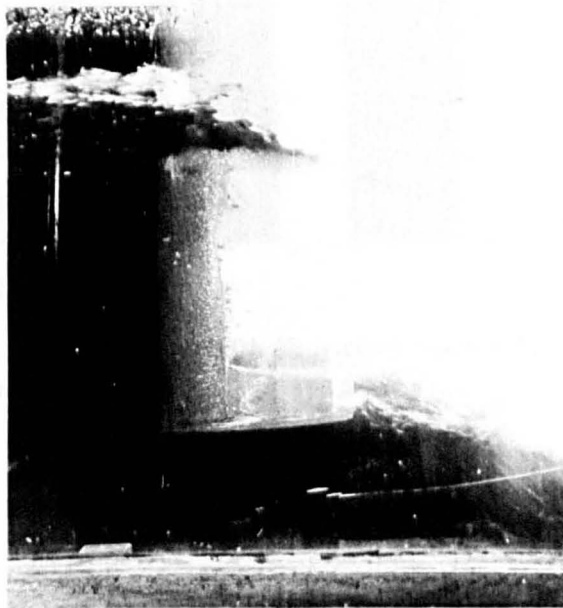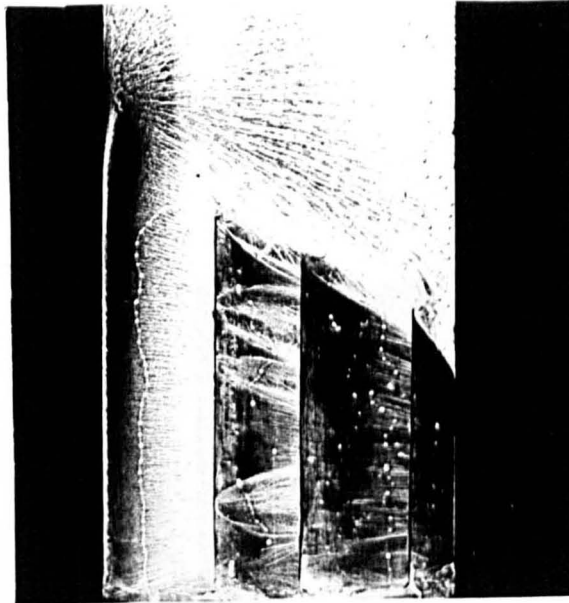
Figure 9.34 — NACA 16 021 Foil With Shortened, Narrow
Slots, 100 psi (700 kPa) Blowing, 10 ft/s
(3m/s), Immersion 170mm, $\beta = 24$ Degrees.
Lower Photo Shows Partial Vent to
Forward Slot. Upper Photo Shows Low
Shear in Same Place Indicating Weak
Attachment.
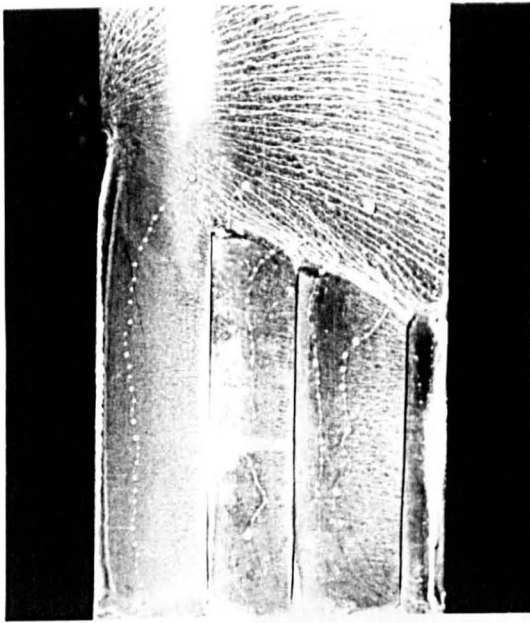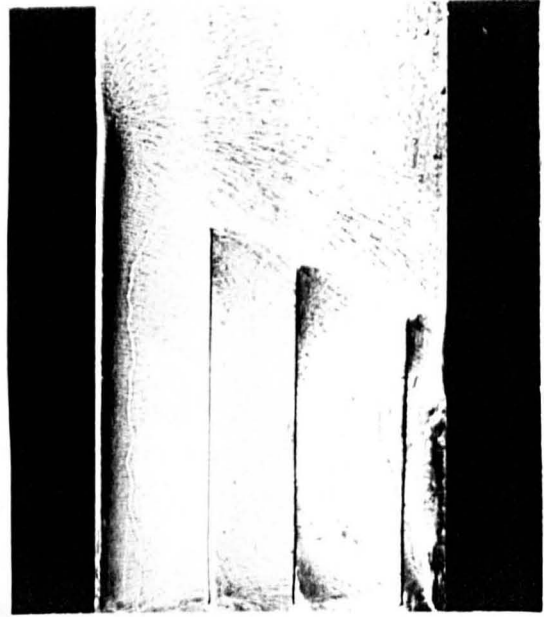
β = 22 Degrees β = 25 Degrees

Figure 9.35 –   NACA 16 021 Foil With Shortened, Narrow Slots, With Suction, 10 ft/s,
Immersion 170mm.
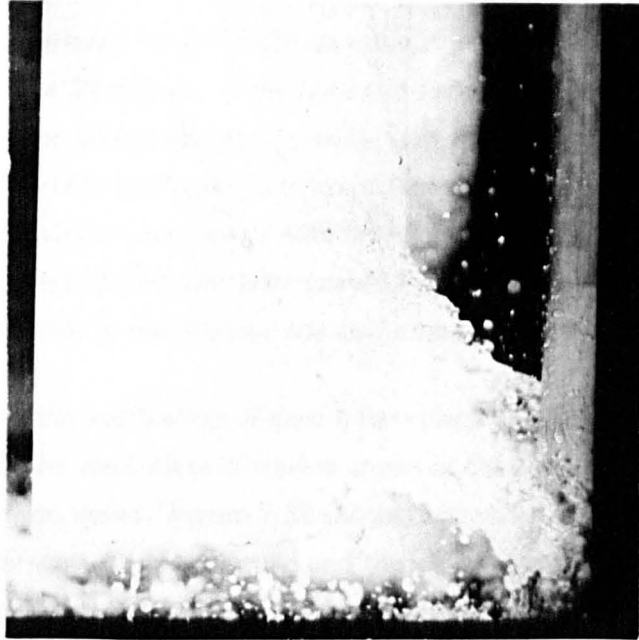
Figure 9.36 — NACA 16 021 Foil With Shortened, Wide Slots, 100 psi (700 kPa) Blowing, Showing Flow From Slots in Air.

Figure 9.37 shows a sequence of photographs of the widened slot model just prior to ventilation at 24 and 25 degrees. In the oil smear pattern can be seen small patches of local separation. These are correlated with bubble entrainment seen near the trailing edge in the flow photographs. One of these shows a partial vent down the forward slot edge.

In general, the thicker slots did not delay inception of ventilation or the spread of separation so well as the thin slotted version with similarly shortened slots. However, spearation was still virtually eliminated at 25 degrees by blowing.

The Mk I Model both with shortened slots and with widened slots re-inforced the hypothesis that the principal practical effect of blowing is to increase the sideforce which can be sustained by a surface-piercing strut without ventilation inception. A spectacular increase in ventilation angle was not possible with the present model, if for no other reason than that full separation from the nose occurred around 28 or 29 degrees. Nose separation could not have been affected by blowing from the existing slots. The maximum angle possible under the circumstances was therefore attained. However, the penalty paid was the introduction of the possibility a new type of ventilation, similar to nose ventilation, associated with very small regions of separation and very low pressures. Like nose ventilation, the new type proved time dependent and erratic. Possible sensitivity to ambient bubbles in the channel was also noted.

Roughness. As expected, the application of glass microspheres to the surface of the Mk I and II Models greatly decreased the ventilation inception angles in the absence of blowing, and also introduced a dependency on speed. Figure 9.38 shows the ventilation inception angles versus speed for the Mk I Model with all slots blocked and the surface roughened, for various immersions. Also included for comparison are the results obtained form the NACA 0012 strut reported in Chapter 5, under similar roughness conditions, immersed to two chord lengths. There is a certain amount of scatter to the results, as anticipated. No dependence on immersion depth was evident over the range tested, in contrast to the smooth model results. This corroborated the observations made during tests of taped configurations.

The average values of the ventilation angles are re-plotted in Figure 9.39 to serve as a reference for comparison with the results of the Mk I Model, similarly roughened, with blowing, at various immersions as shown. The ventilation angles obtained for the smooth Mk I Model with blowing and the same slot geometry are also shown.

There are several trends which can be deduced from Figure 9.39. The most important and obvious is the improvement in ventilation angle made by blowing at 10 ft/s (3 m/s). At 170mm immersion, the ventilation angle was the same as that of the plain smooth model and nearly equalled that of the smooth, blown model value. The maximum improvement was 7 degrees above the baseline value of 19 degrees for the unblown, roughened strut.
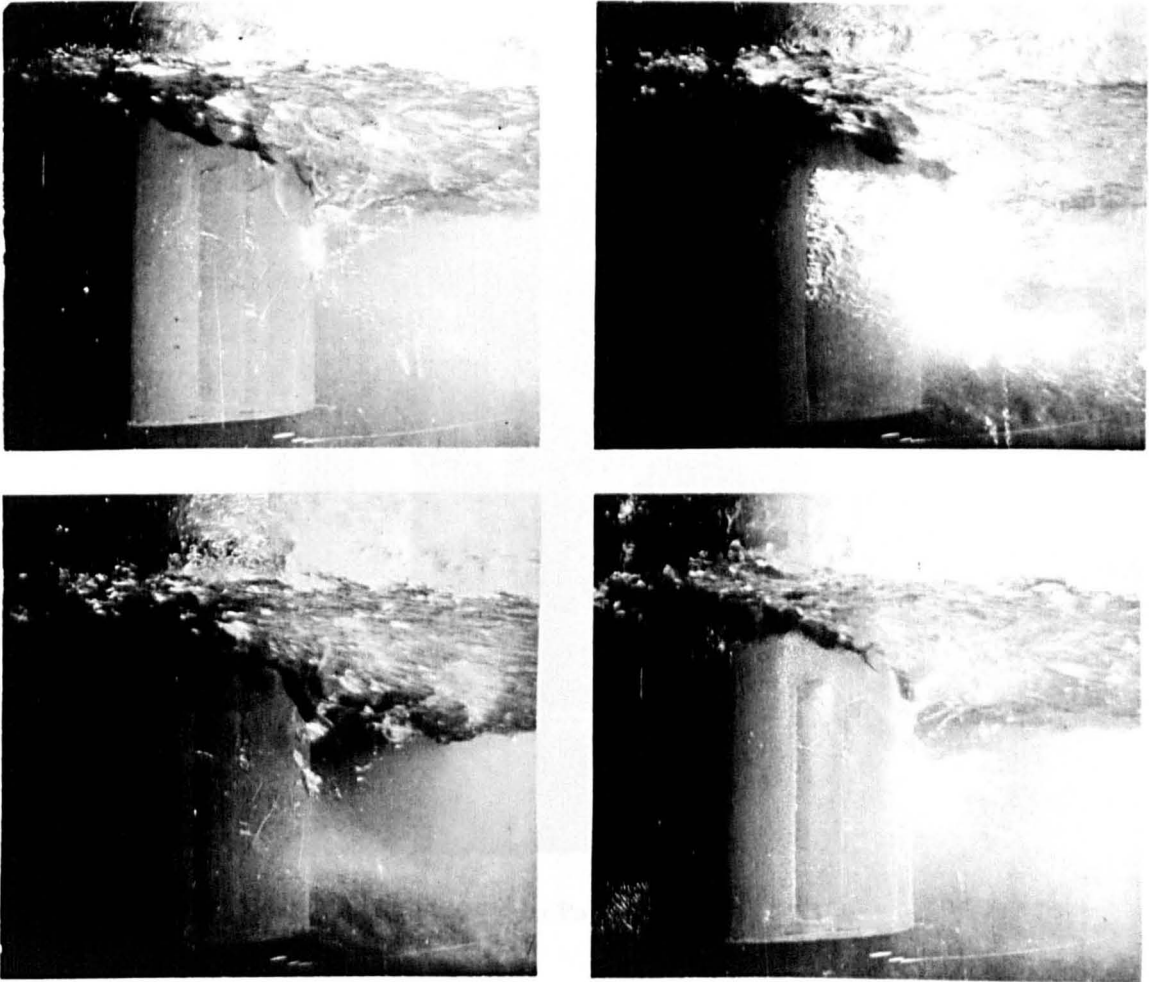
Figure 9.37a – NACA 16 021 Foil With Shortened, Wide Slots, 100 psi (700 kPa) Blowing, Immersion 170 mm, 10 ft/s (3m/s), β = 25 Degrees.
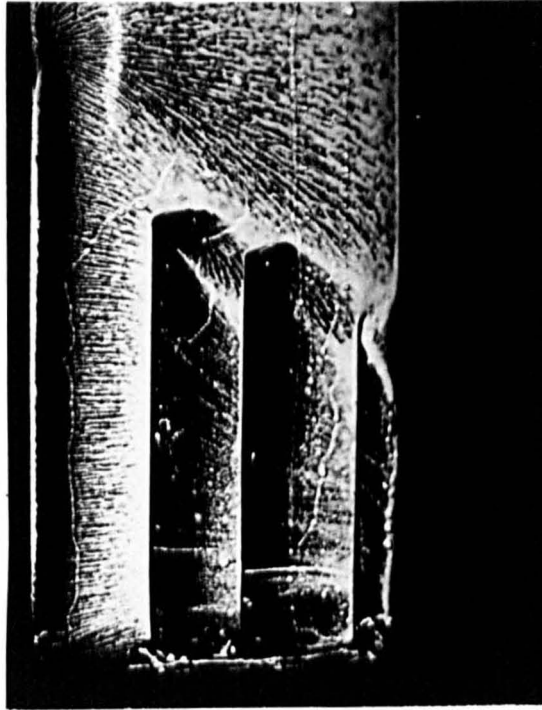
Figure 9.37b – Oil Smear Pattern, β = 24 Degrees.
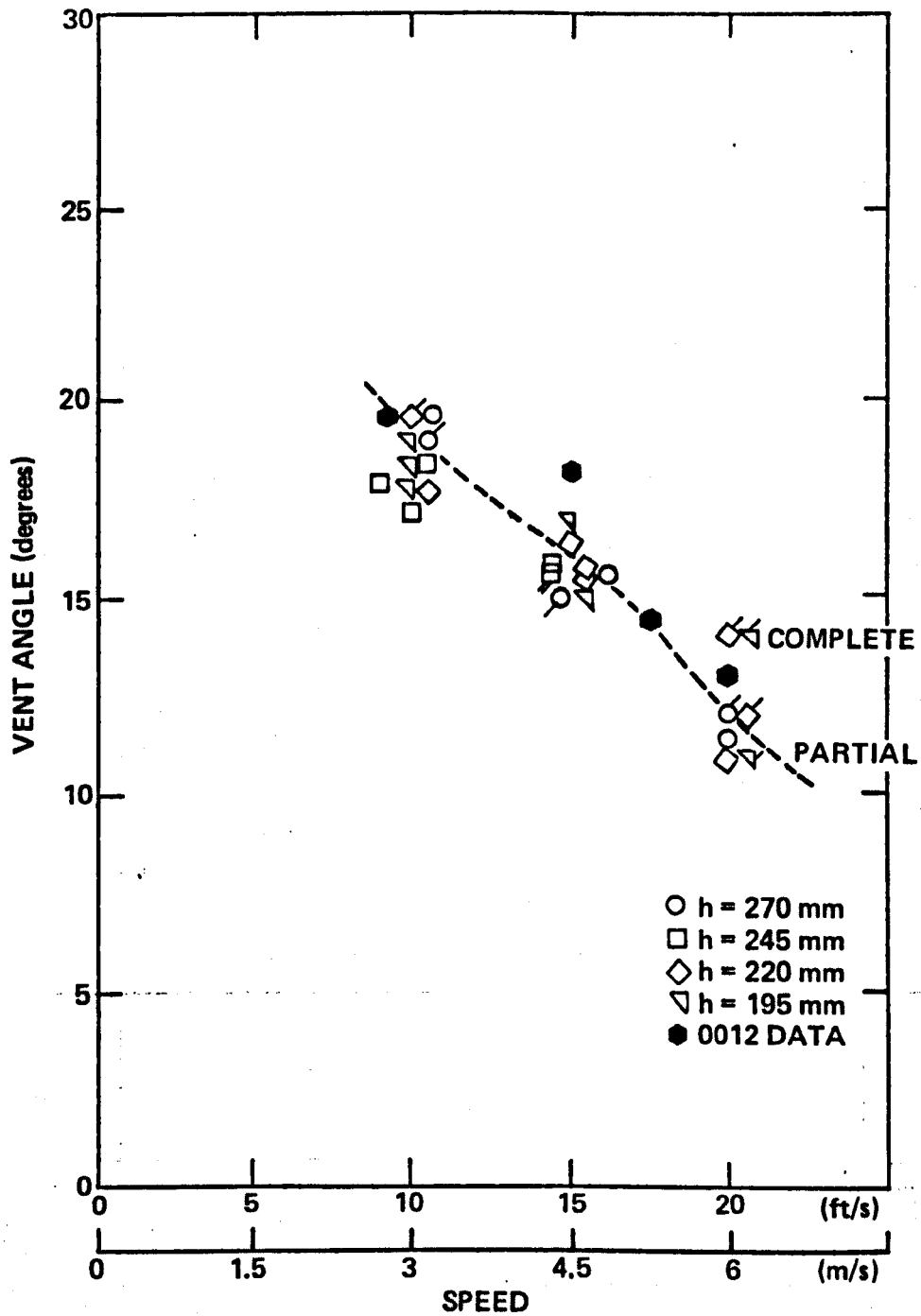
Figure 9.38 — Ventilation Angle Versus Speed For NACA 16 021 Foil With 11
Grade Microsphere Roughness Applied.

289
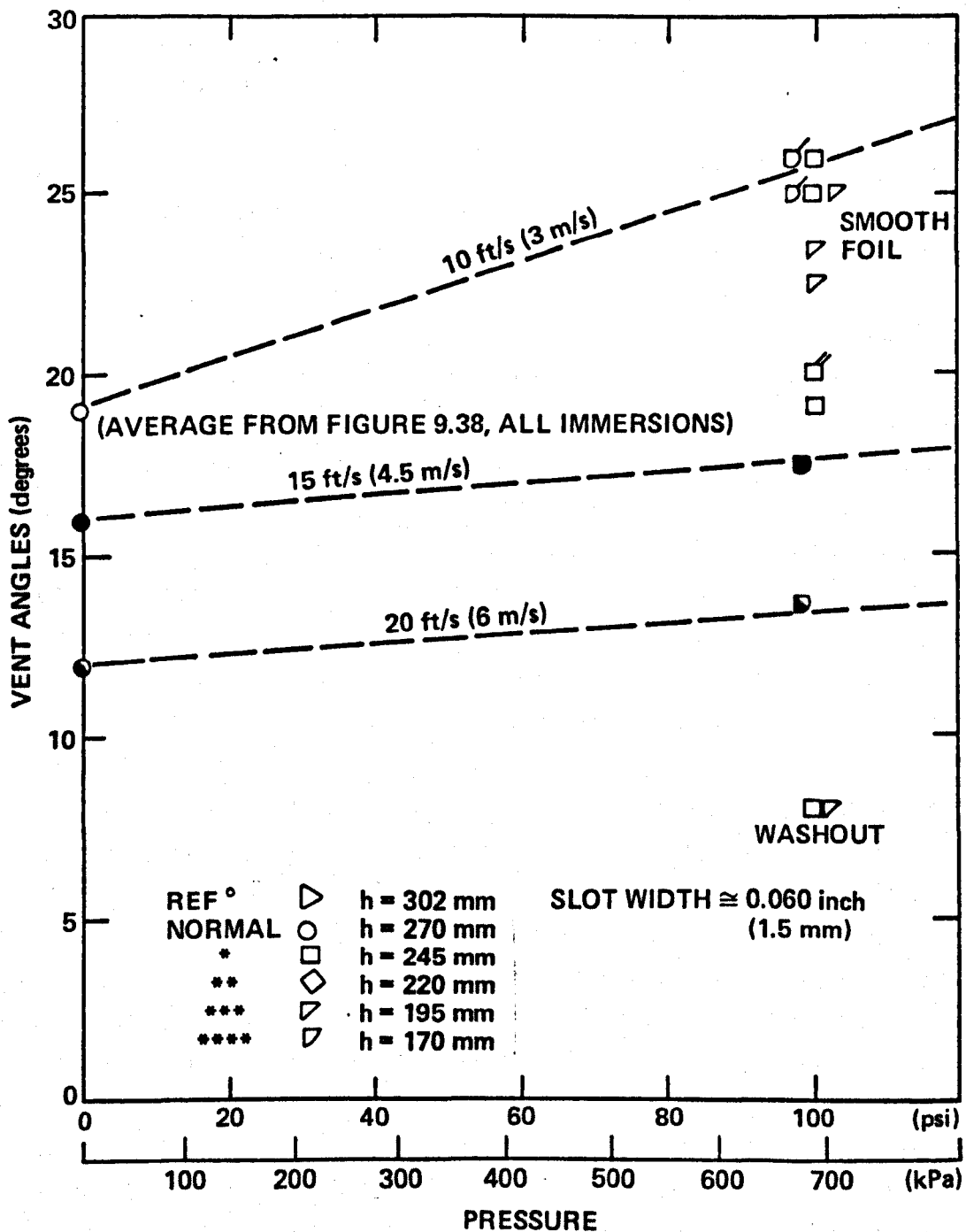
Figure 9.39 — Ventilation Angle Versus Blowing Reservoir Pressure, NACA 16 021 Foil With Shortened, Wide Slots, With Roughness.

Compared to the plain strut and the smooth blown strut, a strong dependence of inception angle on immersion depth is evident from the data collected at 10 ft/s (3 m/s). Also, the improvement in ventilation angle is reduced to one or two degrees at speeds of 15 and 20 ft/s (4.5 and 6 m/s). These two tendencies, coupled with the prior observation that the jet flow velocity increased appreciably nearer the strut bottom, indicate that the blowing momentum or velocity was marginally effective in overcoming the tendency to separate, and then only when the high velocity portion of the jet flow was brought sufficiently close to the free surface, and the channel flow was not too fast in comparison.

Figure 9.40 shows the flow through the slots of the roughened model out of the water with 100 psi (690 kPa) reservoir pressure. Comparing this with Figure 9.36, which similarly shows the smooth model, the flow appears faster through the roughened slots. Probably, this is due to the blockage effect of the microspheres at the slot exit. The sheet of water flowing from the slots appears scarcely less uniform than in the smooth case.

Figure 9.41 shows a sequence of photographs taken of the flow and the oil smear pattern generated by the roughened strut. No evidence of separation can be found in the oil smear pattern up to 25 or 26 degrees. Then, ventilation was preceded by the distinct appearance of leading edge separation. Referring to the below-water photographs, no significant bubble entrainment occurred prior to 22 degrees, in great contrast to all previous tests with roughened models.

The characteristic persistence of the ventilated cavity in the presence of roughness was noted. Figure 9.42 is a photograph of a double sub-surface vent at +5 degrees which persisted until washout at −2 degrees in spite of continuous blowing. Subsurface vents are typically observed on prototype craft, but not generally on smooth models. The general effect of blowing was to induce closure of the ventilated cavity at higher sideslip angles than normally expected, although without a high degree of consistency.

The implications of the roughness-with-blowing experiment are significant. Chapter 5 showed that the effect of roughness alone tends to supplant surface instabilities as the mechanism which breaks down the surface seal. Both increasing roughness and higher speeds encourage the breakdown of the surface seal farther forward. In Chapter 5, it was left open whether roughness encouraged premature ventilation by providing small air pathways, or by generating turbulent flow with associated mixing. The latter explanation was favoured as accounting for both a threshold effect and an incremental effect observed with increasing roughness. The smooth nature of the slot flux over the roughened surface undoubtedly contributed to the suppression of the roughness effect, insofar as the effect is related to disorderly or turbulent flow generation. However, the slot flux would have no effect on possible microscopic air passages between roughness elements. This suggests that the turbulence hypothesis is the correct one.
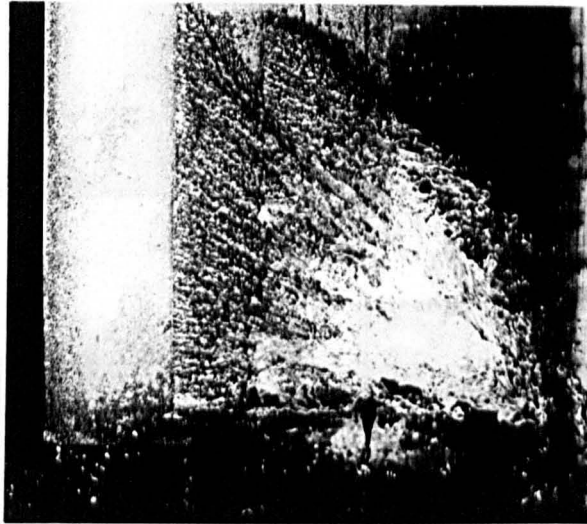
Figure 9.40 – Flow From Slots in Air, NACA 16 021 Foil With Shortened,
Wide Slots, With Roughness, 100 psi (700 kPa) Blowing.
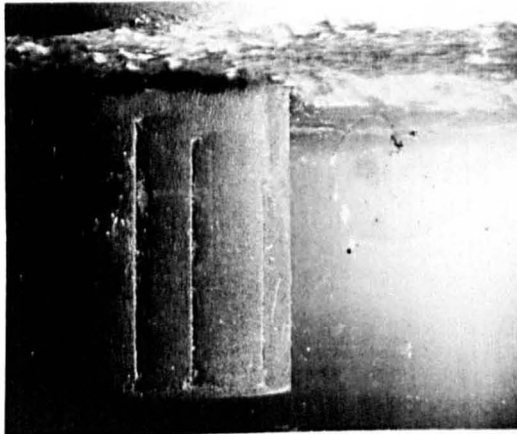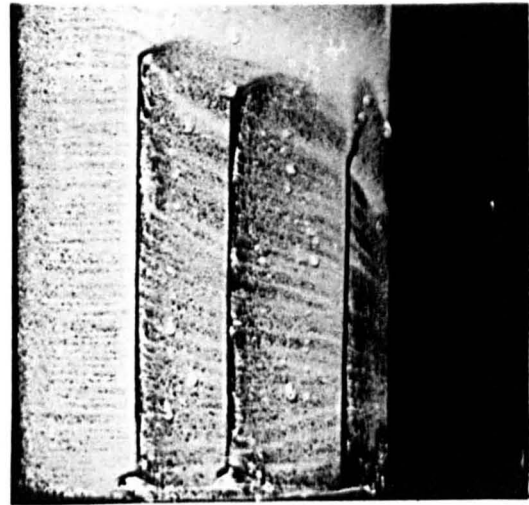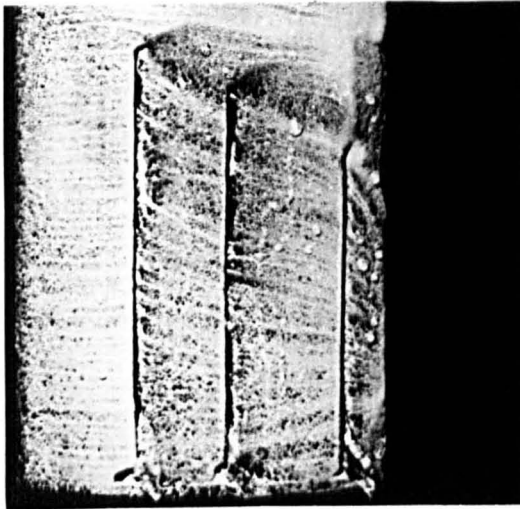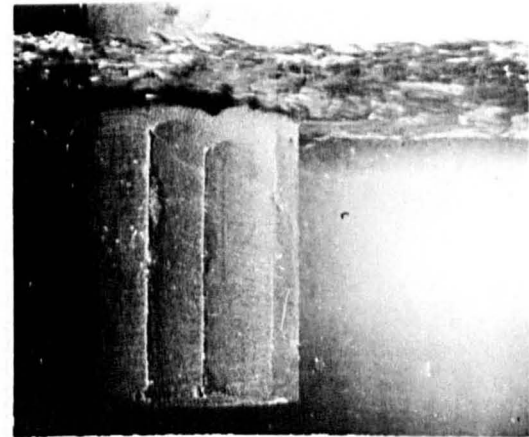
β = 0 Degrees β = 5 Degrees

Figure 9.41a — NACA 16021 Foil with Shortened, Wide Slots,
with Roughness, 100 psi (700 kPa) Blowing,
170 mm Immersion, 10 ft/s (3 m/s).

293
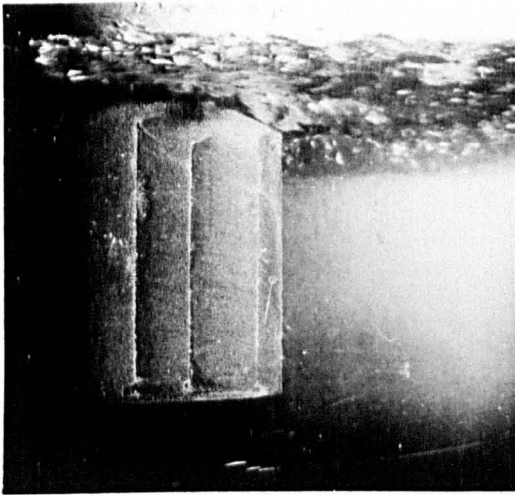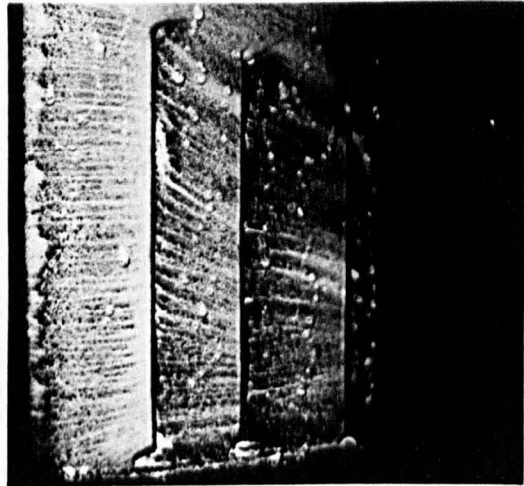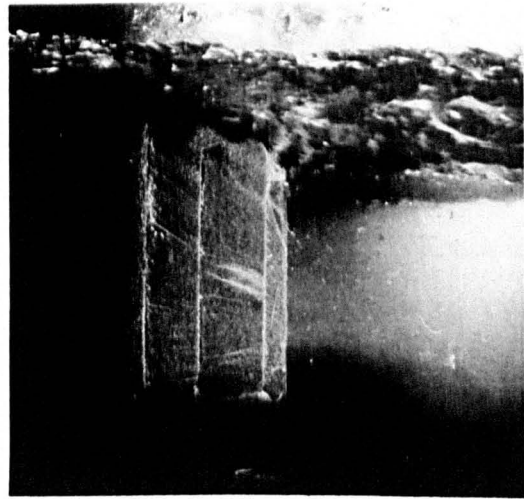
$\beta = 10$ Degrees $\beta = 15$ Degrees

Figure 9.41b

294
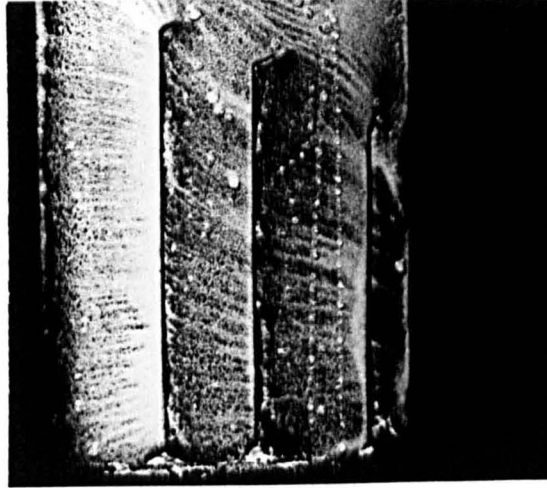
β = 20 Degrees
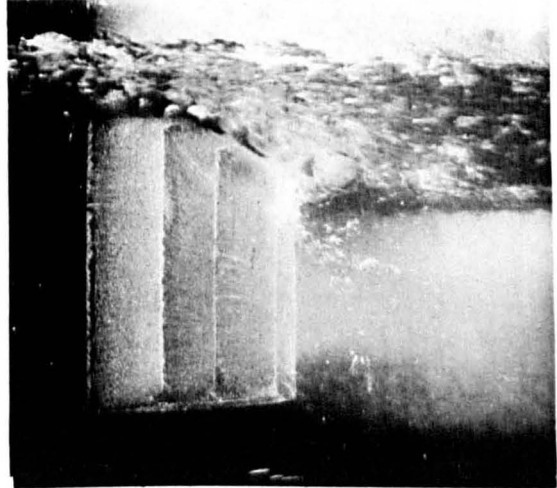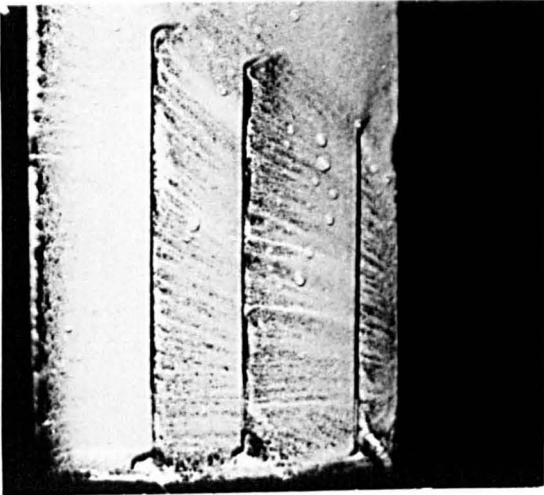
β = 22 Degrees

Figure 9.41c
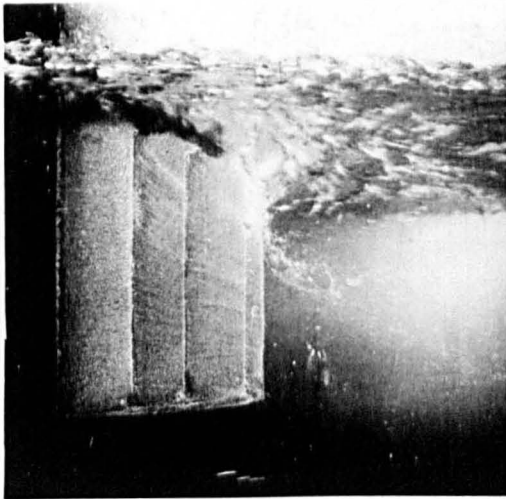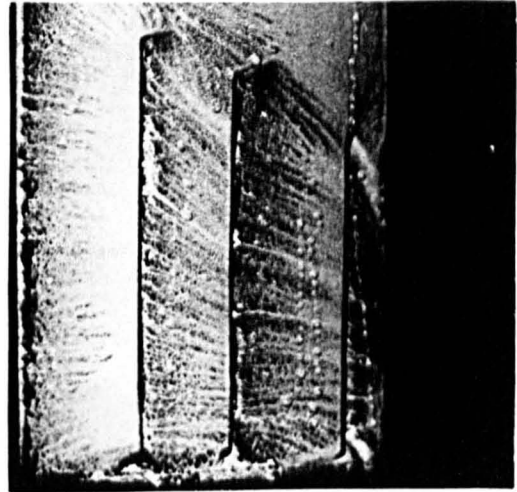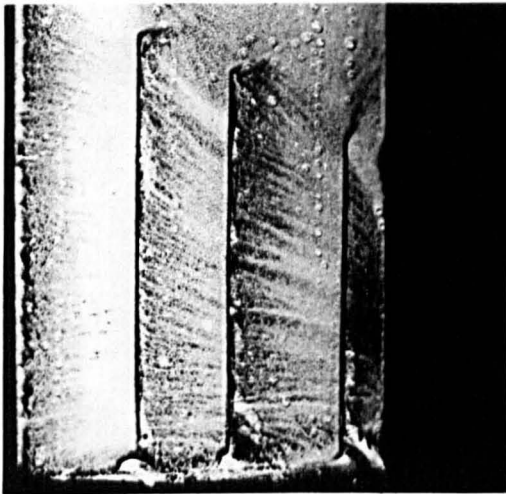
$\beta = 23$ Degrees $\qquad\qquad\qquad\qquad \beta = 24$ Degrees

Figure 9.41d
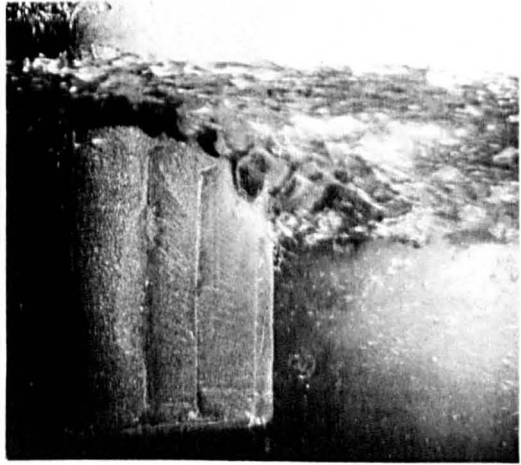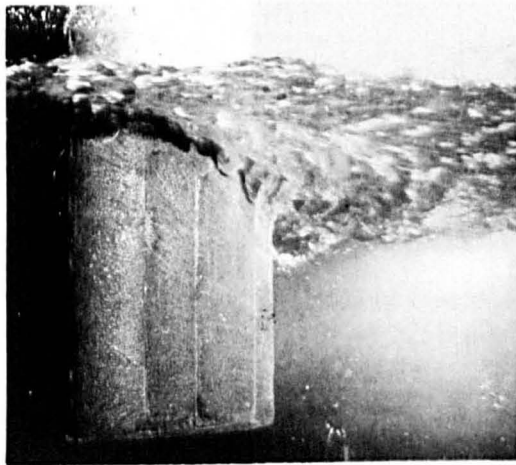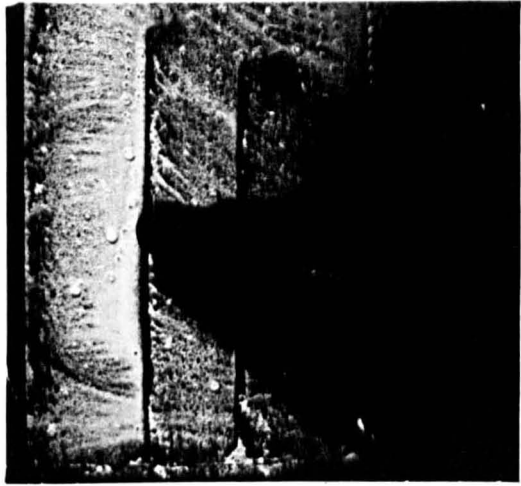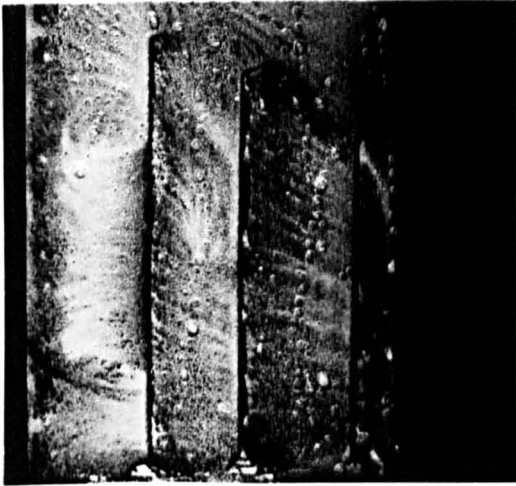
$\beta = 25$ Degrees $\beta = 26$ Degrees

Figure 9.41e

297
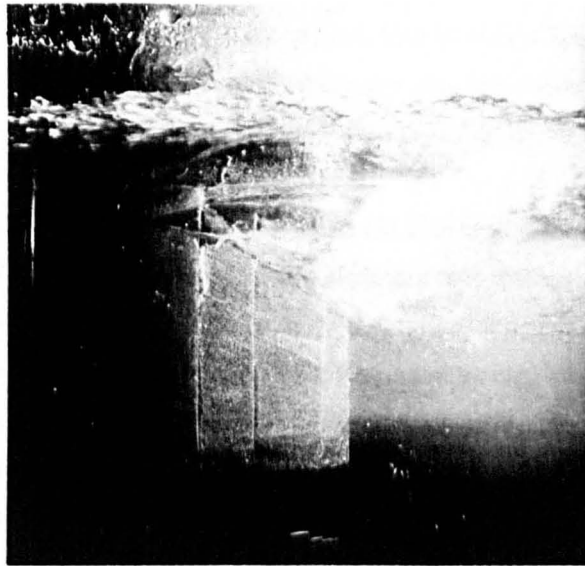
Figure 9.42 – Example of Double Subsurface Ventilated Cavity. Roughened NACA 16 021 Foil, 100 psi (700 kPa) Blowing, 10 ft/s (3m/s), β = 5 Degrees.

If the analogy of speed and size with roughness effect is correct with respect to ventilation, then the technique of blowing to retard ventilation inception could be more effective in increasing the inception angle at prototype speeds and sizes than at model scale. There is no reason to believe that it would not be possible to increase the lift or sideforce which prototype hydrofoils may sustain prior to ventilation. Of course, the problem of vapour cavitation has not been addressed, but there are still many applications for which vapour cavitation would not be a significant factor. In addition, the results of Baily[27] indicate that blowing may be possible and useful even in a cavitating environment.

Comparison with Predicted Jet Momentum. Calculating momentum flux from jet slots is difficult because it requires knowledge of the velocity and mass flux, or the pressure, mass flux and exact slot dimensions. Because of distortions of the model, and pressure losses in the supply system, the only parameter known with any degree of assurance was the volume flux corresponding to a particular supply pressure. Within the scope of the experimental objectives, the effort to acquire the additional information was not justifiable.

However, a reasonable approximation can be made if it is assumed that the flow through the slots was uniform, and that the dimensions of the slots did not change under pressure. For the long, narrow-slotted Mk I Model with three slots of 0.5mm width and 298mm (2.3c) length, $A_j = 149mm^2$. Expressed in terms of proportion of planform area, $A = 2.3c^2$, then $A_j = 0.012A$. The flux as given in Figure 9.7 for 70 psig (480 kPa) blowing, the lowest ratio for which separation was effectively eliminated, was 0.05 ft^3/s(1.4 x 10^{-3}m^3/s). This resulted in a value of V_j/U_∞ of just greater than 1.0. The corresponding value of momentum coefficient was

$$C_\mu = 0.024$$

This was nearly equal to that predicted, within the range of experimental error.

CONCLUSIONS

It is possible to increase the ventilation inception angle of a surface piercing strut which normally experiences tail ventilation by eliminating the region of separation with tangential slot blowing.

Ventilation occurred when leading edge separation was imminent. The maximum benefit was obtained by blowing near the free surface and ignoring sub-surface separation.

Blowing to increase the ventilation sideforce bound was more effective in proportionate improvement than blowing to increase inception angle.

Blowing was more effective in improving ventilation angle bounds for a roughened strut, which may reflect prototype conditions more accurately than a smooth model.

The analogy between blowing to increase lift on elliptic cylinders and blowing to prevent separation on aerofoil shapes was adequate to make good predictions of the momentum coefficient required to delay ventilation to a given angle and speed.

9.1   Wright, A.J., and McGregor, R.C., *"DREA Hydrofoil Project Interim Report,"* University of Leeds Dept. of Mech. E. Rept. TP/DREA/4, Mar 1972.

9.2   Wright, A.J., McGregor, R.C., and Swales, P.D., *"Time Dependency of Ventilation,"* Hovering Craft and Hydrofoils, Vol. 12, No. 9, 1973.

9.3   Ward, Kenneth E., and Land, Norman S., *"Preliminary Tests in the NACA Tank to Investigate the Fundamental Characteristics of Hydrofoil,"* NACA Wartime Report L-766, originally issued as ACR, Sep 1940.

9.4   Gartshore, I.S., and Newman, B.G., *"The Turbulent Wall Jet in an Arbitrary Pressure Gradient,"* Aero. Quart.,Vol. XX, Part 1, Feb 1969.

9.5   Kind, R.J., and Maull, D.J., *"An Experimental Investigation of a Low Speed Circulation Control Aerofoil,"* Aero. Quart., Vol. XIX, Part II, May 1968.

9.6   Kind, R.J., *"A Calculation Method for Circulation Control by Tangential Blowing Around a Bluff Trailing Edge,"* Aero. Quart., Vol. XIX, pp. 205 - 223, continued under same title in Trans. Canadian Aero. & S. Inst., Vol. IV, No. 2, Sep 1971.

9.7   Wyganski, I., and Newman, B.G., *"The Effect of Jet Entrainment on Lift and Moment for a Thin Airfoil with Blowing,"* Aero. Quart., Vol. XV, Part 2, May 1964.

9.8   Williams, Robert M., and Howe, H.J., *"Two Dimensional Subsonic Wind Tunnel Tests on a 20 Percent Thick, 5 Percent Cambered Circulation Control Airfoil,"* NSRDC Tech. Note AL 176, AD 877-764, Aug 1970.

9.9   Anon., *"Study of Variable Deflection Thruster for Hydrofoil Applications,"* Honeywell doc. 6DF22, no date.

9.10   Cheeseman, I.C., and Seed, A.R., *"The Application of Circulation Control by Blowing to Helicopter Rotors,"* Jour. Aero. Sci., Vol. 71, No. 679, p. 451 ff, Jul 1967.

9.11   Cheeseman, I.C., *"Circulation Control and its Application to Stopped Rotor Aircraft,"* J.R.A.S., Jul 1968.

9.12   Dunham, J., *"A Theory of Circulation Control by Slot Blowing Applied to a Circular Cylinder,"* J.F.M., Vol. 33, Part 3, pp. 495 - 514, 1968.

9.13   Englar, R.J., *"Investigation into and Application of the High Velocity Circulation Control Wall Jet for High Lift and Drag Generation of STOL Aircraft,"* AIAA Seventh Fluid and Plasma Dynamics Conference, Palo Alto, California, Jun 1974.

9.14   Englar, R.J., *"Subsonic Wind Tunnel Investigation of the Lift Capability of a Circulation Controlled Wing on a T-2C Aircraft Model,"* NSRDC TN AL-299, May 1973.

9.15   Dinh, Nguyen Ngoc, *"Some Experiments on a Supercavitating Hydrofoil with Jet Flap,"* J. Sh. Res., Vol. 13, No. 3, pp. 207-219, Apr 1969.

9.16 Englar, R.J., *"Experimental Investigation of the High Velocity Coanda Wall Jet Applied to Bluff Trailing Edge Circulation Control Airfoils,"* DTNSRDC A&SE Dept. TN AL-308, Jun 1973.

9.17 Englar, R.J., and Williams, R.M., *"Design of a Circulation Control Stern Plane for Submarine Application,"* DTNSRDC A&SE Dept. TN AL-200, Mar 1971.

9.18 Englar, R.J., *"Two Dimensional Subsonic Wind Tunnel Test of Two 15 Percent Thick Circulation Control Airfoils,"* DTNSRDC A&SE Dept. TN AL-211, Aug 1971.

9.19 Englar, R.J., *"Two Dimensional Transonic Wind Tunnel Tests of Three 15 Percent Thick Circulation Control Airfoils,"* DTNSRDC A&SE Dept. TN AL-182, 1970.

9.20 Englar, R.J., *"Two Dimensional Subsonic Wind Tunnel Tests of a 30 Percent Thick Cambered 30 Percent Thick Circulation Control Airfoil,"* DTNSRDC A&SE TN AL-201, May 1972.

9.21 English, et al, *"Some Manoeuvring Devices for Use at Low Ship Speed,"* NPL Ship Div. Rept. 163, Mar 1972.

9.22 Kaplan, P., and Goodman, T.R., *"Use of Jet Flapped Hydrofoils as Ship Anti-Pitching Fins,"* Oceanics, Inc., AD 604 011, Jul 1964.

9.23 Lacy and Hemmerly, *"A Preliminary Evaluation of the Low Speed Performance and Handling Quality of a T-2C Aircraft Modified with a Circulation Control Flap System,"* NSRDC Rept. ASED 318, Mar 1974.

9.24 Lachmann, G.V., (ed), *"Boundary Layer and Flow Control,"* Pergamon, 1961.

9.25 Walters, Myer and Holt, *"Circulation Control by Steady and Pulsed Blowing from a Cambered Elliptical Airfoil,"* W. Va. Univ. Dept of A.E., Jul 1974 (ONR Contract N00014-68-A-0512)

9.26 Wright, A.J., and McGregor, R.C., *"DREA Hydrofoil Project Interim Report,"* University of Leeds Dept. of Mech. E. Rept. TP/DREA/4, Mar 1972.

9.27 Franklin, R.E., and Bailey, A.B., *"Preliminary Experiment on a Jet Flapped Hydrofoil,"* Oxford University, 1974.

CHAPTER 10

USE OF A LIQUID FENCE
TO SUPRESS VENTILATION

INTRODUCTION

Background of Fences as a Practical Means of Ventilation Control. Besides surface piercing hydrofoils and struts, the problem of ventilation, or air ingestion, arises elsewhere in marine engineering. For example, air may be drawn down surface piercing shaft housings to propellors or rudders. If ventilation is a problem, a natural attempt at a solution is imposition of a solid barrier between the atmosphere above the water surface, and the submerged or semisubmerged affected appendage. Thus, in the case of the outboard motor, there is a "cavitation" plate between the propeller and the water surface. For purposes of this discussion, such devices will be identified generally as "fences." Von Schertel made use of fences in his early struggle with the ventilation problem, and they may still be seen on Supramar and many other hydrofoil boats. Even hydrofoil craft which use fully submerged foils may require the addition of fences to avoid ventilation problems on surface piercing supporting struts. It is interesting that, in spite of their obvious and practical applicability to ventilation problems, prior to the University of Leeds work, no systematic investigation of the properties of fences was to be found.

Leeds Fence Studies. McGregor et al[10.1] established some rudimentary properties of fences in experiments on vertical, surface piercing struts in the Leeds Channel. One of the more significant results was the determination of the size of fence required to inhibit tail ventilation: a small fence sufficed to prevent nose ventilation but comparatively great breadth was required to affect tail ventilation other than adversely. Figure 10.1 shows a typical fence which was effective against tail ventilation.

Besides the excessive breadth which was required to prevent tail ventilation, it was also found that the fence had to be inclined to the horizontal at an angle of 30 degrees. Otherwise, the vorticity generated by the non-alignment of the fence with the local flow allowed air to curl around the edges of the fence. In spite of the seemingly radical alterations to the strut appearance, it was difficult to increase the ventilation inception angle by more than a few degrees for struts which were susceptible to tail ventilation.

As might be expected, the drag associated with the large, wedge-shaped fences was large, amounting to two or three times the zero sideslip drag of the unfenced strut.

It is not clear what the fence study implied concerning full scale applications, and the investigators specifically disclaimed any attempt to extrapolate their findings. Evidence exists, that with increased size or speed, certain aspects of the ventilation mechanism are altered in such a way as to be more amenable to interdiction by fences. For example, in Chapters 5 and 6 it was suggested that the point of inception of ventilation moves forward with increasing speed or roughness. This would have a significant influence on the usefulness of a fence.

304
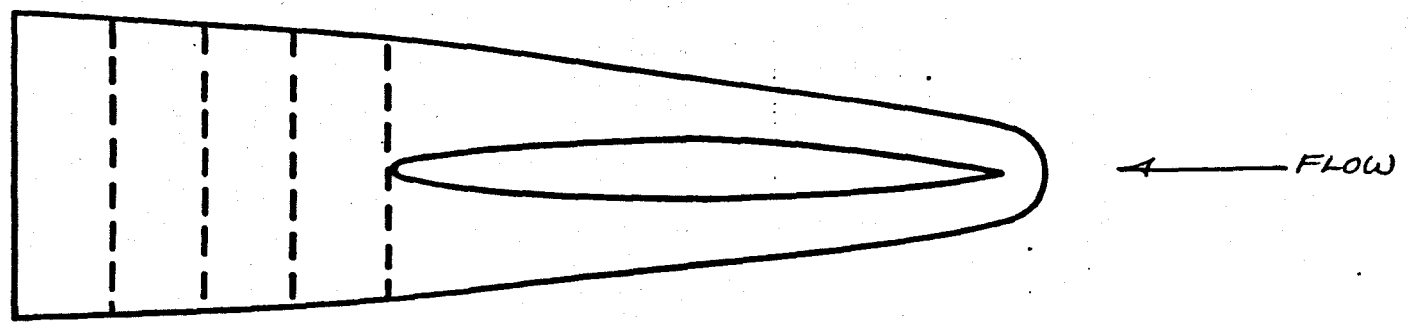
Figure 10.1 — **Proportions of Typical Fence Found Effective Against Tail Ventilation. From McGregor et al[1].**

Whatever the modifications to the fence study conclusions might be at full scale, it is certainly true that in many cases, the addition of even conventional solid fences to surface piercing strut and foils systems could have serious drawbacks. Besides the obvious ones, such as high drag and poor flow characteristics, there is occasionally a requirement for retractability.

Liquid Fence. Therefore, as part of a comprehensive exploration of methods of control of ventilation, an investigation was planned of a device which would retain the intuitively attractive and simple feature of preventing ventilation by barring air paths, while perhaps eliminating some of the objections associated with conventional fences and, especially, the very broad fences developed in the Leeds studies. A horizontally ejected jet of water which would form a uniform sheet was proposed as being analogous to a solid fence, in much the same way that a jet flap is analogous to a conventional flap.

The momentum of the jet would prevent the ingress of air, while at the same time allowing the flow around the strut to assume its natural contours to the greatest extent possible. This would reduce the tendency toward separation and cavitation engendered by conventional fences and cause the least degradation of the properties of the bare strut or foil. Such a device, a liquid fence, would also interfere least with the mechanical properties of struts or foils, and, in particular, would allow the desirable capability of retraction into the hull.

Ideally, a liquid fence could also be turned off or on as the occasion demanded, as, "on" during manoeuvres or in heavy seas, or "off" in straight ahead, cruise conditions in light weather. Generally, conventional fences are used in stacks to account for variation in submergence of the strut-foil system due to differing operating requirements. With liquid fences, it would be possible to turn off unnecessary fences in the stack with consequent savings in drag.

OBJECT OF THE EXPERIMENT

The experimental objective was straighforward and limited: to determine whether a horizontally ejected jet of water would behave similarly to a solid fence in suppressing ventilation at model scale speeds and sizes, and to make observations and measurements which would aid in interpretation of the results and in defining possible limitations on their extrapolation to full scale.

METHOD AND APPROACH

Choice of Model Size and Section. The NACA 16-021 section with 127mm chord at a nominal submergence of two chord lengths was chosen for the reasons described in the previous chapter. Specifically, the section exhibits:

1. Well behaved and defined ventilation characteristics
2. Tail separation and tail mode ventilation only
3. Sufficient thickness for internal water ducting
4. Applicability to full scale craft

The 16-021 planform and section is shown in Figure 10.2 as modified for the liquid fence.

Choice of Test Speed. The factors which influenced the choice of test speed were the same as those which were important in determining the test speed for the boundary layer blowing experiment of the previous chapter. It was felt that the lowest speed which satisfied those requirements would reduce the necessary momentum of the liquid fence jet. A speed of 3 metres/second was chosen as being above lowest at which complete ventilation would occur. It was also a speed free from time dependent ventilation effects, free of anomalous separation effects, and relatively free from the effects of air entrainment in the Water Channel. Some exploratory runs were conducted at 4.5 and 9 m/s to ascertain whether speed effects were being overlooked. These speeds were also included in the series of experiments in which the strut surface was roughened with glass microspheres. In this case, increased speed had a pronounced effect.

Flow Visualisation and Photography. Photographs of the ultraviolet illuminated oil smear flow visualisation pattern were taken in conjunction with photographs of the flow during the run using stroboscopic lighting as described in the preceding two chapters. These photographs illustrated the important features of the flow, such as the area of fence breakdown and the extent of separation.

EXPERIMENTAL APPARATUS

The experimental equipment used in the Free Surface Water Channel for providing high pressure jet water, immersing and removing the model, acquiring the proper sideslip angle and taking photographs was identical to that of the previous chapter.

The Mk II Model shown in Figure 10.2 was used in the experiment of the previous chapter with its blowing slots filled in, as a control. As previously described, the model was filled from

0.6c

0.2c
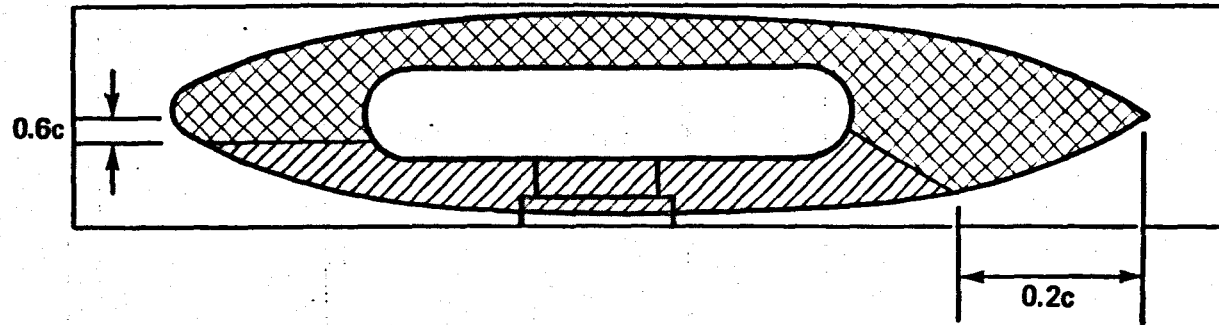
Figure 10.2 –   NACA 16 021 Section and Planform as Modified for Horizontal Slot Blowing.
Chordlength 127mm, Slot Width 0.8mm, Design Submergence 2.0c.

phosphorbronze using a profiled milling cutter. The chord length was 127 mm and the profile was maintained for 3 chord lengths from the strut tip. An 0.8 mm slot was cut perpendicular to the plane of symmetry of the strut, across the chord, forming an angle of 20 degrees with the horizontal as shown in Figure 10.2. The cut was made through the port side (normally low pressure) and intersected the interior plenum through which was supplied the high pressure water. The slot was cut through slightly to the starboard side at the nose, and at the tail extended forward 5 percent of the chord length. The intersection of the slot with the leading edge was about 1½ chord lengths from the strut tip. Slightly above the first slot, a second was cut at an angle of 10 degrees with the horizontal. This slot was filled with epoxy and smoothed to the contours of the strut. It was intended to be used contingent upon results of the 20 degree slot. Modifications made to the 20 degree slot added to the complexity of the model so that the 10 degree slot was never utilised.

The modifications were made when it was observed that the majority of the flow excited from the 20 degree slot at the midchord section, "starving" the fence at the nose and tail. To reduce this tendency, a flow guide was installed in the plenum to direct the flow toward the nose and tail at the expense of the midsection. When this did not prove satisfactory, the slot was enlarged to about 15 mm thickness, leaving the lower edge intact. A thin wall of epoxy approximately 1 mm thick was then moulded into the shape of the exterior, restoring the slot thickness to 0.8 mm. The effect was to enlarge the plenum so that only a very thin wall separated the plenum from the exterior, in the hope that the pressure drop across the slot would then be fairly constant around the perimeter, equalising the flow. This scheme was moderately successful, except that the momentum was lower at the tail than elsewhere. To correct this, the slot at the tail was enlarged slightly. The flow was still weaker at the tail, but further modification was not possible. In retrospect, it seems that attempting to match the momentum flux density emanating from a pointed tail (point-source) with that emanating from a plane surface was inherently hopeless.

The model was later modified by the application of glass microsphere roughness as described in the previous chapter and in Chapter 5.

EXPERIMENTAL PROCEDURE

The experimental procedure and techniques used were virtually the same as those described in the preceding chapter for the Mk I vertical slot model, including the use of suction through the blowing slots to refill the pressurised reservoir. The immersion depths were the same, ranging from 1.3 to 2.4 chord lengths in increments of approximately 0.2 chord. The main difference in experimental procedure was that, for the horizontal slot model, blowing was not started prior to

immersion. Generally, the strut was immersed to the required depth, blowing commenced, then the sideslip angle was acquired. As previously, the blowing pressure was set at the reservoir and the flow rate measured by timing the fall in the reservoir level. The various conditions are referenced to the reservoir pressure, rather than flow rate. Flow rate versus reservoir pressure is shown plotted in Figure 10.3 for the Mk II Model.

OUTLINE OF THE EXPERIMENT

The horizontal slot model was tested in three Series. In Series I, the reservoir pressure was limited to 15 psig (100 kPa) to protect the strut from damage in the early phases of the test. Series II was the test of the roughened strut, and the third Series extended the test of the smooth model to the maximum safe blowing pressure, 100 psig (700 kPa). Flow visualisation photographs were made for most runs.

Series I — Smooth Model, Low Blowing Pressure. The Mk II horizontal slot model was tested at 3 m/s in all Series I runs. The first runs were performed with three different internal baffles or flow guides and then with the trailing edge section of the slot opened slightly. The reservoir pressure was mostly 6 psig (40 kPa) and the immersion 302 mm (2.4 chords). Two runs were made at 6 m/s to ensure that there were no significant changes over the available speed range.

This was followed by a group of runs aimed at revealing the effect of immersion, which was varied from 195 mm to 302 mm, with 15 psig (100 kPa) blowing pressure. This sequence was repeated, adding a run with 170 mm immersion, but with 9 psig (60 kPa) blowing, and including some runs for which the internal baffles were removed. The baffles did not appear to have any effect, and so were removed for the remainder of the tests of the Mk II strut.

The final runs of Series I were performed with the slot partly taped to concentrate the jet flow afterwards.

Series II — Roughness. The microsphere-roughened Mk II Model was tested at 3, 4.5, and 6 m/s at immersions of 195 and 245 mm with reservoir pressures of 10, 15, 30, and 45 psig (70, 100, 205, and 310 kPa). It was also tested with the slot completely sealed to provide a reference base.

Series III — Smooth Model, High Blowing Pressure. For the final Series, the Mk II Model was tested with the roughness removed and reservoir pressures of 30 psig (205 kPa) at a speed of 3 m/s and immersion depths of 195 and 245 mm. For the 245 mm immersion, tests were conducted at 60 and 100 psig (410 and 675 kPa).

310

$$\text{FLOW (FT}^3\text{/S)} = \sqrt{\frac{\text{TANK PRESS} - 2.32\ \text{PSI}}{30400}} \quad \text{(SOLID LINE)}$$

SLOT 67% BLOCKED
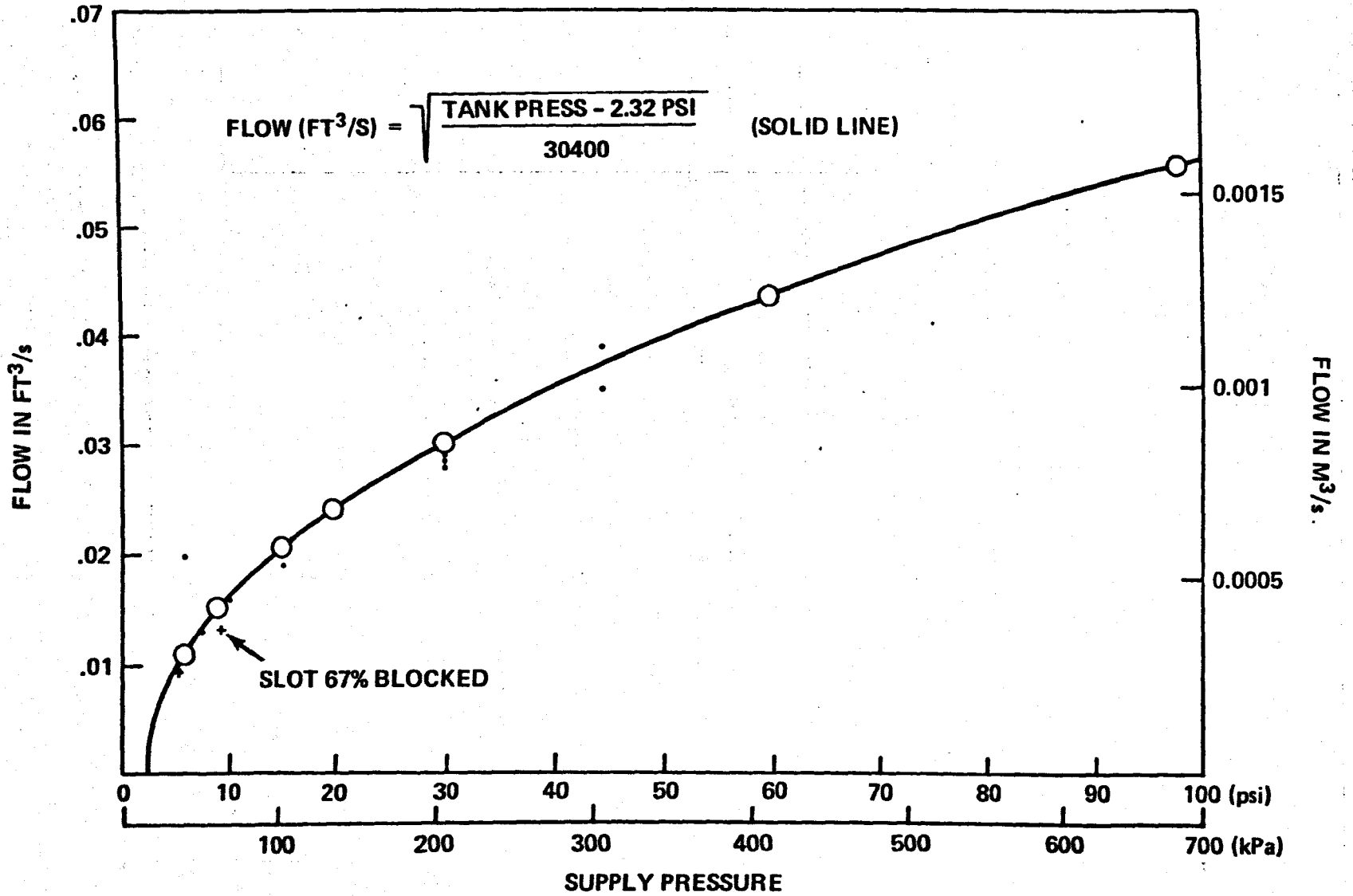
Figure 10.3 — Flow in Slots Versus Reservoir Pressure.

311

RESULTS AND DISCUSSION

Series I — Smooth Model, Low Pressure. Figure 10.4 shows the ventilation inception and washout angles plotted versus blowing pressure for the Mk II horizontal slot model for pressures up to 15 psig (100 kPa). Also included on the figure are the points obtained with the slot partially taped as shown in Figure 10.5. As can be seen from Figure 10.4, the liquid fence had hardly any positive influence on the ventilation inception boundary, although a trend toward improvement with increasing pressure may be noted. The tape was an attempt to concentrate more of the liquid fence flow aftward, where the breakdown seemed to be occurring. This met with no success, probably because the tape tended to pull away from the strut surface and directed the fence flow more downward than aft, entraining air into the separated region.

Although the experiment was not specifically designed to observe or study washout angle, it is interesting to note that the greatest effect of the liquid fence was to increase the washout angle with increasing fence pressure, particularly for the case of 302mm immersion. This is in agreement with the McGregor et al[10.1] observations. Solid fences did not improve the ventilation inception angles a great deal, but were often strikingly effective in increasing washout angles.

Observation revealed that the liquid fence replicated the water sheet which naturally precedes closure, at least as the situation existed in the Leeds Water Channel. This closure mechanism is more thoroughly described by McGregor, et al. It is interesting that, especially for the 302mm immersion, the mere existence of the horizontal slot encourages washout at higher angles than would "normally" occur. Washout on the plain strut under similar conditions was observed to occur at about 5 degrees, as was "complete" washout with the liquid fence in operation. However, washout from the tip to the height of the fence occurred at 11 degrees with no pressure applied to the fence. At 6 psig (41 kPa), the washout angle (to the fence) increased to 15 degrees. At 15 psig (100 kPa) washout increased to 17 degrees, while complete washout remained relatively constant, at about 5 or 6 degrees.

The slot with no forced flow emanating from it was able to increase washout angle by virtue of the ram head at the forward part of the slot. This created a sheet of water, encouraging closure over the after portion of the strut. The effect was similar to that observed in the suction slot experiment discussed in Chapter 8, whereby some suction took place due to the spanwise pressure gradient along the slot. In the present case, the pressure gradient and the slot were both parallel to the chord.

It would not be prudent to attach great significance to the effect of the liquid fence on washout angle. Firstly, the mechanism of washout observed at this scale was that of closure of the top of the ventilated cavity by a clear, uniform water sheet. It is highly doubtful that this
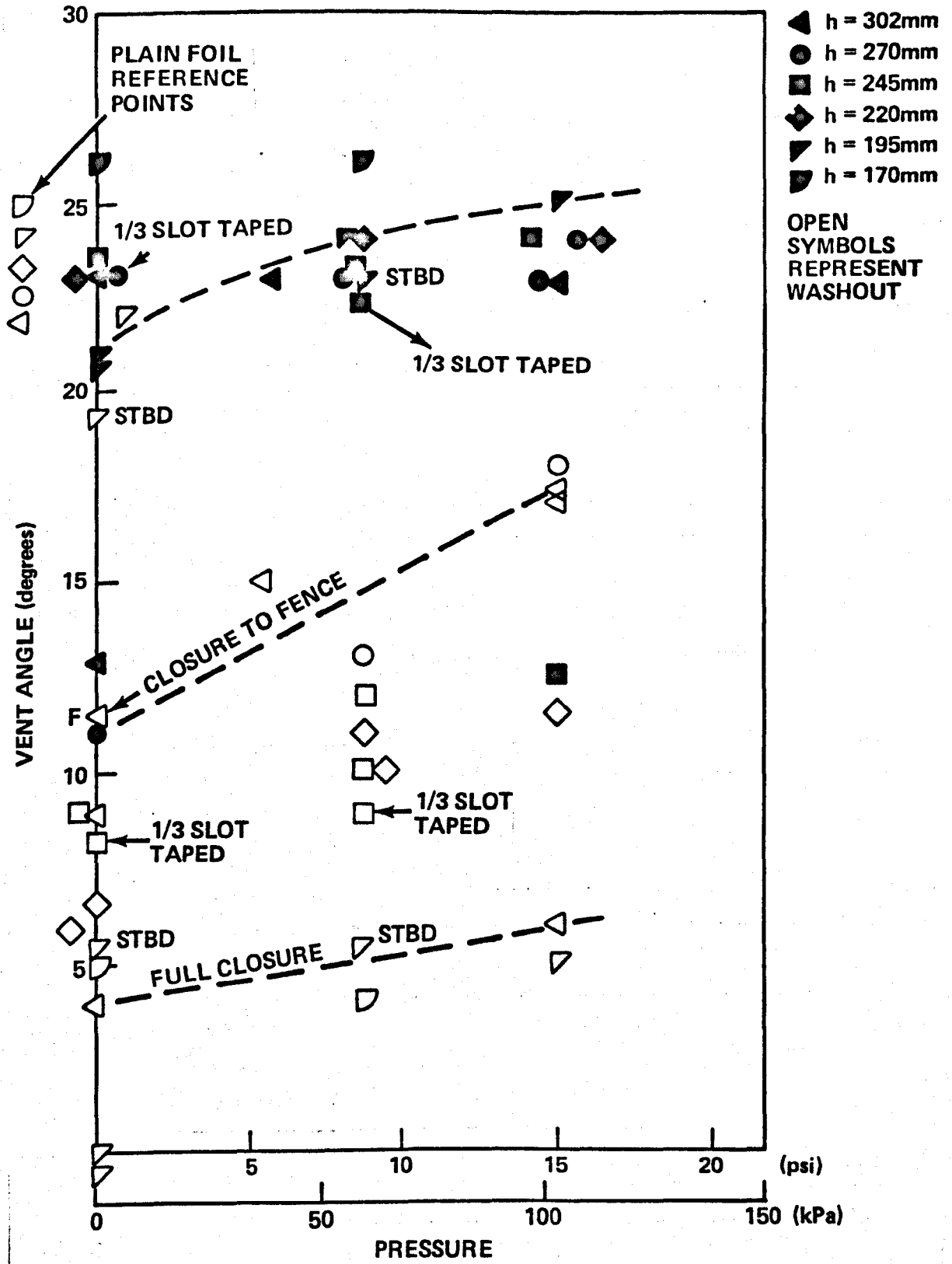
Figure 10.4 — Ventilation Angle Versus Reservoir Pressure, NACA 16 021 Foil With Horizontal Slot Blowing, 10 ft/s (3m/s).

313

Figure 10.5 – NACA 16 021 Horizontal Slot Model Partially Taped to Improve Rearword Slot Flow.

mechanism would be preserved at higher speeds and larger sizes, where such sheets would be unstable, coagulating into droplets which would not form a barrier to the cavity air supply. Secondly, the observations of Chapters 5 and 6 demonstrate that washout angle is extremely sensitive to roughness and speed, even at small scale. Therefore the results would be difficult to extrapolate, or even to duplicate.

Flow Visualisation. The photographs of the flow and oil smear patterns are helpful in interpreting and explaining the observed results. One of the most interesting pairs of photographs, taken of the strut at 302mm immersion with 6 psig (41 kPa) blowing at a speed of 3 m/s, is shown in Figure 10.6. Full separation from the leading edge was indicated by the oil smear pattern, while the flow is seen to have been completely wetted. A minor amount of air was entrained aft of the trailing edge. Such a complete separation had never been observed on an unmodified strut prior to ventilation. This implies that the liquid fence was effective in terms of the amount of separation that could be sustained prior to ventilation. Further insight is revealed in Figure 10.7 which shows a sequence of photographs taken at the same speed and immersion as previously, except that the fence was alternately blowing at 15 psig (100 kPa) or turned off as the sideslip angle was increased from 10 to 23 degrees. This sequence is fairly representative of most of the conditions tested in this Series. It will be noted that separation increased more rapidly with the water emerging than otherwise. At 20 degrees, the separation appears to be about 30 percent more extensive with the fence "on." This is probably related to the greater amount of surface drawdown which can be seen at the 20 degree angle with the fence "off." The fence has a flow-straightening effect which undoubtedly increased the pressure gradient, resulting in separation farther forward. Greater sideforces may also have been generated by the flow straightening.

The sequence shown in Figure 10.7 also shows the initial typical vent to the depth of the slot, observed whether or not the fence was turned on. Generally, the strut ventilated to the depth of the fence between 15 degrees and 20-22 degrees of sideslip.

Other photographs which illustrate the action of the liquid fence are shown in Figures 10.8 and 10.9. Figure 10.8 shows sub-surface ventilated cavities above the slot, at 10 degrees without blowing and at 15 degrees with blowing. Generally, the more deeply immersed configurations experienced first a sub-surface vent, followed by a full vent to the fence. Following the vent to the fence, the strut then behaved as if the immersion were shallower. Figure 10.9 shows a deep partial vent below the fence at 24 degrees, which the fence was preventing from growing to a full cavity, probably by limiting the cavity air supply.

Figure 10.10 is a sequence of photographs which particularly illustrates the mechanism of fence breakdown. These photos were taken with a fence pressure of 15 psig (100 kPa) and with

Figure 10.6 —   No Ventilation Despite Full Separation, NACA 16 021 With Horizontal Slot
Blowing, 6 psi (41 kPa), 10 ft/s (3m/s), Immersion 302mm.
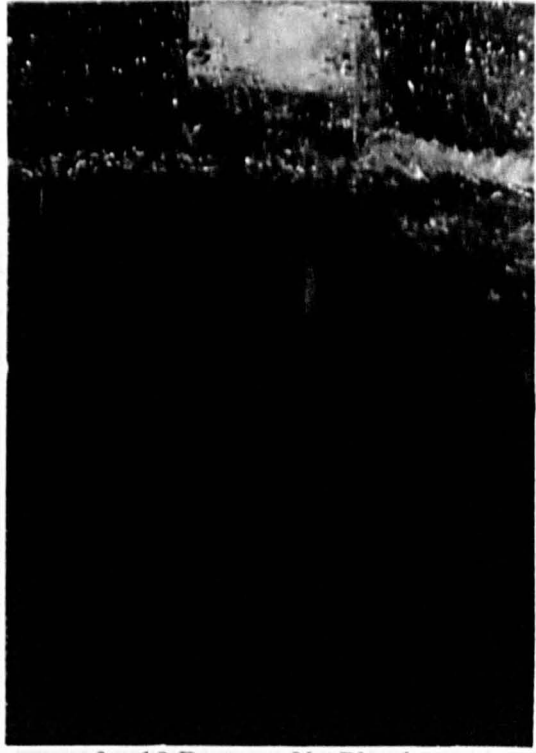
β = 10 Degrees, 15 psi (100 kPa) Blowing β = 10 Degrees, No Blowing

Figure 10.7a – Comparison of Blowing and Non-Blowing, NACA 16 021 With Horizontal Slot, 10 ft/s (3m/s), Immersion 302mm.

317
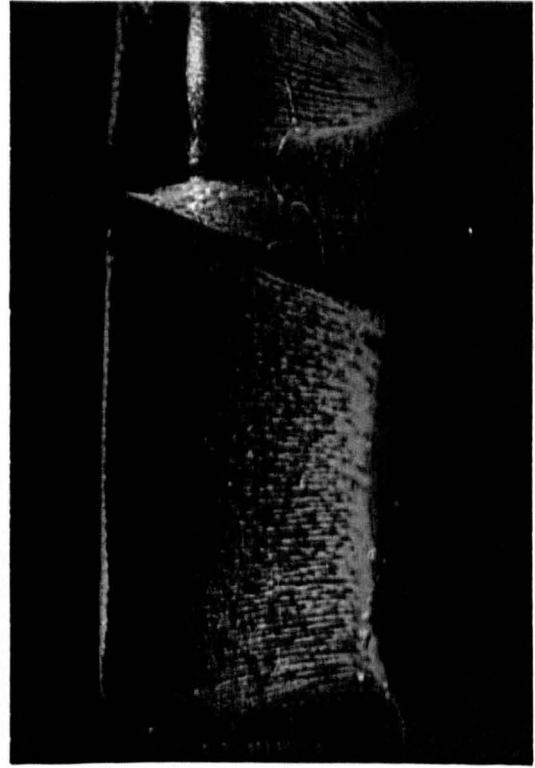
β = 15 Degrees, 15 psi (100 kPa) Blowing   β = 15 Degrees, No Blowing

Figure 10.7b
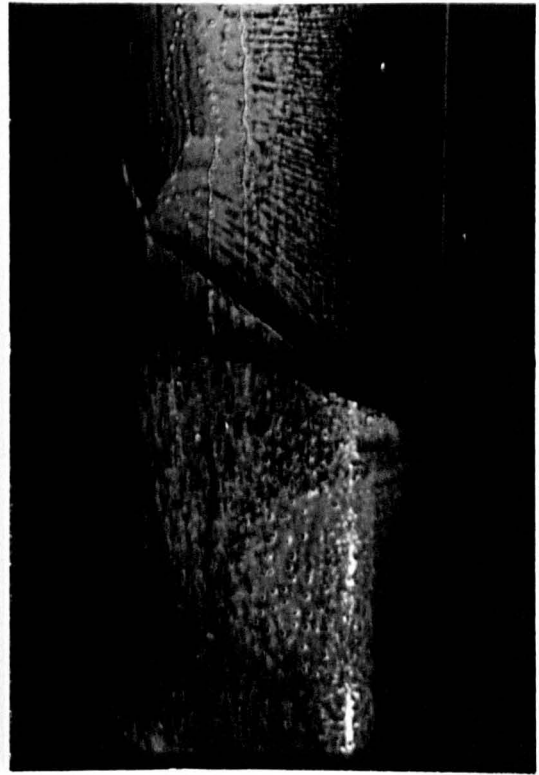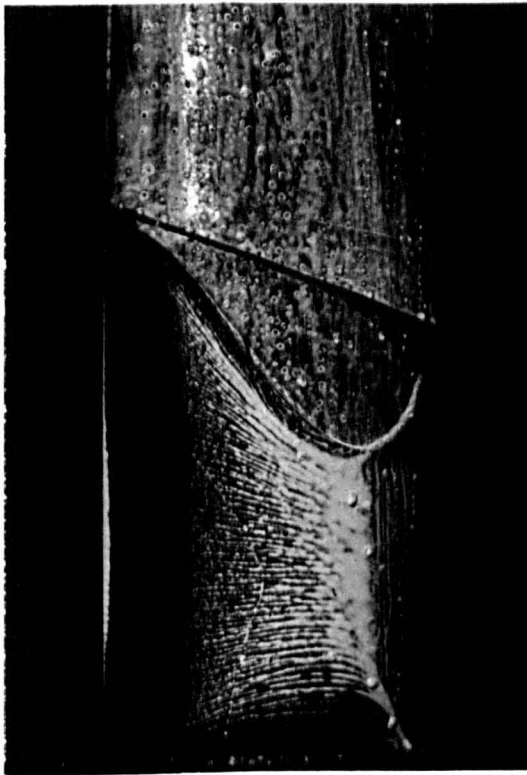
β = 20 Degrees, 15 psi (100 kPa) Blowing β = 20 Degrees, No Blowing

Figure 10.7c

319

β = 23 Degrees, 15 psi (100 kPa) Blowing
Vent Occurred Before Oil Pattern Developed.

Figure 10.7d

No Blowing

15 psi (41 kPa) Blowing

Figure 10.8 — Examples of Subsurface Ventilated Cavities Above the Slot, NACA 16 021 With Horizontal Slot, 10 ft/s (3m/s), Immersion 210mm, β = 15 Degrees.

321
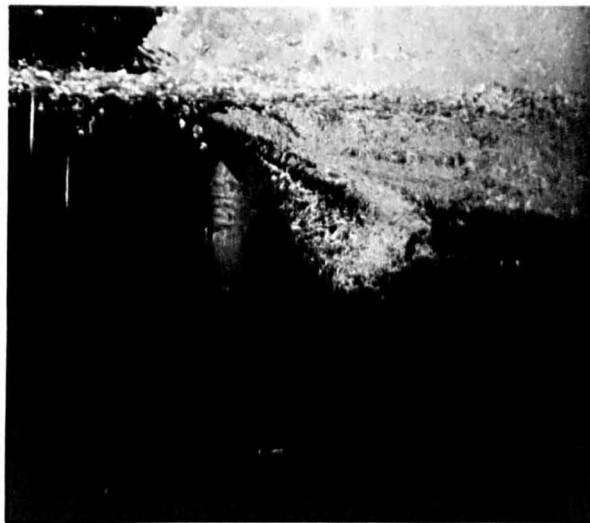
Figure 10.9 – Deep Partial Vent, NACA 16 021 With Horizontal Slot, 10 ft/s (3m/s), Immersion 195mm, β = 24 Degrees, 15 psi (100 kPa) Blowing.
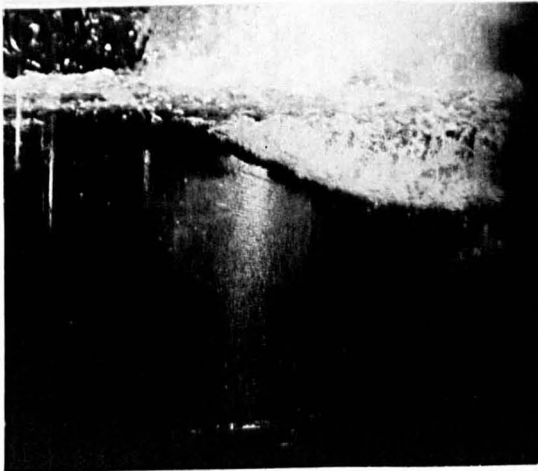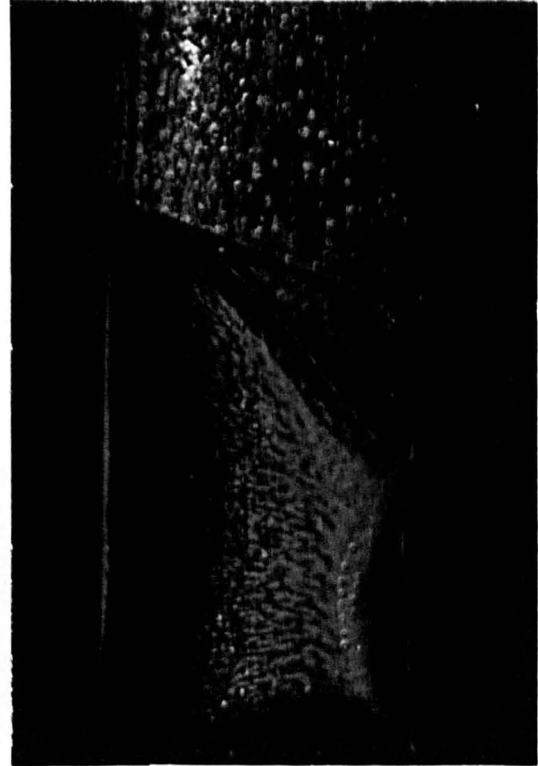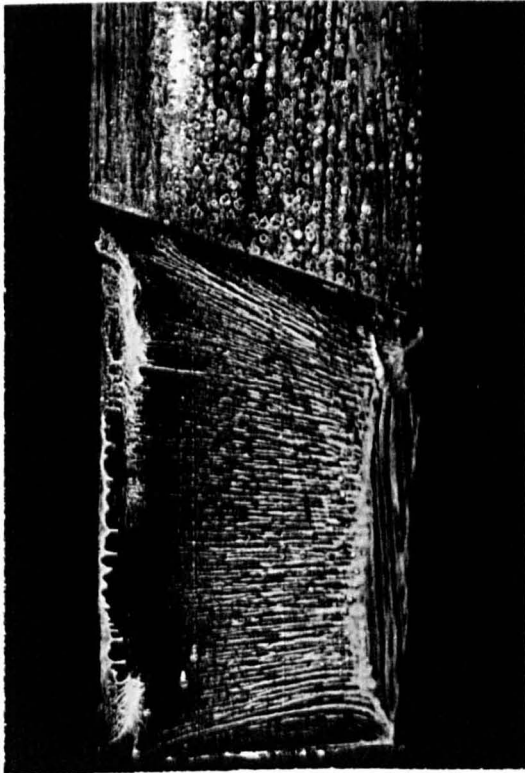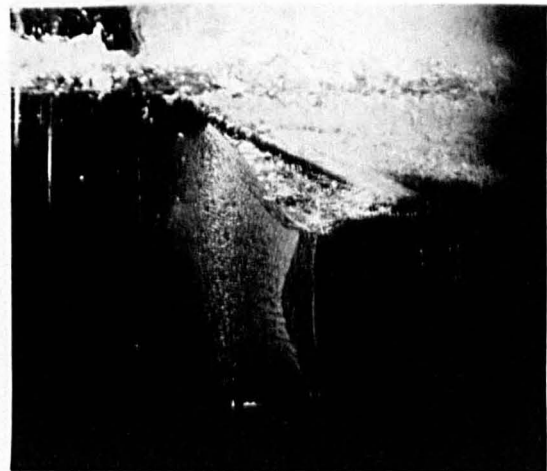
$\beta = 15$ Degrees $\beta = 20$ Degrees

Figure 10.10a – Sequence of Photos Illustrating Mechanism of Fence Breakdown.
NACA 16 021 Fail With Horizontal Slot, 10 ft/s (3m/s), Immersion
195mm, 15 psi (100 kPa) Blowing.
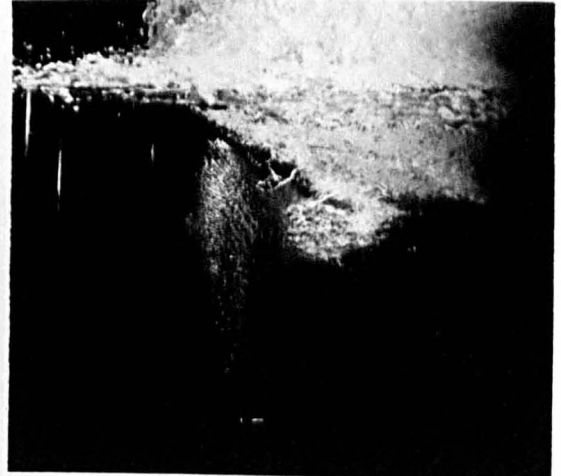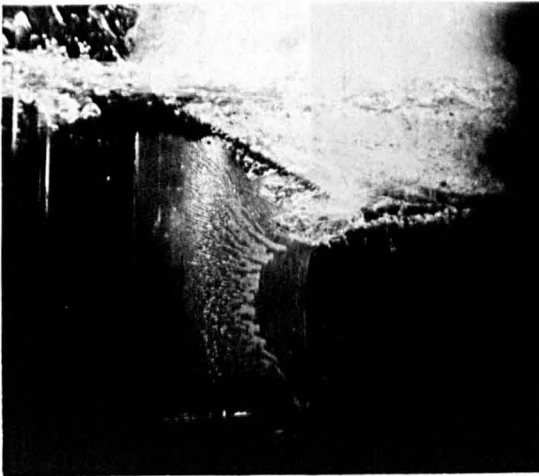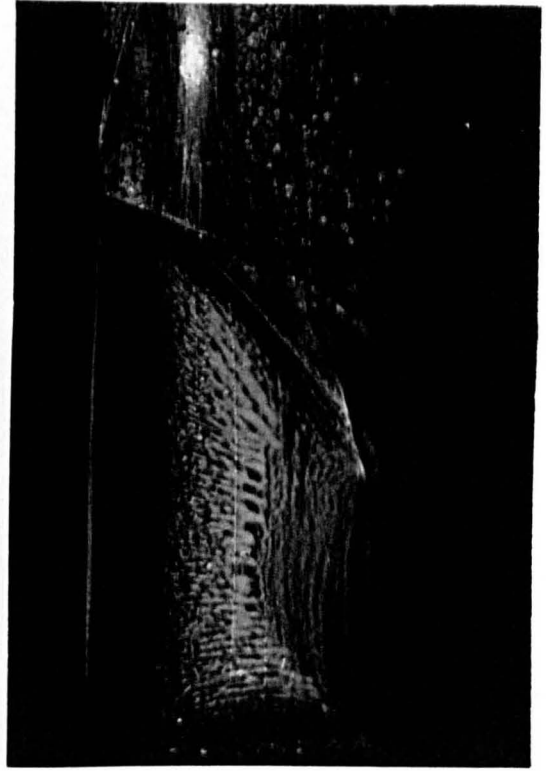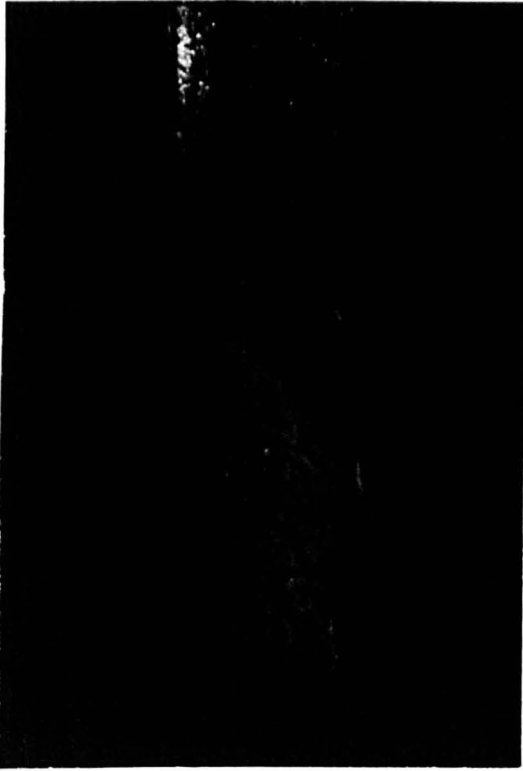
β = 22 Degrees

β = 23 Degrees

Figure 10.10b
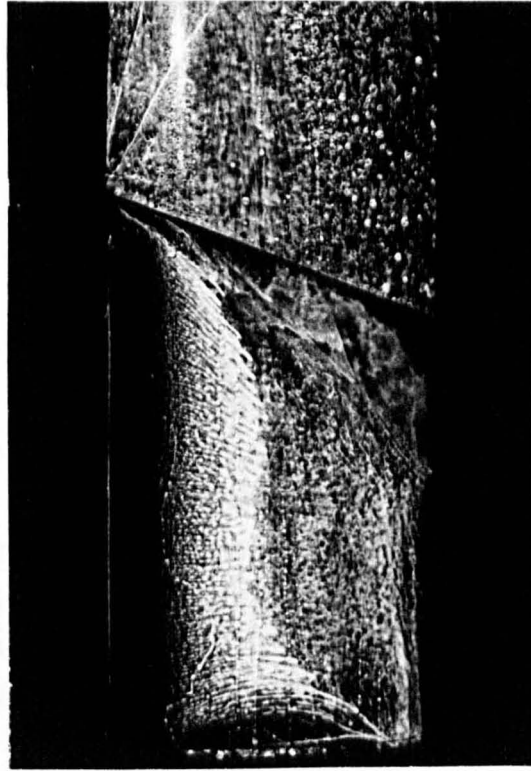
β = 24 Degrees

Figure 10.10c

the immersion such that the fence was just at the apparent water surface as viewed from the lower camera, which was aimed horizontally at the mid-depth of the channel. Specifically, the immersion was 195mm (1.5c). The increase in air entrainment, surface drawdown and area of separation can be clearly seen. Most of the air entrainment took place behind the strut.

Figure 10.11 shows the development with increasing sideslip angle of a subsurface vent followed by a full vent to the depth of the fence, typical of the deeper immersions.

A comparison of the flow visualisation photographs for pressures of 9 psig (62 kPa) and 15 psig (100 kPa) revealed no difference in the amount of air entrainment or surface drawdown near the after part of the fence. No difference was revealed with or without the various types of internal baffles. This seems to indicate that the fence characteristics were not sensitive to minor variations in the fence flow. The exception to this was the test with the forward part of the slot blocked with tape in an attempt to concentrate more of the flow aftwards. The effect was slightly detrimental, with the ventilation angle dropping by 1½ degrees.

Series III – Smooth Model, High Pressure. The effects on the ventilation and washout angles of blowing with pressures up to 100 psig (675 kPa) are shown graphically in Figure 10.12. As in Series I, the most pronounced effect of the liquid fence was on washout angle. As previously stated, washout angles are subject to many factors which were not controlled in this experiment, and which mitigate against extrapolation of results. However, it seems impossible to ignore the trend of increasing washout angle, and the fact that the washout angle approached the inception angle in the most favourable case.

Figure 10.13 shows the data from Series I and Series III plotted on the same graph. The faired solid lines show the trends in ventilation inception and washout angles with increasing fence pressure for the cases which demonstrated consistent improvement. The top two curves represent inception and washout for 245mm (1.9c) immersion and the lowest line represents washout for 195mm (1.5c) immersion.

If just the high pressure series were considered, it would appear that there was a "threshold" pressure for fence effectiveness in suppressing ventilation at the 245mm immersion which was somewhere between 30 and 45 psig (206 and 309 kPa). For 195mm immersion, the fence appeared to have achieved effectiveness below 30 psig (206 kPa), but the increase in inception angle was not as significant as the maximum improvement attained in the previous case.

The trend in washout angles was somewhat more inconsistent between Series I and III. In Series I, the washout angle increased monotonically and nearly linearly with supply pressure with no apparent minimum of pressure, down to 8 psig (55 kPa), the lowest pressure tested. In Series III, 30 psig (206 kPa) did not have much or any effect, but beginning with 45 psig (309 kPa), washout angle was rather consistently increased with increasing supply pressure, up to the
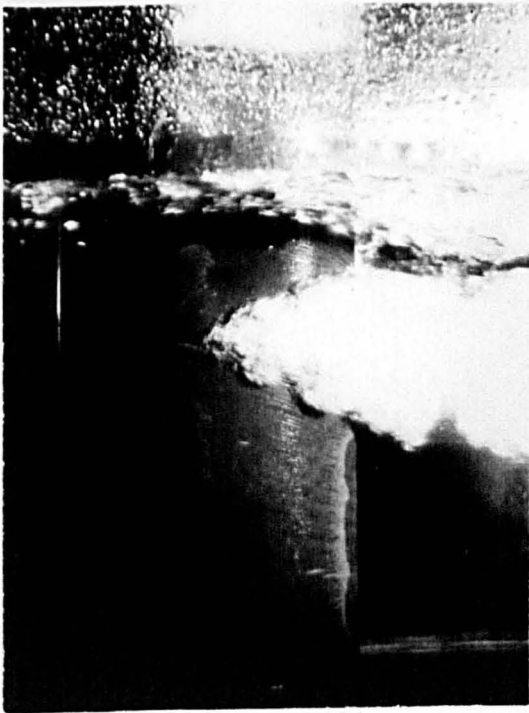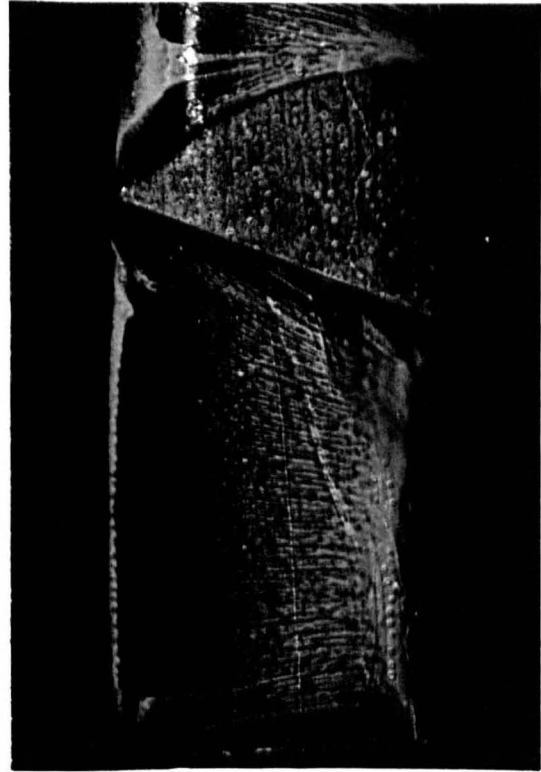
$\beta = 10$ Degrees

$\beta = 15$ Degrees

Figure 10.11a – Development of a Subsurface Vent With Increasing Sideslip Angle, NACA
16 021 Fail With Horizontal Slot, 10 ft/s (3m/s), Immersion 270mm,
9 psi (62 kPa) Blowing.

327
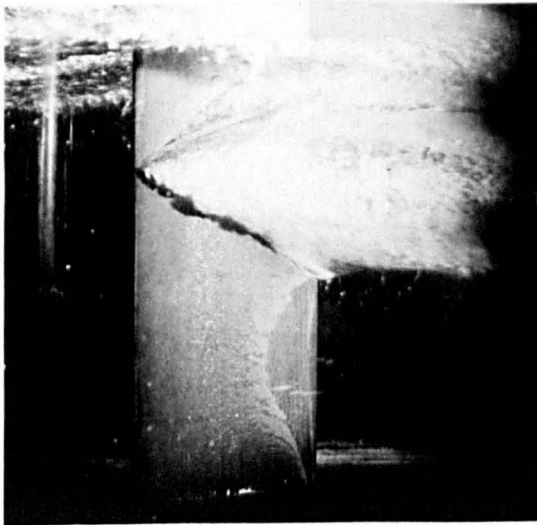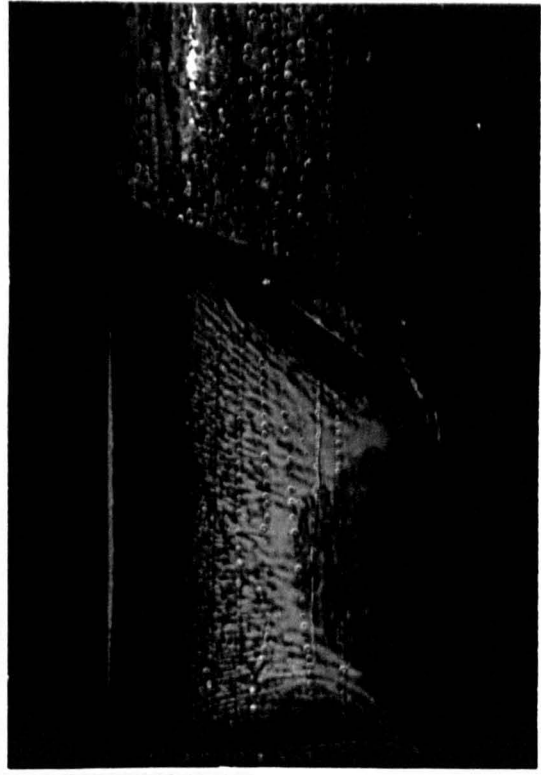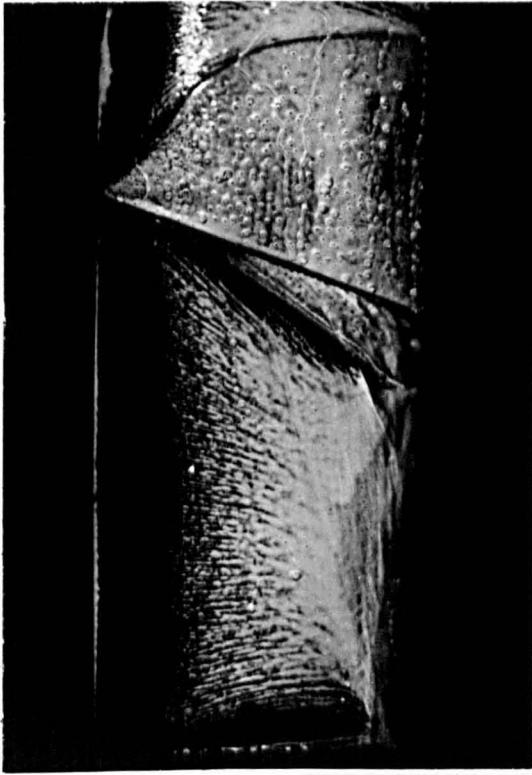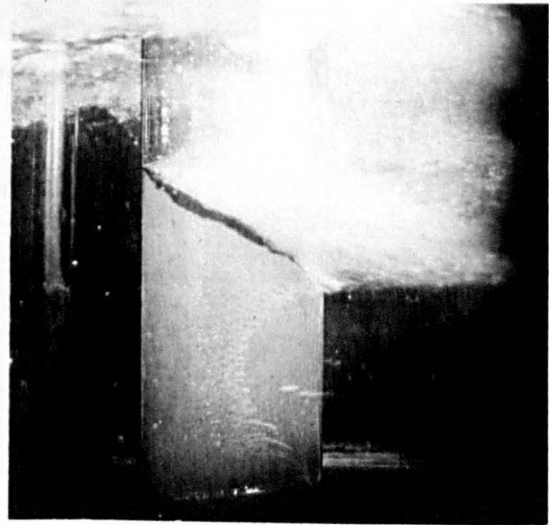
$\beta = 20$ Degrees $\beta = 22$ Degrees

Figure 10.11b

328

β = 23 Degrees

Figure 10.11c
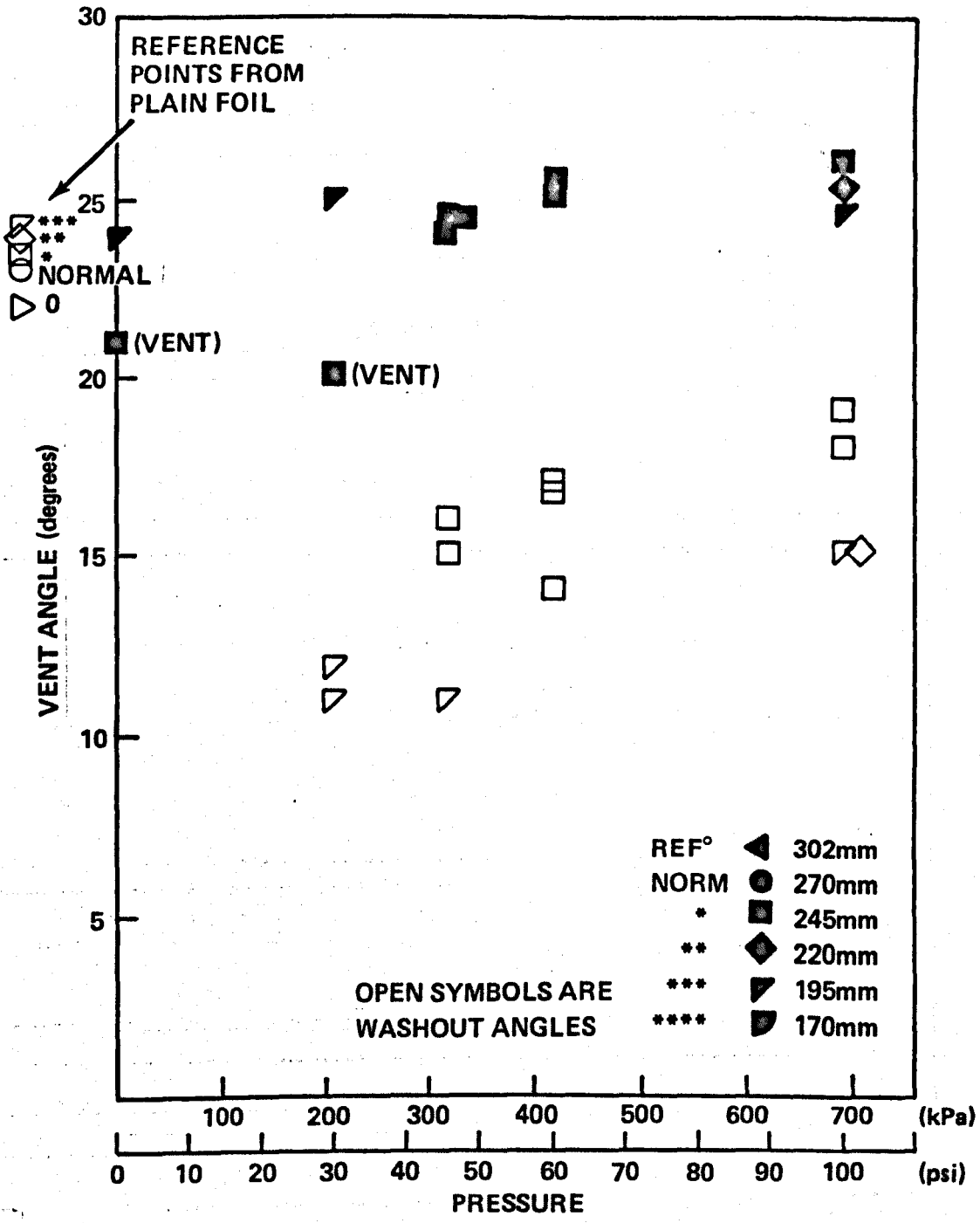
Figure 10.12 — Ventilation Angle Versus Reservoir Pressure, NACA 16 021 Foil With Horizontal Slot Blowing, 10 ft/s (3m/s) High Pressure Series (III).
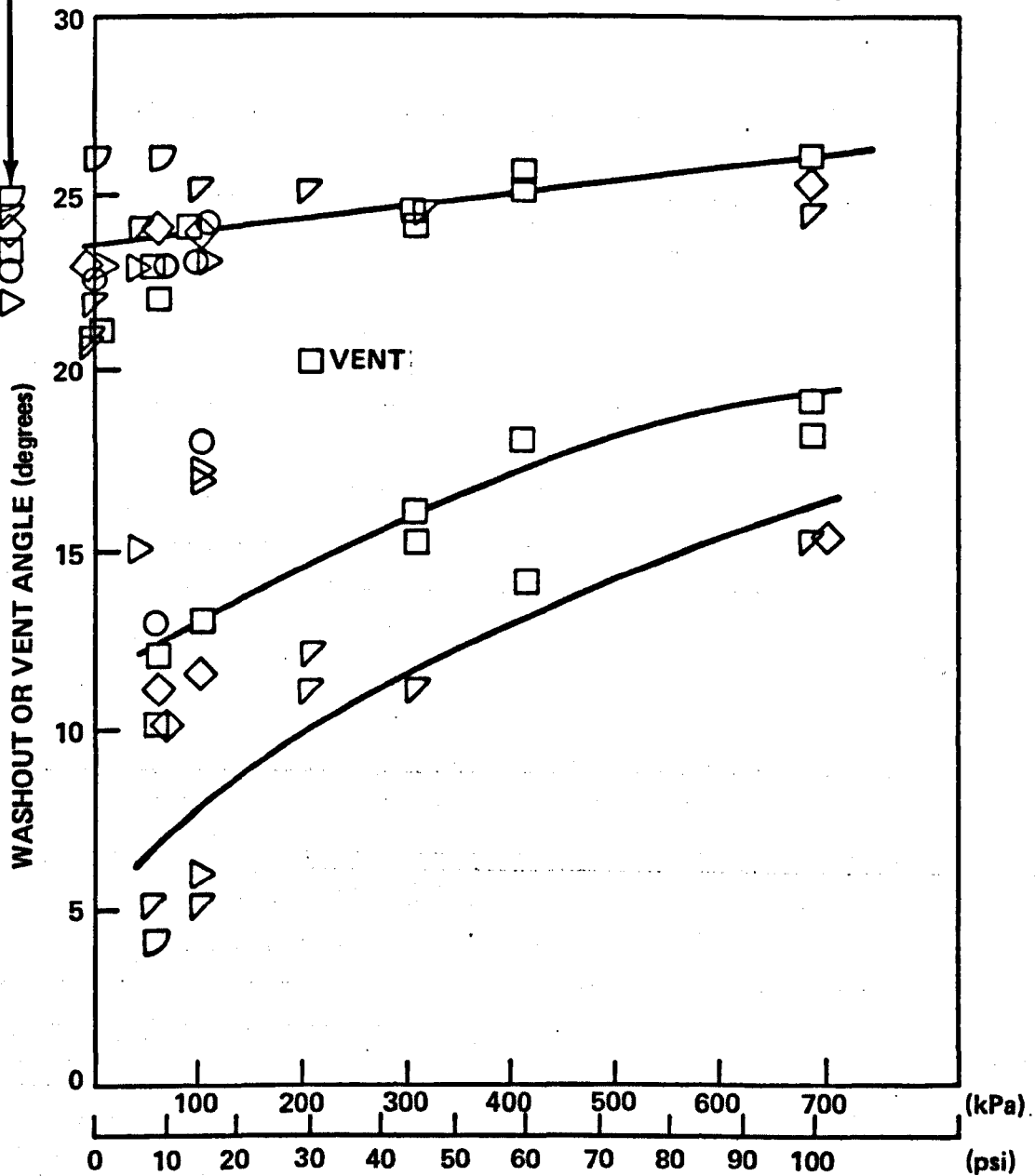
Figure 10.13 — Ventilation Angle Versus Reservoir Pressure, NACA 16 021 Foil With Horizontal Slot Blowing, 10 ft/s (3m/s) Combined Low and High Pressure Series (I & III).

331

maximum 100 psig (675 kPa). This could be related to lack of consistency in the parameters affecting washout angle, including certain experimental procedures, such as the rate of sideslip angle decrease.

An interesting result of the two series of tests is that the 195mm immersion was most vent-resistant at low fence pressure but the 245mm immersion was best at higher pressures. It is possible that this is related to the differences in threshold pressures.

Flow Visualisation — Series III. Four photographs taken of the flow in Series III are shown in Figure 10.14. Comparison of these photographs with similar ones taken in Series I revealed less air entrainment at the higher blowing pressures. A seemingly anomalous phenomenon is the appearance of distinct Taylor surface instabilities in the photographs of high fence pressure runs. These instabilities are characteristic of the surface flow around unmodified struts prior to venti-lation, as discussed in Chapter 2. However, the instabilities observed in the present case are of much smaller size, indicating that the liquid fence did have a stabilising effect, as predicted. (The decrease in surface drawdown is related to less downward acceleration of the surface. The growth of Taylor instabilities is proportional to this acceleration.)

Series II — Roughness. Figure 10.15 is a graph of the inception and washout angles versus fence supply pressure for Channel speeds of 3, 4.5 and 6 m/s for immersions of 195, 220, and 245 mm. The short, horizontal bars on the ordinate indicate average values for the roughened strut with the slot filled in. For this strut, depth of immersion did not affect the results significantly over the range tested. Points to the left of the ordinate represent suction through the fence slot. Points labelled "DLA" are averages of the filled-in slot results at the immersion indicated by the symbol.

At the higher speeds, the air bubble content of the Water Channel built up during the run, and appeared to affect the results. This was also observed in the nose suction experiment. Figure 10.16 shows a sequence of photographs taken during a run at 6 m/s which shows the succesive increase in bubbles. Two points in Figure 10.15 are labelled "no air in channel" and "excess air in channel." During the runs in which those points were collected, the ventilation angle decreased steadily from an initial value of 22 degrees at a rate of a degree or so per run as the bubble population increased. Finally, the ventilation angle stabilised between 17 and 18 degrees.

Washout angles lie mostly within the dotted region on the graph of Figure 10.15. Major trends are indicated by the faired lines between points. Two highly significant trends are evident which are in complete opposition to those observed on the smooth strut. Firstly, increasing

β = 19 Degrees
100 psi (700 kPa) Blowing
245mm Immersion

β = 25 Degrees
100 psi (700 kPa)
195mm Immersion

β = 24 Degrees
45 psi (309 kPa) Blowing
245mm Immersion
Just Prior to Ventilation

β = 24 Degrees
60 psi (410 kPa) Blowing
170mm Immersion

Figure 10.14 – NACA 16 021 Foil With Horizontal Slot Blowing, 10 ft/s (3m/s).
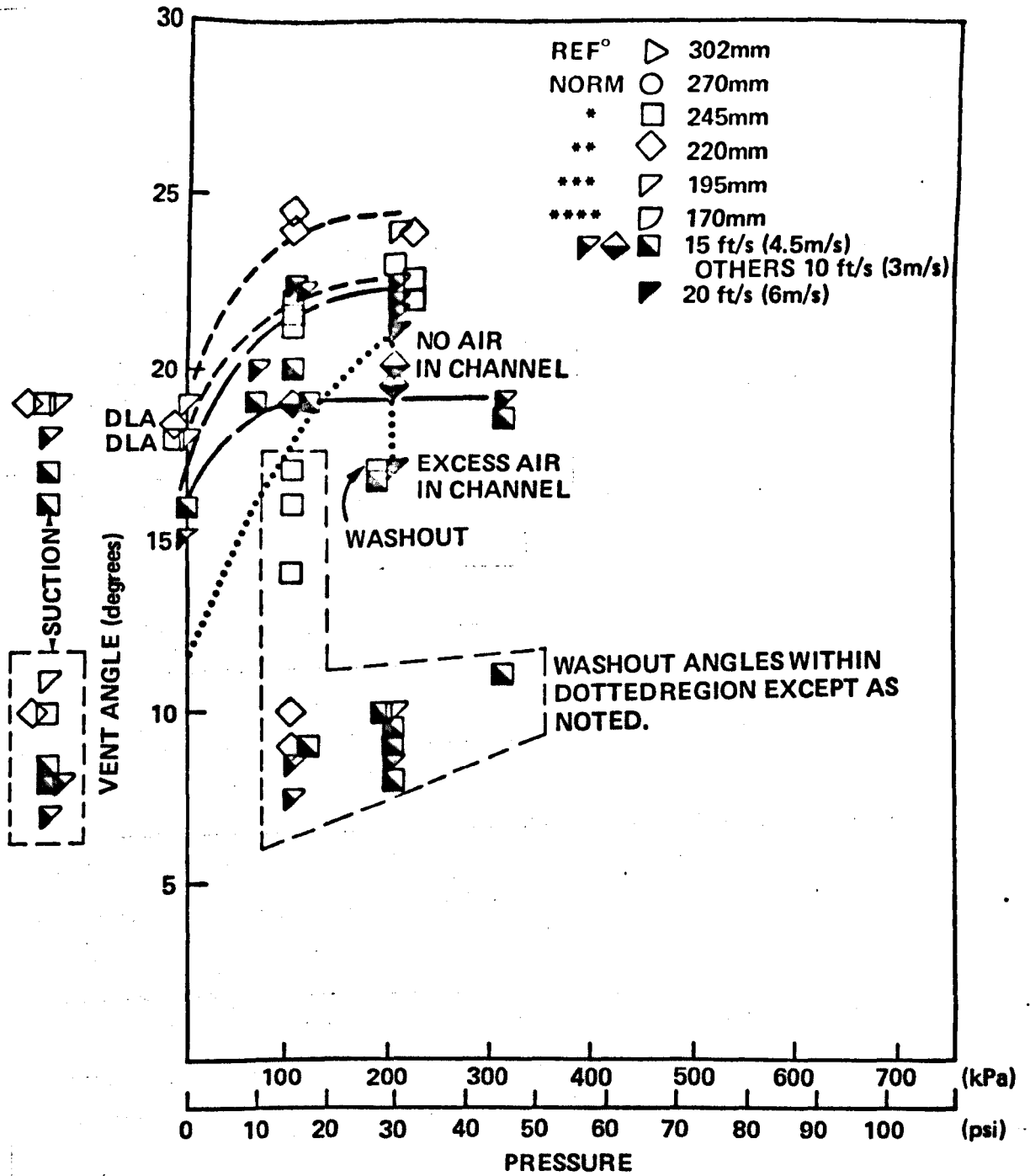
Figure 10.15 — Ventilation Angle Versus Blowing Reservoir Pressure, NACA 16 021 Foil With Horizontal Slot, Roughened With 11 Grade Glass Microspheres.

334
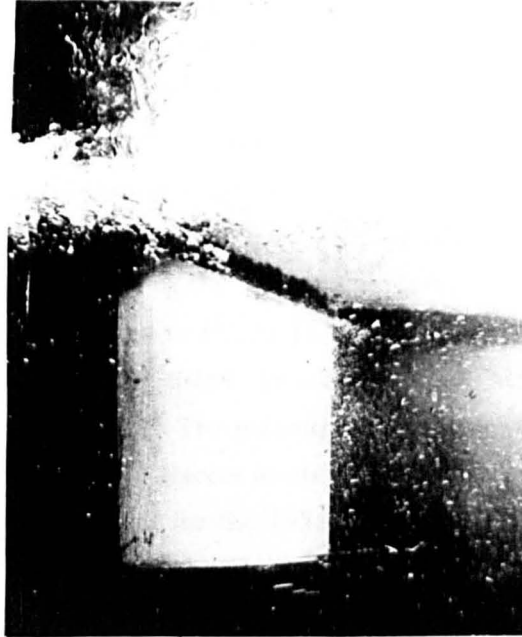
β = 12 Degrees
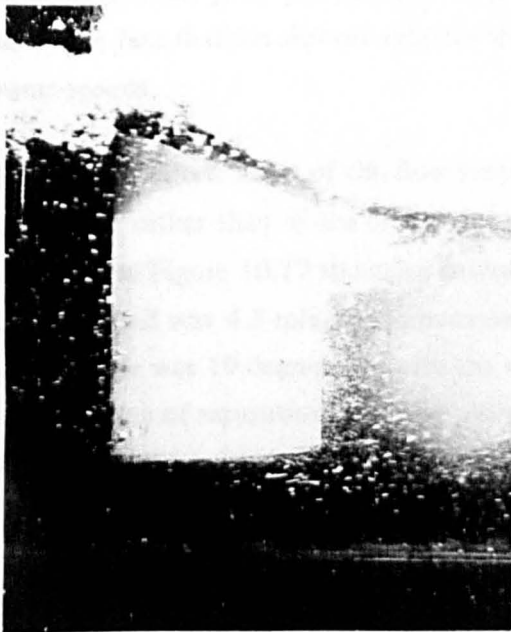
β = 15 Degrees

β = 16 Degrees

Figure 10.16 – Buildup of Bubbles in the Free Surface Water Channel. Roughened NACA 16 021 Foil With 30 psi (209 kPa) Horizontal Slot Blowing, 20 ft/s (6m/s), Immersion 195mm.

335

fence supply pressure had a beneficial effect on inception angle, right up to the maximum pressure applied. Secondly, the fence did not affect the washout angle as much as inception angle, particularly at the higher speed tested.

These phenomena are consistent with the concept of a weakened surface seal engendered by the added roughness. This weakness is a manifestation of the lowered momentum close to the strut boundary, due to the roughness-thickened boundary layer. There may also be a contribution due to the presence of flow disturbances which can be amplified by the Taylor mechanism. Of crucial importance is the fact that these effects are precisely those associated with higher speeds and larger sizes — that is, higher Reynolds Number. This concept has already been expounded in Chapters 5, 6, and 9, and the behaviour of the liquid fences provides a convincing confirmation.

The other important trend revealed in Figure 10.15 is that the relative increase in ventilation inception angle increases with increasing speed. In most cases, the absolute increase in ventilation angle becomes greater with higher speed. The inception angle at 3 m/s increased about 6 degrees upon activation of the fence, from 18½ degrees to about 24 degrees. At 6 m/s, the increase was 7 degrees, from 15 to 22 degrees, at least for the 195mm immersion. For 9 m/s, the increase was nearly 10 degrees, from 11 to 21 degrees, if the datum representing the bubble-free channel condition can be taken as representative. This trend is extremely promising with regard to full scale application, and was not observed in the boundary layer control of method of ventilation suppression described in the previous chapter. Rather than a fundamental defect in the concept, the comparatively poor performance of the vertical slot model at higher speeds may have been due to the fact that the slot-jet velocity was so low that it was not fully effective except at the lowest speeds.

Flow Visualisation. Most of the flow visualisation photographs were taken of the model immersed in the flow, rather than of the oil smear pattern at the end of the run. A few patterns were photographed, and Figure 10.17 shows an interesting example, paired with the flow photograph. The Channel speed was 4.5 m/s, the immersion 195 mm and the fence pressure 45 psig (310 kPa). The sideslip angle was 19 degrees, exactly the ventilation inception angle for that case. There was little evidence of separation in the oil smear pattern, except at the trailing edge. The flow photo shows entrained bubbles striking forward in a flow region clearly indicated by the oil smear as attached. A problem is posed as to the mechanism by which these bubbles are transported forward. It is well known that a ventilated cavity will generally extend farther forward than the separated region which precedes its inception, and it is understandable that, once an air filled cavity is formed in a region previously separated, the new dynamics of the flow situation could cause the entire cavity to spread forward. Mere entrainment of a few bubbles is a different case.
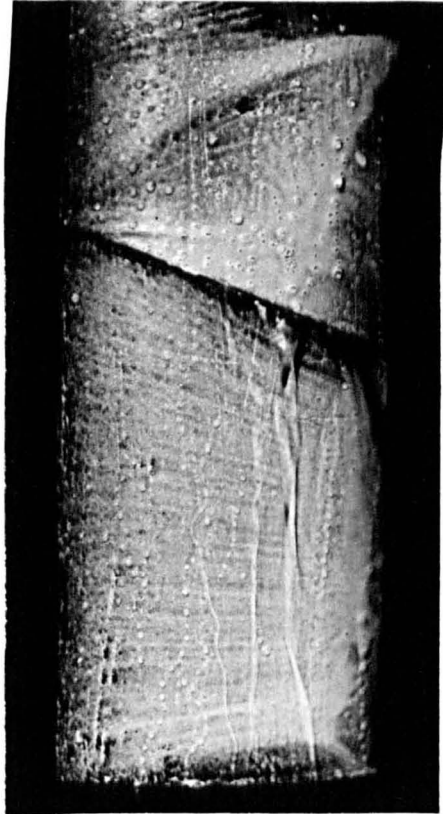
Figure 10.17 – Bubble Transport Phenomenon. Roughened NACA 16 021 Foil With 45 psi
(309 kPa) Horizontal Slot Blowing, β = 19 Degrees, 15 ft/s (4.5m/s),
Immersion 195mm.

Perhaps there is an intermediate stage where the properties of the fluid in the separated region are sufficiently different from water and similar to air to allow the type of transport displayed in Figure 10.17. In no case was a great area of separation apparent in the oil smear pattern prior to ventilation, in contrast to the smooth strut and the Mk I strut with blowing, smooth or rough.

Figures 10.18, 10.19, 10.20 and 10.21 are sequences all photographed at the same sideslip angles, up to the angle of ventilation inception. Immersion was 195mm in all cases but one. The principal differences between the conditions in each of the figures were:

Figure 10.18   3 m/s, slot blocked
Figure 10.19   4.5 m/s, slot blocked
Figure 10.20   4.5 m/s, slot open, no blowing
Figure 10.21   4.5 m/s, slot open, 10 and 30 psi (68 and 206 kPa) blowing.

By comparing Figures 10.18 and 10.19, the effect of speed on the plain, roughened strut can be seen. The main effect of speed seems to have been on the surface quality of the water in the Channel upstream of the strut. At 4.5 m/s, it was rougher than at 3 m/s. At 6 m/s, (not shown) the surface was very much more rough. At 3 m/s, no visible air was drawn down the strut trailing edge at sideslip angles less than 15 degrees. At 4.5 m/s, air drawdown was evident at 5 degrees, and pronounced at 10 degrees.

Comparing Figures 10.19 and 10.20 shows the effect of simply opening the slot without blowing. In spite of the fact that air was purged from the blowing system before the photographs were taken, the open slot with no blowing encouraged air entrainment. This did not seem to affect inception angles (significantly), but the open slot may have had a somewhat favourable influence on washout angle due to residual flow in the slot driven by the ram pressure at the nose.

Comparing Figures 10.20 and 10.21 shows the effect of increasing fence supply pressure. Successively less air was drawn down with increased fence pressure. A direct comparison of the open slot case in Figure 10.20 with the fence-active cases in Figure 10.21 is not possible because the sideslip angles in Figure 10.20 were greater than the vent angle in Figure 10.19.

All the flow visualisation points to the fact that the weak (most easily ruptured) area of the fence was near the trailing edge. Because one of the demonstrated effects of roughness is to move the inception point forward, the fence may have been acting more in the region of maximum effectiveness than it was in the smooth strut cases.

The effect of immersion is not clear. In the photographs, no more bubbles were observed to be drawn down for the 245mm than the 195mm immersion under similar conditions, but at the greater submergence, the inception angle was decreased by 2 degrees or so. This difference is more than would be expected, based on the immersion dependence of the smooth, unmodified strut.

β = 0 Degrees

β = 5 Degrees

β = 10 Degrees

β = 15 Degrees

β = 18 Degrees

β = 18 Degrees

Figure 10.18 — Roughened NACA 16 021 Foil, Slot Blocked, 10 ft/s (3m/s), Immersion 195mm.
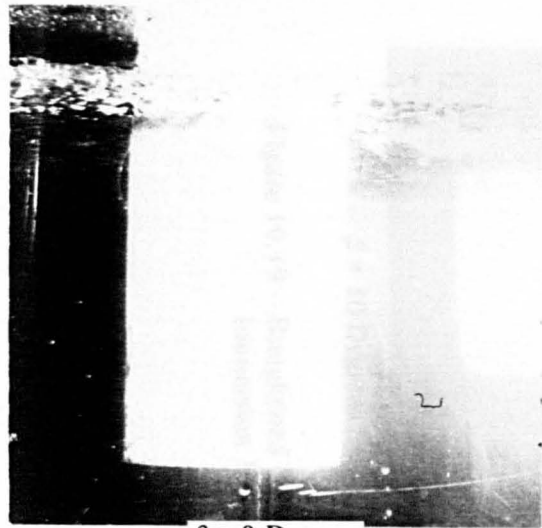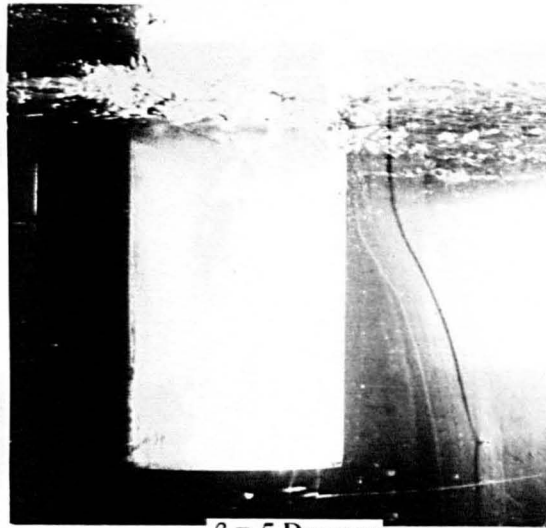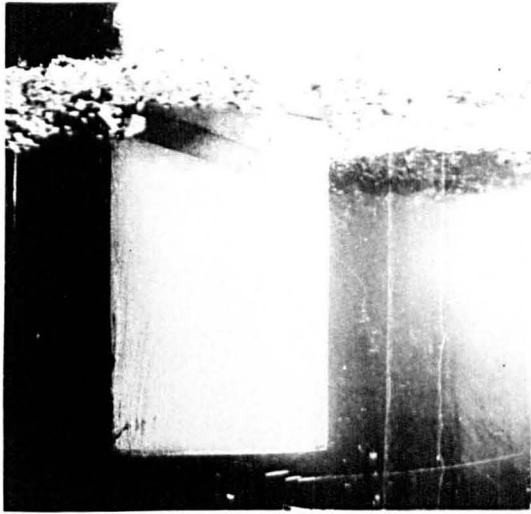
$\beta = 0$ Degrees
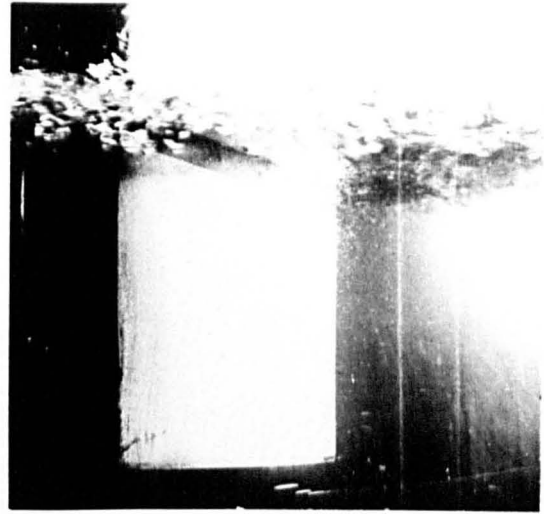
$\beta = 5$ Degrees

$\beta = 10$ Degrees
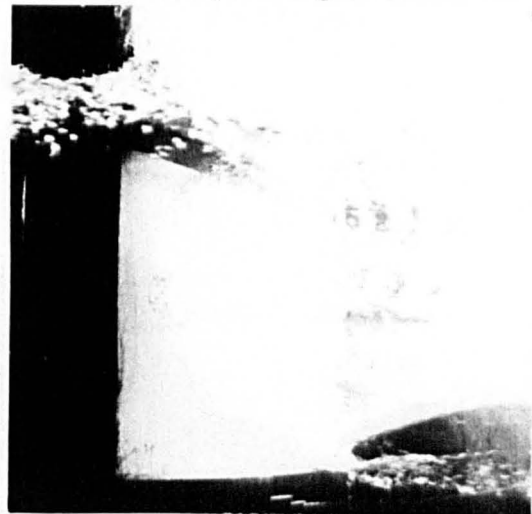
$\beta = 15$ Degrees

Figure 10.19 – Roughened NACA 16 021 Foil, Slot Blocked, 15 ft/s (3m/s), Immersion 195mm.

β = 0 Degrees
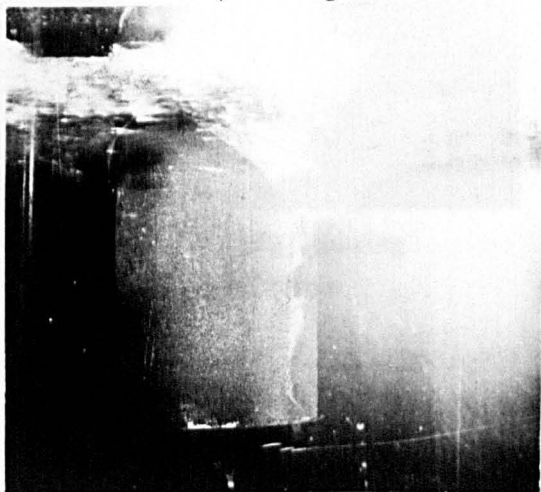
β = 5 Degrees

β = 10 Degrees

β = 15 Degrees

Figure 10.20 – Roughened NACA 16 021 Foil With Horizontal Slot, 15 ft/s (3m/s) No Blowing, Immersion 170mm.

341

10 psi (68 kPa) Blowing
Immersion 245mm

30 psi (206 kPa) Blowing
Immersion 195mm

Figure 10.21 – Roughened NACA 16 021 Foil With Horizontal Slot Blowing, 15 ft/s (3m/s)
β = 18 Degrees.

The trend in washout angle with immersion seemed to be contrary to the trend in inception angle, but this is not considered significant in view of the unreliability of the washout data.

An interesting sequence of photographs is shown in Figure 10.22, in which a vent was washed out at 10 degrees by turning on the liquid fence, and partly re-established after the fence had been turned off.

CONCLUSIONS

A near horizontal sheet of liquid ejected from a surface piercing strut acts similarly to a solid ventilation fence in suppressing ventilation.

For the smooth model, washout angle was most affected by the liquid fence, increasing with fence flow rate (above a threshold pressure) to nearly the inception angle. Inception angles were increased by 3 or 4 degrees in the most favourable cases.

The fence had a flow-straightening effect which caused steeper pressure gradients, resulting in premature separation. Based on the separation patterns, the fence was more effective than the increase in angle would indicate.

Fence breakdown occurred near and perhaps aft of the tail, where the fence flow was inherently weak (in velocity). Taylor instabilities were present in the fence flow, but were not as prominent prior to breakdown as they were in the unmodified strut case.

For the roughened strut, ventilation inception angle was more improved than was washout angle. Inception angles were increased by nearly a multiple of two compared to the unfenced roughened strut, at the highest channel speed. Inception angle increased with increasing supply pressure, in nearly every case, up to the maximum pressure applied.

The similarity of the effect of roughness to higher Reynolds Number and the trend of increased relative improvement with increasing speed indicates that the liquid fence may have promise for application to full scale.

No Blowing

45 psi (309 kPa) Blowing   No Blowing

Figure 10.22 – Effect of Turning Blowing On, Then Off. Roughened NACA 16 021 Foil With
Horizontal Slot, 15 ft/s (3m/s), β = 10 Degrees, Immersion 245mm.

Chapter 10 References

10.1 McGregor, R.C., Foster, J.L., Rothblum, R.S., Swales, P.D., *"The Influence of Fences on Surface Piercing Struts and Foils,"* 10th Office of Naval Research Symposium, Boston, Massachusetts, 1974.

The first four chapters of this thesis were concerned with tracing the history of the problem of hydrofoil ventilation, expounding the mechanism, the possibilities for suppression and control, and establishing the scaling laws. In these chapters were raised or implied the questions to which the remainder of the thesis was addressed.

In Chapter Two, it was noted that the mechanism of ventilation was unverified at full scale and that there was no evidence that the modes of inception were the same as those observed in the laboratory. The point was raised that although separation or cavitation was always observed prior to ventilation, this was not conclusive evidence of a prerequisite. Possibly at larger sizes, the requirement for a low momentum region could be satisfied by ordinary growth of the unseparated boundary layer. It was noted that for the longer residence times for some full scale situations that the growth of Taylor instabilities would be nonlinear with time.

Chapter Three suggested that elimination of separation by boundary layer energisation by either suction or blowing might be a feasible method of suppression of ventilation. The possibility of a liquid fence barrier to the path of air was also discussed.

In Chapter Four on Scaling, an explanation was sought for the success of fences at full scale, when model scale experiments indicated that fences were relatively ineffective against tail ventilation. Also examined was the hypothesis that if the surface seal were weakened by higher speeds and larger sizes, then ventilation would take place gradually, rather than suddenly as observed in the laboratory. A question was posed by the observation of partial ventilation on prototypes and the failure to observe a similar phenomenon at model scale, even at very high speeds. The effect of the ocean environment was also questioned – the influence of waves, background turbulence and dissolved and dispersed gases. The possibility was raised that effects might be present at model scale, such as surface wettability and roughness, which would not extrapolate to full scale.

The conclusions of Chapter Four were that, for similar geometry, a large variety of model scale results could be reduced to a function of cavitation number and Froude number alone. For nearly arbitrary geometry, including cases with and without vapour cavitation, an empirical relationship between a dimensionless velocity and the ratio of surface drawdown to chord length was sufficient information to predict inception for as many cases as could be assessed from available data, including results obtained in waves.

In Chapter Five, on Roughness and Wettability, it was concluded that the application of roughness above a minimum size to a surface piercing strut reduced the ventilation angle at a

given speed, the effect becoming more pronounced with increasing speed and increasing roughness size. This was explained as an effect of the roughness weakening the surface seal, first by causing transition to turbulence and then encouraging the growth of the boundary layer. The roughness did not appear to affect the extent of the separated region. In spite of the weakening of the surface seal, transition to ventilation did not take place gradually. Roughness generally had a delaying effect on washout, with a tendency of cavities to cling to isolated roughnesses. Because the minimum roughness size which had an effect was considerably larger than the roughness found on ordinarily smooth models, this effect was discounted as an explanation for variation between otherwise similar model tests. Surface contact angle (wettability) had no effect at the sizes and speeds tested in this study.

Chapter Six, which extended the study of Chapter Five to high speeds, allowed some very interesting conclusions to be drawn. The mode of inception of ventilation on the NACA 0012 strut changed from tail to nose and then back to tail with increasing speed, the last change being made as vapour cavitation became significant. At an intermediate speed, a new mode of ventilation, not previously observed, was noted. In the new mode, aerated water in a tail separated region interacted with a pulsating nose vapour cavity, the air path being introduced to the cavity completely below the water surface, at about midspan. Comparison with towing tank data suggested that the reason that nose ventilation became less likely to occur with increasing speed was that the momentum of the surface seal became greater without being counterbalanced by a corresponding growth in the extent of the separated region. Even though the mode of inception changed to the tail type at the highest speeds, it was also observed that the point of inception moved relatively forward. This could provide an explanation of the success of nose fences at prototype speeds.

The effect of roughness was to introduce scatter, especially at low and intermediate speeds. With increasing speed, the ventilation boundary seemingly approached a least angle asymptote. The necessity for large regions of separation prior to ventilation was reduced or possibly eliminated by roughness. The frequent partial vents observed were reminiscent visually of full scale observations, and compatible with a physical model in which the surface seal is weakened by boundary layer growth, turbulence and mixing action. Accurate modeling of prototype performance will probably require the inclusion of controlled roughness on the model.

Chapter Eight described how by modifying a theoretical two dimensional pressure distribution to account for the free surface and finite span, it was possible to predict the depth to which a region of nose separation could be eliminated by suction. Unfortunately, complete elimination of the separated region over the entire span was not achieved, so it was not

347

possible to conclude whether separation was a necessary precondition for ventilation inception. A slot only partially open near the free surface was effective in preventing nose ventilation, and a reduction in the extent of the separated region reduced the tendency to ventilation.

Chapter Nine reported the results of an experiment to eliminate tail separation by boundary layer blowing, thus suppressing ventilation, providing that the separated region is a precondition to inception. An analogy between blowing to increase lift on elliptic cylinders and blowing to prevent separation on aerofoil shapes was used to develop a theory which gave a surprisingly accurate prediction of the blowing momentum coefficient required to delay ventilation to a given angle and speed. It proved possible to increase the ventilation inception angle somewhat over the normal inception angle for the strut tested. Usually, leading edge separation was imminent at ventilation inception with blowing. The success of the experiment was greater in terms of the implied force coefficient attained prior to ventilation than in terms of actual angle. The maximum increase in inception angle was obtained by blowing near the free surface and ignoring subsurface separation, much as in the case of the suction experiment. The fact that ventilation occurred when the oil smear patterns indicated that separation was virtually eliminated shakes the hypothesis that separation is a necessary precondition. At the most, it can be said that a very small amount of separation is necessary, an amount so small as never to be eliminated under practical conditions. The effect of blowing was much more pronounced in the case of a roughened strut. In fact, the results with the roughened strut were nearly as good as an unmodified smooth strut without blowing. This lends weight to the conclusion that the principal effect of the roughness in initiating earlier ventilation was due to the enhanced growth of the boundary layer.

The liquid fence experiment of Chapter Ten showed that a nearly horizontal sheet of liquid ejected from a strut acted similarly to a solid ventilation fence in suppressing ventilation. For the smooth model, washout angle was most affected by the liquid fence, increasing with fence flow rate (above a threshold) to nearly the inception angle. Inception angles were increased by three or four degrees in the most favourable cases. For the roughened strut, ventilation inception angle was more improved than was washout angle. Inception angles were increased by nearly a multiple of two compared to the unfenced roughened strut, at the highest channel speed. Inception angle increased with increasing supply pressure, in nearly every case, up to the maximum pressure applied. The similarity of the effect of roughness to larger sizes and the trend of increased relative improvement with increasing speed indicates that the liquid fence may have promise for full scale applications.